

DTIC  
①

AD-A151 846



INVESTIGATION OF A FAILURE DETECTION/  
IDENTIFICATION SYSTEM FOR A TACTICAL  
AIRCRAFT NAVIGATION SYSTEM

THESIS

Gary R. Johnston  
First Lieutenant, USAF

AFIT/GE/ENG/84D-36

DISTRIBUTION STATEMENT A

Approved for public release  
Distribution Unlimited

DTIC  
ELECTE  
MAR 29 1985  
S B D

DEPARTMENT OF THE AIR FORCE  
AIR UNIVERSITY

**AIR FORCE INSTITUTE OF TECHNOLOGY**

Wright-Patterson Air Force Base, Ohio

85 08 13 064

DTIC FILE COPY

AFIT/GE/ENG/84D-36

INVESTIGATION OF A FAILURE DETECTION/  
IDENTIFICATION SYSTEM FOR A TACTICAL  
AIRCRAFT NAVIGATION SYSTEM

THESIS

Gary R. Johnston  
First Lieutenant, USAF

AFIT/GE/ENG/84D-36

DTIC  
ELECTE  
MAR 29 1985  
S B D

Approved for public release; distribution unlimited

AFIT/GE/ENG/84D-36

INVESTIGATION OF A FAILURE DETECTION/  
IDENTIFICATION SYSTEM FOR A TACTICAL  
AIRCRAFT NAVIGATION SYSTEM

THESIS

Presented to the Faculty of the School of Engineering  
of the Air Force Institute of Technology  
Air University  
in Partial Fulfillment of the  
Requirements for the Degree of  
Master of Science in Electrical Engineering

Gary R. Johnston, B.S.E.E.  
First Lieutenant, USAF

December 1984

Approved for public release; distribution unlimited

## Preface

The purpose of this thesis was to develop a filter model and failure detection/identification system for the initial phase of an adaptive tactical navigation (ATN) simulation program. This thesis topic was suggested by Mr. Brian Mahon to support a current Air Force Avionics Laboratory research effort.

The filter model, as well as the failure detection/identification system (designed, tuned, and tested against no-failure and failed sensor conditions in both benign and highly dynamic flight scenarios) demonstrated good performance and provided some expected results. However, additional filter tuning and threshold adjustments are needed to optimize the system's performance.

I am proud to have been associated with and am truly indebted to my faculty advisor, Dr. Peter S. Maybeck and thesis reader, Captain Stephen E. Cross. I also wish to thank Stan Musick and Sandy Berning of the Avionics Lab for their assistance. I wish to express a heart felt thanks to my wife, Bonnie, and my sons, Brent and Greg. Their love and untiring support has helped me through the thesis as well as the academic program that has brought me to this point in my formal education.

Gary R. Johnston



## Table of Contents

|  | Page |
|--|------|
| Preface . . . . .                      | ii   |
| List of Figures . . . . .              | v    |
| List of Tables . . . . .               | xiv  |
| Abstract . . . . .                     | xvi  |
| I. Introduction . . . . .              | 1-1  |
| Overview . . . . .                     | 1-1  |
| Background . . . . .                   | 1-3  |
| Problem . . . . .                      | 1-15 |
| Scope . . . . .                        | 1-15 |
| Assumptions . . . . .                  | 1-17 |
| Standards . . . . .                    | 1-18 |
| Approach . . . . .                     | 1-18 |
| Outline of Thesis . . . . .            | 1-19 |
| II. The System Truth Model . . . . .   | 2-1  |
| The Truth Model . . . . .              | 2-1  |
| Simulation . . . . .                   | 2-30 |
| Flight Trajectory . . . . .            | 2-30 |
| Monte Carlo Analysis . . . . .         | 2-32 |
| The Unaided Simulation . . . . .       | 2-32 |
| III. The Filter Design . . . . .       | 3-1  |
| Introduction . . . . .                 | 3-1  |
| The Baro-Altimeter . . . . .           | 3-3  |
| Doppler Radar . . . . .                | 3-5  |
| Radar Altimeter . . . . .              | 3-10 |
| Map Correlator . . . . .               | 3-12 |
| Satellite Position System . . . . .    | 3-14 |
| Gyro and Accelerometer . . . . .       | 3-16 |
| Filter Tuning . . . . .                | 3-19 |
| IV. The FDI System . . . . .           | 4-1  |
| Background . . . . .                   | 4-1  |
| Failure Detection Concept . . . . .    | 4-3  |
| Observability Criteria . . . . .       | 4-5  |
| Detectability Criteria . . . . .       | 4-5  |
| Fault Isolation . . . . .              | 4-6  |
| FDI Technique Review . . . . .         | 4-6  |
| Stochastic Failure Detection . . . . . | 4-6  |

|  |         |
|--|---------|
| The SPRT . . . . .   | 4-8     |
| Voting Systems . . . . .                                       | 4-9     |
| FDI System Design. . . . .                                     | 4-10    |
| Failure Detection System . . . . .                             | 4-11    |
| The Isolation/Identification Process . . . . .                 | 4-22    |
| <br>V. FDI Analysis . . . . .                                  | <br>5-1 |
| Simulation Overview . . . . .                                  | 5-1     |
| No-Failure Likelihood Functions. . . . .                       | 5-3     |
| Satellite Failure Detection (Benign) . . . . .                 | 5-4     |
| Satellite Failure Detection (Dynamic) . . . . .                | 5-8     |
| Doppler Failure Detection (Benign) . . . . .                   | 5-10    |
| Doppler Failure Detection (Dynamic) . . . . .                  | 5-12    |
| Terrain Correlator Failure Detection (Benign) . . . . .        | 5-14    |
| Terrain Correlator Failure Detection (Dynamic) . . . . .       | 5-15    |
| Another Detection Approach . . . . .                           | 5-18    |
| No-Failure Slope Detection . . . . .                           | 5-19    |
| Satellite Slope Failure Detection (Benign) . . . . .           | 5-20    |
| Satellite Slope Failure Detection (Dynamic) . . . . .          | 5-20    |
| Doppler Slope Failure Detection (Benign) . . . . .             | 5-20    |
| Doppler Slope Failure Detection (Dynamic) . . . . .            | 5-21    |
| Terrain Correlator Slope Failure Detection (Benign) . . . . .  | 5-21    |
| Terrain Correlator Slope Failure Detection (Dynamic) . . . . . | 5-21    |
| Slope Detection Analysis . . . . .                             | 5-21    |
| The FDI Detection Processor. . . . .                           | 5-26    |
| <br>VI. Conclusions and Recommendations . . . . .              | <br>6-1 |
| Conclusions . . . . .  | 6-1     |
| Recommendations . . . . .                                      | 6-2     |
| <br>Appendix . . . . .   | <br>A-1 |
| <br>Bibliography . . . . .                                     | <br>B-1 |
| <br>Vita . . . . .   | <br>V-1 |



|  |                         |
|--|-------------------------|
| <input checked="checked" type="checkbox"/> Unannounced<br><input type="checkbox"/> Justification |                         |
| By _____   |                         |
| Distribution/ _____  |                         |
| Availability Codes _____   |                         |
| Dist   | Avail and/or<br>Special |
| A-1  |                         |

### List of Figures

| Figure |   | Page |
|--------|---|------|
| 1.1    | Sensor-Aided INS/FDI System .....                         | 1-16 |
| 2.1    | X-Sensitive Gyro Error Model .....                        | 2-11 |
| 2.2    | Accelerometer Error Model For X Axis .....                | 2-12 |
| 2.3    | Baro-Altimeter Error Model .....                          | 2-14 |
| 2.4    | User Clock Error Model .....                              | 2-16 |
| 2.5    | Doppler Radar Error Model For<br>Along-Track Error .....  | 2-17 |
| 2.6    | Radar Altimeter Error Model .....                         | 2-18 |
| 2.7    | Terrain Correlation Error Model .....                     | 2-19 |
| 2.8    | Fundamental Matrix .....                                  | 2-24 |
| 2.9    | $F_{11}$ Partition 35 x 35 of<br>Fundamental Matrix ..... | 2-25 |
| 2.10   | $F_{22}$ Partition 36-39 of<br>Fundamental Matrix .....   | 2-27 |
| 2.11   | $F_{33}$ Partition 40-45 of<br>Fundamental Matrix .....   | 2-27 |
| 2.12   | $F_{44}$ Partition 48-52 of<br>Fundamental Matrix .....   | 2-28 |
| 2.13   | Latitude/Longitude Flight Profile .....                   | 2-34 |
| 2.14   | Altitude Flight Profile .....                             | 2-35 |
| 2.15   | Yaw Flight Profile .....                                  | 2-36 |
| 2.16   | Pitch Flight Profile.....                                 | 2-37 |
| 2.17   | Roll Flight Profile .....                                 | 2-38 |
| 2.18   | Longitude Error For Unaided INS .....                     | 2-39 |
| 2.19   | Latitude Error For Unaided INS .....                      | 2-40 |
| 2.20   | Altitude Error For Unaided INS .....                      | 2-41 |

|      |   |      |
|------|---|------|
| 2.21 | East Velocity For Unaided INS .....                         | 2-42 |
| 2.22 | North Velocity Error For Unaided INS .....                  | 2-42 |
| 2.23 | Vertical Velocity Error For Unaided INS .....               | 2-44 |
| 2.24 | East Attitude Error For Unaided INS .....                   | 2-45 |
| 2.25 | North Attitude Error For Unaided INS .....                  | 2-46 |
| 2.26 | Vertical Attitude Error For Unaided INS .....               | 2-47 |
| 2.27 | Vertical Acceleration Error .....                           | 2-48 |
| 3.0  | Vehicle Track to Navigation Frame<br>Transformation .....   | 3-7  |
| 3.1  | Longitude Error For Satellite Measurement ...               | 3-23 |
| 3.2  | Latitude Error For Satellite Measurement.....               | 3-24 |
| 3.3  | Altitude Error For Satellite Measurement.....               | 3-25 |
| 3.4  | East Velocity Error For Satellite<br>Measurement .....      | 3-26 |
| 3.5  | North Velocity Error For Satellite<br>Measurement .....     | 3-27 |
| 3.6  | Vertical Velocity Error For Satellite<br>Measurement .....  | 3-28 |
| 3.7  | Satellite Position Error For Satellite<br>Measurement ..... | 3-29 |
| 3.8  | Satellite Velocity Error For Satellite<br>Measurement ..... | 3-30 |
| 3.9  | Longitude Error For Doppler Measurement.....                | 3-31 |
| 3.10 | Latitude Error For Doppler Measurement .....                | 3-32 |
| 3.11 | Altitude Error For Doppler Measurement .....                | 3-33 |
| 3.12 | East Velocity Error For Doppler Measurement..               | 3-34 |
| 3.13 | North Velocity Error For Doppler Measurement .              | 3-35 |
| 3.14 | Vertical Velocity Error For Doppler<br>Measurement .....    | 3-36 |
| 3.15 | Doppler Beam Error For Doppler Measurement ...              | 3-37 |

|      |   |      |
|------|---|------|
| 3.16 | Doppler Scale Factor Error For Doppler Measurement .....                                  | 3-38 |
| 3.17 | Longitude Error For Terrain Correlator Measurement .....                                  | 3-39 |
| 3.18 | Latitude Error For Terrain Correlator Measurement .....                                   | 3-40 |
| 3.19 | Altitude Error For Terrain Correlator Measurement .....                                   | 3-41 |
| 3.20 | East Velocity Error For Terrain Correlator Measurement .....                              | 3-42 |
| 3.21 | North Velocity Error For Terrain Correlator Measurement .....                             | 3-43 |
| 3.22 | Vertical Velocity Error For Terrain Correlator Measurement .....                          | 3-44 |
| 3.23 | Radar Altimeter Error For Terrain Correlator Measurement .....                            | 3-45 |
| 3.24 | East Terrain Correlator Position Error For Terrain Correlator Measurement .....           | 3-46 |
| 3.25 | North Terrain Correlator Position Error For Terrain Correlator Measurement .....          | 3-47 |
| 3.26 | Vertical Terrain Correlator Position Error For Terrain Correlator Measurement .....       | 3-48 |
| A.1  | Hard Satellite Receiver - Satellite Velocity Measurement #4 - Benign Flight .....         | A-2  |
| A.2  | Hard Satellite Receiver Failure - Satellite Velocity Measurement #5 - Benign Flight ..... | A-3  |
| A.3  | Hard Satellite Receiver Failure - Satellite Velocity Measurement #6 - Benign Flight ..... | A-4  |
| A.4  | Soft Satellite Failure - Satellite Position Measurement #1 - Benign Flight .....          | A-5  |
| A.5  | Soft Satellite Failure - Satellite Position Measurement #2 - Benign Flight .....          | A-6  |
| A.6  | Soft Satellite Failure - Satellite Measurement #3 - Benign Flight .....                   | A-7  |

|      |   |      |
|------|---|------|
| A.7  | Hard Accelerometer 3 Failure - Satellite<br>Position Measurement #3 - Benign Flight ..... | A-8  |
| A.8  | Hard Accelerometer 3 Failure - Satellite<br>Velocity Measurement #4 - Benign Flight ..... | A-9  |
| A.9  | Hard Accelerometer 3 Failure - Satellite<br>Velocity Measurement #5 - Benign Flight ..... | A-10 |
| A.10 | Hard Accelerometer 3 Failure - Satellite<br>Velocity Measurement #6 - Benign Flight ..... | A-11 |
| A.11 | Hard Accelerometer 2 Failure - Satellite<br>Velocity Measurement #5 - Benign Flight ..... | A-12 |
| A.12 | Hard Accelerometer 1 Failure - Satellite<br>Velocity Measurement #4 - Benign Flight ..... | A-13 |
| A.13 | Hard Accelerometer 1 Failure - Satellite<br>Velocity Measurement #5 - Benign Flight ..... | A-14 |
| A.14 | Hard Accelerometer 1 Failure - Satellite<br>Velocity Measurement #6 - Benign Flight ..... | A-15 |
| A.15 | Soft Accelerometer 2 Failure - Satellite<br>Velocity Measurement #4 - Benign Flight ..... | A-16 |
| A.16 | Soft Accelerometer 2 Failure - Satellite<br>Velocity Measurement #5 - Benign Flight ..... | A-17 |
| A.17 | Soft Accelerometer 1 Failure - Satellite<br>Velocity Measurement #4 - Benign Flight ..... | A-18 |
| A.18 | Soft Accelerometer 1 Failure - Satellite<br>Velocity Measurement #6 - Benign Flight ..... | A-19 |
| A.19 | Hard Gyro 2 Failure - Satellite Velocity<br>Measurement #4 - Benign Flight .....          | A-20 |
| A.20 | Hard Gyro 2 Failure - Satellite Velocity<br>Measurement #5 - Benign Flight .....          | A-21 |
| A.21 | Hard Gyro 2 Failure - Satellite Velocity<br>Measurement #6 - Benign Flight .....          | A-22 |
| A.22 | Hard Gyro 1 Failure - Satellite Velocity<br>Measurement #4 - Benign Flight .....          | A-23 |
| A.23 | Hard Gyro 1 Failure - Satellite Velocity<br>Measurement #6 - Benign Flight .....          | A-24 |
| A.24 | No Failure Condition - Satellite Position<br>Measurement #1 - Benign Flight .....         | A-25 |

|      |   |      |
|------|---|------|
| A.25 | No Failure Condition - Satellite Position<br>Measurement #2 - Benign Flight .....         | A-26 |
| A.26 | No Failure Condition - Satellite Position<br>Measurement #3 - Benign Flight .....         | A-27 |
| A.27 | No Failure Condition - Satellite Position<br>Measurement #4 - Benign Flight .....         | A-28 |
| A.28 | No Failure Condition - Satellite Position<br>Measurement #5 - Benign Flight .....         | A-29 |
| A.29 | No Failure Condition - Satellite Velocity<br>Measurement #6 - Benign Flight .....         | A-30 |
| A.30 | Soft Satellite Failure - Satellite Position<br>Measurement #2 - Dynamic Flight .....      | A-31 |
| A.31 | Soft Satellite Failure - Satellite Position<br>Measurement #1 - Dynamic Flight .....      | A-32 |
| A.32 | Soft Satellite Failure - Satellite Position<br>Measurement #3 - Dynamic Flight .....      | A-33 |
| A.33 | Hard Accelerometer 3 Failure - Satellite<br>Velocity Measurement #6 - Dynamic Flight .... | A-34 |
| A.34 | Hard Accelerometer 2 Failure - Satellite<br>Velocity Measurement #4 - Dynamic Flight .... | A-35 |
| A.35 | Hard Accelerometer 1 Failure - Satellite<br>Velocity Measurement #4 - Dynamic Flight .... | A-36 |
| A.36 | Hard Accelerometer 1 Failure - Satellite<br>Velocity Measurement #5 - Dynamic Flight .... | A-37 |
| A.37 | Soft Accelerometer 2 Failure - Satellite<br>Velocity Measurement #4 - Dynamic Flight .... | A-38 |
| A.38 | No Failure Condition - Satellite Position<br>Measurement #1 - Dynamic Flight .....        | A-39 |
| A.39 | No Failure Condition - Satellite Position<br>Measurement #2 - Dynamic Flight .....        | A-40 |
| A.40 | No Failure Condition - Satellite Position<br>Measurement #3 - Dynamic Flight .....        | A-41 |
| A.41 | No Failure Condition - Satellite Velocity<br>Measurement #4 - Dynamic Flight .....        | A-42 |
| A.42 | No Failure Condition - Satellite Velocity<br>Measurement #5 - Dynamic Flight .....        | A-43 |

|      |   |      |
|------|---|------|
| A.43 | No Failure Condition - Satellite Velocity<br>Measurement #6 - Dynamic Flight .....      | A-44 |
| A.44 | No Failure Condition - Doppler Velocity<br>Measurement #1 - Benign Flight .....         | A-45 |
| A.45 | No Failure Condition - Doppler Velocity<br>Measurement #2 - Benign Flight .....         | A-45 |
| A.46 | No Failure Condition - Doppler Velocity<br>Measurement #3 - Benign Flight .....         | A-47 |
| A.47 | Hard Gyro 1 Failure - Doppler Velocity<br>Measurement #1 - Benign Flight .....          | A-48 |
| A.48 | Hard Gyro 1 Failure - Doppler Velocity<br>Measurement #2 - Benign Flight .....          | A-49 |
| A.49 | Hard Gyro 2 Failure - Doppler Velocity<br>Measurement #1 - Benign Flight .....          | A-50 |
| A.50 | Hard Gyro 2 Failure - Doppler Velocity<br>Measurement #2 - Benign Flight .....          | A-51 |
| A.51 | Soft Accelerometer 1 Failure - Doppler<br>Velocity Measurement #1 - Benign Flight ..... | A-52 |
| A.52 | Soft Accelerometer 1 Failure - Doppler<br>Velocity Measurement #2 - Benign Flight ..... | A-53 |
| A.53 | Soft Accelerometer 2 Failure - Doppler<br>Velocity Measurement #1 - Benign Flight ..... | A-54 |
| A.54 | Soft Accelerometer 2 Failure - Doppler<br>Velocity Measurement #2 - Benign Flight ..... | A-55 |
| A.55 | Hard Accelerometer 2 Failure - Doppler<br>Velocity Measurement #1 - Benign Flight ..... | A-56 |
| A.56 | Hard Accelerometer 2 Failure - Doppler<br>Velocity Measurement #2 - Benign Flight ..... | A-57 |
| A.57 | Hard Accelerometer 3 Failure - Doppler<br>Velocity Measurement #1 - Benign Flight ..... | A-58 |
| A.58 | Hard Accelerometer 3 Failure - Doppler<br>Velocity Measurement #3 - Benign Flight ..... | A-59 |
| A.59 | Soft Doppler Failure - Doppler Velocity<br>Measurement #1 - Benign Flight .....         | A-60 |
| A.60 | Soft Doppler Failure - Doppler Velocity<br>Measurement #2 - Benign Flight .....         | A-61 |



|      |   |      |
|------|---|------|
| A.61 | Soft Doppler Failure - Doppler Velocity<br>Measurement #3 - Benign Flight .....         | A-62 |
| A.62 | Hard Doppler Failure - Doppler Velocity<br>Measurement #3 - Benign Flight .....         | A-63 |
| A.63 | Hard Doppler Failure - Doppler Velocity<br>Measurement #2 - Dynamic Flight .....        | A-64 |
| A.64 | Soft Doppler Failure - Doppler Velocity<br>Measurement #1 - Dynamic Flight .....        | A-65 |
| A.65 | Soft Doppler Failure - Doppler Velocity<br>Measurement #2 - Dynamic Flight .....        | A-66 |
| A.66 | Soft Doppler Failure - Doppler Velocity<br>Measurement #3 - Dynamic Flight .....        | A-67 |
| A.67 | Hard Accelerometer 2 Failure - Doppler<br>Velocity Measurement #1 - Dynamic Flight .... | A-68 |
| A.68 | Hard Accelerometer 2 Failure - Doppler<br>Velocity Measurement #2 - Dynamic Flight .... | A-69 |
| A.69 | Hard Accelerometer 3 Failure - Doppler<br>Velocity Measurement #2 - Dynamic Flight .... | A-70 |
| A.70 | Hard Accelerometer 3 Failure - Doppler<br>Velocity Measurement #3 - Dynamic Flight .... | A-71 |
| A.71 | Hard Accelerometer 1 Failure - Doppler<br>Velocity Measurement #1 - Dynamic Flight .... | A-72 |
| A.72 | Hard Accelerometer 1 Failure - Doppler<br>Velocity Measurement #2 - Dynamic Flight .... | A-73 |
| A.73 | Hard Accelerometer 1 Failure - Doppler<br>Velocity Measurement #3 - Dynamic Flight .... | A-74 |
| A.74 | Soft Accelerometer 2 Failure - Doppler<br>Velocity Measurement #2 - Dynamic Flight .... | A-75 |
| A.75 | Soft Accelerometer 1 Failure - Doppler<br>Velocity Measurement #2 - Dynamic Flight .... | A-76 |
| A.76 | No Failure Condition - Doppler Velocity<br>Measurement #1 - Dynamic Flight .....        | A-77 |
| A.77 | No Failure Condition - Doppler Velocity<br>Measurement #2 - Dynamic Flight.....         | A-78 |
| A.78 | No Failure Condition - Doppler Velocity<br>Measurement #3 - Dynamic Flight.....         | A-79 |

|      |   |      |
|------|---|------|
| A.79 | Soft Accelerometer 1 Failure - Terrain<br>Correlator Position Measurement #1 -<br>Benign Flight ..... | A-80 |
| A.80 | Hard Radar Altimeter Failure - Terrain<br>Correlator Measurement #3 - Benign Flight ....              | A-81 |
| A.81 | Soft Radar Altimeter Failure - Terrain<br>Correlator Measurement #3 - Benign Flight ....              | A-82 |
| A.82 | Hard Accelerometer 3 Failure - Terrain<br>Correlator Measurement #3 - Benign Flight ....              | A-83 |
| A.83 | Hard Baro-Altimeter Failure - Terrain<br>Correlator Measurement #3 - Benign Flight ....               | A-84 |
| A.84 | Hard Accelerometer 2 Failure - Terrain<br>Correlator Measurement #1 - Benign Flight ....              | A-85 |
| A.85 | Hard Accelerometer 2 Failure - Terrain<br>Correlator Measurement #2 - Benign Flight ....              | A-86 |
| A.86 | Soft Accelerometer 2 Failure - Terrain<br>Correlator Measurement #1 - Benign Flight ....              | A-87 |
| A.87 | Hard Accelerometer 1 Failure - Terrain<br>Correlator Measurement #2 - Benign Flight ....              | A-88 |
| A.88 | Hard Accelerometer 1 Failure - Terrain<br>Correlator Measurement #1 - Benign Flight ....              | A-89 |
| A.89 | No Failure Condition - Terrain Correlator<br>Measurement #1 - Benign Flight .....                     | A-90 |
| A.90 | No Failure Condition - Terrain Correlator<br>Measurement #2 - Benign Flight .....                     | A-91 |
| A.91 | No Failure Condition - Terrain Correlator<br>Measurement #3 - Benign Flight .....                     | A-92 |
| A.92 | No Failure Condition - Terrain Correlator<br>Measurement #1 - Dynamic Flight.....                     | A-93 |
| A.93 | No Failure Condition - Terrain Correlator<br>Measurement #2 - Dynamic Flight.....                     | A-94 |
| A.94 | No Failure Condition - Terrain Correlator<br>Measurement #3 - Dynamic Flight.....                     | A-95 |
| A.95 | Soft Accelerometer 2 Failure - Terrain<br>Correlator Measurement #1 - Dynamic Flight ...              | A-96 |

|       |  |       |
|-------|--|-------|
| A.96  | Soft Accelerometer 3 Failure - Terrain<br>Correlator Measurement #1 - Dynamic Flight ... | A-97  |
| A.97  | Hard Accelerometer 1 Failure - Terrain<br>Correlator Measurement #1 - Dynamic Flight ... | A-98  |
| A.98  | Hard Accelerometer 1 Failure - Terrain<br>Correlator Measurement #2 - Dynamic Flight ... | A-99  |
| A.99  | Hard Accelerometer 2 Failure - Terrain<br>Correlator Measurement #1 - Dynamic Flight ..  | A-100 |
| A.100 | Hard Accelerometer 3 Failure - Terrain<br>Correlator Measurement #1 - Dynamic Flight ..  | A-101 |
| A.101 | Soft Radar Altimeter Failure - Terrain<br>Correlator Measurement #1 - Dynamic Flight ..  | A-102 |
| A.102 | Soft Radar Altimeter Failure - Terrain<br>Correlator Measurement #2 - Dynamic Flight ..  | A-103 |
| A.103 | Soft Radar Altimeter Failure - Terrain<br>Correlator Measurement #3 - Dynamic Flight ..  | A-104 |
| A.104 | Hard Radar Altimeter Failure - Terrain<br>Correlator Measurement #3 - Dynamic Flight ..  | A-105 |
| A.105 | Hard Baro-Altimeter Failure - Terrain<br>Correlator Measurement #3 - Dynamic Flight ..   | A-106 |

# List of Tables

| Table |  | Page |
|-------|--|------|
| I     | Error Model State Variables .....  | 2-20 |
| II    | Notation Used in Figure 2.9 .....  | 2-26 |
| III   | Error Source Statistics .....  | 2-29 |
| IV    | Flight Profile Statistics .....  | 2-31 |
| V     | Additional Filter Error States .....   | 3-2  |
| VI    | The Filter Error Model .....   | 3-17 |
| VII   | Q Values for Filter Tuning .....   | 3-21 |
| VIII  | Measurement Processing .....   | 4-16 |
| IX    | Sensor Fault Classification .....  | 4-20 |
| X     | Gyro and Accelerometer Error Tracking .....  | 4-21 |
| XI    | Simulation Times of Interest .....   | 5-2  |
| XII   | Satellite Likelihood Function Failure<br>Statistics for Benign Flight .....                  | 5-7  |
| XIII  | Satellite Likelihood Function Failure<br>Statistics for Dynamic Flight .....                 | 5-9  |
| XIV   | Doppler Likelihood Function Failure<br>Statistics for Benign and Dynamic (@)<br>Flight ..... | 5-13 |
| XV    | Terrain Correlator Likelihood Function<br>for Benign and Dynamic (@) Flight .....            | 5-17 |
| XVI   | Slope Failure Detection Results .....  | 5-22 |
| XVII  | Slope Failure Sequence for Satellite<br>Likelihood Functions (Benign Flight) .....           | 5-23 |
| XVIII | Slope Failure Sequence for Doppler<br>Likelihood Functions (Dynamic Flight).....             | 5-23 |
| XIX   | Slope Failure Sequence for Doppler<br>Likelihood Functions (Benign Flight) .....             | 5-24 |
| XX    | Slope Failure Sequence For Doppler<br>Likelihood Functions (Dynamic Flight) .....            | 5-24 |

| Table  |  | Page |
|--------|--|------|
| XXI    | Slope Failure Sequence for Terrain<br>Correlator Likelihood Functions (Benign<br>Flight) .....                 | 5-25 |
| XXII   | Slope Failure Sequence for Terrain<br>Correlator Likelihood Functions (Dynamic<br>Flight).....                 | 5-25 |
| XXIII  | Combined Failure Detection Capability .....  | 5-30 |
| XXIV   | Combined Failure Isolation Capability for<br>Satellite Likelihood Functions (Benign<br>Flight) .....           | 5-31 |
| XXV    | Combined Failure Isolation Capability for<br>Satellite Likelihood Functions (Dynamic<br>Flight) .....          | 5-32 |
| XXVI   | Combined Failure Isolation Capability for<br>Doppler Likelihood Functions (Benign<br>Flight) .....             | 5-33 |
| XXVII  | Combined Failure Isolation Capability for<br>Doppler Likelihood Function (Dynamic<br>Flight) .....             | 5-34 |
| XXVIII | Combined Failure Isolation Capability for<br>Terrain Correlator Likelihood Functions<br>(Benign Flight) .....  | 5-35 |
| XXIX   | Combined Failure Detection Capability for<br>Terrain Correlator Likelihood Functions<br>(Dynamic Flight) ..... | 5-36 |

Abstract

This research effort aimed at the design of a suitable filter model and failure detection/identification (FDI) processor as a basis for the development of a fully simulated adaptive tactical navigation (ATN) system. A 52-state "truth" error model was developed from which a 26-state filter error model was derived. The measurement process utilizes a six measurement satellite positioning system (three velocity measurements and three position measurements), a three measurement Doppler radar (three velocity measurements), and a terrain correlation system (three position measurements). The filter residuals for the different measurement processes are then utilized in N-step likelihood function computations to observe the residual behavior. Two different testing criteria have been developed for failure declaration. Simple threshold establishment and the tracking of the likelihood function N-step slope characteristics are utilized for this purpose. Based on the statistics of the observed failure characteristics, an isolation/identification processor isolates the fault and makes the correct identification.

The analysis was performed by simulating both "soft" and "hard" failures and monitoring the likelihood function behavior. The observed failure characteristics then triggered the appropriate isolation/identification logic and the failed sen-

sor decision was made. The test results indicate that this FDI process warrants further consideration. Readdressing the basic issues of filter state reduction, tuning, threshold settings, and "window" size will undoubtedly improve the performance of this system.

# INVESTIGATION OF A FAILURE DETECTION/IDENTIFICATION SYSTEM FOR A TACTICAL AIRCRAFT NAVIGATION SYSTEM

## I. Introduction

### Overview

The requirement for precise weapon delivery has generated the need for highly accurate navigation during a tactical mission. Without this accuracy, weapon delivery will most likely be ineffectual. During the tactical mission, selecting sensors for updating the navigation system can become very time consuming and complex for the aircrew. This could force the aircrew to spend a substantial amount of time concerned about what suite of sensors will ensure the success of their particular mission. Their time could be more effectively used for activities that may be important at that particular mission phase. For the purpose of this paper, accurate weapon delivery will represent the measure of meeting the mission objective.

An automated system is desired which will use the probability of target kill and the probability of aircraft survival when making a sensor suite selection. This automated system may consider such data as prestored map features, threat information, flight plan, sensor characteristics (e.g., signatures to the enemy and the sensor's accuracy in the current environment) as well as the



degree of navigation accuracy required for the particular mission phase. Also, real-time information, such as radar illumination from an unknown site (due to a sensor or sensors presently in use), a change in route, a change in target, a sensor failure/degradation, or sensor jamming must also be taken into account when optimizing the navigation system.

A key element for this automated system, referred to as adaptive tactical navigation (ATN), is the failure detection and identification (FDI) system. The FDI system has the essential job of ensuring that an accurate sensor suite is functioning at all times. This will ultimately ensure the peak performance of the ATN system. The FDI system must continuously monitor the performance of the inertial navigation system (INS) and any external aiding sensors to ensure that they are functioning within acceptable limits. If a sensor or sensors are malfunctioning, the FDI system must detect the malfunction, identify the failed sensor or sensors, and then pass this information to the ATN system computer for sensor removal, compensation, or reselection. There are several FDI processes which have been developed (30). Each of them have both positive and negative attributes. Positive attributes would be represented by ease of implementation and reduced computational load. Negative attributes are exemplified by high false alarm rates (declaring a failure when no failure has occurred) or non-detection of low-level ("soft") failures. An "optimal" (in

this case, optimal implies minimal false alarms and timely detection and identification) FDI process is needed which has a high degree of reliability. Without this reliability, the ATN system will not achieve the peak performance needed to contribute to the success of a tactical mission.

### Background

The following information is included to provide the reader with the historical perspective of FDI process development and to make a distinction between the objective of this thesis and the works of others.

Before an explanation of the FDI processes can occur, an overview of the filtering process is in order (24:3-7). For an aircraft navigation problem, the quantities that describe the "state" of the system cannot be measured directly, therefore, the desired values must be derived from the available data (e.g., an air data system directly provides static and pitot pressures, the aircraft heading and reference system provides Euler angles, etc.). From this data, velocity and position can be determined. The system is typically driven by inputs other than those that are known and the correlation among the states is only known with a degree of certainty. The measurement of these quantities is also corrupted by noise, bias, and inaccuracy. If a number of measuring devices are available, some means of combining their measurement information in an optimal and systematic

fashion is needed. The Kalman filter combines this available measurement data with apriori information about the system and measurement devices to provide a statistically error-minimized solution.

The FDI process has the responsibility for the detection of undesirable characteristics in the system. For actuators these characteristics are exhibited by shifts in the control input gains (B matrix), increased processing noise, or a bias in the measurements. On the other hand, sensor failures usually manifest themselves as abrupt changes in the measurement gain (H matrix), increases in measurement noise, or as biases in the measurements themselves. The characteristics usually are strongly exhibited in the residuals generated by the filter or in related difference expressions (difference expressions not considered residuals would be the equations which compare failed-state modeling to the measured quantity and the difference is not used for filter update but for failure detection) (11:47). For the purpose of this paper, the issue of sensor failure detection will be addressed.

There are several FDI techniques which offer various tradeoffs, advantages, and disadvantages. Based on the general approach of the FDI technique, it can be placed into one of the following categories (47):

- (1) failure sensitive filter
- (2) voting systems

- (3) multiple hypothesis filter-detectors
- (4) jump process formulations
- (5) innovations - based detection systems

Failure-sensitive filters (12:17;44) are aimed at the "oblivious" filter. If the filter, because of its structure, learns the state too well, (as a result of too small of a filter covariance,  $P$ , and filter gain,  $K$ ), it will tend to rely heavily on old measurement data and will neglect new measurement data. Therefore, if an abrupt change occurs, the filter will not react in a timely manner. The 1964 work of Fagin (12) produced an exponentially age-weighted filter. This technique reduced the filter's reliance on old data in an exponential fashion. In 1970, this technique was further explored by Tarn and Zaborsky (17). The efforts of Jazwinski in 1968 (44), produced the finite - memory filter. He also proposed methods such as increasing the noise covariance or fixing filter gain in a 1970 paper (18). These techniques offer indirect failure information, which means this type of filter responds faster than the base filter to abrupt changes. The drawback to this approach is the increase in filter bandwidth due to the increased allowance of new data to influence filter behavior. This increased bandwidth degrades the performance of the filter under normal operating conditions. One possible solution is a two-filter system (a normal mode filter and a failure mode filter). Several

methods have been developed which model the failure of sensors as states in the filter which are then directly compared to their nominal values, to declare or not declare a failure based on the results of the comparison. This technique provides quick response at the expense of increased filter dimensionality and some performance degradation due to the increased bandwidth caused by the additional states. The further effort of Beard (46) and Jones (47) in 1973, produced a design procedure which allows particular failure modes to manifest themselves as residuals which remain in a fixed direction or in a fixed plane in the failure subspace. This failure subspace is the set of vectors which represent the failure modes which could occur. These vectors generate a subspace from which it is possible to determine the failure mode. By the construct of this algorithm, the residual remains in a fixed direction and has a magnitude which is proportional to the failure size. The Jones method can be used to detect a wide variety of failures and provides detailed failure isolation information; however, it is not an optimal estimator (optimal in the sense that it can only handle specific types of failures with specific characteristics). This implies this type of filter would be slow or completely oblivious to detect a failure which has not been addressed in the failure filter design. Furthermore, its construct is only applicable to the time-invariant system.

Voting systems are useful in systems that possess a high degree of parallel hardware redundancy. The work of Gilmore and McKern (1970) (13) discusses the use of this technique to detect "hard" gyro failures. Standard voting schemes require at least three identical devices to determine which device has failed (with two devices, only a discrepancy between them can be determined but not an indication of which one actually failed). In 1974, Broen (2) proposed a voter - estimator scheme which generates a "soft" voting procedure that removes the data from a failed sensor in a weighted fashion so as to reduce false alarms caused by transients (rapid removal of this sensor could cause a large change in the measurement residual). This technique uses a variable which is a function of the like - sensor measurements. This variable has a small value if the measurement of a particular sensor is different from the others and a large value if it is close to the others. The variable is then used to find the value of a filter state that minimizes a likelihood function for the innovations sequence. Since the likelihood function output is not directly used to determine which sensor has failed, a failed sensor still has this "soft" vote. This approach greatly lessens false alarms but requires on-line computation of the filter gain. In general, voting schemes are easy to implement and provide fast detection of hard failures, but can only be implemented in systems that have a high degree of parallel hardware redundancy. They cannot

take advantage of information from unlike sensors and are extremely poor at detecting "soft" failures.

Multiple hypothesis filter detectors are based on different hypotheses concerning system behavior. A "bank" of (linear) filters is utilized, each of which models a different hypothesis. This approach requires both the filter modeling of the hypotheses and a conditional probability generated from the filter's residuals. This information is then used to determine the probability that each hypothesis is correct. The technique allows simultaneous state estimation and failure identification. Willsky, Deyst, and Crawford (1974, 1975) (48:51) applied the methodology developed by Buxbaum and Haddad (1969) (4) for the detection of failures in an INS. The theoretically optimum implementation of the algorithm requires an exponentially growing bank of filters due to the fact that each filter is associated with a time history of hypothesis decisions, and the number of such sequences grows exponentially with time. Several approximation techniques have been proposed to alleviate this problem. This proposal of Willsky, Deyst, and Crawford used an "N-step" window. The "shift" (growth) of the residual bias due to failed behavior is hypothesized as occurring once in the N-steps. If no abnormal behavior is observed in the N-steps, the N conditional densities (these densities represent the probability of a shift conditioned on the measurement history) are fused into a single density and

the N-step process is repeated. The fused density allows the filter bank to be reinitialized which means it will essentially remain sensitive to new information. Another approach using the N-step window was proposed by Newbold and Ho (1968) (16). The approach is called a sequential probability ratio test (SPRT). It operates based on a two-hypothesis decision rule (e.g., system character changed/didn't change) and compares aposteriori probabilities of the two hypotheses by means of the log ratio of the two probabilities. This log ratio is then compared to predetermined thresholds (these thresholds have been empirically established based on desired detection sensitivity) and then either no decision is made, in which case another measurement is brought in and added to the previous N inputs, or a decision is made. This means that the value of N is dynamic and enhances the detection capability of the detection process; however, the "soft" failure of a device which occurs in the middle of an N-step process may go undetected until the next test occurs. Further techniques proposed by Nahi (1969) (38) considered the use of multiple hypothesis modeling to develop a linear estimator for the system which accounts for any measurement that might contain only noise. For a measurement that contains only noise, the H matrix for that hypothesis is a matrix of zeroes. This in effect models "hard" sensor failure which was unaddressed in earlier work. The multiple decision process remains intact.



This technique does not remove bad measurements or allow the filter structure to adapt.

Jump process formulations are the result of the requirement of an FDI system to detect abrupt changes in a dynamic system in the shortest possible amount of time. Basically, this technique involves the characterization of apriori information concerning failure rates. The magnitude of possible failures is assumed to be known value which allows the designer to model the detection system to hypothesize a certain threshold based on a detected rate of growth in the residual. Work by Sworder and Robinson, (1973) (41), and Ratner and Luenberger (1973) (40) have focused on the finite jump of system matrices among a finite set of possible matrices which are generated apriori for different failures and for the no-failure condition. The major deficiency in this approach is the unaddressed issue of system randomness (e.g., the lack of statistically describing the jump characteristics). Since the jump matrices are for a specific set of failure descriptions, there is no flexibility in this approach to detect unmodeled jump failures. Davis (1975) (10) has worked the fault detection problem using nonlinear methodology (e.g., he has modeled his detection formulation based on nonlinear state equations and measurement formulations). At the time of this writing, no study of this technique had been made which would establish its performance; however, this technique is suboptimal as a

state estimator since its tuning has been based on failed-sensor statistics. Chien (1972) (3) devised a failure detection method which circumvents the suboptimal state estimate problem and provides detection of a jump or ramp in the system. The approach demonstrated detector simplicity and use of a scalar stochastic equation which allows direct failure estimates (one equation for each failure type). The method also has built-in robustness to account for modeling errors (through incorporation of white noise processes), eliminates suboptimal filter performance for no-failure operation, through the use of a time-probability description for the failure description, alleviates the problem of the previously addressed "oblivious" filter. The design method utilizes a nominal size bias and steady-state evaluation of the failure/residual relationship to establish a stochastic differential equation for the probability of a failure given the measurement.

Failure transients have not been properly addressed, which means that a time delay for failure detection may result while waiting for the failure to reach steady-state condition.

Innovations - based detection systems involve the residual monitoring of a filter based on normal and/or failed hypotheses. Chien's method (30) which was addressed in the previous paragraph, can also be placed in this group due to his method of residual usage. The flexibility of this

methodology is obvious. Since the filter model operates under no-failure conditions (statistics are for no-failure condition), the FDI system uses the residuals generated by the filter state estimate and the measurement to determine the sensor or sensors' operating condition. This technique exploits the characteristics of the residuals (e.g., the residual should be zero-mean, white, Gaussian, and have a covariance of  $(HP^{-1}H^T + R)$ , as computed in the filter if the filter is well tuned, and if its hypothesis under no-failure conditions is correct). The residuals under failed conditions would exhibit biases or amplitude increases. The FDI system may also have to distinguish between different failure modes which would require techniques such as multiple hypotheses or likelihood function or ratio formulations to perform adequately. Mehra and Peschon (31) have proposed several different statistical tests to be performed on residuals. One proposed method involves the chi-squared test as utilized by Willsky, Deyst, and Crawford (1974-75) (48;50). This method relies on  $Np$  degrees of freedom, where  $N$  represents the residual "window" length and  $p$  represents the  $p$ -dimensional residual vector. The operation of this approach is based on the chi-squared random variable exceeding some predetermined threshold which has been established by the previously described residual characteristics. The chi-squared variable is the  $(\text{residual}^2 / \text{sigma}^2)$ , where sigma was previously defined by  $HP^{-1}H^T + R$  and

the residual is the difference of the measurement and the filter's estimate. Under the conditions of no uncertainty this value would have a mean value of 1, since the filter's estimated variance would equal the residual squared, on the average. Deficiencies of the N-step window size (e.g., too large or too small a value of N) may result in the non-detection or late-detection of failures due to too large a value of N and on the other hand, too small a value of N may result in a high false alarm rate. Merrill (1972) (30) developed a technique whereby bad sensor data is suppressed. Another technique compares the actual measurement at any point in time to the predicted value of the measurement based on the weighted history of previous data and incorporates this into the algorithm as an additional measurement of the present state. This method, which was researched by Peterson (1975) (30), involves the incorporation of work done with weighted residual tests done by Chow, Dunn, and Willsky (1975) (8) and the previous work of Merrill (30). Another technique which has been explored by such researchers as Willsky, Jones, McAulay, Denlinger, Deyst, Deckert, Sanyal, Shen, Chow, and Dunn (7;8;9;30;42;46), is the use of what is referred to as the generalized likelihood ratio (GLR), which was motivated by the deficiencies of the chi-squared procedure. The GLR method utilizes knowledge of the effects particular failures have on the measurement residual. In general, this method provides an optimum decision rule for

failure detection and provides failure identification information to aid the system reconfiguration after a failure has been detected. This technique utilizes the precomputation of a "failure signature matrix" which provides an explicit description of how various failures propagate through the system. Also, the "time-to-failure", modeled as a random variable, is determined from the maximum likelihood function using the residuals of the measurement process. This variable keeps the detection system open to new data and gives the system's FDI processor time to adjust to dynamic characteristics of the flight. Full implementation of this technique requires a linearly growing bank of matched filters. Simplifications, such as "windowing" the "time-to-failure" random variable, will help eliminate the growing complexity of the detection scheme. Further simplification of the "failure signature matrix" to eliminate transient effects (e.g., develop a steady-state matrix which neglects the time-varying characteristics of the matrix design) and specifying the failure magnitude apriori will reduce the computational burden.

The work of these researchers has highlighted key issues that should be considered when weighing the various detection methods. The most important issues are:

- (1) Types of failure modes that can be detected
- (2) Complexity of implementation

- (3) Performance as measured by false alarms, delays in detection, missed alarms
- (4) Robustness in the face of modeling errors.

Each of the various addressed detection schemes have both advantages and drawbacks which must be measured against the aforementioned criteria.

#### Problem

This thesis will address the issue of performance with respect to the four criteria just listed, for prospective designs of the FDI system of a high performance aircraft operating in a highly dynamic environment.

#### Scope

The investigation of this problem will consist of an analysis of the present FDI technical groupings as previously discussed in this chapter. Computer modeling of the FDI technique or techniques which warrant further consideration will then be addressed.

The computer model to simulate the real world environment consists of a local-level strapdown INS and an external aiding sensor set consisting of a global (satellite) positioning system (GPS), a radar altimeter, a terrain map/correlation system, and Doppler Radar (see Figure 1.1). The INS/external aiding package will then have the FDI modeling package appended for an analysis of the various FDI features.

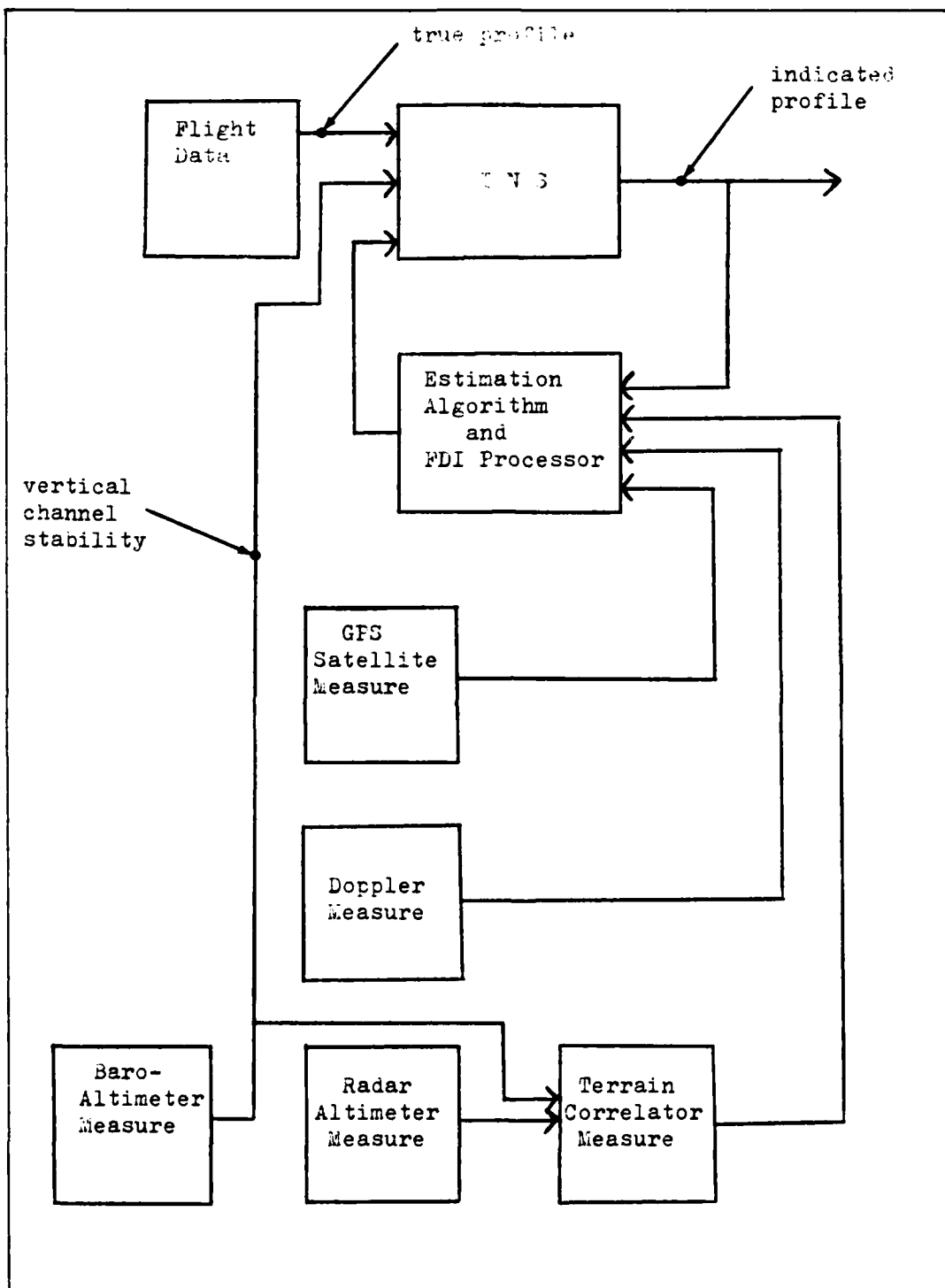


Figure 1.1. Sensor-Aided INS/FDI System

The externally sensor-aided INS/FDI package will then be "flown" against a simulated (computer generated) flight profile which will offer different dynamic features to exercise the FDI system fully and establish its strengths and weaknesses. Further, this will provide a basis for the simulation of various sensor failure/degradations due to the presence of noise/jamming or their own internal failures.

#### Assumptions

The following list of assumptions represent the practical limits which will be placed on the development of this thesis:

1. The modeling of the basic INS will be based on a 35-state error model (1:35) for a dry-tuned strapdown system that maintains navigation information in a local-level coordinate frame.
2. The states associated with the external aiding sensors will be augmented to the basic INS to generate the desired "truth" model.
3. The error analysis will be based on a set of linearized INS/external sensor error equations.
4. The FDI techniques addressed in this thesis represent those that are currently known and documented.
5. The generic modeling information for the sensors and INS to be used is accurate.



6. The information to be derived from available computer simulation program for the flight profile and the filter design program are accurate.

7. Information gathered from published documents represent facts which require no proof.

### Standards

The measure of the performance of the FDI processor will be based on its ability to detect failures/degradations and to report the deficiency in a timely manner. Also, the deficient sensor must be properly identified.

### Approach

The first phase of the thesis will be the generation of a "truth" model for the INS and the sensors. From this model, a Kalman filter package will be developed which will be tuned against the error-state "truth" model to provide an accurate on-board filter representation.

The second phase will be the design of an FDI system. This system will be developed as the result of an in-depth analysis of currently documented FDI techniques. Based on this analysis, a decision will be made as to which technique or techniques will be addressed further. The FDI system will then be combined with the INS/sensor package to provide a satisfactory computer model for the flight test.

The third phase will result in the test of this FDI system with the flight profile simulation. The complete

package will be exercised to simulate various sensor failures/degradations due to excessive measurement noise, jamming, and internal sensor failure.

Performance sensitivity analyses will also be performed. The analyses will focus on the adequacy of the FDI system as a function of the measuring device accuracy. This approach will separate the issues of how FDI performance is affected by measurement inaccuracy from the fundamental performance bound of the FDI system with perfect measurements.

Phase four will be the analysis of post-flight data to establish the performance characteristics of the FDI system. Recommendations and conclusions will then be extracted from this analysis to provide a basis for further research.

#### Outline of Thesis

This thesis is divided into five chapters. Included in Chapter I is an overview of the ATN concept, a discussion of the research in FDI methodology which provides a basis for this thesis, and a discussion of the assumptions and limitations pertaining to the objective of this thesis.

Chapter II includes a description of the "truth" model, a discussion of the simulation philosophy, a description of the simulation software, a definition of the flight profile, a description of the Monte Carlo technique for the simulation and analysis, and a presentation of the simulation results for an unaided INS. The unaided INS results provide credibility

for the truth model since the plots are representative of errors seen in flight testing (45).

Chapter III includes a definition of the reduced error model used in the filter, the filter time propagation and update equations, and the presentation of aided INS simulation results under no-failure conditions.

Chapter IV presents the currently documented FDI methodologies and a decision as to which techniques will be incorporated into the FDI system. A failure mode analysis will be included in this chapter. Also included in this chapter are the simulation results for this FDI system.

Chapter V presents an analysis of the FDI system based on its performance with the INS/sensor package. The performance measure will be based on the comparison of the time and type of failure/degradation and the system's ability to identify the failed sensor. Finally, conclusions and recommendations will be set forth to provide a basis for the next step in establishing the benchmark for an ATN system.

## II. The System Truth Model

### The Truth Model

A "truth model" is what the system designer perceives to be the best description of the real world behavior of the system. This particular system consists of the basic INS, a baro-altimeter, a satellite-positioning system, a terrain correlation system, and Doppler radar. In this section, a 52-state system error model is developed in the form of a linear stochastic vector differential equation as shown in Eq(2-1).

$$\dot{\underline{x}}(t) = \underline{F} \underline{x}(t) + \underline{G}(t) \underline{w}(t) \quad (2-1)$$

where:

$\underline{x}(t)$  is the 52-dimensional state vector

$\underline{F}(t)$  is the (52 x 52) fundamental matrix

$\underline{w}(t)$  is a (15 x 1) vector of white noise forcing functions, and

$\underline{G}(t)$  is a (52 x 15) input matrix

Eq(2-1) represents a set of 52 first-order linear differential equations which model the errors and error sources in the externally-aided INS.

The INS which is modeled in this thesis is an 0.8 nautical mile per hour (NM/HR), local-level, strapdown system. It is designed to be representative of medium

accuracy INSs currently developed for tactical aircraft. Gyroscopes and accelerometers are mounted on a navigation base or platform that is directly attached to the vehicle. No gimbals isolate the instruments from the angular velocity of the vehicle. To keep track of accelerometer orientation, gyros or other rate sensors are used to measure the angular velocity of the vehicle in inertial space. Transformation from platform to geographic ("navigation") coordinates is handled by maintaining the current solution for the direction cosine matrix differential equation (45:72):

$$\dot{C}_p^N = C_p^N \Omega_{ip}^p - \Omega_{in}^N C_p^N \quad (2-2)$$

where:

$\Omega_{ip}^p$  is a skew symmetric matrix of angular velocity of the platform (in platform coordinates as measured by rate gyros).

$\Omega_{in}^N$  is the skew-symmetric matrix form of the angular velocity of the ("navigation") local-level frame in inertial space, and  $C_p^N$  is the direction cosine transformation matrix from the platform to the navigation frame.

A barometric altimeter is used to aid the INS by controlling the unstable INS errors in the vertical channel. The INS has a position growth error of approximately 0.8 NM/hr RMS due to Schuler effects, instrument errors (input axis misalignments, instrument biases, drifts, and scale factor errors), and environmental errors (gravity uncertainties and pressure variations).

The following equations represent the mechanization equations that are in the INS computer to determine velocity and position (45:10-17):

$$\dot{\lambda} = V_e / (R_\lambda + h) \cos L \quad (2-3)$$

$$\dot{L} = V_N / (R_L + h) \quad (2-4)$$

$$\dot{h} = V_z - K_1 (h - h_{ref}) \quad (2-5)$$

$$\dot{V}_x = f_x + g_x - (w_y - \Omega_y) V_z + (w_z + \Omega_z) V_y \quad (2-6)$$

$$\dot{V}_y = f_y + g_y - (w_z + \Omega_z) V_x + w_x V_z \quad (2-7)$$

$$\begin{aligned} \dot{V}_z = f_z + g_z - w_x V_y + (w_y + \Omega_y) V_x \\ - K_2 (h - h_{ref}) - \delta \hat{a} \end{aligned} \quad (2-8)$$

$$V_e = V_x \cos \alpha - V_y \sin \alpha \quad (2-9)$$

$$V_n = V_x \sin \alpha + V_y \cos \alpha \quad (2-10)$$

$$\dot{\alpha} = -V_e \tan L / R \quad (2-11)$$

$$\delta \hat{a} = K_3 (h - h_{ref}) \quad (2-12)$$

where,

$\lambda$  = longitude

$L$  = geographic latitude

$h$  = INS indicated altitude

$V_x, V_y, V_z$  = velocity in wander azimuth frame

$V_e, V_n$  = east and north velocities

$\alpha$  = wander azimuth angle: (angle between local-level axes and wander azimuth horizontal axes):  
 $\alpha$  is the clockwise rotation of X,Y,Z from E,N,U about the vertical axis

$\delta \hat{a}$  = best estimate of acceleration error due to accelerometer and gravity errors based on altimeter input

$f_{x,y,z}$  = specific forces in wander azimuth frame

$g_{x,y,z}$  = gravity components in wander azimuth frame

$h_{ref}$  = baro-altimeter indicated altitude (see truth state 35)

$K_1, K_2, K_3$  = damping loop gains of vertical channel third-order damping of INS vertical channel with baro-altimeter)

$\Omega_{y,z}$  = components of earth angular velocity in wander azimuth frame (x is orthogonal to  $\Omega$  )

$R_{\lambda,L}$  = east-west/north-south radius of curvature of the earth reference ellipsoid (9)

$w_{x,y,z}$  = angular velocity of wander azimuth frame with respect to inertial space.

These equations could then be reproduced in computer software to compute position and velocity in the wander azimuth frame. From these equations, the following basic INS error equations are derived wrt the east, north, up (ENU) frame. By fixing alpha ( $\alpha$ ) in Eqs (2-9) and (2-10) to -90 degrees referenced from north, the following solutions are found:

$$V_e = V_x \quad (2-13)$$

$$V_N = V_y \quad (2-14)$$

These solutions can then be substituted into Eqs (2-3) thru (2-8) and the appropriate attitude error equations (45:26) to

produce the following results:

$$\dot{\delta\lambda} = (p_z/\cos L) \delta L - (p_N/R \cos L) \delta h + \delta V_e/R \cos L \quad (2-15)$$

$$\dot{\delta L} = (p_e/R) \delta h + \delta V_N/R \quad (2-16)$$

$$\dot{\delta h} = \delta V_z - K_1 \delta h \quad (2-17)$$

$$\begin{aligned} \dot{\delta V_e} = & (2(\Omega_n V_n + \Omega_z V_z) + p_n V_n \cos^2 L) \delta L \\ & + (p_n p_e + p_n K_z) \delta h - (p_e \tan L + K_z) \delta V_e \\ & + (w_z + \Omega_z) V_n - (w_n + \Omega_n) \delta V_z + \delta f_e + \delta g_e \end{aligned} \quad (2-18)$$

$$\begin{aligned} \dot{\delta V_n} = & -(2\Omega_n V_e + p_n V_e \cos^2 L) \delta L \\ & + (p_n p_z - p_e K_z) \delta h - 2w_z \delta V_e - K_z \delta V_n \\ & + p_e \delta V_z + \delta f_n + \delta g_n \end{aligned} \quad (2-19)$$

$$\begin{aligned} \dot{\delta V_z} = & -2\Omega_z V_e \delta L - p_n^2 + p_e^2) \delta h \\ & + 2w_n \delta V_e - 2p_e \delta V_n + \delta f_z + \delta g_z - K_2 \delta h \end{aligned} \quad (2-20)$$

$$\dot{\epsilon_e} = (-p_e/R) \delta h - \delta V_n/R + w_z \epsilon_n - w_n \epsilon_z + \delta w_e \quad (2-21)$$

$$\dot{\epsilon_n} = -\Omega_z \delta L - (p_n/R) \delta h + \delta V_e/R - w_z \epsilon_e + w_e \epsilon_z + \delta w_n \quad (2-22)$$

$$\begin{aligned} \dot{\epsilon_z} = & (w_n + p_n \tan L) - (p_z/R) \delta h \\ & + (\tan L/R) \delta V_e + w_n \epsilon_e + \delta w_z \end{aligned} \quad (2-23)$$

$$\dot{\delta \hat{a}} = K_3 \delta h = K_3 (h - h_{ref}) \quad (2-24)$$



where:

$\epsilon_{e,n,z}$  = platform misalignment angles (see (45:193-195) for an explanation of transformation to E-N-U frame)

$\delta f_{e,n,z}$  = accelerometer errors, as transformed to E-N-U frame (gravity knowledge errors are not explicitly modeled)

$\delta w_{e,n,z}$  = gyroscope errors, as transformed into ENU frame

$P_{e,n,z}$  = angular velocity of ENU frame w.r.t. earth (45:12)

$\delta h$  = altitude errors, where  $h$  and  $h_{ref}$  were previously defined.

Other errors and their equations are gyroscope errors, gravity uncertainties, baro-altimeter errors, satellite positioning system receiver errors, terrain correlation errors, radar altimeter errors, and Doppler radar errors. Components of these errors are modeled as random constants, random walks, and first-order Markov processes.

A random constant is modeled as the output of an integrator with zero input and a (Gaussian) random initial condition which has a zero mean and a variance,  $P$ . This type of model is suitable for describing an instrument bias that changes each time the device is turned on, but remains constant while it is on.

A random walk is the output of an integrator driven by zero-mean, white, Gaussian noise. The defining equations are given below:

$$\dot{x}(t) = w(t), \quad x(t_0) = 0 \quad (2-25)$$

$$E(w(t)) = 0 \quad (2-26)$$

$$E [w(t) w(t + \tau)] = Q \delta(\tau) \quad (2-27)$$

$$E [x^2(t)] = Q(t - t_0) \quad (2-28)$$

where  $Q$  is the strength of the white Gaussian noise and  $\delta(\tau)$  is the Dirac delta function. The random walk is suitable for describing errors that grow without bound or are slowly varying (a pseudonoise driver addition to a random constant integrator model).

A first-order Markov process is the output of a first-order lag driven by a zero-mean, white, Gaussian noise of strength,  $Q$ . The model is described by the following equations:

$$\dot{x}(t) = (-1/T) x(t) + w(t) \quad (2-29)$$

$$E [x(t)^2] = Q T/2 \quad (2-30)$$

where:

$$Q = 2\sigma^2/T \quad (2-31)$$

$$\sigma = (E [x(t)^2])^{1/2} \quad (2-32)$$

$T$  = correlation time

A first-order Markov model is used to represent the exponentially time-correlated noises. The autocorrelation kernel function for this process is (24:178):

$$E [x(t) x(t + \tau)] = \sigma^2 e^{-|\tau|/T} \quad (2-33)$$

where,

$\sigma$  and  $T$  are defined above

$\tau$  = time interval

All modeled errors are assumed to be independent (45:20)  
with initial covariances described by:

$$P_{ij}(0) = 0, i \neq j \quad (2-34)$$

$$P_{ii}(0) = x_i^2 \quad (2-35)$$

where  $x_i$  is the initial condition on the standard deviation of the  $i^{\text{th}}$  truth state at time  $t_0$ .

The gyroscope errors (45:75-101;9) are gyro drift (g-insensitive, g-sensitive and  $g^2$ -sensitive), scale factor errors, and input axis misalignments.

G-insensitive gyro drift exhibits growth in time. It is modeled by a random walk for each gyro and is one of the most significant error sources for the INS. G-sensitive drift produces a gyro output drift which is proportional to the specific force and is applied to each gyroscope. The g-sensitive drift is modeled by a random constant coefficient which is multiplied by the appropriate component of actual specific force.  $G^2$ -sensitive gyro drifts are the result of anisoelastic torques and are also modeled by random constants and coefficients which are then multiplied by products of two appropriate components of true specific force. For the purposes of this research, gyro drift will be modeled as a random constant and a random walk to account for the gyro

drift errors; i.e. g-sensitive and  $g^2$ -sensitive components are not explicitly modeled.

Gyro scale factor errors and misalignment are the result of the error occurring from the measured voltage being translated to a torque reading and installation errors. The scale factor error is modeled as a random constant. The six misalignment angles are due to the three gyros being displaced into directions about the rotational axis.

The gyro drift model is shown in the following equations (one equation for each platform axis):

$$\epsilon_x = DX_f + w_{icy} XG_y + w_{icz} XG_z + w_{icx} GSF_x \quad (2-36)$$

$$\epsilon_y = DY_f + w_{icx} YG_x + w_{icz} YG_z + w_{icy} GSF_y \quad (2-37)$$

$$\epsilon_z = DZ_f + w_{icx} ZG_x + w_{icy} ZG_y + w_{icz} GSF_z \quad (2-38)$$

where,

$\epsilon_{x,y,z}$  = total error along x,y,z axes

$DX_f, DY_f, DZ_f$  = gyro drift rate bias error (see Table I)

$w_{icx,y,z}$  = computer frame angular rate w.r.t. inertial space

$X,Y,ZG_{x,y,z}$  = gyro input axis misalignment (see Table I)

$GSF_{x,y,z}$  = gyro scale factor errors

Fig. 2.1 represents the typical model for gyro errors in the X-sensitive direction.

Accelerometer errors (45:105-118;9) are modeled as input axis misalignment, scale factor error, and biases.

There are six accelerometer misalignment angles which follow the same argument as gyro misalignment. Each misalignment angle is modeled as a random constant. Accelerometer biases induce a constant force measurement error and are adequately modeled by random walks. Scale factor errors are the result of translating voltage to specific force readings and each is modeled as a random constant since the scale factor is assumed linear over the operating range of the accelerometer.

The total accelerometer error model is shown in the equations below:

$$\delta A_x = AB_x + f_x ASF_x + f_y XA_y + f_z XA_z \quad (2-39)$$

$$\delta A_y = AB_y + f_y ASF_y + f_x YA_x + f_z YA_z \quad (2-40)$$

$$\delta A_z = AB_z + f_z ASF_z + f_x ZA_x + f_y ZA_y \quad (2-41)$$

where:

$\delta A_{x,y,z}$  = total error in x,y,z direction

$AB_{x,y,z}$  = accelerometer bias error (see Table I)

$f_{x,y,z}$  = specific force in x,y,z direction

$ASF_{x,y,z}$  = accelerometer scale factor error (see Table I)

$X,Y,ZA_{x,y,z}$  = accelerometer misalignment error (see Table I)

The total error model for x axis accelerometer errors is shown in Fig. 2.2.

Gravity errors are not explicitly modeled. The gravity errors are typically generated by using a reference ellipsoid

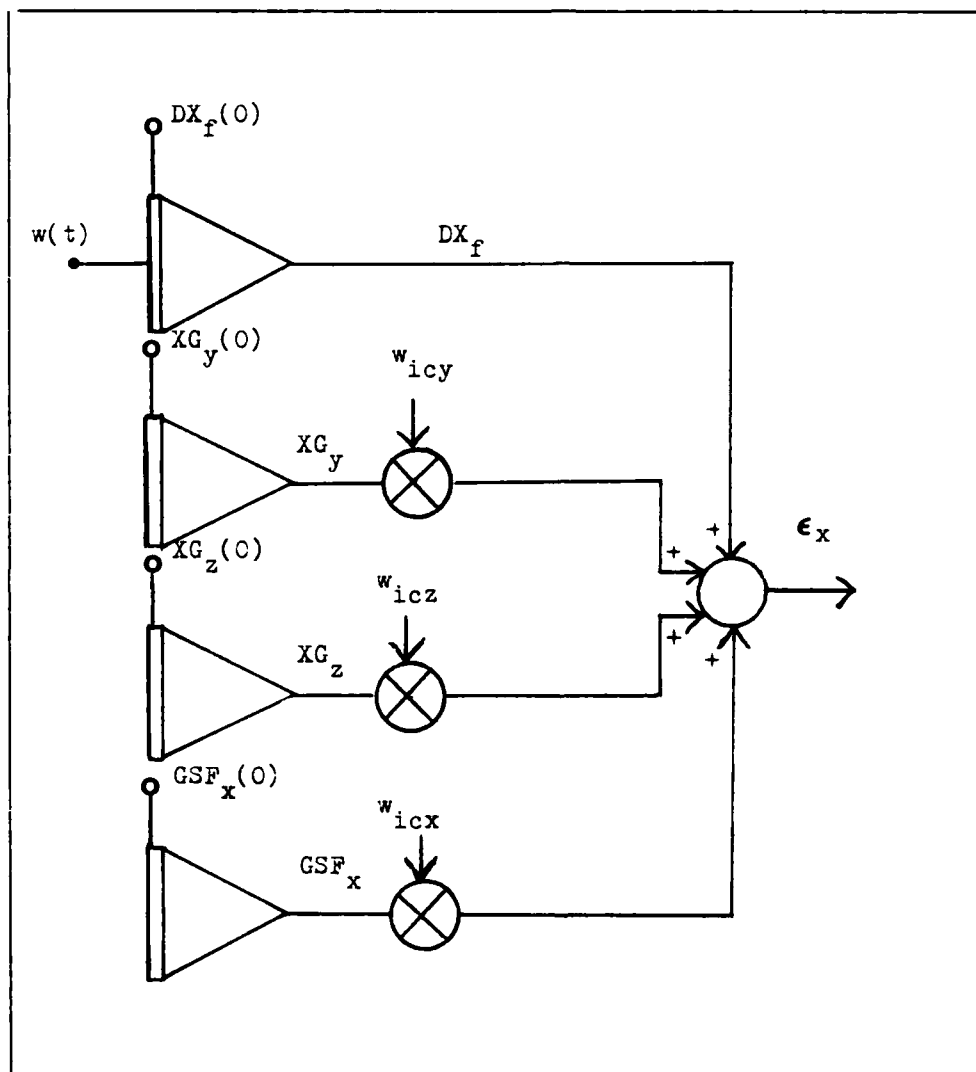


Fig. 2.1. X-Sensitive Gyro Error Model

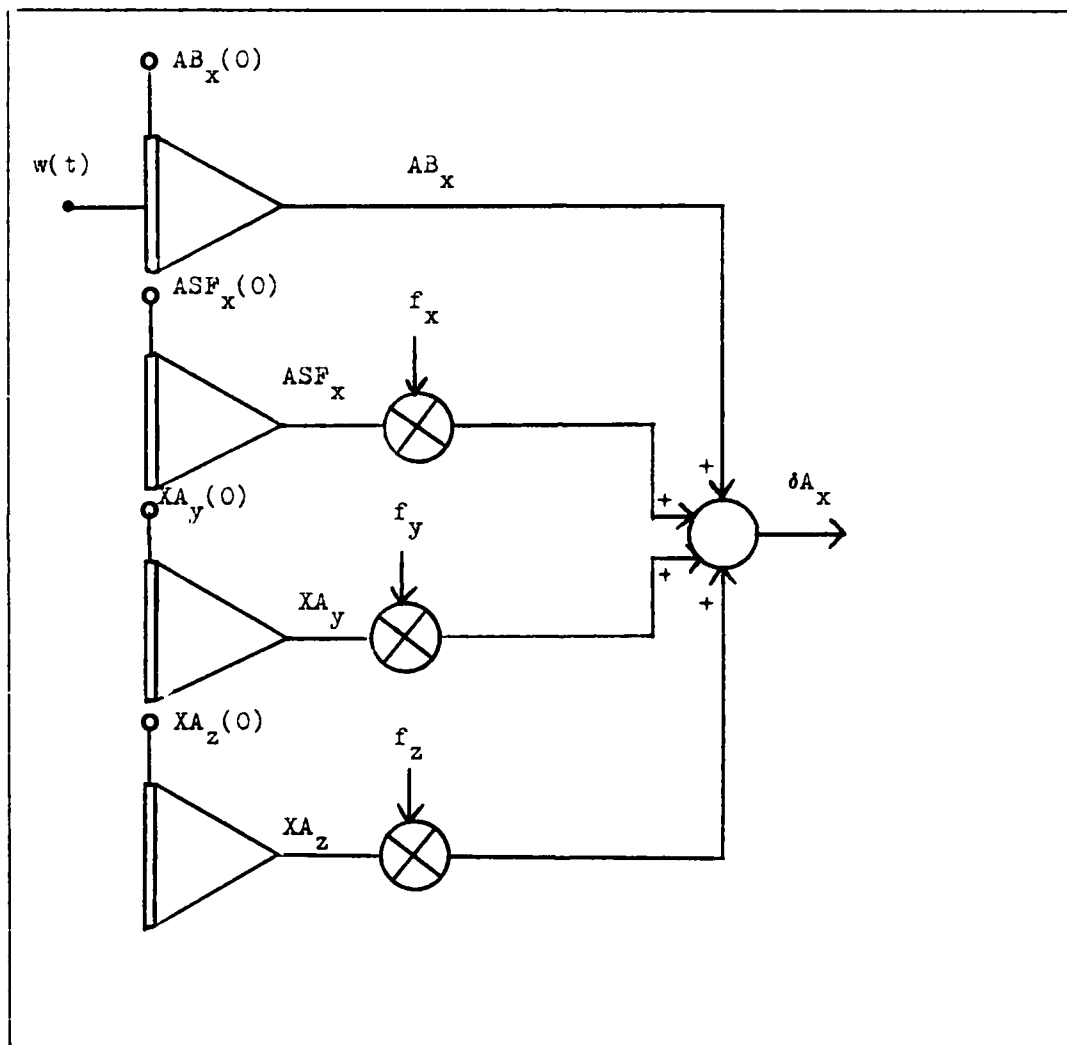


Fig. 2.2. Accelerometer Error Model For X Axis

for the specific force computations. This modeling fails to account for the geoidal local variations which produce an acceleration error in the three axes. Gravity modeling requires modeling these local variations and correcting acceleration error for the gravity modeling error. This error does not represent a serious correction until one is interested in generating a .25 NM/hr or better INS. For this reason, gravity errors are not modeled for this research.

Baro altimeter error (15:3-46) is represented as a single state model which accounts for calibration and reference bias, weather variations, and static pressure error changes with airspeed. This bias model is modeled as a first-order Markov process to account for isobaric variations which have constant correlation distances and thus much lower correlation times for high-performance aircraft, letting the "correlation time" be the correlation distance divided by vehicle velocity.

The barometric-altimeter error model is shown in the equation below:

$$\dot{e}_{po} = (-V_g/D_{alts}) e_{po} + w(t) \quad (2-42)$$

where,

$e_{po}$  is the error due to variation in altitude of a constant pressure surface

$V_g$  is the ground velocity of the aircraft

$D_{alts}$  is the correlation distance

$w(t)$  is the white noise driving process



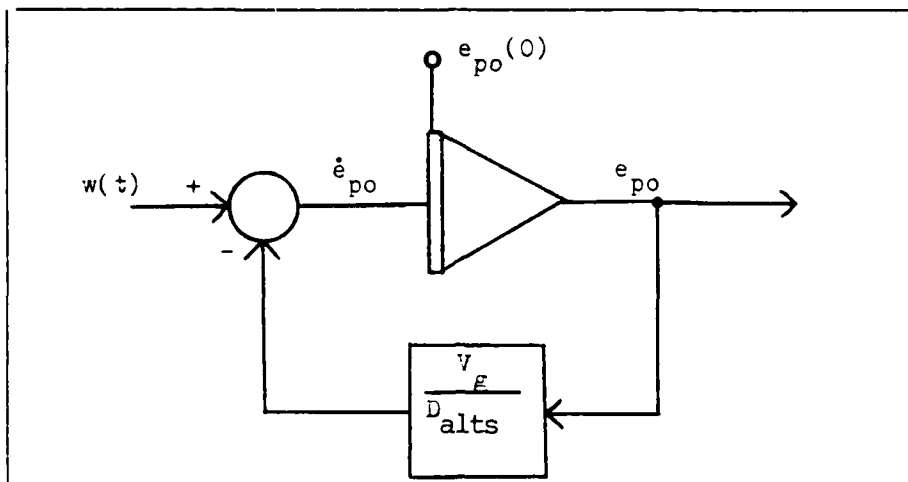


Fig. 2.3. Baro-Altimeter Error Model

The GPS satellite positioning system is modeled under the assumptions that the satellite clocks are synchronized (and periodically updated from ground stations) and operate with negligible error, and transmissions are accurate. With these assumptions, satellite positioning errors can be attributed to the user receiver clock alone. The clock error is the sum of four processes (15:C-9-15); initial phase error accounts for the actual difference between the user clock and the master clock; initial frequency offset errors refer to the difference in frequency between the user and master clock immediately after synchronization; long term stability errors are used to account for crystal aging; random errors account for short-term stability errors, temperature variations, and vibration-induced errors.

The clock errors are established along three orthogonal axes such that no clock errors are shared between any two axes, i.e., such that error ellipsoids are perfectly spherical (this implies a particularly convenient orientation of the satellites w.r.t. the navigation frame and it is assumed that satellite selection algorithms will produce results similar to this performance). Since clock errors are established in both phase (position) and frequency (velocity), these errors will be used to correct INS errors in both position and velocity. The measurement model takes both position and velocity measurements.

The satellite positioning system error model is shown in the equation below:

$$\dot{\delta t}_u = \dot{\delta t}_{bu} + \dot{\delta t}_{ru} + w_1(t) \quad (2-43)$$

where,

$\delta t_u$  is the total phase (position) error

$\dot{\delta t}_{bu}$  is the frequency bias

$\dot{\delta t}_{ru}$  is the random frequency error (modeled as first-order Markov)

$w_1(t)$  is the white noise process.

Doppler radar is modeled to compensate for errors in beam direction, temperature, installation alignment, INS attitude, tracker time constant, surface motion, and beamwidth (15:3-32-40). Under the assumption that Doppler errors are dominated by alignment/pitch calibration errors

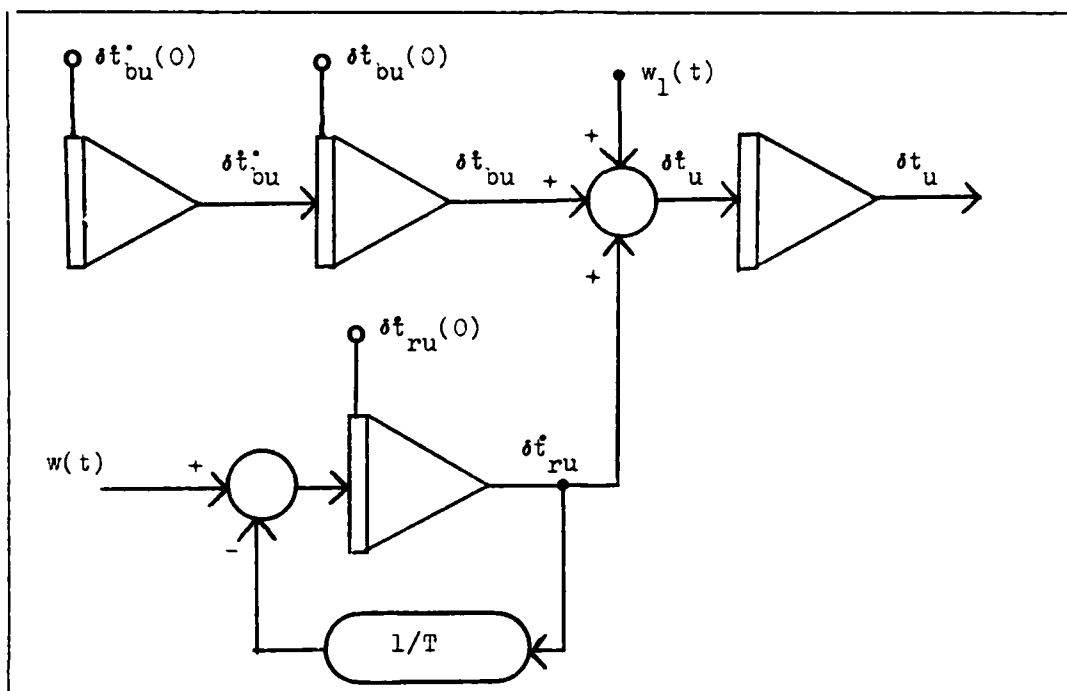


Fig. 2.4. User Clock Error Model

and scale factor errors, these errors will be explicitly represented in the "truth" model (15:3-40-42). This simplification is also possible due to the restriction to overland flight which eliminates the surface motion errors. The alignment/pitch calibration errors will be modeled as random constants, and the scale factor errors will be modeled as first-order Markov processes (15:3-35-37).

The Doppler radar error model is shown in the following equations:

$$\delta V_{D_\lambda} = V_\lambda b_\lambda + \delta V_{S_\lambda} \quad (2-44)$$

$$\delta V_{Du} = V_u b_u + \delta V_{su} \quad (2-45)$$

$$\delta V_{Dh} = V_h b_h + \delta V_{sh} \quad (2-46)$$

where,

$\delta V_D$  is the total Doppler velocity error

$V$  is the along-track, cross-track, and vertical velocity

$\delta V_s$  is the scale factor error

Radar altimeter errors are typically modeled as two errors (15:3-46-47). The largest errors in using this as an altitude reference are the zero offset and scale factor. Both of these errors are modeled as random constants. This model does not account for terrain variation effects since no actual data for ground characteristics are available.

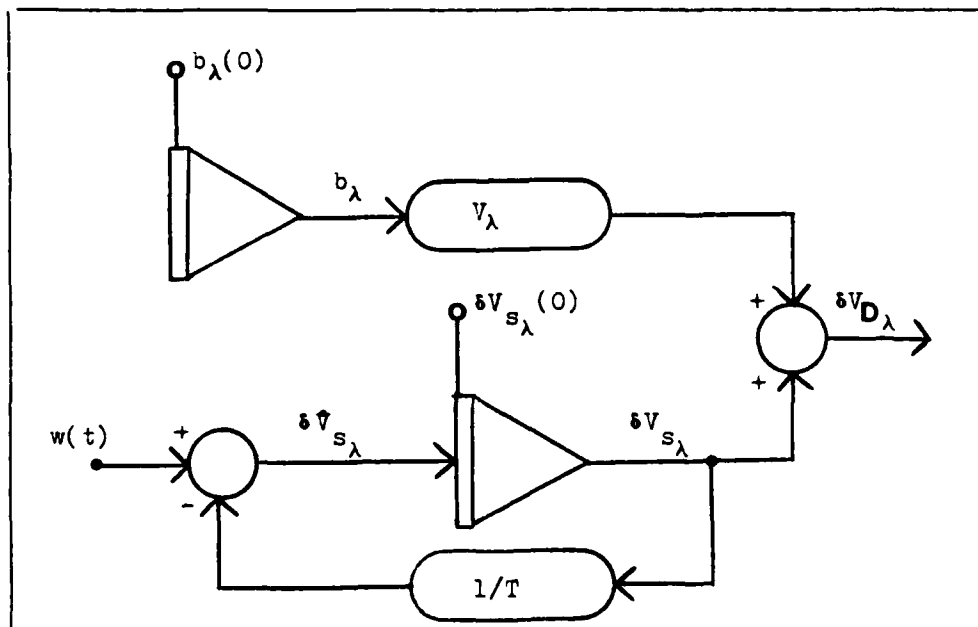


Fig. 2.5. Doppler Radar Error Model  
For Along-Track Error

The flight profile tape does not provide any knowledge of terrain characteristics such as altitude-above-sea-level, slopes, tree-covered, rocky, etc.

The radar altimeter error model is described by the following equation:

$$\delta h_{RA} = \gamma h_{gn} + \delta h_{zo} \quad (2-47)$$

where,

$\delta h_{ra}$  is the total radar altimeter error

$\gamma$  is the scale factor error

$h_{gn}$  is the aircraft altitude above ground

$\delta h_{zo}$  is the zero offset error

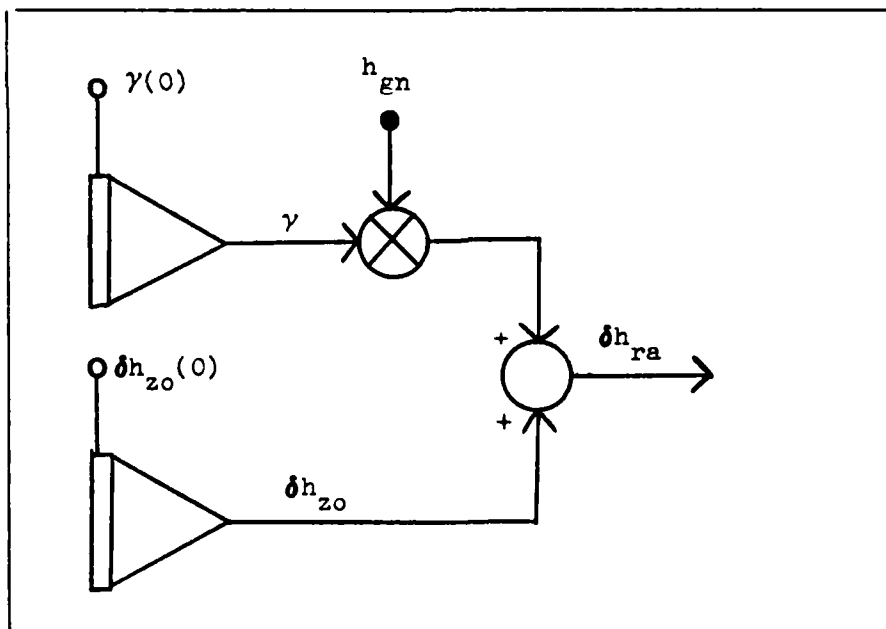


Fig. 2.6. Radar Altimeter Error Model

Terrain correlator errors can be modeled as map errors. These errors are modeled with a 5-state "shaping filter". Three states account for errors in north, east and vertical. The other two states are north and east velocity errors. The velocity errors are modeled as random constants with pseudonoise addition. The positional errors for horizontal are driven by the velocity states with a random constant. The vertical position error is modeled as a random constant and a pseudonoise.

The terrain correlation system is modeled by the following equation:

$$\dot{\delta \underline{P}} = \delta \underline{V} + \underline{w}(t) \quad (2-48)$$

$$\dot{\delta A} = w_z(t) \quad (2-49)$$

where,

$\delta \underline{P}$  represents the east and north position errors

$\delta \underline{V}$  represents the east and north velocity errors

$\underline{w}(t)$  is a white noise process for east and north velocity.

$\delta A$  is the vertical position error

$w_z(t)$  is the vertical white noise process

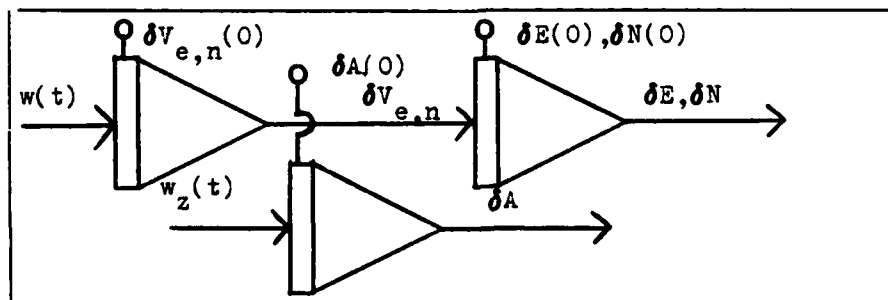


Fig. 2.7. Terrain Correlation Error Model

The 52-state variables are summarized with their initial conditions in Table I. The Fundamental Matrix,  $F(t)$ , is represented by Figures 2.1 - 2.5. A list of error source initial values and statistics is shown in Table III. The initial conditions are representative of a medium-grade strapdown INS.

Table I  
Error Model State Variables

| State Variable                                   | Initial Condition<br>(Standard Deviation) |
|--|---|
| <u>Basic Inertial Navigation Errors</u>          |   |
| 1. $\lambda$ east longitude error                | .05 arc min                               |
| 2. $\delta L$ north latitude error               | .05 arc min                               |
| 3. $\delta h$ altitude error                     | 30 ft                                     |
| 4. $\delta V_e$ east velocity error              | .1 ft/sec                                 |
| 5. $\delta V_n$ north velocity error             | .1 ft/sec                                 |
| 6. $\delta V_z$ vertical velocity error          | .1 ft/sec                                 |
| 7. $\epsilon_e$ east attitude error              | .05 arc min                               |
| 8. $\epsilon_n$ north attitude error             | .05 arc min                               |
| 9. $\epsilon_z$ vertical attitude error          | .4 arc min                                |
| <u>Vertical Channel Error Variable</u>           |   |
| 10. $\delta \hat{a}$ vertical acceleration error | .006 ft/sec <sup>2</sup>                  |

Table I. (cont'd)

| State Variable  | Initial Condition<br>(Standard Deviation) |
|---|---|
| <u>Gyro Drift</u>   |   |
| NOTE: This drift is an approximation to account for g-insensitive, g-sensitive and $g^2$ -sensitive errors. |   |
| 11. $DX_f$ x gyro drift   | .008°/hr                                  |
| 12. $DY_f$ y gyro drift   | .008°/hr                                  |
| 13. $DZ_f$ z gyro drift   | .008°/hr                                  |
| <u>Gyro Scale Factor Error</u>  |   |
| 14. $GSF_x$ X gyro scale factor   | 2 ppm                                     |
| 15. $GSF_y$ Y gyro scale factor   | 2 ppm                                     |
| 16. $GSF_z$ Z gyro scale factor   | 2 ppm                                     |
| <u>Gyro Input Axis Misalignment</u>   |   |
| 17. $XG_y$ X gyro about Y   | 5 arc sec                                 |
| 18. $XG_z$ X gyro about Z   | 5 arc sec                                 |
| 19. $YG_x$ Y gyro about X   | 5 arc sec                                 |
| 20. $YG_z$ Y gyro about Z   | 5 arc sec                                 |
| 21. $ZG_x$ Z gyro about X   | 5 arc sec                                 |
| 22. $ZG_y$ Z gyro about Y   | 5 arc sec                                 |
| <u>Accelerometer Biases</u>   |   |
| 23. $AB_x$ X accelerometer bias   | 40 $\mu$ g                                |
| 24. $AB_y$ Y accelerometer bias   | 40 $\mu$ g                                |



Table I. (cont'd)

| State Variable   |   | Initial Condition<br>(Standard Deviation)             |
|--|---|---|
| 25. AB <sub>z</sub>  | Z accelerometer bias  | 40 μg   |
| <u>Accelerometer Scale Factor Error</u>                                |   |   |
| 26. ASF <sub>x</sub>   | X accel scale factor  | 60 ppm  |
| 27. ASF <sub>y</sub>   | Y accel scale factor  | 60 ppm  |
| 28. ASF <sub>z</sub>   | Z accel scale factor  | 60 ppm  |
| <u>Gravity Uncertainties</u>   |   |   |
| NOTE: Gravity uncertainties are not modeled due to medium accuracy INS |   |   |
| <u>Accelerometer Input Axis Misalignment</u>                           |   | NOTE: X,Y,Z are for platform not wander azimuth frame |
| 29. XA <sub>y</sub>  | X accel about Y   |   |
| 30. XA <sub>z</sub>  | X accel about Z   |   |
| 31. YA <sub>x</sub>  | Y accel about X   |   |
| 32. YA <sub>z</sub>  | Y accel about Z   |   |
| 33. ZA <sub>x</sub>  | Z accel about X   |   |
| 34. ZA <sub>y</sub>  | Z accel about Y   |   |
| <u>Barometer Altimeter Error</u>                                       |   |   |
| 35. e <sub>po</sub>  | error due to variation in altitude of a constant pressure surface | 500 ft  |

Table I. (cont'd)

| State Variable                            |                           | Initial Conditions<br>(Standard Deviation) |
|---|---------------------------|--|
| <u>Satellite Positioning System Error</u> |                           |  |
| 36. $\delta t_u$                          | clock phase bias          | 1000 ft                                    |
| 37. $\dot{\delta t}_u$                    | clock frequency error     | 1 ft/sec                                   |
| 38. $\ddot{\delta t}_u$                   | clock aging bias          | $2 \times 10^{-7}$ ft/sec <sup>2</sup>     |
| 39. $\delta t_{Ru}$                       | clock frequency bias      | 10 ft/sec                                  |
| <u>Doppler Radar System Errors</u>        |                           |  |
| 40. $\delta B_\mu$                        | longitudinal beam error   | 2 arc min                                  |
| 41. $\delta B_\lambda$                    | latitude beam error       | 2 arc min                                  |
| 42. $\delta B_h$                          | vertical beam error       | 2 arc min                                  |
| 43. $\delta V_{s\mu}$                     | along-track scale factor  | .3 ft/sec                                  |
| 44. $\delta V_{s\lambda}$                 | across-track scale factor | .3 ft/sec                                  |
| 45. $\delta V_{sh}$                       | vertical scale factor     | .3 ft/sec                                  |
| <u>Radar Altimeter System Error</u>       |                           |  |
| 46. $\delta h_{zo}$                       | zero offset error         | 2 ft                                       |
| 47. $\delta \gamma$                       | scale factor              | .025                                       |
| <u>Terrain Correlation Errors</u>         |                           |  |
| 48. $\delta E$                            | easting map error         | 320 ft                                     |
| 49. $\delta N$                            | northing map error        | 320 ft                                     |
| 50. $\delta A$                            | vertical map error        | 98 ft                                      |
| 51. $\delta V_e$                          | east velocity error       | 2 ft/sec                                   |
| 52. $\delta V_n$                          | north velocity error      | 2 ft/sec                                   |

| 1-35                 | 36-39                | 40-47           | 48-50           | 51-55                |
|----------------------|----------------------|-----------------|-----------------|----------------------|
| $\underline{E}_{11}$ | $\underline{0}$      | $\underline{0}$ | $\underline{0}$ | $\underline{0}$      |
| $\underline{0}$      | $\underline{E}_{22}$ | $\underline{0}$ | $\underline{0}$ | $\underline{0}$      |
| $\underline{0}$      | $\underline{E}_{33}$ | $\underline{0}$ | $\underline{0}$ | $\underline{0}$      |
| $\underline{0}$      | $\underline{0}$      | $\underline{0}$ | $\underline{0}$ | $\underline{0}$      |
| $\underline{0}$      | $\underline{0}$      | $\underline{0}$ | $\underline{0}$ | $\underline{E}_{44}$ |

Fig. 2.8. Fundamental Matrix

```

XDOT (1) = F9x9 (1)*XS(2)+F9x9 (7)*XS(3)+F9x9(16)*XS(4)
XDOT (2) = F9x9 (8)*XS(3)+F9x9(22)*XS(5)
XDOT (3) = F9x9 (9)*XS(3)+XS(6)+CK1*XS(35)
XDOT (4) = F9x9 (2)*XS(2)+F9x9(10)*XS(3)+F9x9(17)*XS(4)
          +F9x9(23)*XS(5)+F9x9(28)*XS(6)+F9x9(34)*XS(8)
          +F9x9(38)*XS(9)
          +CNP(1)*XS(23)+CNP(4)*XS(24)+CNP(7)*XS(25)
          +CNP(1)*FX*XS(26)+CNP(4)*FY*XS(27)+CNP(7)*FZ*XS(28)
          -CNP(1)*FZ*XS(29)+CNP(1)*FY*XS(30)+CNP(4)*FZ*XS(31)
          -CNP(4)*FX*XS(32)-CNP(7)*FY*XS(33)+CNP(7)*FX*XS(34)
XDOT (5) = F9x9 (3)*XS(2)+F9x9(11)*XS(3)+F9x9(18)*XS(4)
          +F9x9(24)*XS(5)+F9x9(29)*XS(6)+F9x9(30)*XS(7)
          +F9x9(39)*XS(9)
          +CNP(2)*XS(23)+CNP(5)*XS(24)+CNP(8)*XS(25)
          +CNP(2)*FX*XS(26)+CNP(5)*FY*XS(27)+CNP(8)*FZ*XS(28)
          -CNP(2)*FZ*XS(29)+CNP(2)*FY*XS(30)+CNP(5)*FZ*XS(31)
          -CNP(5)*FX*XS(32)-CNP(8)*FY*XS(33)+CNP(8)*FX*XS(34)
XDOT (6) = F9x9 (4)*XS(2)+F9x9(12)*XS(3)+F9x9(19)*XS(4)
          +F9x9(25)*XS(5)+F9x9(31)*XS(7)+F9x9(35)*XS(8)-XS(10)
          +CNP(3)*XS(23)+CNP(6)*XS(24)+CNP(9)*XS(25)
          +CNP(3)*FX*XS(26)+CNP(6)*FY*XS(27)+CNP(9)*FZ*XS(28)
          -CNP(3)*FZ*XS(29)+CNP(3)*FY*XS(30)+CNP(6)*FZ*XS(31)
          -CNP(6)*FX*XS(32)-CNP(9)*FY*XS(33)+CNP(9)*FX*XS(34)
          +CK2*XS(35)
XDOT (7) = F9x9(13)*XS(3)+F9x9(26)*XS(5)+F9x9(36)*XS(8)
          +F9x9(40)*XS(9)
          +CNP(1)*XS(11)+CNP(4)*XS(12)+CNP(7)*XS(13)
          +CNP(1)*WCX*XS(14)+CNP(4)*WCY*XS(15)+CNP(7)*WCZ*XS(16)
          +CNP(1)*WCZ*XS(17)-CNP(1)*WCY*XS(18)-CNP(4)*WCZ*XS(19)
          +CNP(4)*WCX*XS(20)+CNP(7)*WCY*XS(21)+CNP(7)*WCX*XS(22)
XDOT (8) = F9x9 (5)*XS(2)+F9x9(14)*XS(3)+F9x9(20)*XS(4)
          +F9x9(32)*XS(7)+F9x9(41)*XS(9)
          +CNP(2)*XS(11)+CNP(5)*XS(12)+CNP(8)*XS(13)
          +CNP(2)*WCX*XS(14)+CNP(5)*WCY*XS(15)+CNP(8)*WCZ*XS(16)
          +CNP(2)*WCZ*XS(17)-CNP(2)*WCY*XS(18)-CNP(5)*WCZ*XS(19)
          +CNP(5)*WCX*XS(20)+CNP(8)*WCY*XS(21)-CNP(8)*WCX*XS(22)
XDOT (9) = F9x9(6)*XS(2)+F9x9(15)*XS(3)+F9x9(21)*XS(4)
          +F9x9(33)*XS(7)+F9x9(37)*XS(8)
          +CNP(3)*XS(11)+CNP(6)*XS(12)+CNP(9)*XS(13)
          +CNP(3)*WCX*XS(14)+CNP(6)*WCY*XS(15)+CNP(9)*WCZ*XS(16)
          +CNP(3)*WCZ*XS(17)-CNP(3)*WCY*XS(18)-CNP(6)*WCZ*XS(19)
          +CNP(6)*WCX*XS(20)+CNP(9)*WCY*XS(21)-CNP(9)*WCX*XS(22)
XDOT (10) = CK3*XS(3)-CK3*XS(35)
XDOT (11) thru XDOT (34) = 0
XDOT (35) = (-Vg/Dalts) XS(35)

```

Fig 2.9. F<sub>11</sub> Partition 35 x 35 of Fundamental Matrix

Table II

Notation Used in Figure 2.9

|  |  |
|--|--|
| $F_{9 \times 9}(1) - F_{9 \times 9}(41)$ | Basic 9 x 9 non-zero locations for Fundamental Matrix (45:26) baro-altimeter terms added |
| $XS(1) - XS(35)$                         | Error states 1-35  |
| $CK1, CK2, CK3$                          | baro-altimeter damping coefficients  |
| $CNP(1) - CNP(9)$                        | Direction cosine matrix for transformation from platform to navigation frame             |
| $F_x, F_y, F_z$                          | specific forces  |
| $WCX, WCY, WCZ$                          | Angular velocity of E-N-U frame w.r.t. inertial space                                    |
| $V_g / D_{alts}$                         | Aircraft ground speed / correlation distance   |

|    | 36 | 37 | 38 | 39        |
|----|----|----|----|-----------|
| 36 | 0  | 1  | 0  | 1         |
| 37 | 0  | 0  | 1  | 0         |
| 38 | 0  | 0  | 0  | 0         |
| 39 | 0  | 0  | 0  | $-1/7200$ |

Fig. 2.10.  $F_{22}$  Partition 36-39  
of Fundamental Matrix

|    | 40 | 41 | 42 | 43       | 44       | 45       |
|----|----|----|----|----------|----------|----------|
| 40 | 0  | 0  | 0  | 0        | 0        | 0        |
| 41 | 0  | 0  | 0  | 0        | 0        | 0        |
| 42 | 0  | 0  | 0  | 0        | 0        | 0        |
| 43 | 0  | 0  | 0  | $-1/900$ | 0        | 0        |
| 44 | 0  | 0  | 0  | 0        | $-1/900$ | 0        |
| 45 | 0  | 0  | 0  | 0        | 0        | $-1/900$ |

Fig. 2.11.  $F_{33}$  Partition 40-45  
of Fundamental Matrix

|    | 48 | 49 | 50 | 51 | 52 |
|----|----|----|----|----|----|
| 48 | 0  | 0  | 0  | 1  | 0  |
| 49 | 0  | 0  | 0  | 0  | 1  |
| 50 | 0  | 0  | 0  | 0  | 0  |
| 51 | 0  | 0  | 0  | 0  | 0  |
| 52 | 0  | 0  | 0  | 0  | 0  |

Fig. 2.12.  $F_{44}$  Partition 48-52  
of Fundamental Matrix

Table III  
Error Source Statistics

| <u>Random Walks (<math>\dot{x} = w</math>)</u>  |   |  |
|---|---|--|
| <u>State</u>  | <u>Variable</u>                         | <u>Noise Spectral Density (Q)</u>  |
| 11  | X Gyro Bias                             | $(.002^\circ/\text{HR})^2 / \text{HR}$   |
| 12  | Y Gyro Bias                             | $(.002^\circ/\text{HR})^2 / \text{HR}$   |
| 13  | Z Gyro Bias                             | $(.002^\circ/\text{HR})^2 / \text{HR}$   |
| 23  | X Accel Bias                            | $(3 \text{ ug})^2 / \text{HR}$   |
| 24  | Y Accel Bias                            | $(3 \text{ ug})^2 / \text{HR}$   |
| 25  | Z Accel Bias                            | $(3 \text{ ug})^2 / \text{HR}$   |
| 36  | Clock Phase error                       | $(.2 \text{ ft})^2 / \text{sec}$   |
| 50  | Terrain Vertical Pos. Error             | $(30 \text{ ft})^2 / \text{sec}$   |
| 51  | Terrain East Velocity Error             | $(1 \text{ ft/sec})^2 / \text{sec}$  |
| 52  | Terrain North Velocity Error            | $(1 \text{ ft/sec})^2 / \text{sec}$  |
| <u>First-Order Markov Processes (<math>\dot{x} = -(1/\tau)x + w</math>) <math>Q = 2\sigma^2/\tau</math></u> |   |  |
| 35  | Baro-Altimeter Error                    | $\frac{\text{value}}{500 \text{ ft}} \quad \frac{\text{Correlation Time}}{(500 \text{ nautical miles})/v_g}$ |
| 39  | Clock Random Frequency                  | $10 \text{ ft/sec} \quad (7200 \text{ sec})$   |
| 43  | Doppler along-track Scale Factor Error  | $(V_x) 5 \times 10^{-4} \text{ ft/sec} \quad (900 \text{ sec})$  |
| 44  | Doppler across-track Scale Factor Error | $(V_y) 5 \times 10^{-4} \text{ ft/sec} \quad (900 \text{ sec})$  |
| 45  | Doppler Vertical Scale Factor Error     | $(V_z) 5 \times 10^{-4} \text{ ft/sec} \quad (900 \text{ sec})$  |



### Simulation

The results obtained in this effort were generated using the SOFE (36) Monte Carlo evaluation, PROFGEN (35) flight profile generator, and SOFEPL (37) sample statistics generation and plotting software packages.

### Flight Trajectory

The flight trajectory is generated with the AFAL program PROFGEN and stored on magnetic tape. Table IV demonstrates the characteristics of the flight trajectory (e.g., takeoff, climbout, dive, jinking (tactical maneuver, etc.)). It is a 7236 second high-performance aircraft flight profile with many dynamic maneuvers. This profile was chosen to be representative of regions of benign dynamics and harsh dynamics to test the ultimate robustness of the FDI system. Fig.'s 2.13 thru 2.17 demonstrate the flight characteristics.

Table IV  
Flight Profile Statistics

| Segment Number | Duration Seconds | Manuever | Acceleration | Roll   | Pitch  | Heading |
|----------------|------------------|----------|--------------|--------|--------|---------|
| 1              | 30               | STRT     | 0.0 grav     | 0.0    | 0.0    | 0.0     |
| 2              | 20               | VERT     | .250         | 0.0    | 10.00  | 0.0     |
| 3              | 205              | VERT     | .050         | 0.0    | 26.00  | 0.0     |
| 4              | 85               | VERT     | .250         | 0.0    | -36.00 | 0.0     |
| 5              | 942              | STRT     | 0.0          | 0.0    | 0.0    | 0.0     |
| 6              | 11               | VERT     | 1.573        | 0.0    | 1.70   | 0.0     |
| 7              | 16               | VERT     | 3.071        | 0.0    | -19.90 | 0.0     |
| 8              | 4                | VERT     | 4.212        | 0.0    | 18.20  | 0.0     |
| 9              | 37               | HORZ     | .200         | 0.0    | 0.0    | 14.10   |
| 10             | 439              | STRT     | 0.0          | 0.0    | 0.0    | 0.0     |
| 11             | 345              | VERT     | .0358        | 0.0    | -10.0  | 0.0     |
| 12             | 66               | VERT     | .197         | 0.0    | 10.0   | 0.0     |
| 13             | 91               | JINK     | 8.528        | 0.0    | 13.0   | 30.00   |
| 14             | 319              | HORZ     | .200         | 0.0    | 0.0    | 90.00   |
| 15             | 29               | VERT     | 3.000        | 0.0    | 13.20  | 0.0     |
| 16             | 10               | VERT     | 4.000        | 0.0    | -45.40 | 0.0     |
| 17             | 2                | ROLL     | 0.0          | 113.40 | 0.0    | 0.0     |
| 18             | 2                | ROLL     | 0.0          | 113.40 | 0.0    | 0.0     |
| 19             | 21               | VERT     | 6.000        | 0.0    | 53.90  | 0.0     |
| 20             | 18               | VERT     | 1.278        | 0.0    | -21.70 | 0.0     |
| 21             | 40               | JINK     | 9.258        | 0.0    | 20.00  | 45.30   |
| 22             | 20               | VERT     | 4.000        | 0.0    | 10.50  | 0.0     |
| 23             | 10               | VERT     | 3.000        | 0.0    | -20.60 | 0.0     |
| 24             | 30               | HORZ     | 2.000        | 0.0    | 0.0    | 85.00   |
| 25             | 10               | VERT     | 5.000        | 0.0    | 10.10  | 0.0     |
| 26             | 61               | VERT     | 5.000        | 0.0    | 15.00  | 0.0     |
| 27             | 20               | ROLL     | 0.0          | 78.80  | 0.0    | 0.0     |
| 28             | 10               | ROLL     | 0.0          | -78.80 | 0.0    | 0.0     |
| 29             | 50               | VERT     | 3.000        | 0.0    | -15.00 | 0.0     |
| 30             | 1863             | STRT     | 0.0          | 0.0    | 0.0    | 0.0     |
| 31             | 45               | VERT     | .500         | 0.0    | 15.50  | 0.0     |
| 32             | 25               | VERT     | .500         | 0.0    | -15.50 | 0.0     |
| 33             | 5                | ROLL     | 0.0          | 50.90  | 0.0    | 0.0     |
| 34             | 5                | ROLL     | 0.0          | -50.90 | 0.0    | 0.0     |
| 35             | 1493             | HORZ     | .500         | 0.0    | 0.0    | 11.20   |
| 36             | 527              | STRT     | 6            | 0.0    | 0.0    | 0.0     |
| 37             | 300              | VERT     | .500         | 0.0    | -6.90  | 0.0     |
| 38             | 30               | VERT     | .050         | 0.0    | 6.90   | 0.0     |

### Monte Carlo Analysis

The results obtained were generated from 10 runs of SOFE. Each run produced a different sequence of random numbers to generate the samples of input white noise processes. Sample statistics were computed for each time point using the equations:

$$\bar{x} = (1/N) \sum_{i=1}^N x_i \quad (2-50)$$

$$\hat{\sigma}^2 = (1/(N-1)) \sum_{i=1}^N x_i^2 - (N/(N-1)) \bar{x}^2 \quad (2-51)$$

where,

$\bar{x}$  is an estimate of the mean of  $x$ ,

$\hat{\sigma}^2$  is an estimate of the variance of  $x$ ;

$N$  is the number of computer runs.

Ten runs were chosen to reduce the variations in the computed standard deviations in the computed standard deviations of the samples for  $x_i$  below an acceptable value. This produces an essentially unbiased estimate of the state's standard deviation (37:8).

### The Unaided Simulation

The position, velocity, and attitude errors for this unaided INS are shown in Fig.'s 2.18 thru 2.27. These plots represent the magnitude of errors that would be seen if a tactical aircraft's INS were operating in an unaided mode

(except for the baro-altimeter which provides vertical channel stability). These plots represent a minimum performance bound against which to evaluate the filter's performance.

The performance plots also verify the desired values expected for this medium accuracy INS. Also evident in the plots are the effects of Schuler frequency and aircraft maneuvering.

The unaided simulation serves as a means of validating the truth model states. In Chapter Three, a reduced order model (derived from the truth model) is generated.

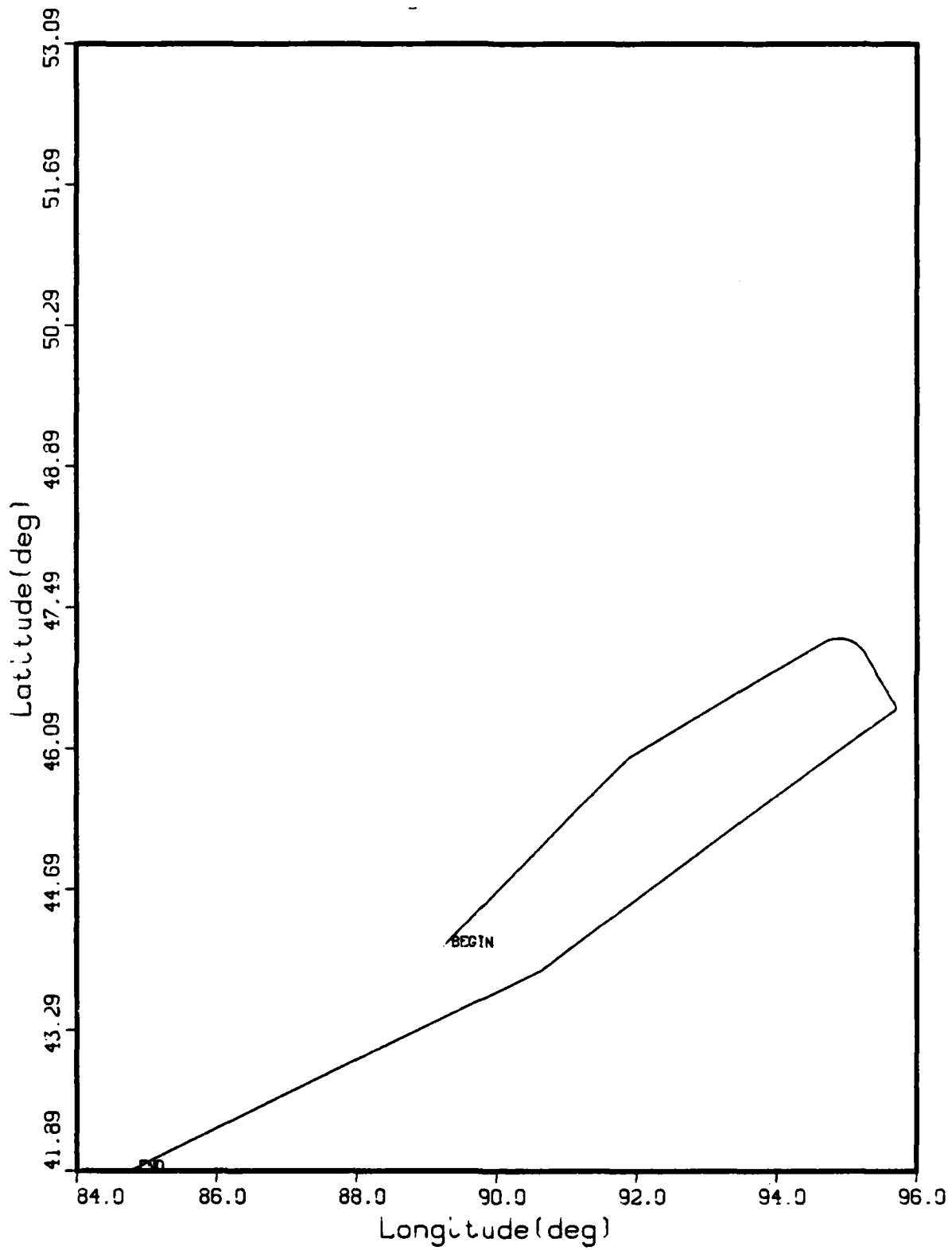


Fig. 2.13. Latitude/Longitude Flight Profile

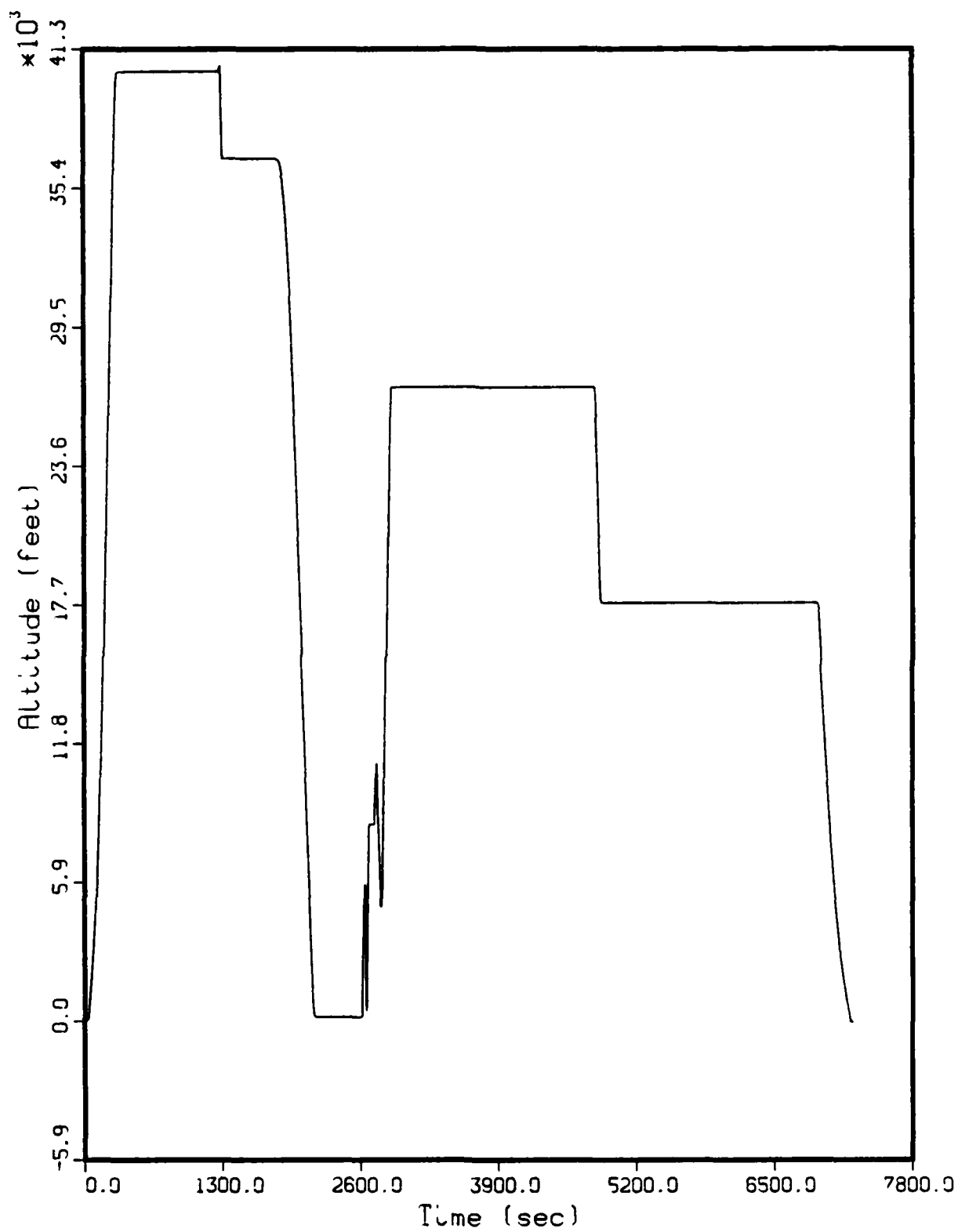


Fig. 2.14. Altitude Flight Profile

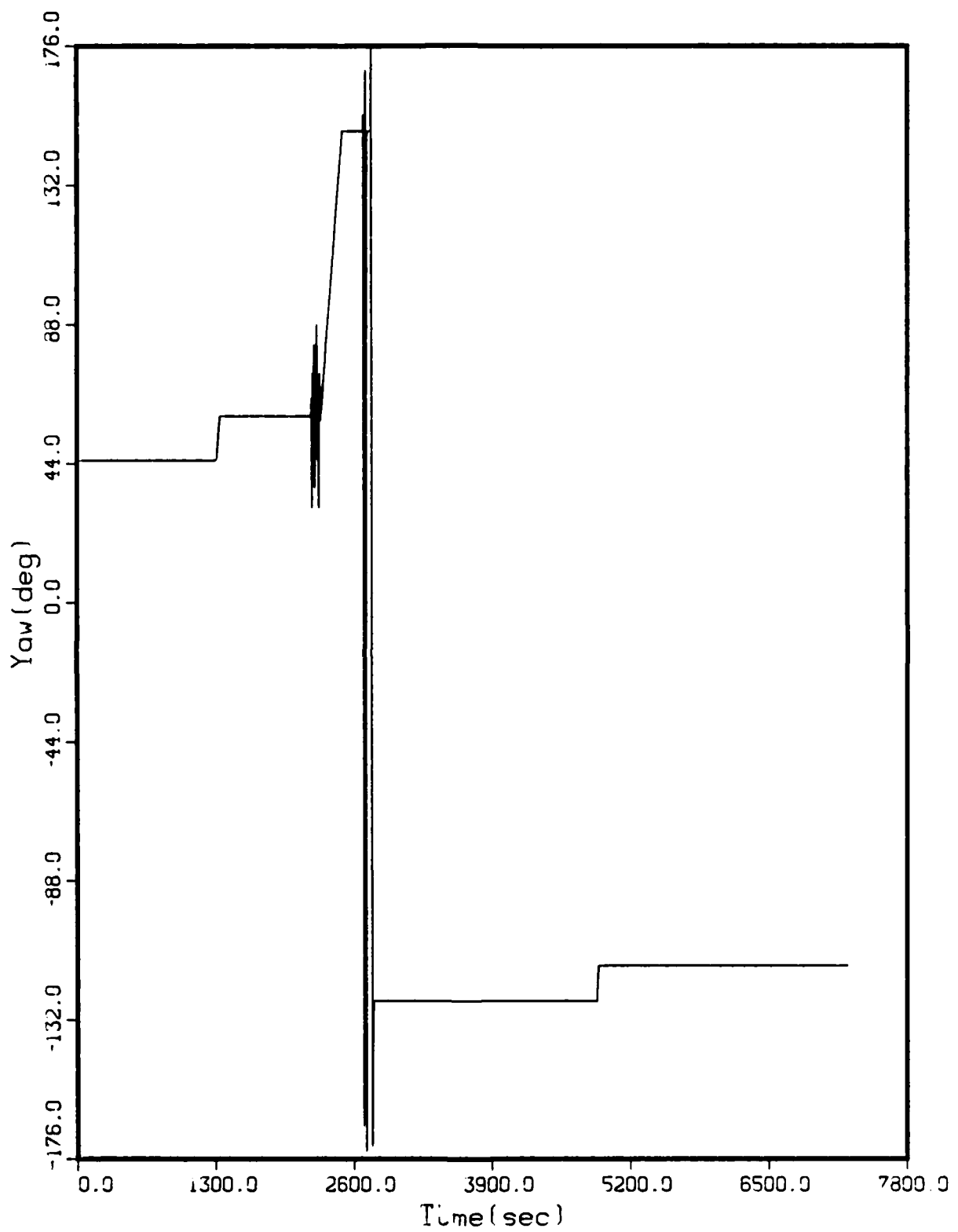


Fig. 2.15. Yaw Flight Profile

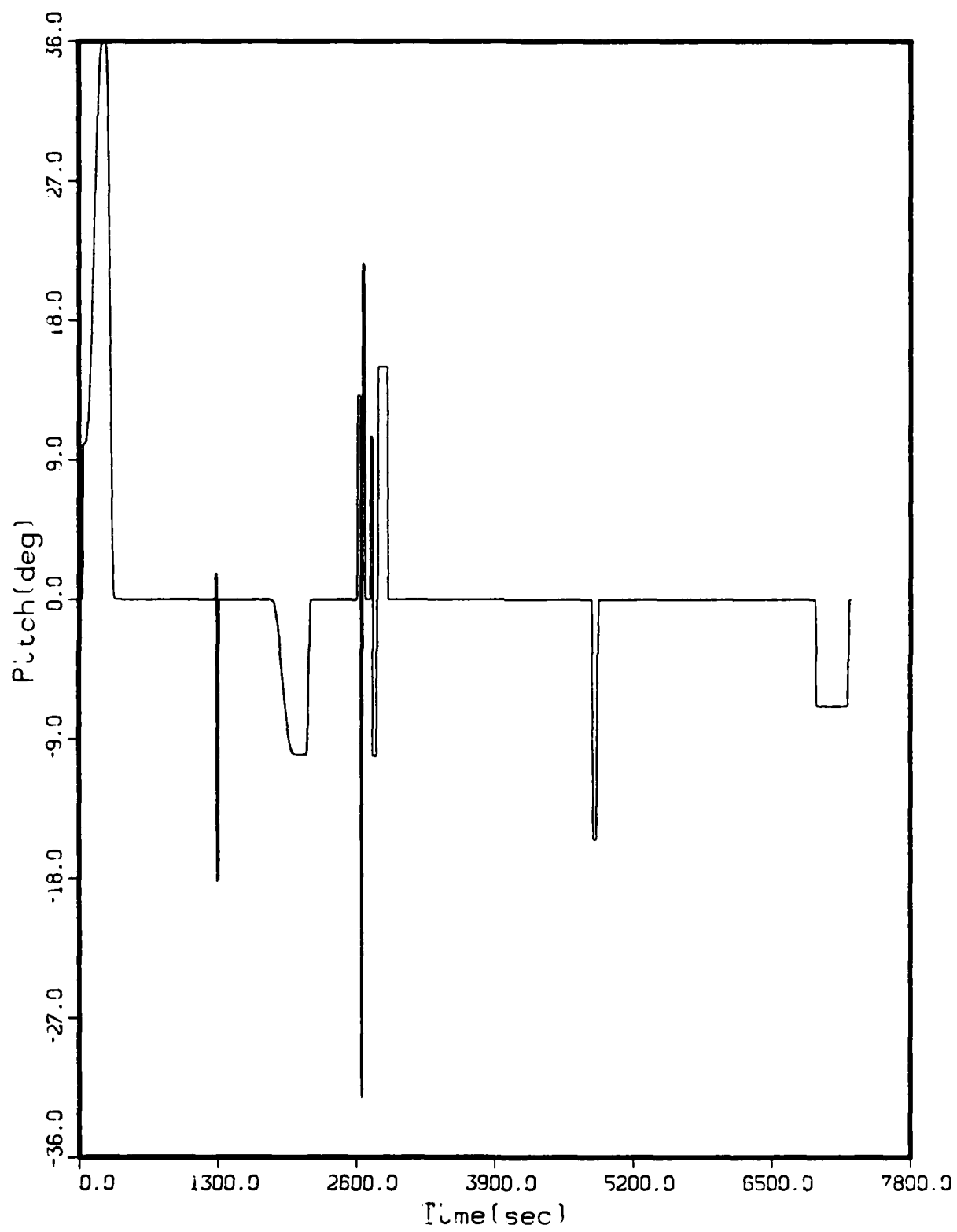


Fig. 2.16. Pitch Flight Profile



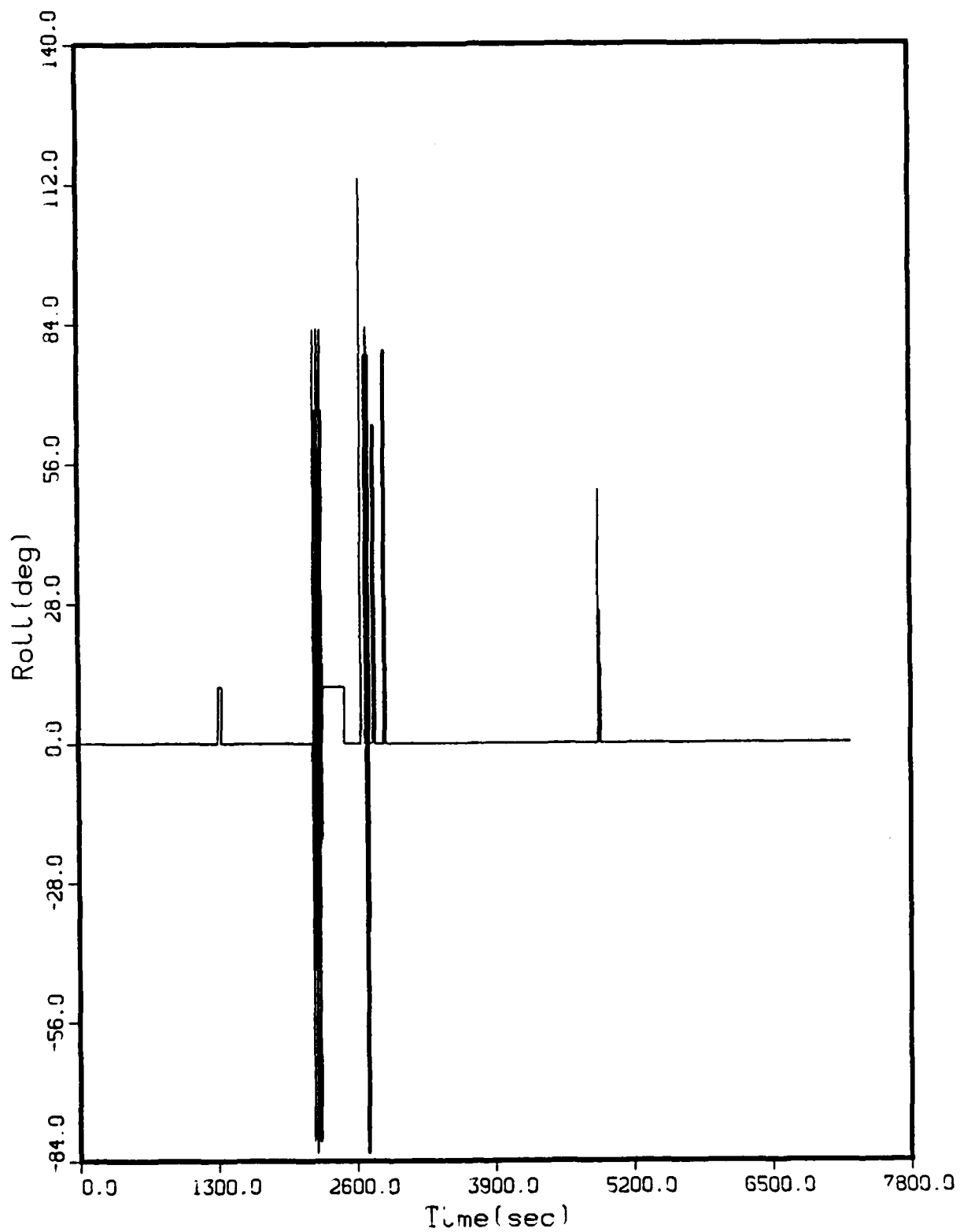


Fig. 2.17. Roll Flight Profile

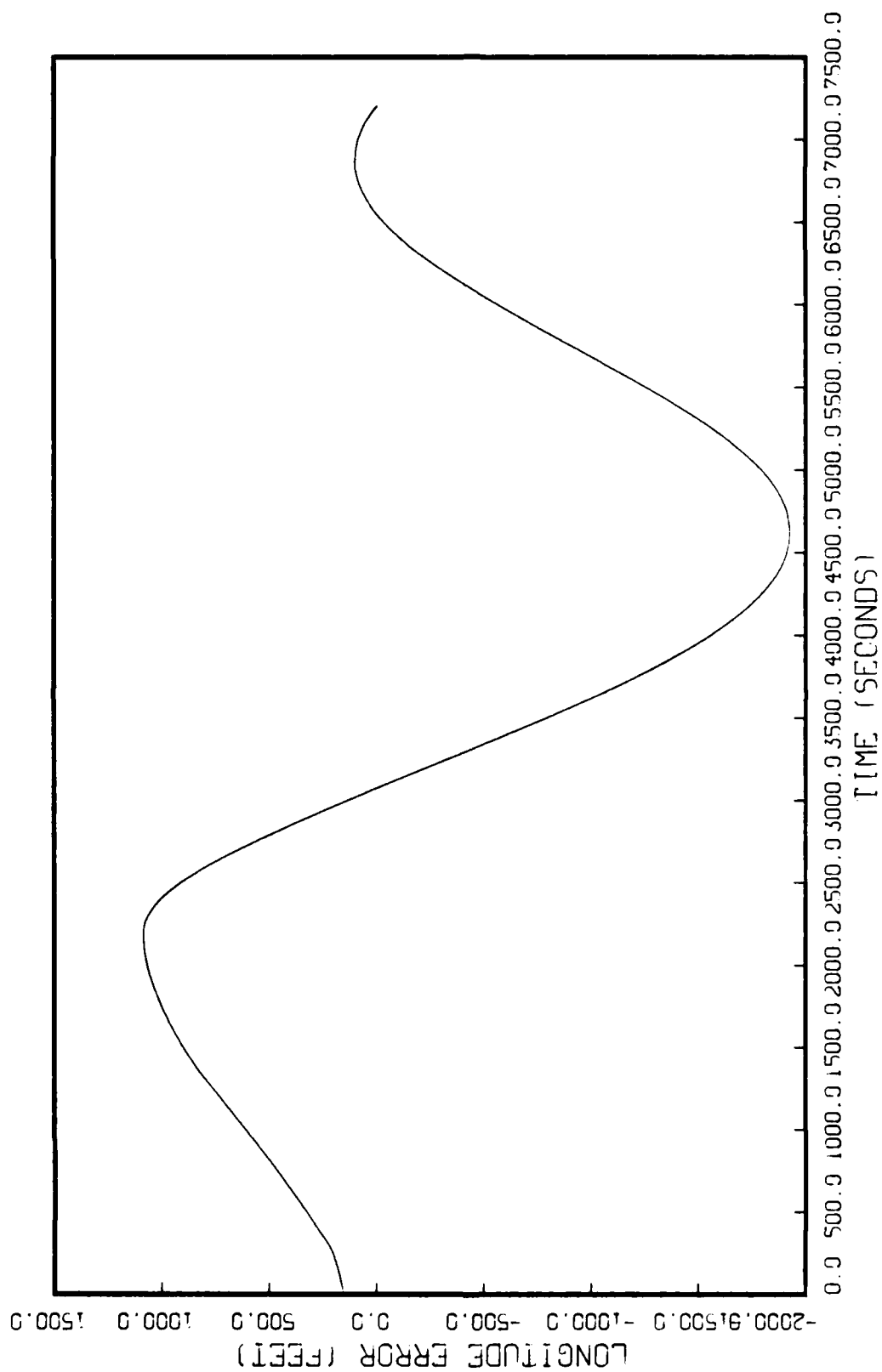


Fig. 2.18. Longitude Error For Unaided INS

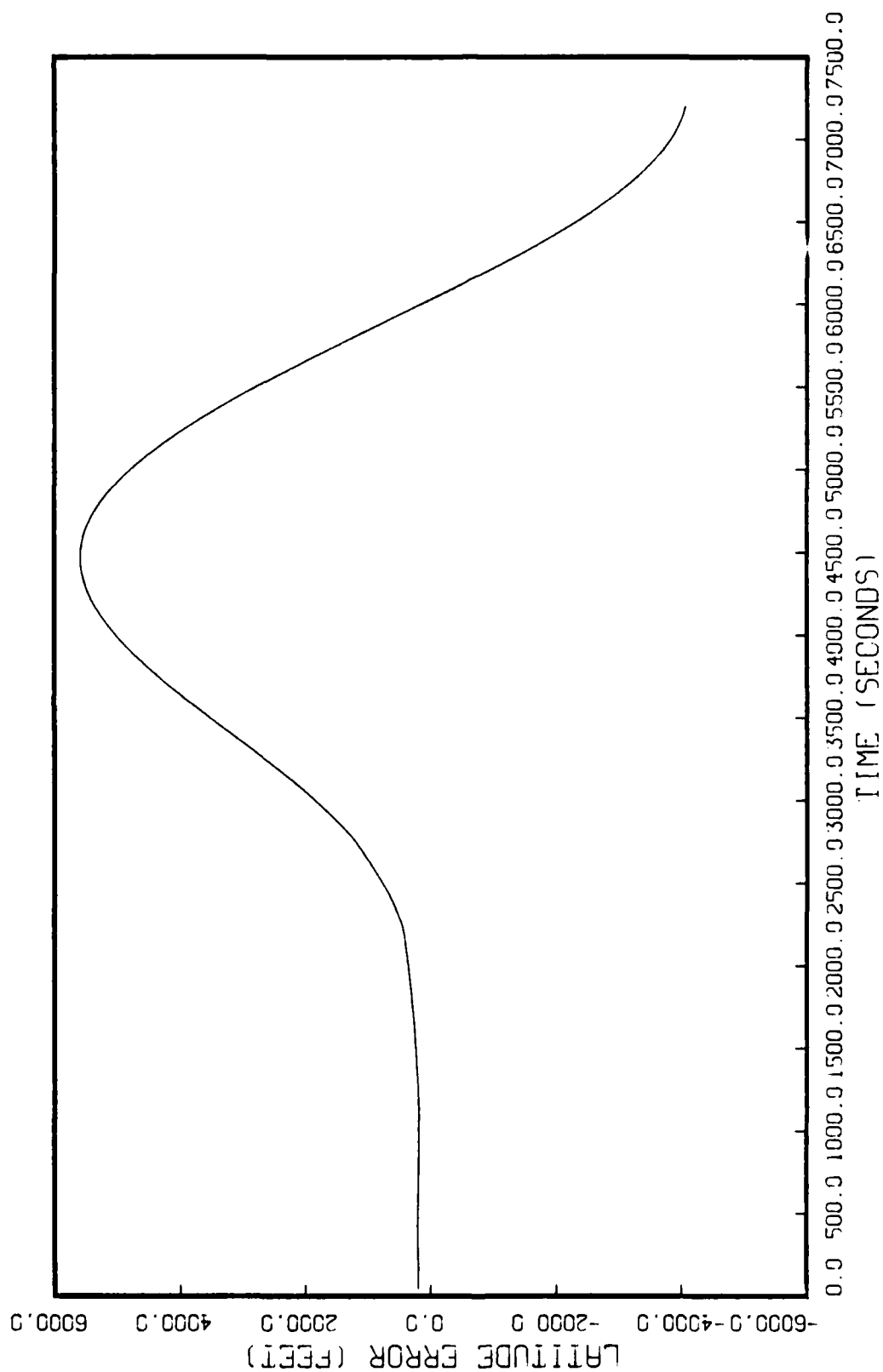


Fig. 2.19. Latitude Error for Unaided INS

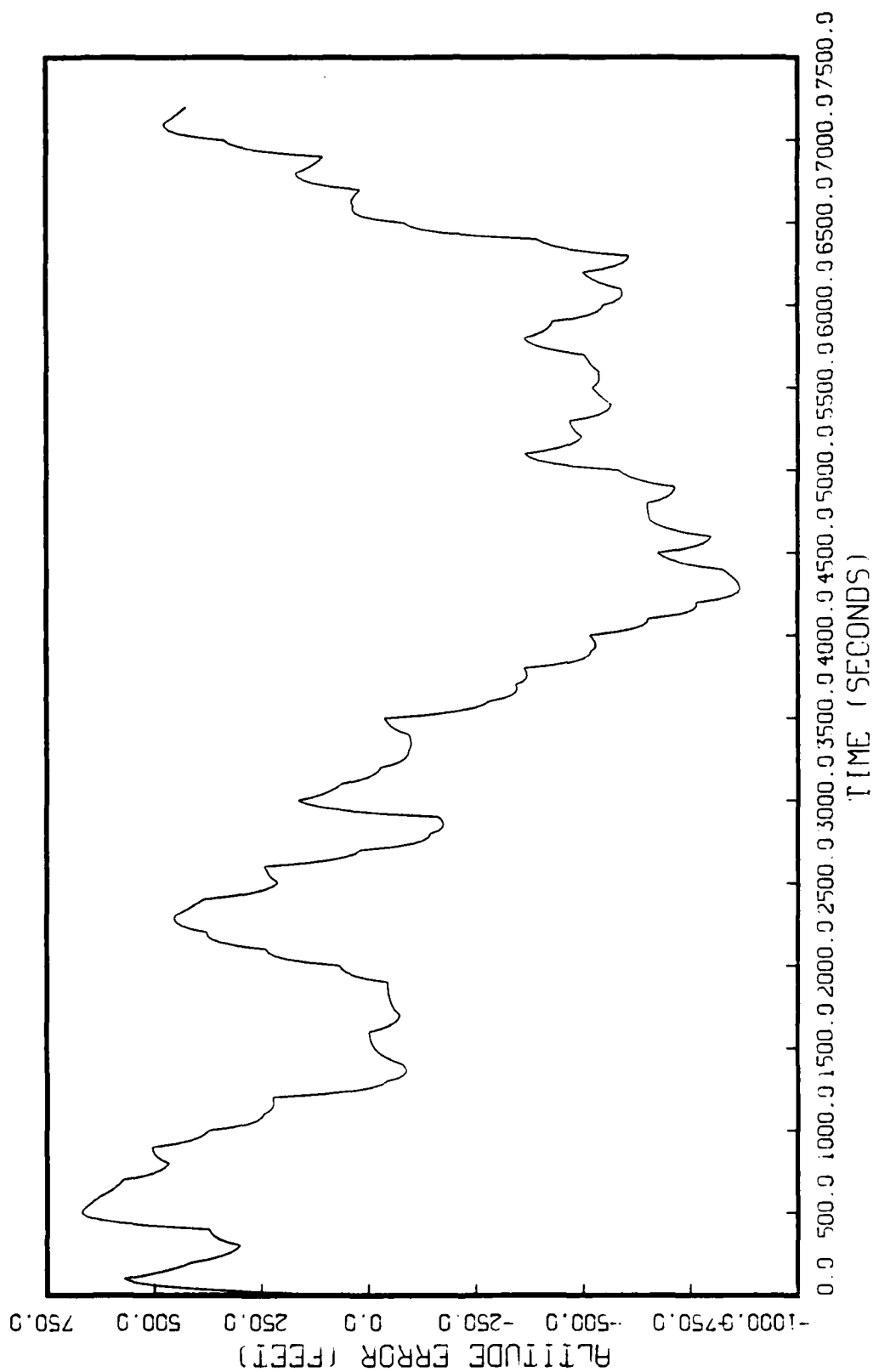


Fig. 2.20. Altitude Error For Unaided INS

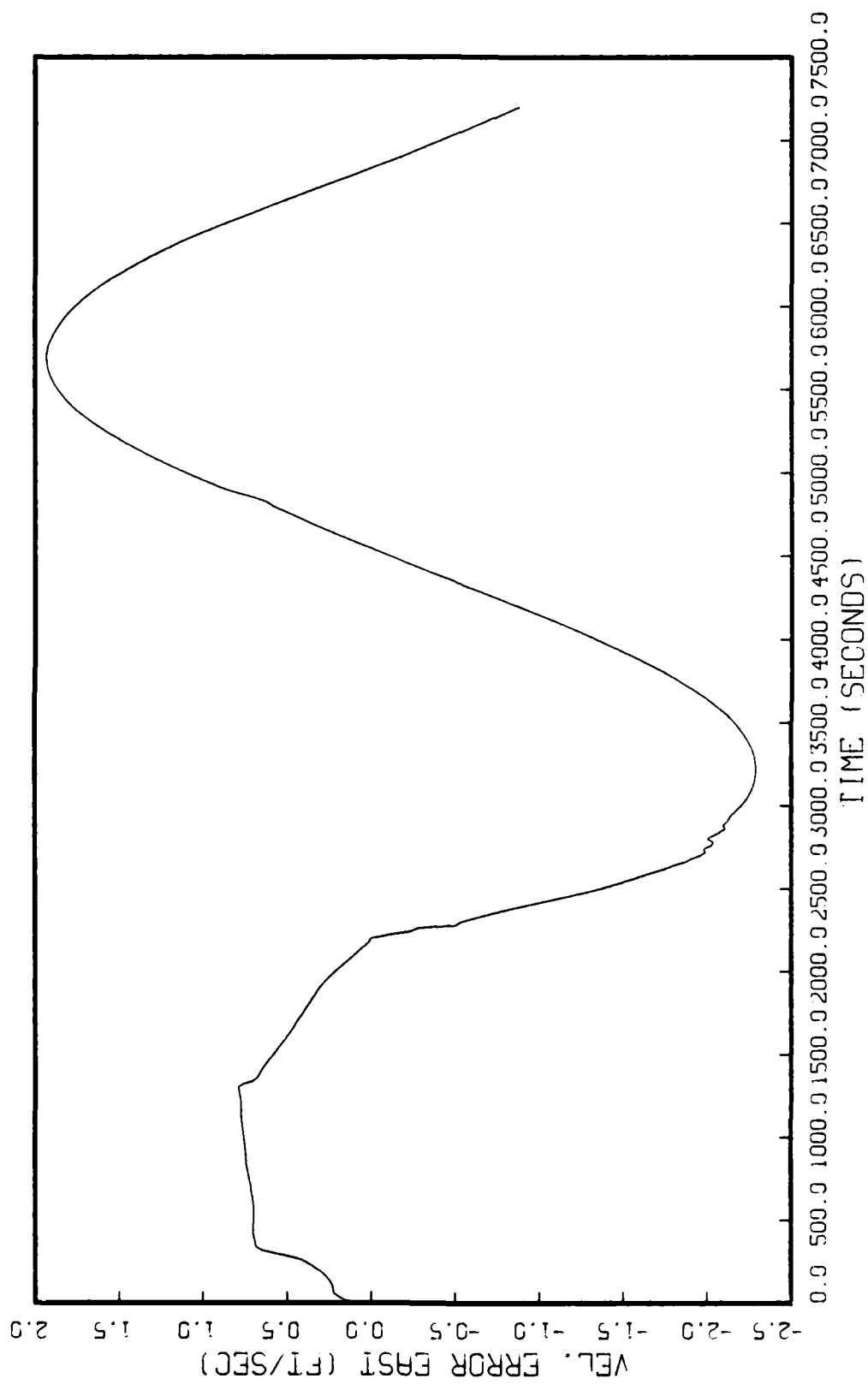


Fig. 2.21 East Velocity Error For Unloaded FMS

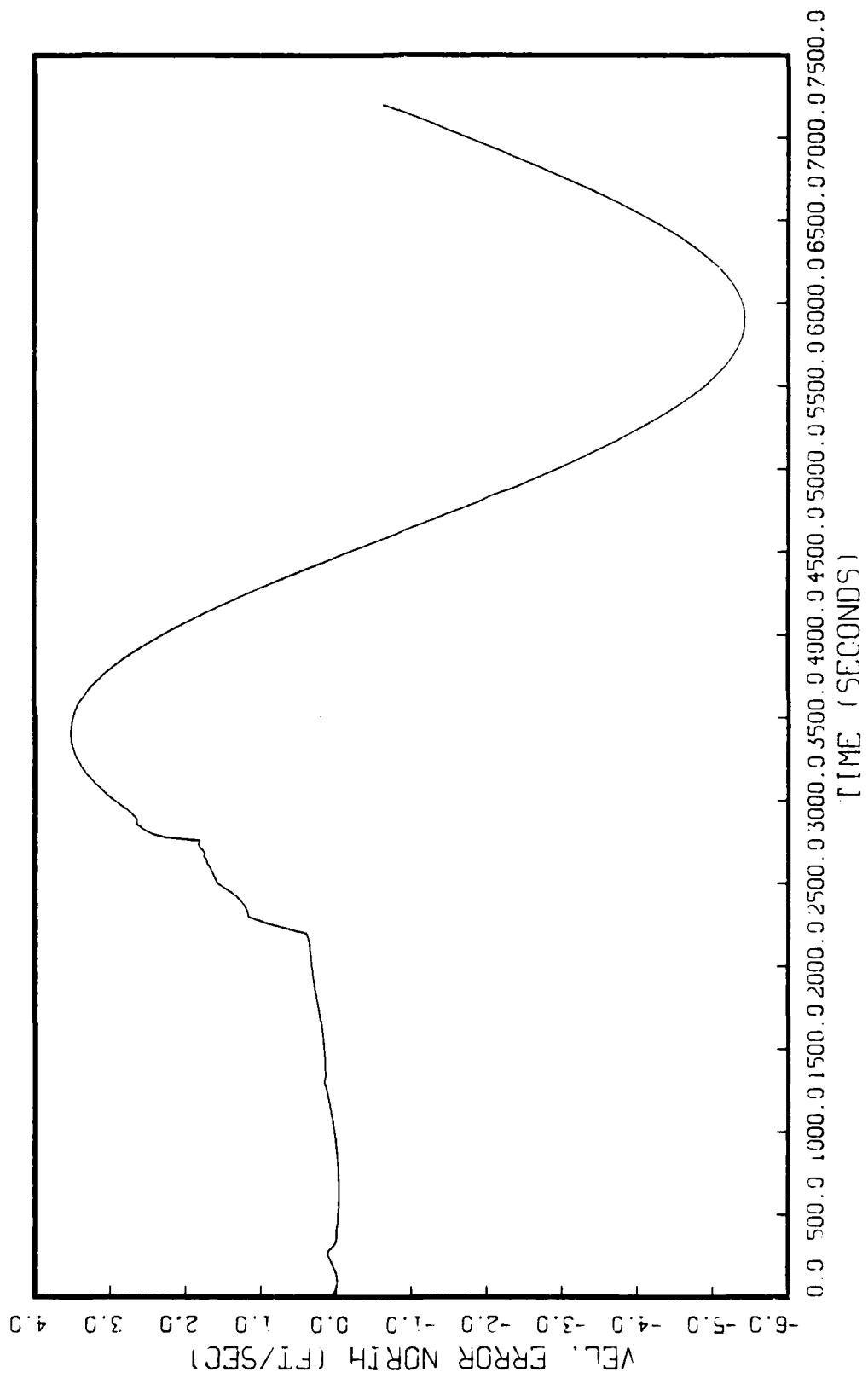
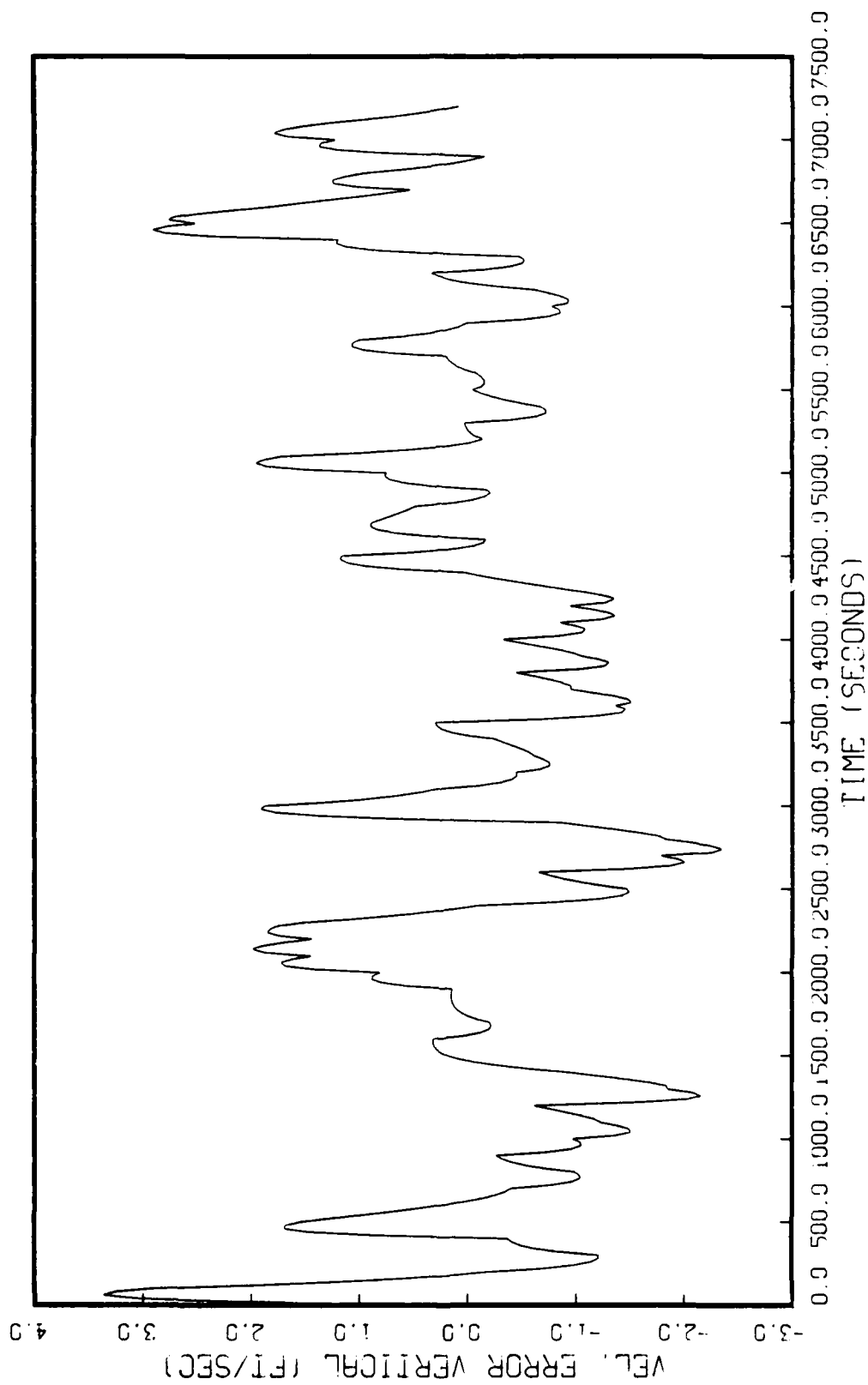


Fig. 2.22. North Velocity Error For Unaided IN3



if. 2.23 Vertical Velocity Error For Unaided INS

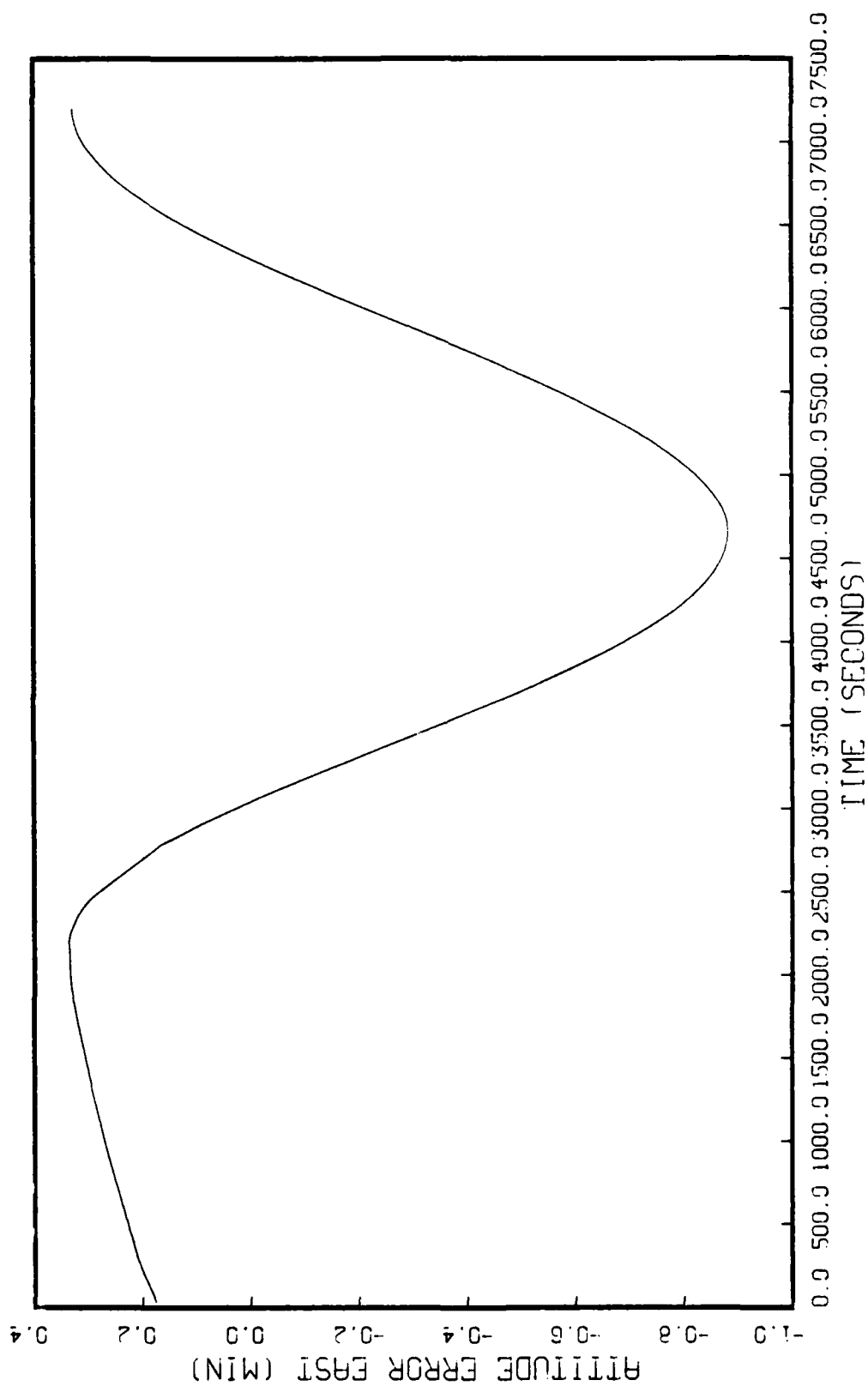


Fig. 2.24. East Attitude Error for Unaided INS



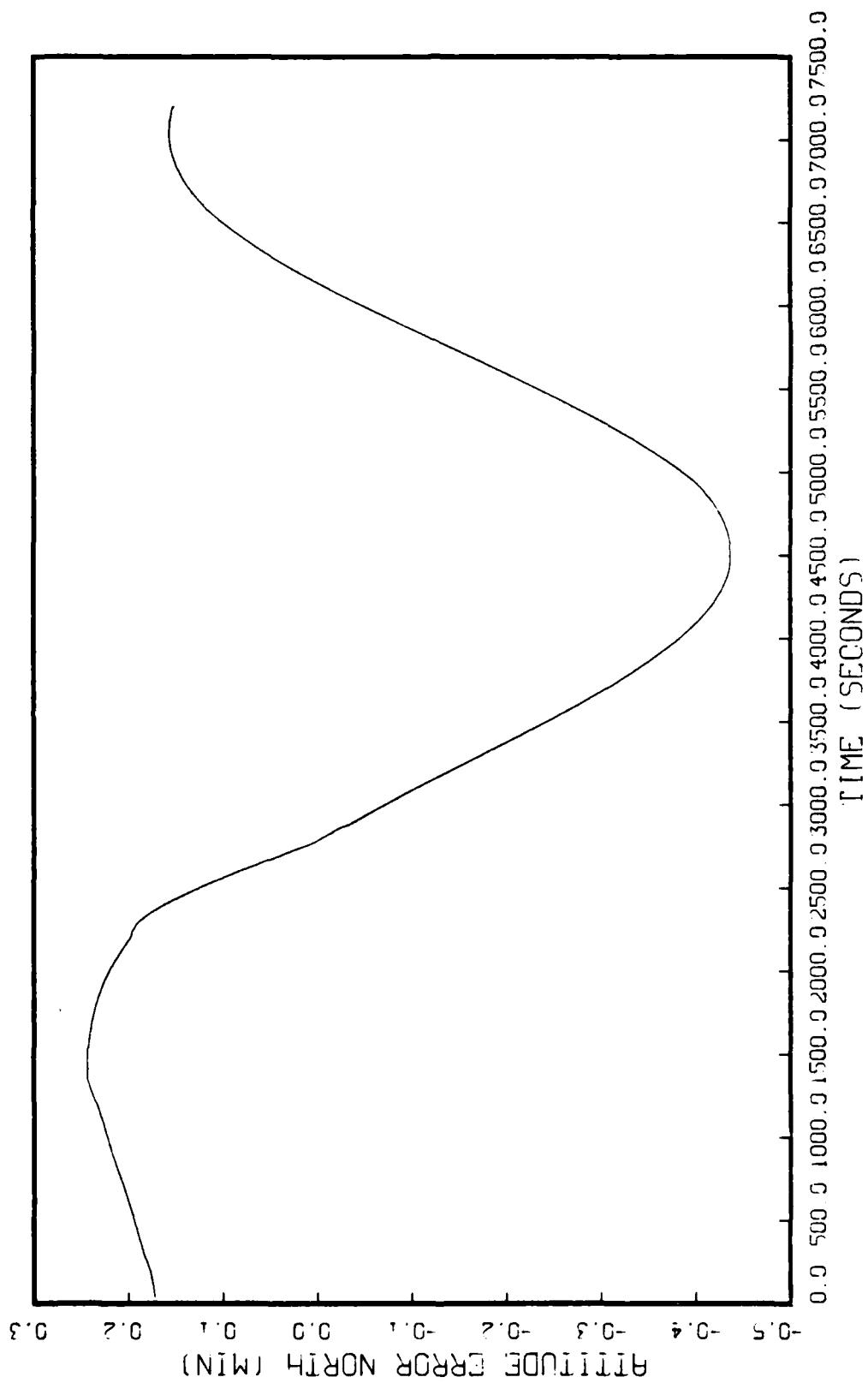


Fig. 2.25 North Attitude Error For Unaided INS

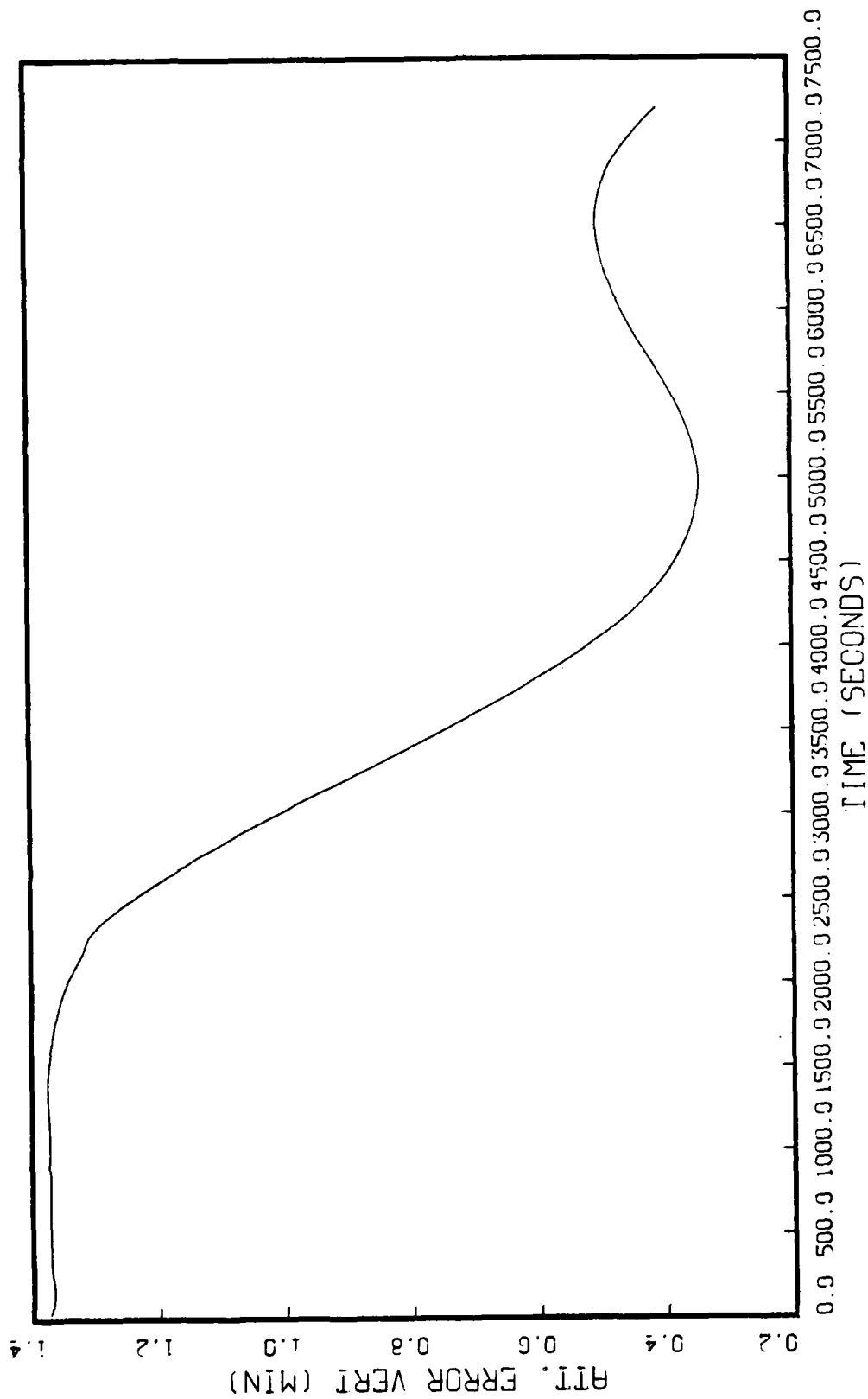


Fig. 2.26. Vertical Attitude Error For Unaided INS

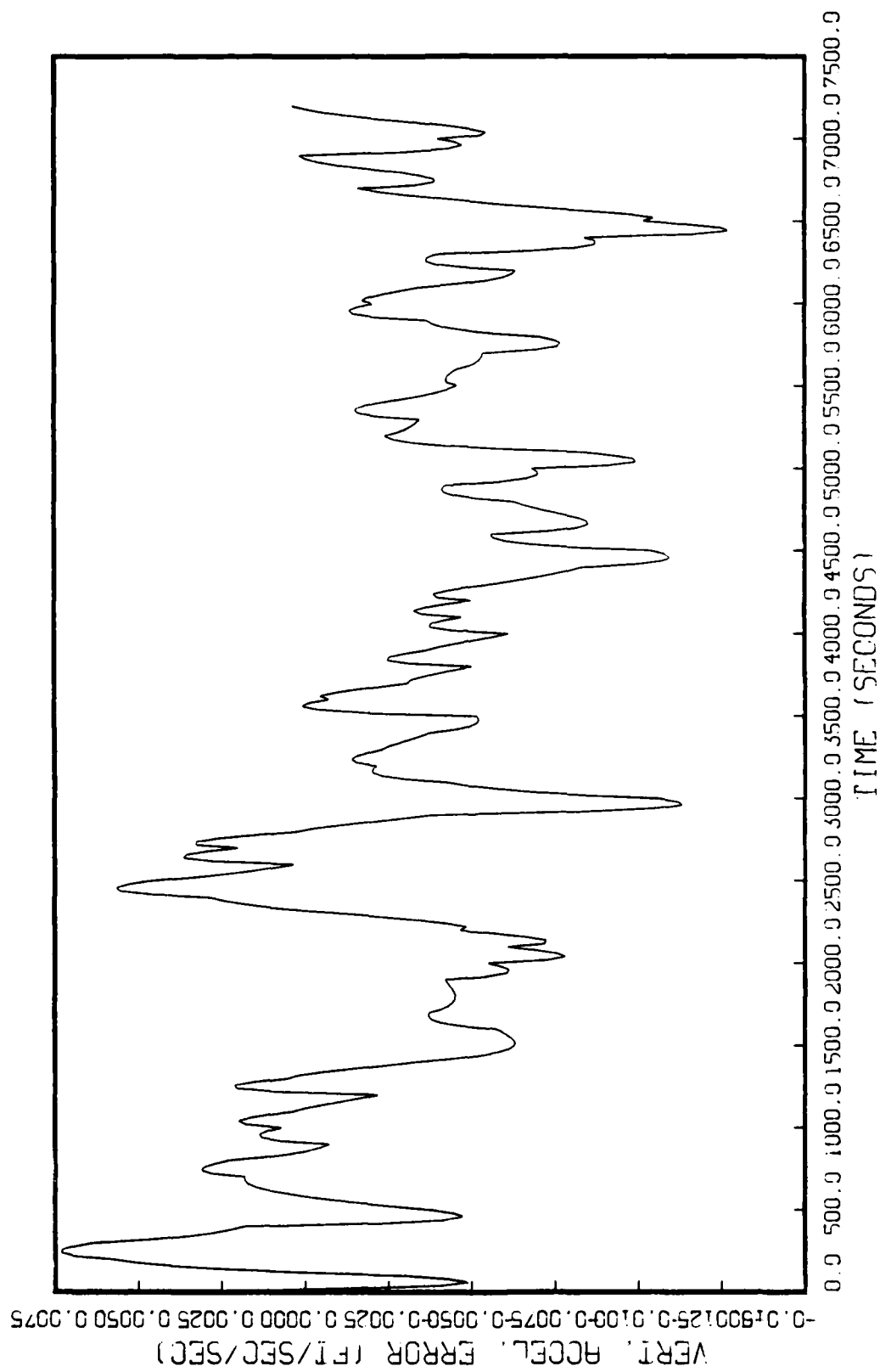


Fig. 2.27. Vertical Acceleration Error For Unaided INS

### III. The Filter Design

#### Introduction

Typical Kalman filter design is an iterative process. The design is based on incorporating modifications and evaluating any such modifications to determine the performance capability of the resulting filter. Performance requirements such as reaching specified RMS errors, and constraints such as cost, sequencing, storage, and computation time, play a major role in the design decision process.

The design of such a filter would be typically structured into the following pattern:

- (1) Develop a "truth" model as the best, all inclusive representation of the real world.

- (2) Propose a Kalman filter design based on the "truth" model.

- (3) Reduce the order of the system model assumed in the filter and incorporate any other purposeful simplifications such as ignoring small matrix coefficients, etc.

- (4) Conduct a covariance analysis and "tune" the filter; iterate back to step 3 as required.

- (5) Perform a Monte Carlo analysis on best designs.

- (6) Study the performance/loading trade-offs and implementation requirements.

(7) Implement the final design on onboard computer.

(8) Perform checkout, final tuning, and testing.

The filter proposed in this study is based on a 26-state model derived from the 52-state "truth" model of the previous chapter. It is composed of the basic 9-state Pinson-Widnall (45) error model for the basic INS errors plus the following additional states:

Table V  
Additional Filter Error States

| <u>Model States</u>   | <u>No. of States</u> |
|---|----------------------|
| Vertical Acceleration Error<br>(needed for 3rd order vertical<br>channel damping for the INS) | 1                    |
| Gyro Drift  | 3                    |
| Accelerometer Bias  | 3                    |
| Baro-Altimeter (error due to the<br>variation in altitude of a<br>constant pressure surface   | 1                    |
| Doppler radar (1 -scale factor<br>and 1-bias)   | 2                    |
| Radar Altimeter (1-zero offset<br>and 1-scale factor)   | 2                    |
| Terrain Correlator (1 for each<br>position error state)                                       | 3                    |
| Satellite Positioning (1-position<br>and 1-velocity)  | 2                    |

The effects of the unmodeled states from the "truth" model were incorporated into the appropriate states in the

filter by increasing the strength of the associated white noise inputs or by changing the physical process as required (e.g., a first-order Markov process with a long correlation time may be somewhat appropriately modeled as a random walk and incorporated into another state).

The basic, driving consideration for the design of this filter model is the conceptual study of an FDI system. The filter was generated to provide the FDI system with a cross-section of sensor error states to examine the effects of different failure modes on the overall filter and also examine the FDI system itself.

The remainder of this chapter provides an overview of the error modeling for the various sensors and also displays the specific error model for each sensor incorporated into the filter.

#### The Baro-Altimeter

The baro-altimeter operates by measuring atmospheric pressure and then scaling the output to obtain the proper exponential altitude versus pressure relation. The error sources which affect barometric measurements are attributable to turbulence and pressure drops at the static pressure vent, temperature variations, and low-pressure gradients. Since the atmospheric pressure decreases exponentially with altitude, the accuracy of the altimeter is greatly reduced above 20,000 feet. Horizontal weather fronts can also induce errors in the barometric altimeter.

The error model for the barometric altimeter can be characteristically generated as a random bias for calibration, reference, weather changes, and static pressure changes. The bias modeling of weather changes and static pressure is appropriate if the aircraft has a slow ground speed for the correlation distance, which produces a large time constant; however, for this particular application, the changes would be more appropriately modeled (45:3-46) as a first-order Markov process with a correlation distance of 500 nautical miles to model isobaric variations on the order of 500 feet. The altimeter lagging effect is not modeled in the filter. For the purposes of this research, the baro-altimeter is primarily utilized as a measurement device at constant altitude to support the terrain correlator. Because of the constant altitude criteria, lagging effect can be ignored. The model utilized for this study is given in the following equation:

$$\dot{e}_{po} = (-V_g/D_{alts}) e_{po} + w \quad (3-1)$$

where,

$V_g$  = velocity w.r.t. ground in ft/sec

$D_{alts}$  = correlation distance (500 n.m.)

$w$  = white noise process

$$E[w] = 0, E[w(t) w(t + \tau)] = Q\delta(\tau) \quad (3-2)$$

$$Q = 2\sigma^2/T = 2(500 \text{ ft})^2 V_g/D_{alts} = 1.6 V_g \quad (3-3)$$

For this particular model, the total error contribution to the baro-error process is:

$$\delta h_B = e_{po} \quad (3-4)$$

The measurement process is given as:

$$h_{MEAS} = h_{true} + e_{po} + v_a \quad (3-5)$$

where:

$v$  represents zero-mean, white Gaussian measurement noise.

#### Doppler Radar

Doppler radar is used to provide a direct measure of aircraft ground speed. The relative motion between the source of the radar beam (e.g., the aircraft) and the target (e.g., the ground) causes a frequency shift in the reflected signal which is proportional to the velocity. By transmitting and receiving several of these beams, a simultaneous measure of the beams will provide information about vehicle ground speed in an along-track, cross-track, and vertical direction (vertical velocity is not an accurate quantity). This system model is based on a four-beam arrangement (two forward-looking and two aft-looking). The system is also modeled as being rigidly attached to the aircraft. The signals are then transformed into navigation coordinates in the navigation computer.



Although the Doppler output is not actually continuous (it is actually a pulse train of several pulses per second), it is modeled as a continuous system. This is reasonable since the time constants of the navigation system errors are much longer than those for the Doppler.

There are several sources of error in the Doppler radar system. Fluctuation noise is due to the variations in the scatter of the beam due to terrain (or water surface) characteristics. These errors are typically modeled as first-order Markov processes in the along-track, cross-track, and vertical directions with correlation times of .25 to 1.0 seconds (45).

Beam direction errors are caused by misalignment or post-calibration uncertainty in antenna direction, refraction from the radome/aircraft boundary, and thermal displacement of the antenna elements. These errors are typically modeled as random constants.

Random scale factor errors are due to aircraft vibration and ground scattering variations with terrain. These errors are modeled as first-order Markov processes with a correlation time of 15 minutes (45:3-36).

The Doppler model used for the study does not account for over water errors since the flight profile does not pass over water.

The filter model is a two-state model which accounts for along-track beam direction error and random scale factor

errors. These errors are then transformed to the navigation frame through the proper direction cosine matrix. This transformation generates a portion of the along-track error in the east, north, and up direction.

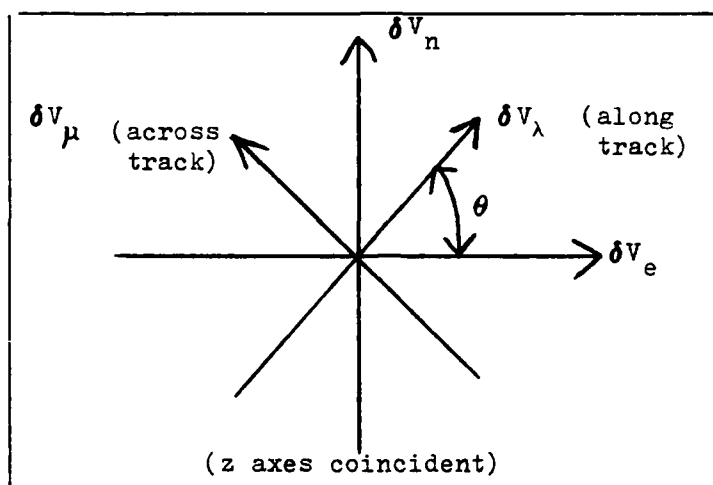


Fig. 3.0. Vehicle Track To Navigation Frame Transformation

To go from an  $\lambda$ ,  $u$ ,  $z$  (along-track, cross-track, vertical) frame to a  $E$ ,  $N$ ,  $U$  (east, north, up) frame requires the following set of equations:

$$\delta V_e = \delta V_\lambda \cos \theta - \delta V_\mu \sin \theta \quad (3-6)$$

$$\delta V_n = \delta V_\lambda \sin \theta + \delta V_\mu \cos \theta \quad (3-7)$$

$$\delta V_z = \delta V_z \quad (3-8)$$

where,

$\delta V_{\lambda,u,z}$  = vehicle track velocities

$\delta V_{e,n,z}$  = navigation frame velocities

$\theta$  = angle between aircraft heading and navigation frame.

Since the error model for the Doppler radar is only tracked for  $\delta V_\lambda$ , then the above equations will simplify to:

$$\delta V_e = \delta V_\lambda \cos \theta \quad (3-9)$$

$$\delta V_n = \delta V_\lambda \sin \theta \quad (3-10)$$

For the Doppler model, the beam direction error is modeled as a random constant:

$$\dot{b}_\lambda = 0 \quad (3-11)$$

where,

$b_\lambda$  is the along-track beam error in ARC MINutes.

For the random scale factor error, a first-order Markov process is used for the error model and is described by the following equation:

$$\dot{\delta V}_{s_\lambda} = -B_s \delta V_{s_\lambda} + w_{s_\lambda} \quad (3-12)$$

where,

$\delta V_{s_\lambda}$  = along-track scale factor error

$B_s$  = inverse time correlation ( $T = 900$  secs)

$w_s$  is the white noise process with the following statistics (15):

$$E [w_{s_\lambda}] = 0, E [w_{s_\lambda}(t)w_{s_\lambda}(t + \tau)] = Q \delta(\tau) \quad (3-13)$$

$$Q = 2(KV_{\lambda})^2/\alpha \quad (3-14)$$

where:

$K = 2 \times 10^{-3}$  for good Doppler

$\alpha = .5 \text{ sec}^{-1}$

$V_{\lambda}$  = along-track velocity

The total error model for the Doppler is then:

$$\begin{aligned} \delta V_{ED} &= b_{\lambda} [V_{\lambda} \cos \theta - V_u \sin \theta] \\ &\quad + \delta V_{s_{\lambda}} [\cos \theta] \end{aligned} \quad (3-15)$$

$$\begin{aligned} \delta V_{ND} &= b_{\lambda} [V_{\lambda} \sin \theta + V_u \cos \theta] \\ &\quad + \delta V_{s_{\lambda}} [\sin \theta] \end{aligned} \quad (3-16)$$

where:

$\delta V_{ED,ND}$  = Total Doppler error for the navigation frame

$V_{\lambda}$  = along-track velocity

$b_{\lambda}$  = beam direction error

$\delta V_{s_{\lambda}}$  = scale factor error

$\theta$  = angle between aircraft heading and navigation frame.

The measurement error is modeled as:

$$V_E = V_E(\text{TRUE}) + \delta V_{ED} + v_{de} \quad (3-17)$$

$$V_N = V_N(\text{TRUE}) + \delta V_{ND} + v_{dn} \quad (3-18)$$

where:

V is the zero-mean, white Gaussian measurement noise

#### Radar Altimeter

Radar altimeters measure delay between transmission of a signal and the reflection of the signal from the ground. A radar altimeter has an inherent accuracy of 25 - 100 feet (15:3-45); however, an unattractive feature of the radar altimeter for use with an INS is that vertical distance is given relative to the surface topography rather than the reference ellipsoid. The direct use of the radar altimeter will not stabilize the vertical INS channel because the radar altimeter errors are not related to the vertical channel INS errors. The radar altimeter "raw" measurements produce a high frequency signal of varying amplitude due to the roughness of the terrain. This high frequency data is usable by the INS but has poor quality for vertical channel damping. The radar altimeter is primarily used for landing, terminal guidance, or as a terrain mapping aid. The radar altimeter used in this study is used as part of the terrain correlation system.

The dominant errors for the radar altimeter are instrument biases and scale factor variation. Another potentially large error source is from interference effects due to terrain irregularities. In addition, the time distribution of the returned signals within the beam pattern

cause the generation of an average for the terrain height over the beam area.

The simplified error model (15:3-46) which accounts for the scale factor errors and bias is given below:

$$\dot{\gamma} = 0 \quad (3-19)$$

where:

$\gamma$  is the scale factor error

$$\dot{\delta h}_{zo} = 0 \quad (3-20)$$

where:

$\delta h_{zo}$  is the zero offset error

These errors are then combined into the total radar altimeter error model in the following equation:

$$\delta h_{RA} = \gamma h_{gn} + \delta h_{zo} \quad (3-21)$$

where,

$\delta h_{RA}$  is the total error

$h_{gn}$  = altitude above ground

$\gamma$  and  $\delta h_{zo}$  were previously defined.

The measurement process is given by the following equation:

$$h_{MEAS} = h_{TRUE} + \delta h_{RA} + v_{ra} \quad (3-22)$$

where:

$v$  represents zero-mean, white Gaussian measurement noise.

Since this particular error model does not have any noise added to account for measurement uncertainty, a pseudonoise will be added to account for finite word length and roundoff errors associated with the airborne computer. It is also needed to prevent filter divergence.

#### Map Correlator

Map correlation techniques involve the comparison of real-time measurements of earth surface properties with a computer stored map. A position-fix is then made when an "in-tolerance" match is made between the measurement data and the map. The actual measurement may be "active" (e.g., radar) or "passive" (resulting from natural phenomena). For this study, the radar altimeter is used as a measurement device.

The actual measurement process utilizes measurements from the radar altimeter and the baro-altimeter to provide a vehicle altitude reference above the terrain. The irregular features of the terrain generates a topographic signature which is then compared to the prestored map.

The error modeling for this terrain correlator is accomplished by assuming errors are appropriately tracked as random walks for the three position error states with the appropriate initial conditions (45). The model for terrain correlation errors is given in the following equations:

$$\dot{\delta E} = w_e \quad (3-23)$$

$$\dot{\delta N} = w_N \quad (3-24)$$

$$\dot{\delta A} = w_Z \quad (3-25)$$

where,

$\delta E, \delta N, \delta A$  are the terrain correlation errors for east, north, and vertical position.

$w_{e,n,z}$  are white noise processes.

where:

$$E[w] = 0, \quad E[w(t)w(t+\tau)] = Q\delta(\tau) \quad (3-26)$$

The strength of the white noise process,  $Q$ , is computed based on the maximum error in velocity in the three coordinates.

The equation for  $Q$  is:

$$Q = (\delta V_E, \delta V_N, \delta V_{Z,max})^2 / ((21 \text{ min}) (60 \text{ sec/min})) \quad (3-27)$$

where:

$\delta V_E, \delta V_N, \delta V_{Z,max}$  represents the maximum velocity error

21 minutes represents the time to quarter wavelength of the Schuler frequency.

The measurement process for this error model is:

$$E_{MEAS} = E_{TRUE} + \delta E + v_{ce} \quad (3-28)$$

$$N_{MEAS} = N_{TRUE} + \delta N + v_{cn} \quad (3-29)$$

$$A_{MEAS} = A_{TRUE} + \delta A + v_{ca} \quad (3-30)$$



where:

$v$  represents zero-mean, white Gaussian noise.

### Satellite Position System

The satellite positioning system is typically modeled based on a four satellite measurement scenario. Range and range rate error information is derived from a pseudo-range measurement (from the satellites), and an estimated pseudo-range computed from the INS-indicated position, and the satellites' position and motion. The observed range and range rate errors are a measure of the user's position, velocity, and clock errors. Clock errors are transformed to distance and velocity by multiplying the clock phase error and frequency error by the speed of light.

Typically, errors in both satellite ephemerides and clock errors will constitute the modeled errors for the measurement process. Since satellite clock synchronization errors and transmitted navigation data errors (transmitted periodically from ground stations to the satellites) are assumed negligible when compared to errors from the user's clock, only user clock errors will be modeled in this study. The clock errors are also not affected by coordinate frame transformation since the errors are not peculiar to any particular orientation of the receiver (15:4-54). Satellites are always assumed chosen such that resulting even ellipsoid in GPS position information is essentially spherical.

The filter error model for the satellite positioning system (9:53) is given in the equations below:

$$\dot{\delta t}_u = w_1 \quad (3-31)$$

where,

$\delta t_u$  = clock phase error

$w_1$  = white noise process

$$E [w_1] = 0, \quad E [w_1(t) w_1(t + \tau)] = Q \delta(\tau) \quad (3-32)$$

$$Q = 1 \text{ ft}^2/\text{sec} \quad (3-33)$$

$$\ddot{\delta t}_{Ru} = (-1/T) \dot{\delta t}_{Ru} + w_2 \quad (3-34)$$

where,

$\dot{\delta t}_{Ru}$  = clock frequency error

$T = 7200$  seconds

$w_2$  = white noise process

$$E [w_2] = 0 \quad E [w_2(t) w_2(t + \tau)] = Q \delta(\tau)$$

$$Q = 2\sigma^2/T = 2(10 \text{ ft/sec})^2/7200 \text{ sec} = .028 \text{ ft}^2/\text{sec}^3 \quad (3-35)$$

As can be seen from Eq (73), the position error is modeled as a random walk with the appropriate initial condition and covariance. The velocity error is modeled as a first-order Gauss-Markov process.

The measurement process is modeled as:

$$V_{e(\text{meas})} = V_{e(\text{true})} + \dot{\delta t}_{Ru} + v_{ve} \quad (3-36)$$

$$V_n(\text{meas}) = V_N(\text{true}) + \delta \dot{t}_{Ru} + v_{vn} \quad (3-37)$$

$$V_z(\text{meas}) = V_z(\text{true}) + \delta \dot{t}_{Ru} + v_{vz} \quad (3-38)$$

and,

$$E_{\text{MEAS}} = E_{\text{TRUE}} + \delta t_u + v_e \quad (3-39)$$

$$N_{\text{MEAS}} = N_{\text{TRUE}} + \delta t_u + v_n \quad (3-40)$$

$$Z_{\text{MEAS}} = Z_{\text{TRUE}} + \delta t_u + v_z \quad (3-41)$$

The filter model is summarized in Table VI. The standard deviations of the states are based on the initial conditions for the truth model. These standard deviations represent the filter's own measure of its estimation uncertainty. These values are identical to the initial conditions seen in Table II except for states 24-26. The increased standard deviations are primarily due to the lower dimensional filter model and the increased acquisition uncertainty for the map measurement process.

#### Gyro and Accelerometer

The reduction in the number of states from the "truth" model for the basic INS to the filter model is due to the elimination of 18 gyro and accelerometer error states.

The gyro error states for misalignment and scale factor were eliminated and their error contribution was modeled as a white noise contribution to the three attitude error states in the filter.

Table VI  
The Filter Error Model

| State Variable  | Initial Condition<br>(Standard Deviation) |
|---|---|
| <u>Basic Inertial Navigation Errors</u>                           |   |
| The 9-state model is identical to the "truth" model               | same as "truth" model                     |
| <u>Vertical Channel Error Variable</u>                            |   |
| 10. $\delta \hat{a}$ vertical acceleration error                  | .006 ft <sup>2</sup> /sec                 |
| <u>Gyro Drift Error</u>   |   |
| 11. $DX_f$ X gyro drift   | .008°/hr                                  |
| 12. $DY_f$ Y gyro drift   | .008°/hr                                  |
| 13. $DZ_f$ Z gyro drift   | .008°/hr                                  |
| <u>Accelerometer Bias</u>   |   |
| 14. $AB_x$ X accelerometer bias                                   | 40μg                                      |
| 15. $AB_y$ Y accelerometer bias                                   | 40μg                                      |
| 16. $AB_z$ Z accelerometer bias                                   | 40μg                                      |
| <u>Baro-Altimeter Error</u>                                       |   |
| 17. $e_{po}$ variation in altitude of a constant pressure surface | 500 ft                                    |

Table VI (cont'd)

| State Variable  | Initial Condition<br>(Standard Deviation) |
|---|---|
| <u>Satellite Positioning Error</u>                        |   |
| 18. $\delta t_u$ clock phase error                        | 1500 ft                                   |
| 19. $\delta \dot{t}_{Ru}$ clock frequency bias            | 15 ft/sec                                 |
| <u>Doppler Radar System Error</u>                         |   |
| 20. $b_\lambda$ along-track beam error                    | 1.75 arc min                              |
| 21. $\delta V_{s_\lambda}$ along-track scale factor error | .4 ft/sec                                 |
| <u>Radar Altimeter System Error</u>                       |   |
| 22. $\delta h_{zo}$ zero offset error                     | 2.5 ft                                    |
| 23. $\gamma$ scale factor error                           | .045                                      |
| <u>Terrain Correlator Errors</u>                          |   |
| 24. $\delta E$ east map error                             | 500 ft                                    |
| 25. $\delta N$ north map error                            | 300 ft                                    |
| 26. $\delta A$ altitude error                             | 100 ft                                    |

The accelerometer states for misalignment and scale factor error were handled in the same manner as the gyro error states except that the noise contributions were added to the filter's velocity states.

Initial noise strengths for the velocity and attitude states were calculated by taking the initial covariance,  $P_0$ , of the unmodeled gyro and accelerometer states through a

direction cosine transformation. This transformation takes the initial covariances from the platform to the navigation frame. The noise strengths are a ~~benchmark~~  $Q$ , from which final tuning of the filter is accomplished. Final noise strengths are given in Table VII.

#### Filter Tuning

The tuning for the filter was accomplished by an iterative process. The dynamic driving noise matrix,  $Q$ , and the measurement noise matrix,  $R$ , were adjusted to provide a "tuned" filter which is usable for the entire mission (e.g., during periods of both benign and highly dynamic behavior). This type of tuning approach requires the filter to overestimate its own errors, especially in benign regions, in order to "capture" harsh dynamic behavior.

The tuning process for the terrain correlator measurements produced poor results. The longitude and latitude error states had no significant error reduction occur as a result of the measurements. Also, the terrain correlator error states, themselves, showed divergent behavior. Even after repeated attempts at adjustments of  $Q$  and  $R$ , no improvement occurred. Because of this, a 3-state "truth" model for the terrain correlator was proposed. This was a reasonable solution since a 3-state model is typical for a terrain correlator acquisition filter model. This 3-state "truth" model is identical in structure to the 3-state

Table VII  
Q Values For Filter Tuning

| Filter State                            | Q (noise strength)                     |
|---|--|
| <u>Random Walks and Pseudonoise (P)</u> |  |
| 1 Longitudinal Error (P)                | 20 ft <sup>2</sup> /sec                |
| 2 Latitude Error (P)                    | 2 ft <sup>2</sup> /sec                 |
| 3 Vertical Position Error (P)           | .025 ft <sup>2</sup> /sec              |
| 4 East Velocity Error (P)               | .025 ft <sup>2</sup> /sec <sup>3</sup> |
| 5 North Velocity Error (P)              | .025 ft <sup>2</sup> /sec <sup>3</sup> |
| 6 Vertical Velocity Error (P)           | .05 ft <sup>2</sup> /sec <sup>3</sup>  |
| 7 East Attitude Error (P)               | .001 rad <sup>2</sup> /sec             |
| 8 North Attitude Error (P)              | .001 rad <sup>2</sup> /sec             |
| 9 Vertical Attitude Error (P)           | .002 rad <sup>2</sup> /sec             |
| 11 x Gyro Drift                         | .002 deg <sup>2</sup> /hr <sup>3</sup> |
| 12 y Gyro Drift                         | .002 deg <sup>2</sup> /hr <sup>3</sup> |
| 13 z Gyro Drift                         | .002 deg <sup>2</sup> /hr <sup>3</sup> |
| 14 X Accelerometer Bias                 | 3 μg <sup>2</sup> /hr                  |
| 15 Y Accelerometer Bias                 | 3 μg <sup>2</sup> /hr                  |
| 16 Z Accelerometer Bias                 | 3 μg <sup>2</sup> /hr                  |
| 18 Satellite Clock Phase Error          | 40000 ft <sup>2</sup> /sec             |
| 24 East Terrain Correlator Error        | 50 ft <sup>2</sup> /sec                |
| 25 North Terrain Correlator Error       | 50 ft <sup>2</sup> /sec                |
| 26 Vertical Terrain Correlator Error    | 10 ft <sup>2</sup> /sec                |

Table VII (cont'd)  
Q Values For Filter Tuning

| First Order Markov Processes ( $\dot{x}=Bx+w$ ) $N=2B \sigma^2$ |                               |                                   |  |
|---|-------------------------------|-----------------------------------|--|
|   | <u>Filter State</u>           | <u><math>1\sigma</math> value</u> | <u>Inverse<br/>Correlation Time(B)</u> |
| 17  | Barometric<br>Altimeter Error | 500 ft                            | $V/(500nm)$                            |
| 19  | Clock Frequency<br>Error      | 10 ft/sec                         | $1/(7200 \text{ sec})$                 |
| 21  | Doppler Scale<br>Factor Error | .3 ft/sec                         | $1/(900 \text{ sec})$                  |



filter model. Initial conditions for the "truth" model are identical to the filter's.

During the retuning of this new terrain correlator truth model and the subsequent measurement simulation, a divergent condition still existed in the longitudinal and latitude error states. This was eliminated by adding a "pseudonoise" to these states. This added uncertainty in the positional error states, in effect, allowed the benefits of the external aiding device (the terrain correlator), to improve the knowledge of the positional error states and generated a convergent or bounded filter.

The final Q values for the filter are shown in Table VII. The results of the tuning are shown in Figures 3.1 thru 3.26. These figures are plotted for the true mean  $\pm$  one sigma, superimposed on the filter-computed  $\pm$  one sigma (- - -). The measurement process begins at 360 seconds.

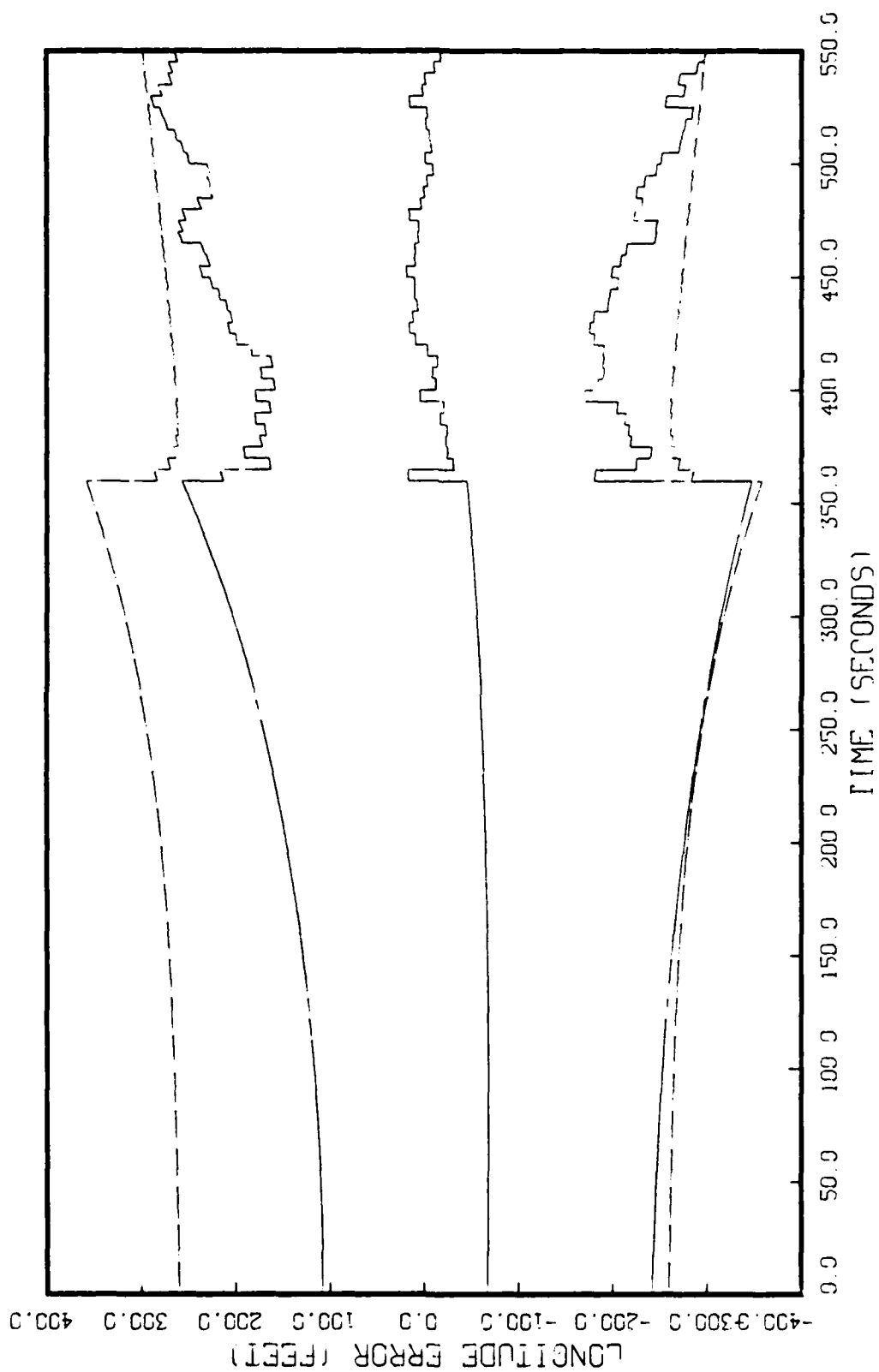


Fig. 3.1. Longitude Error For Satellite Measurement

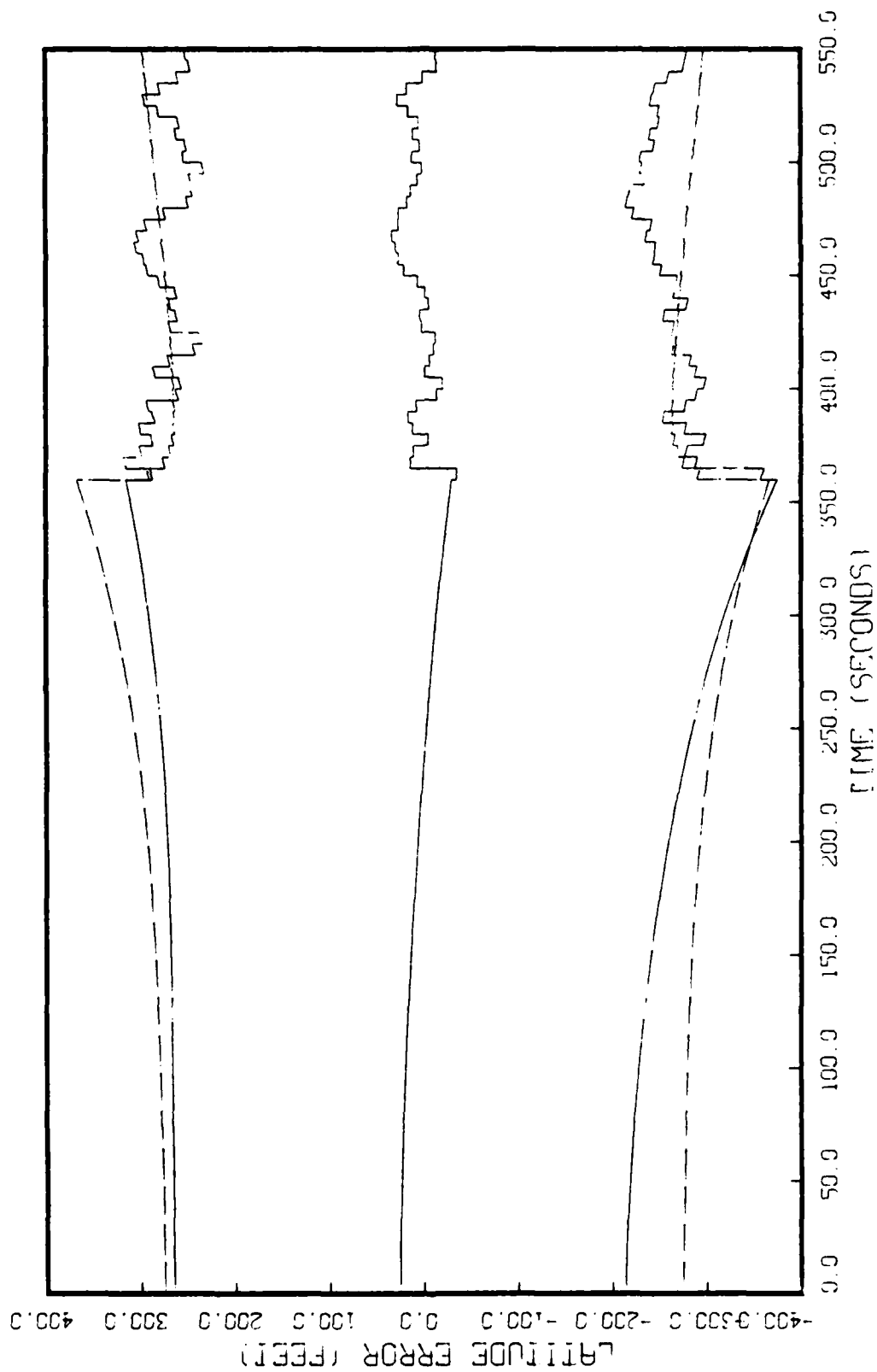


Fig. 3.2. Latitude Error For Satellite Measurement

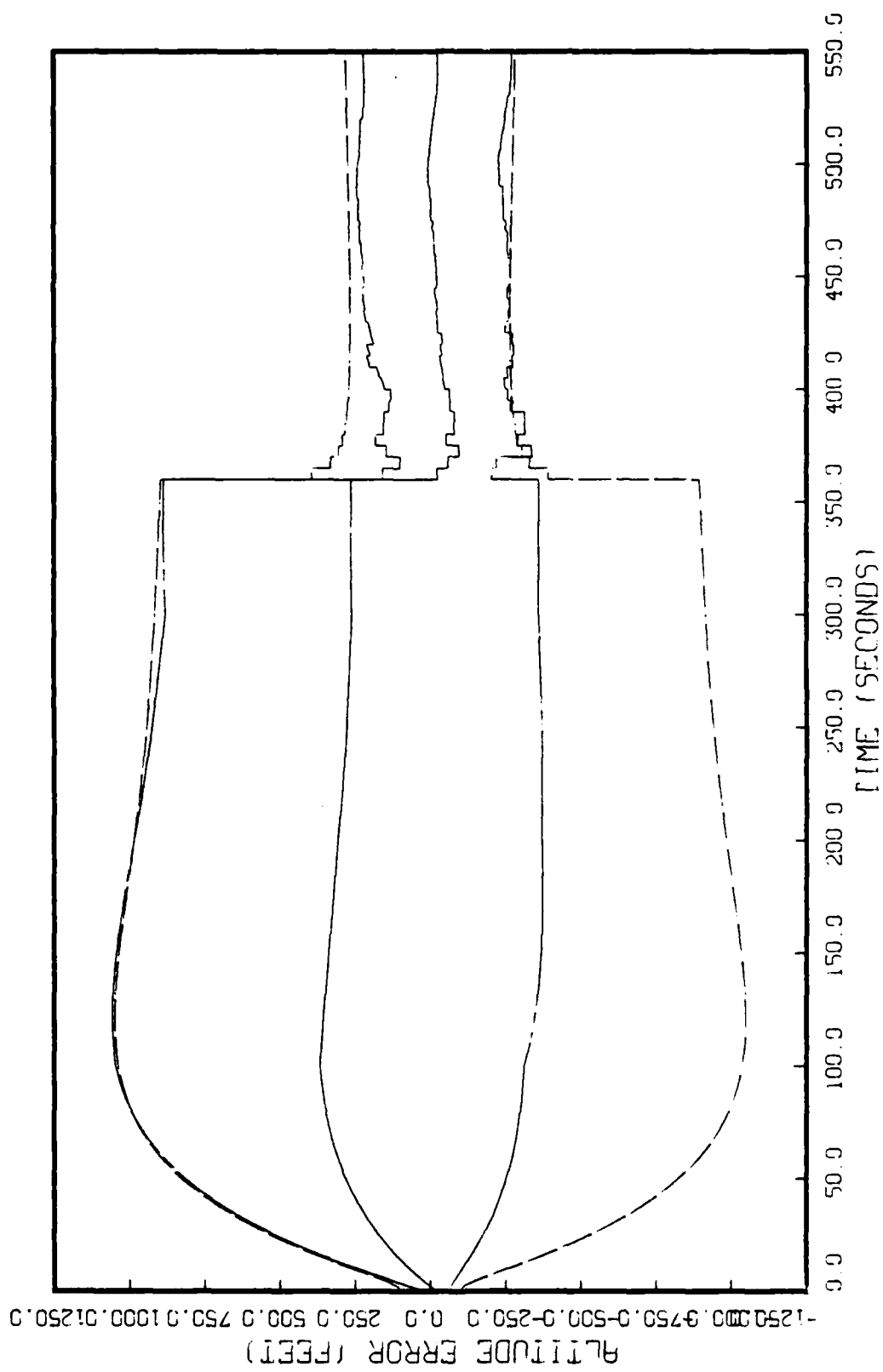


fig. 3.3. Altitude Error For Satellite Measurement

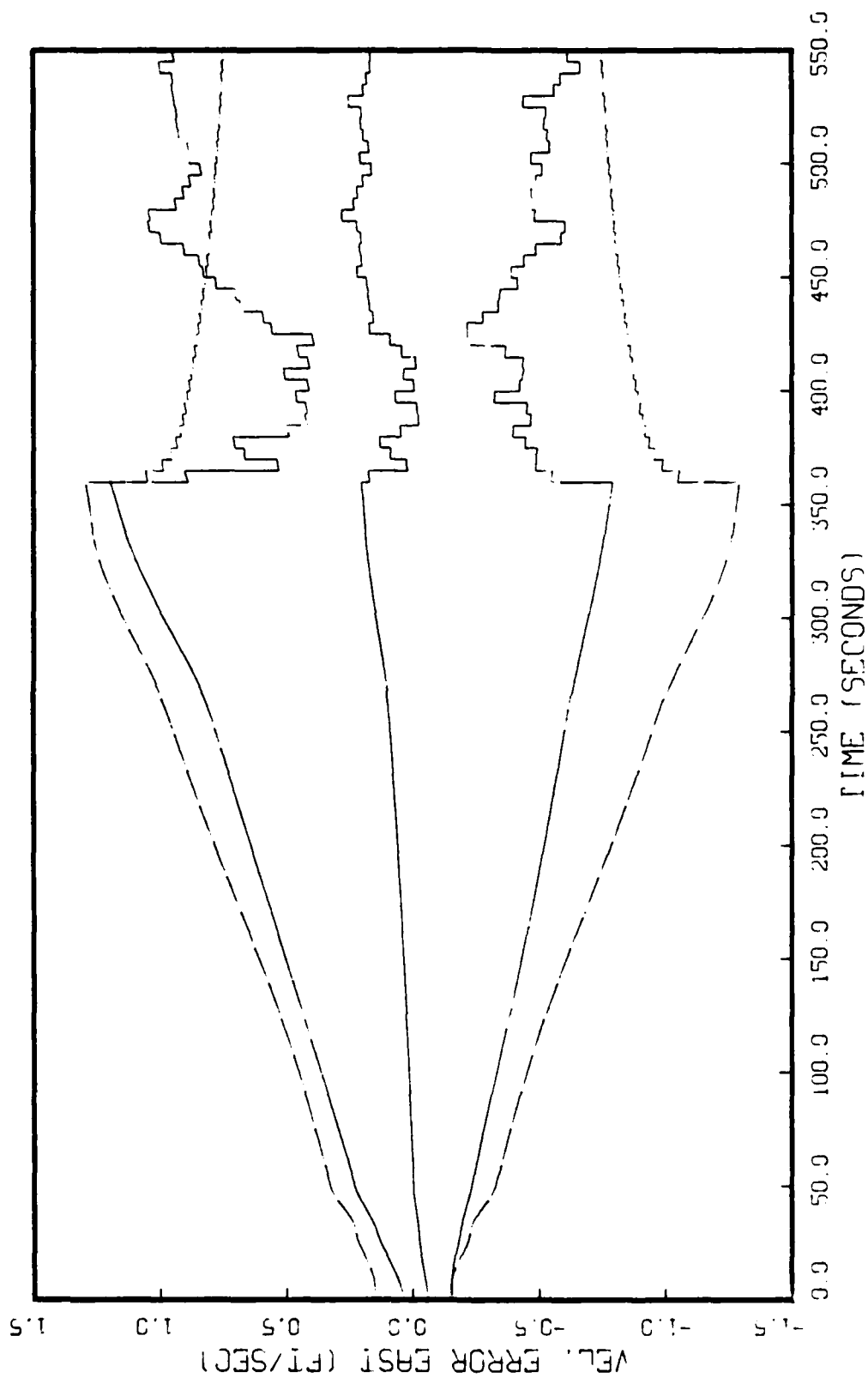


Fig. 3.4. East Velocity Error For Satellite Measurement

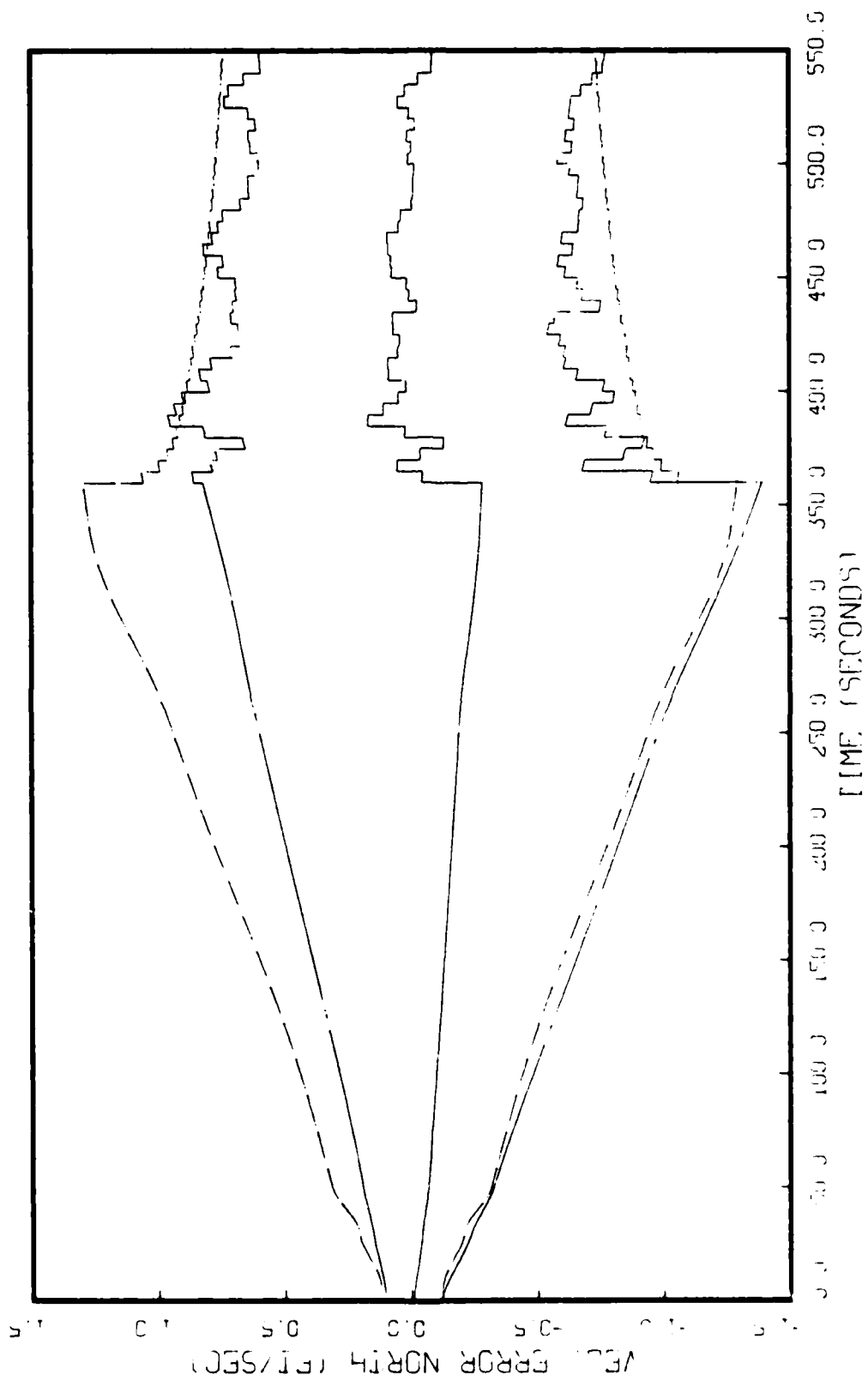


Fig. 3.5. North Velocity Error for Satellite Measurement

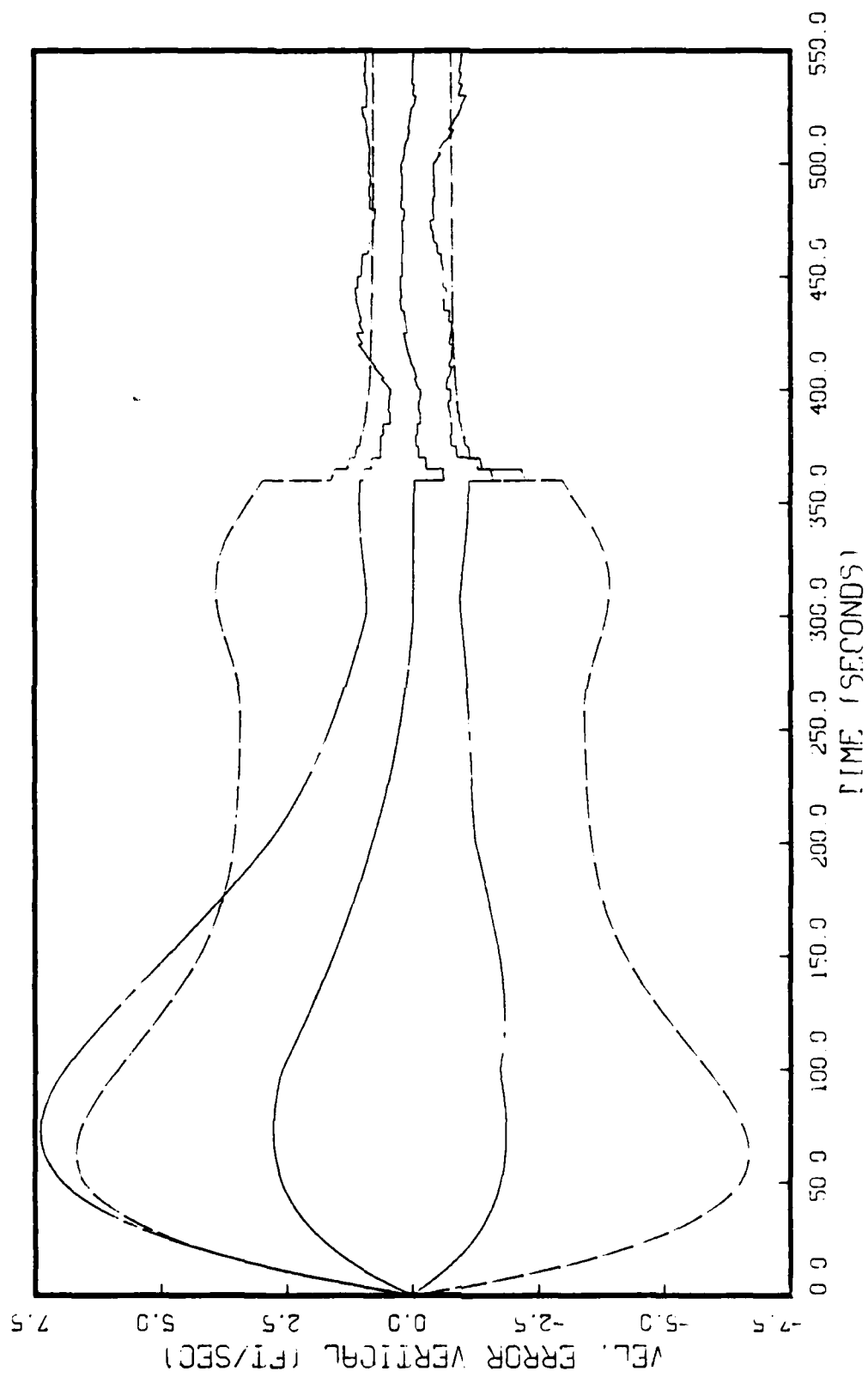


Fig. 3.6. Vertical Velocity Error For Satellite Measurement

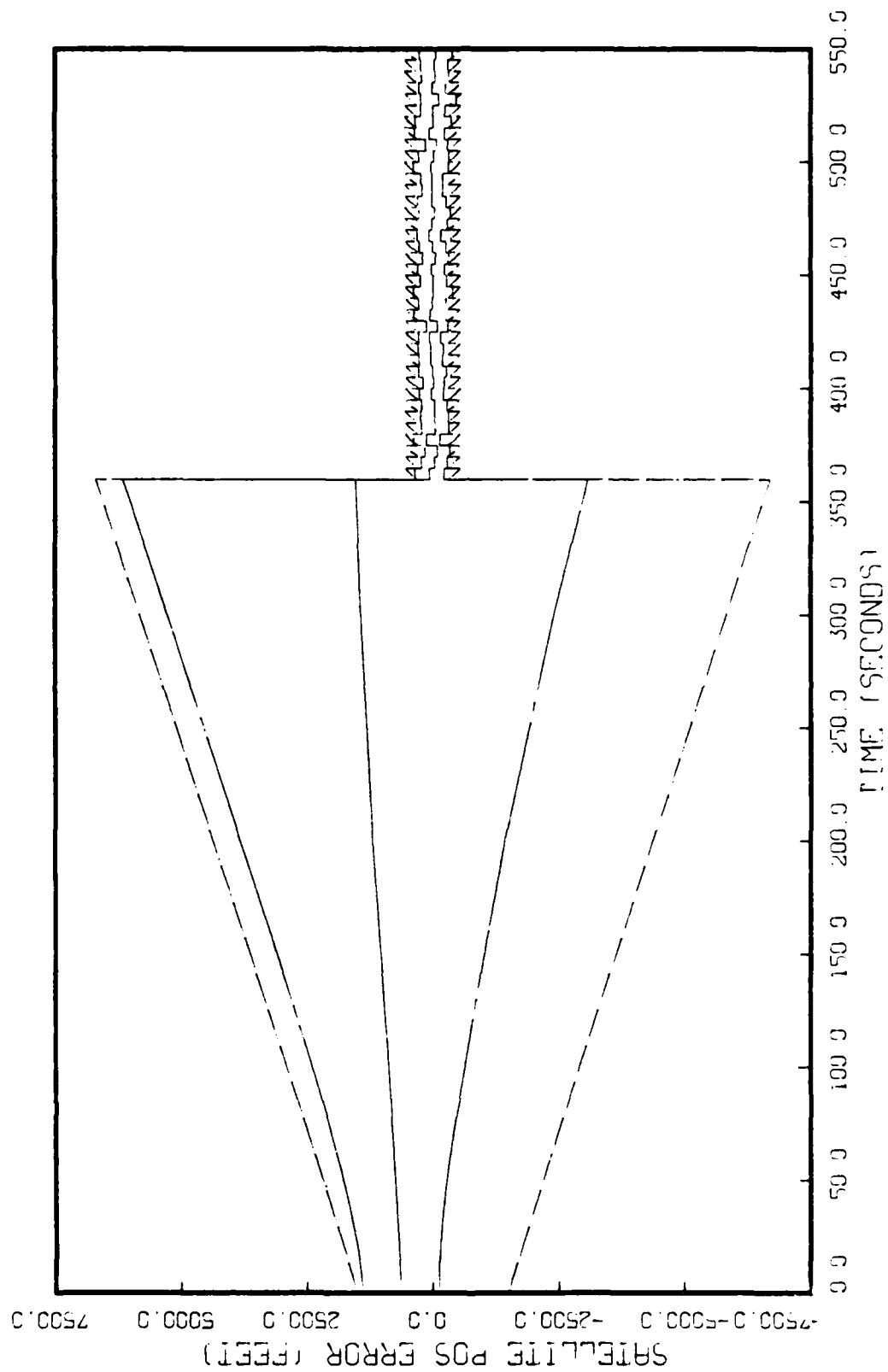


Fig. 3.7. Satellite Position Error For Satellite Measurement



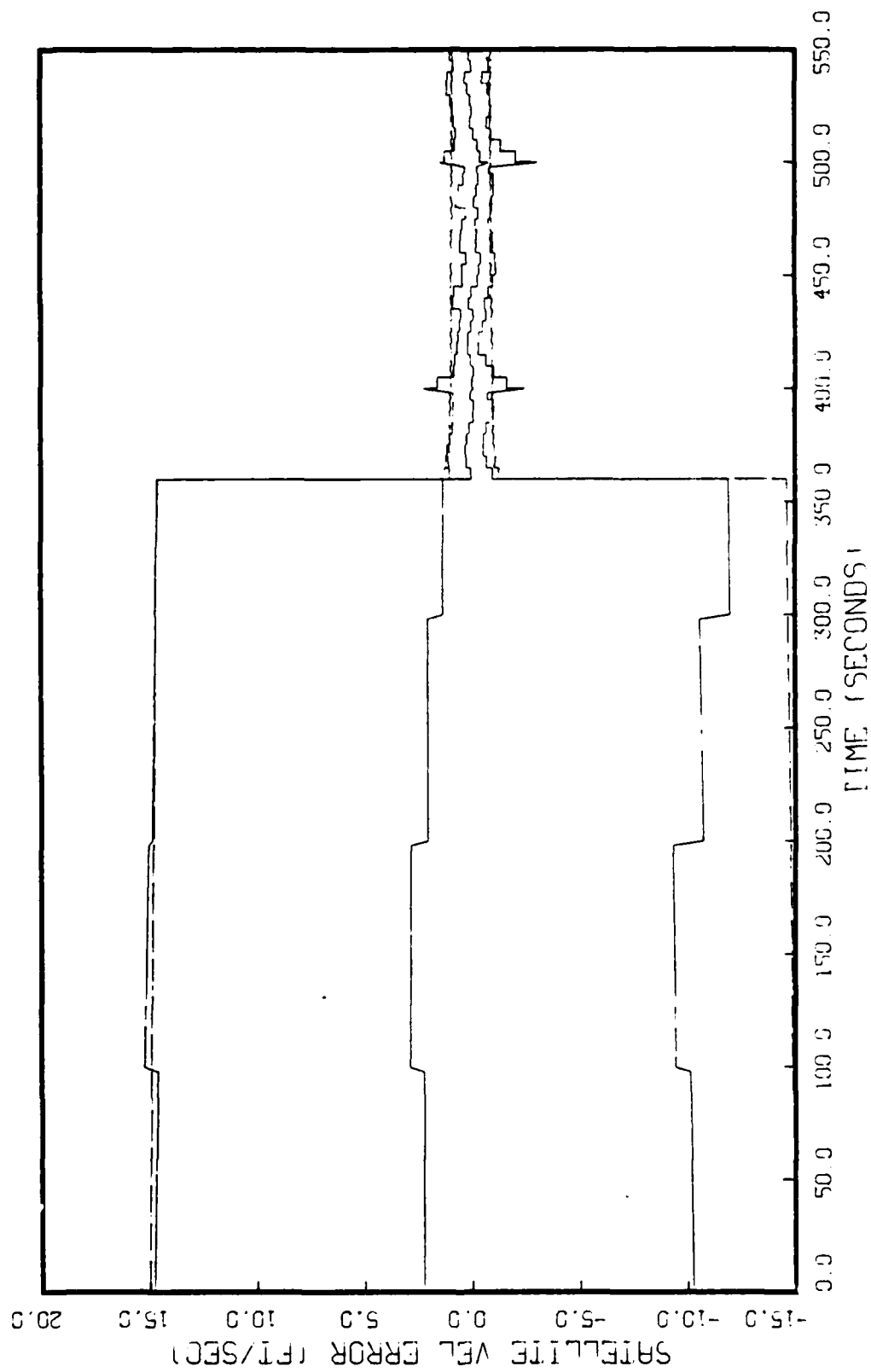


Fig. 3.8. Satellite Velocity Error for Satellite Measurement

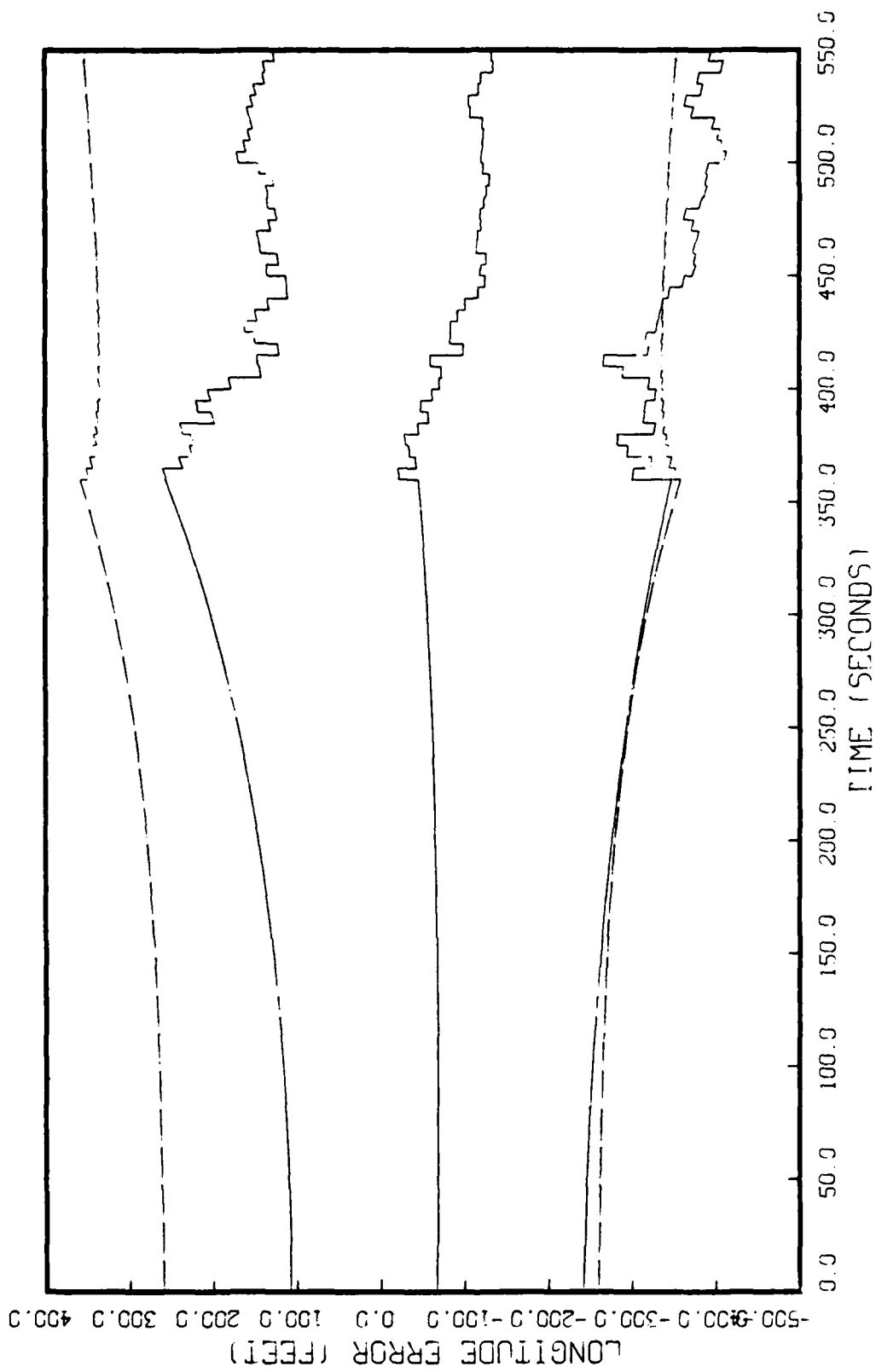


Fig. 3.9. Longitude Error For Doppler Measurement

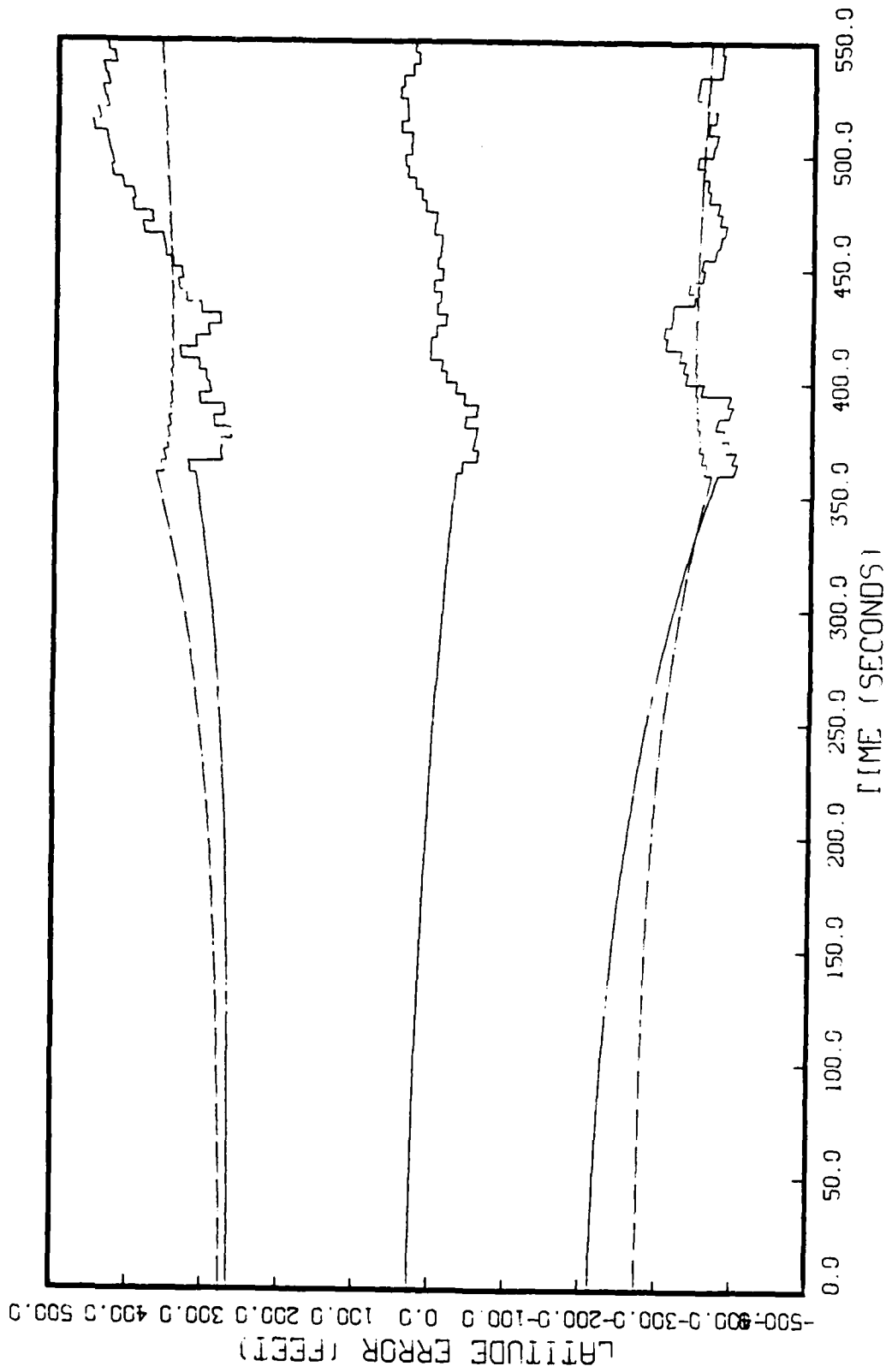


Fig. 3.10. Latitude Error For Doppler Measurement

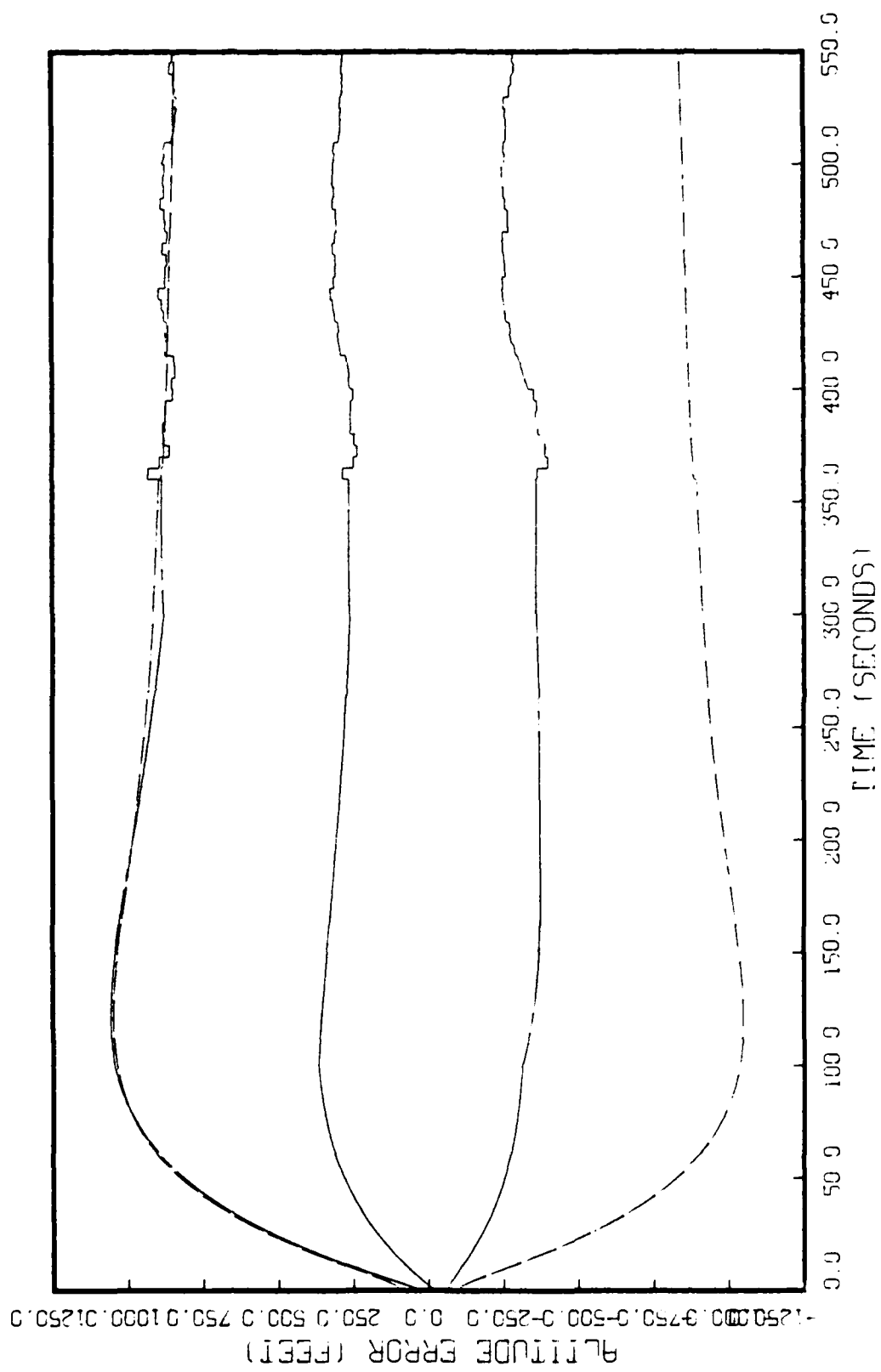


Fig. 3.11. Altitude Error For Doppler Measurement

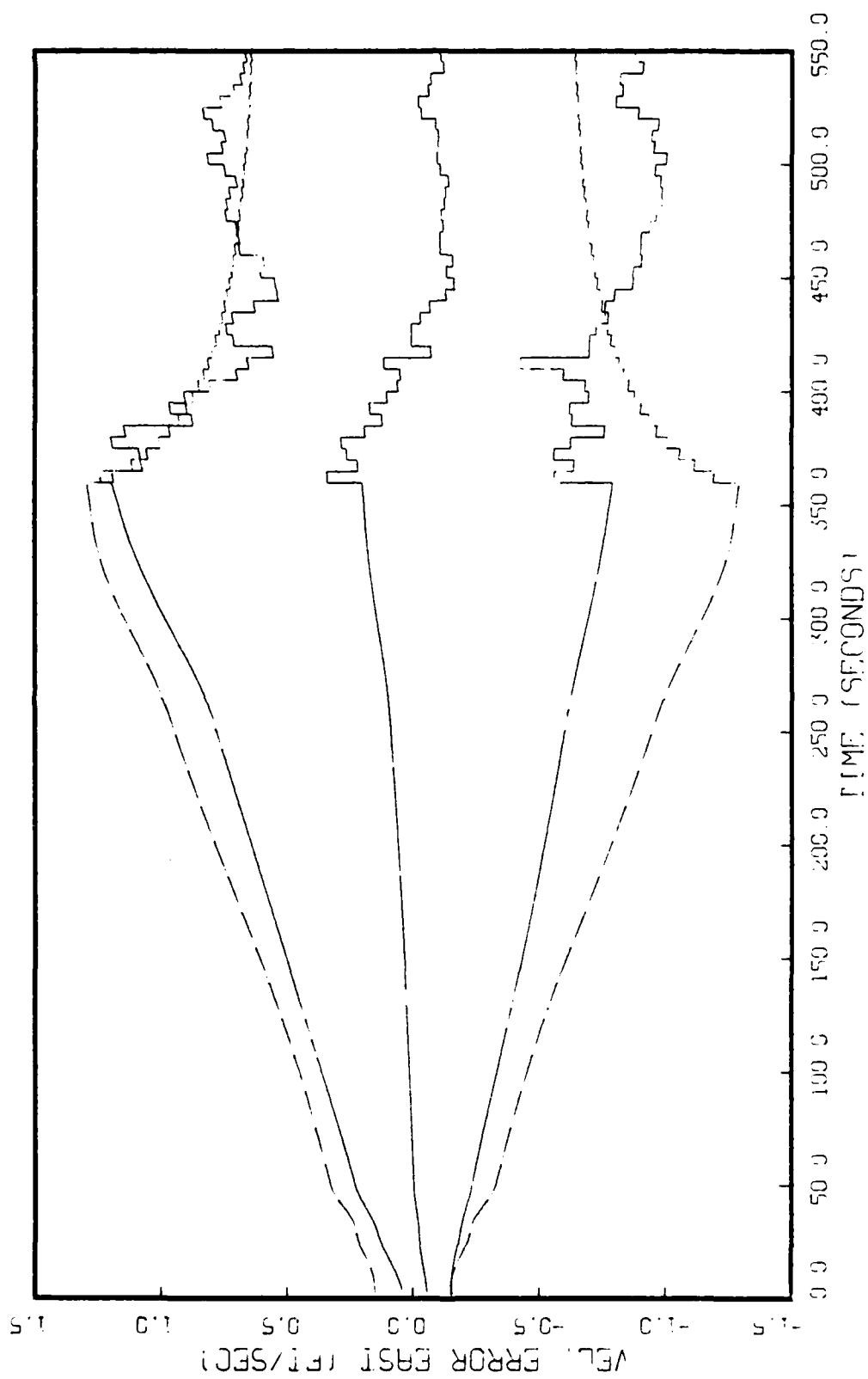


Fig. 3.12. East Velocity Error For Doppler measurement

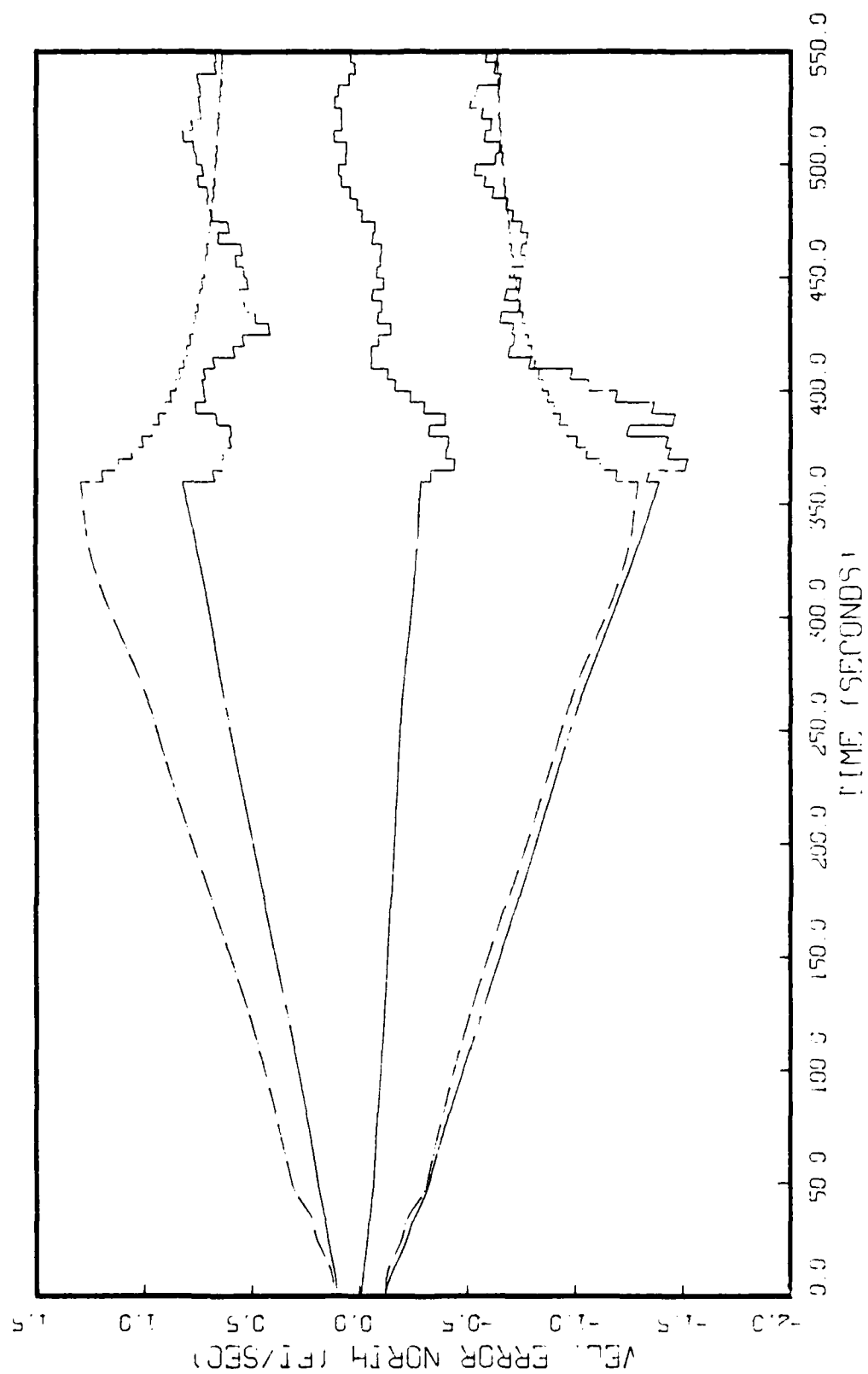


Fig. 3.13. North Velocity Error For Doppler Measurement

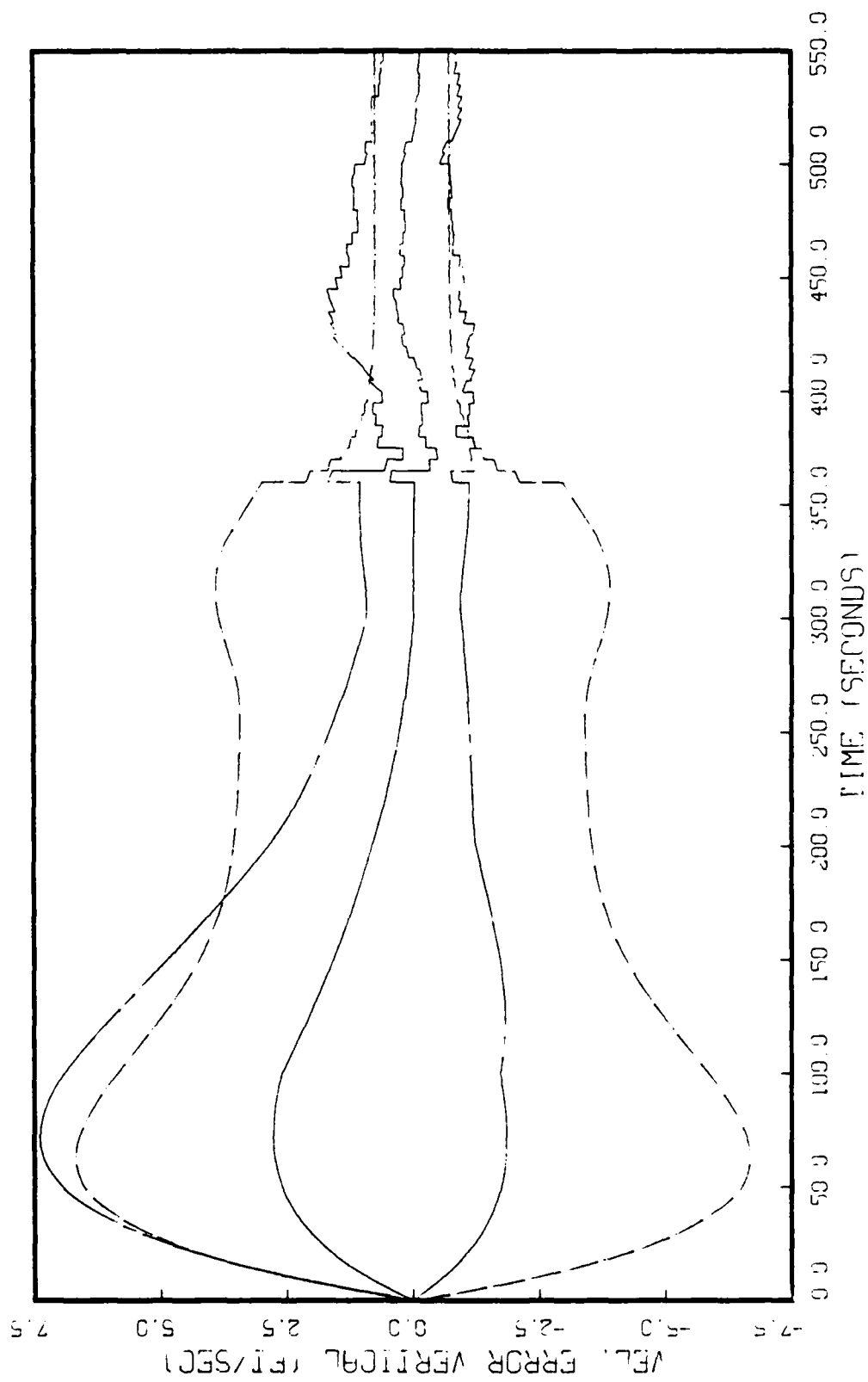


Fig. 3.14. Vertical Velocity Error For Doppler Measurement

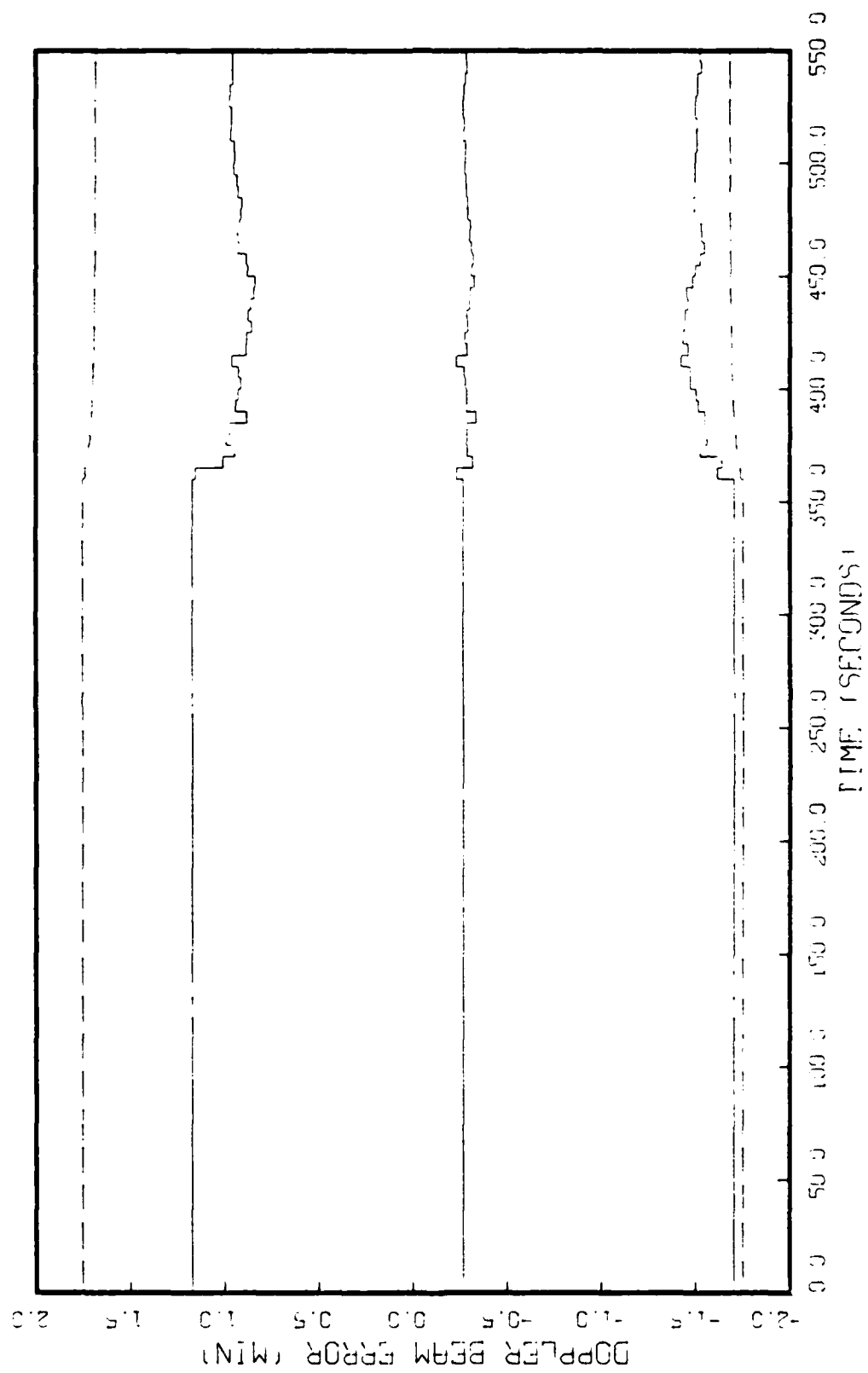


Fig. 3.15. Doppler Beam Error For Doppler Measurement



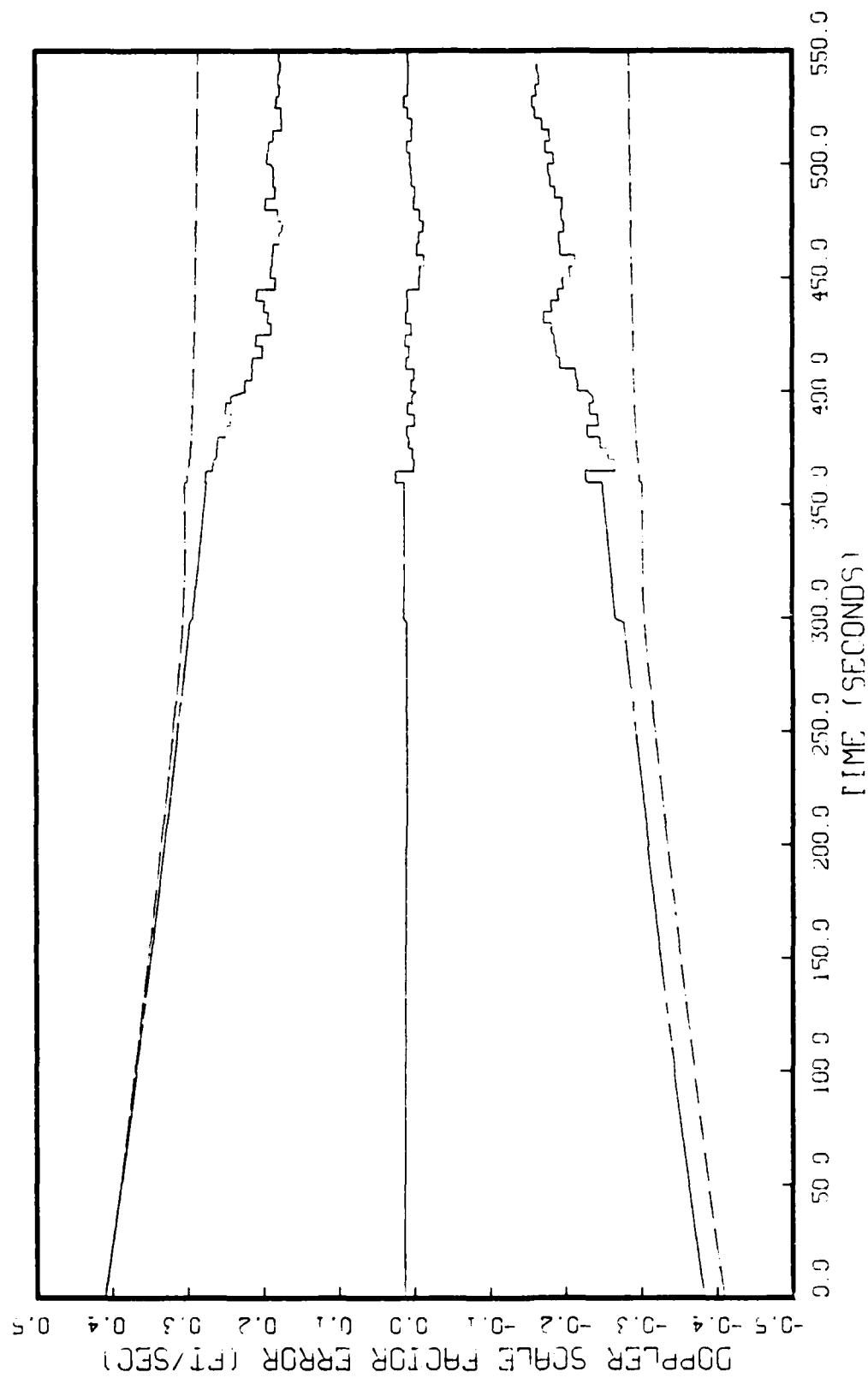


Fig. 3.16. Doppler Scale Factor Error For Doppler Measurement

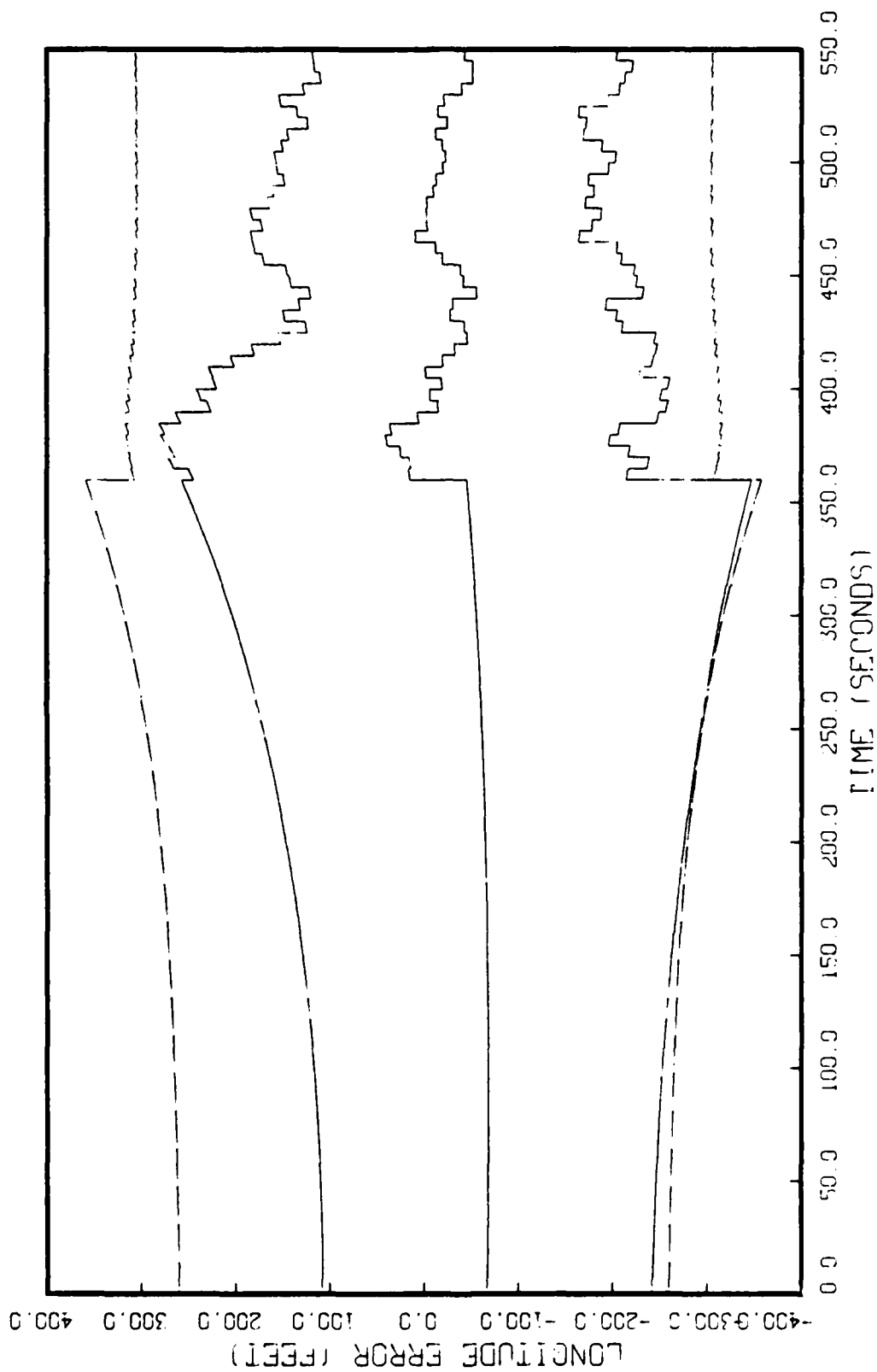


Fig. 3.17. Longitude Error For Terrain Correlator Measurement

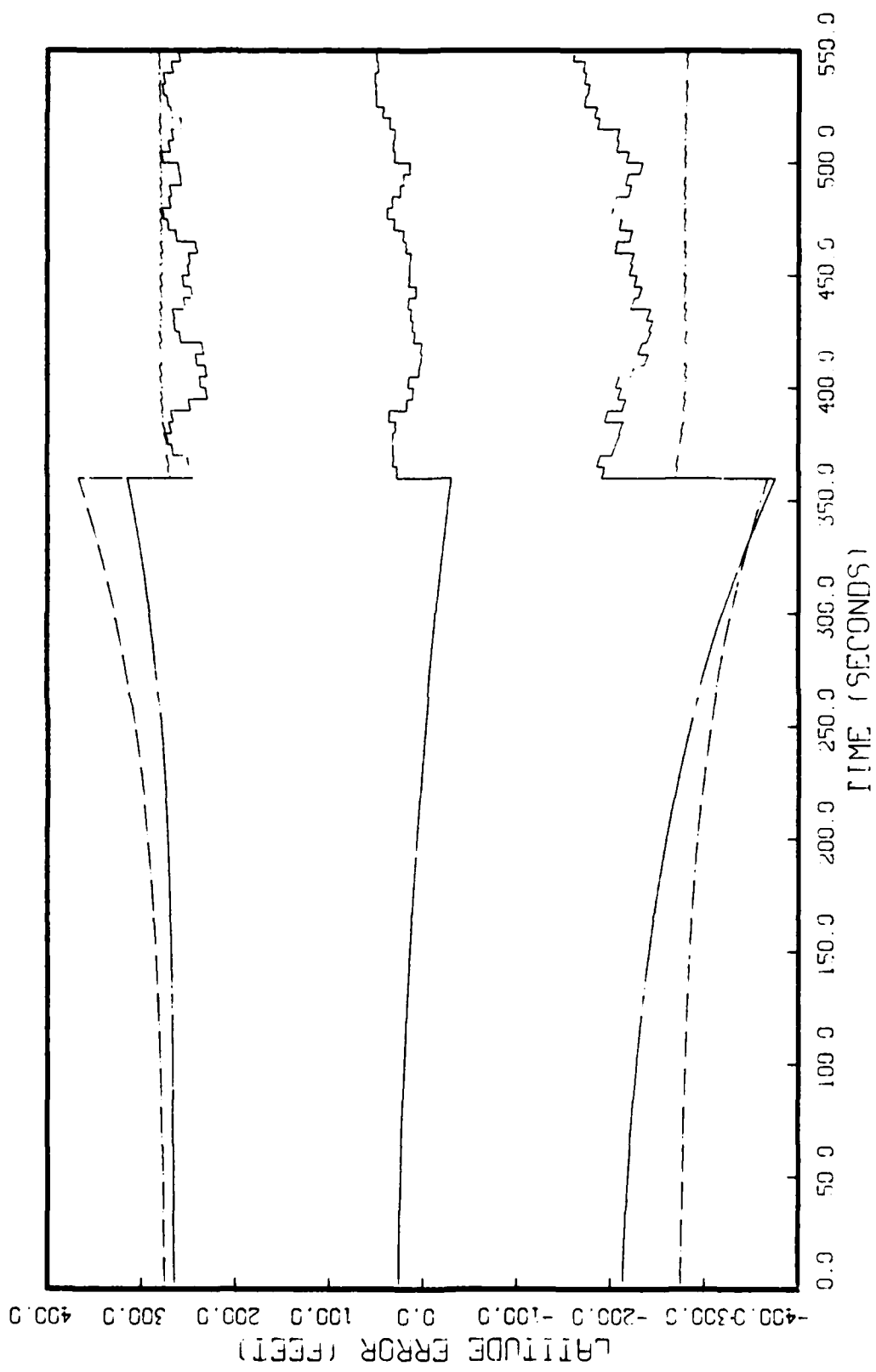


Fig. 3.18. Latitude Error For Terrain Correlator Measurement

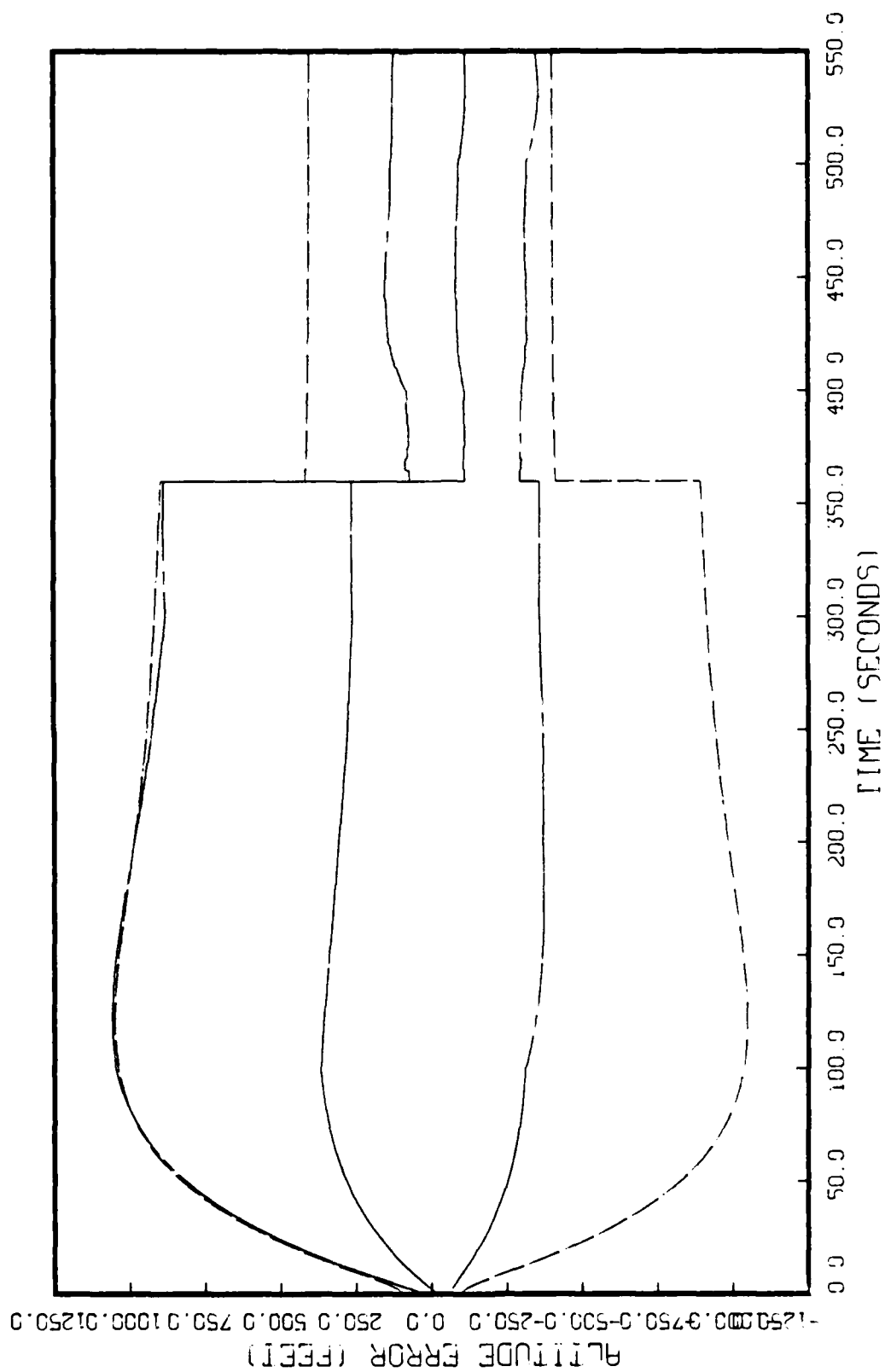


Fig. 3.19. Altitude Error For Terrain Correlator Measurement

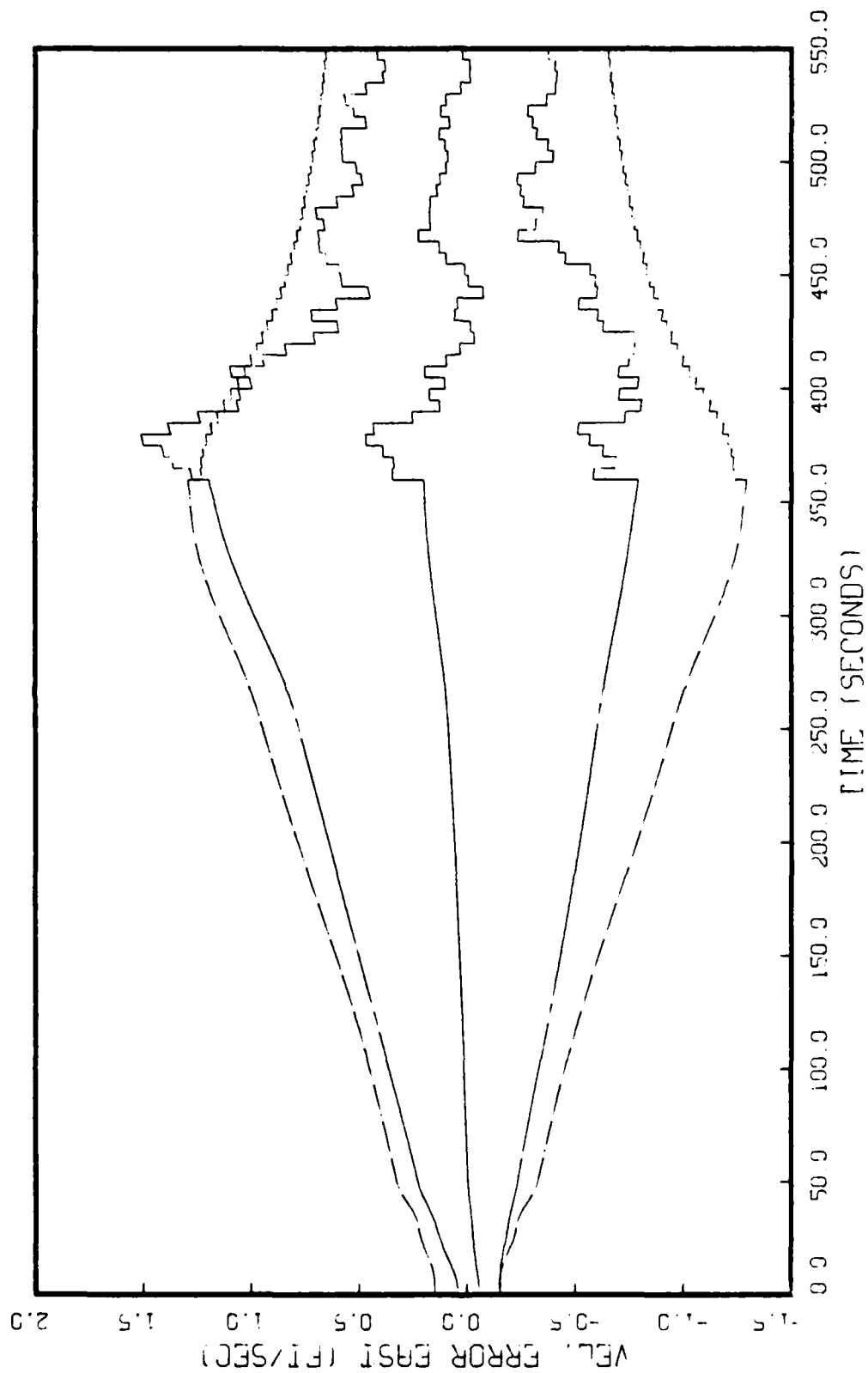


Fig. 3.20. East Velocity Error For Terrain Correlator Measurement

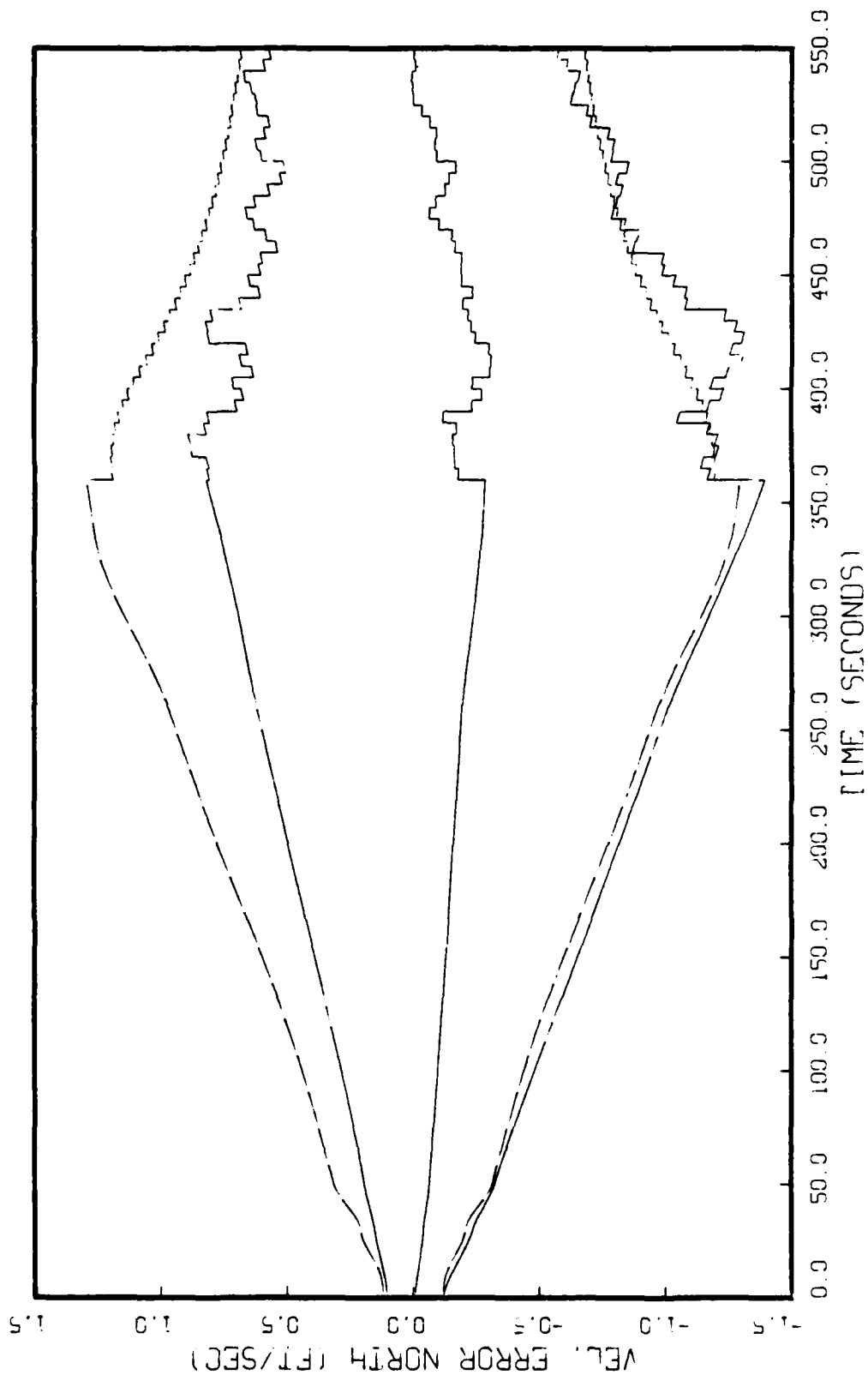


Fig. 3.21. North Velocity Error For Terrain Correlator Measurement

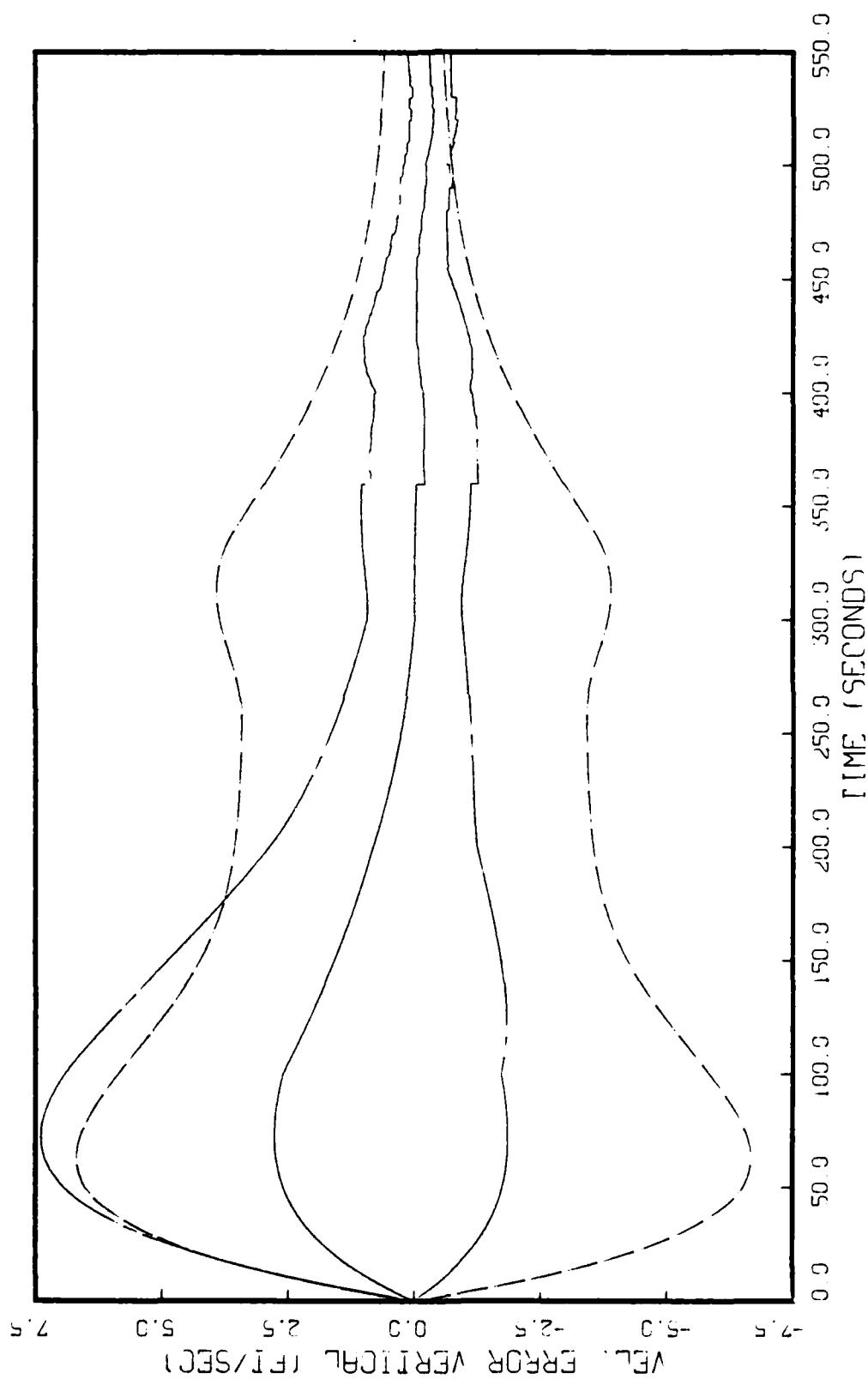


Fig. 3.22. Vertical Velocity Error For Terrain Correlator measurement

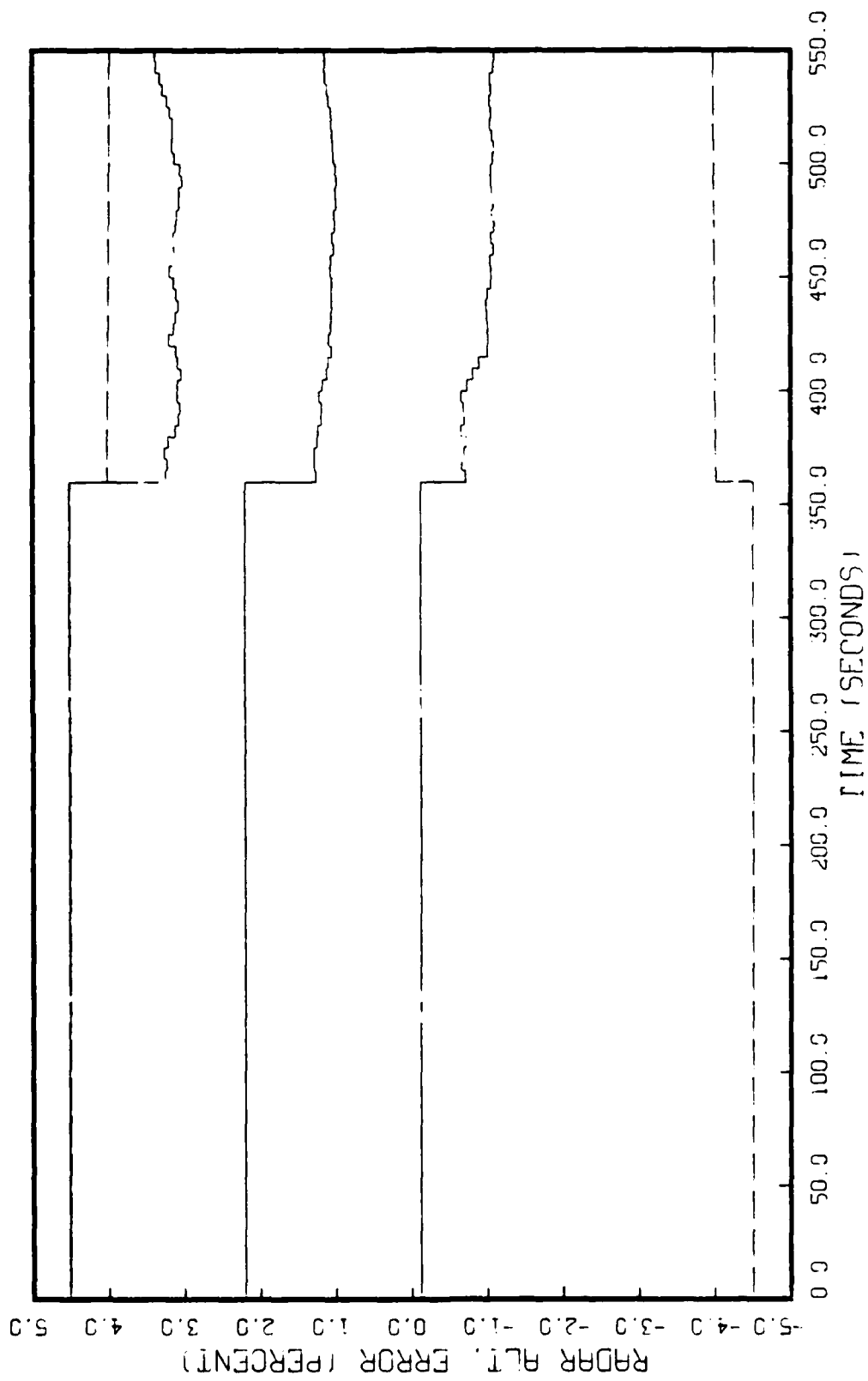


Fig. 3.23. Radar Altimeter Error For Terrain Correlator Measurement



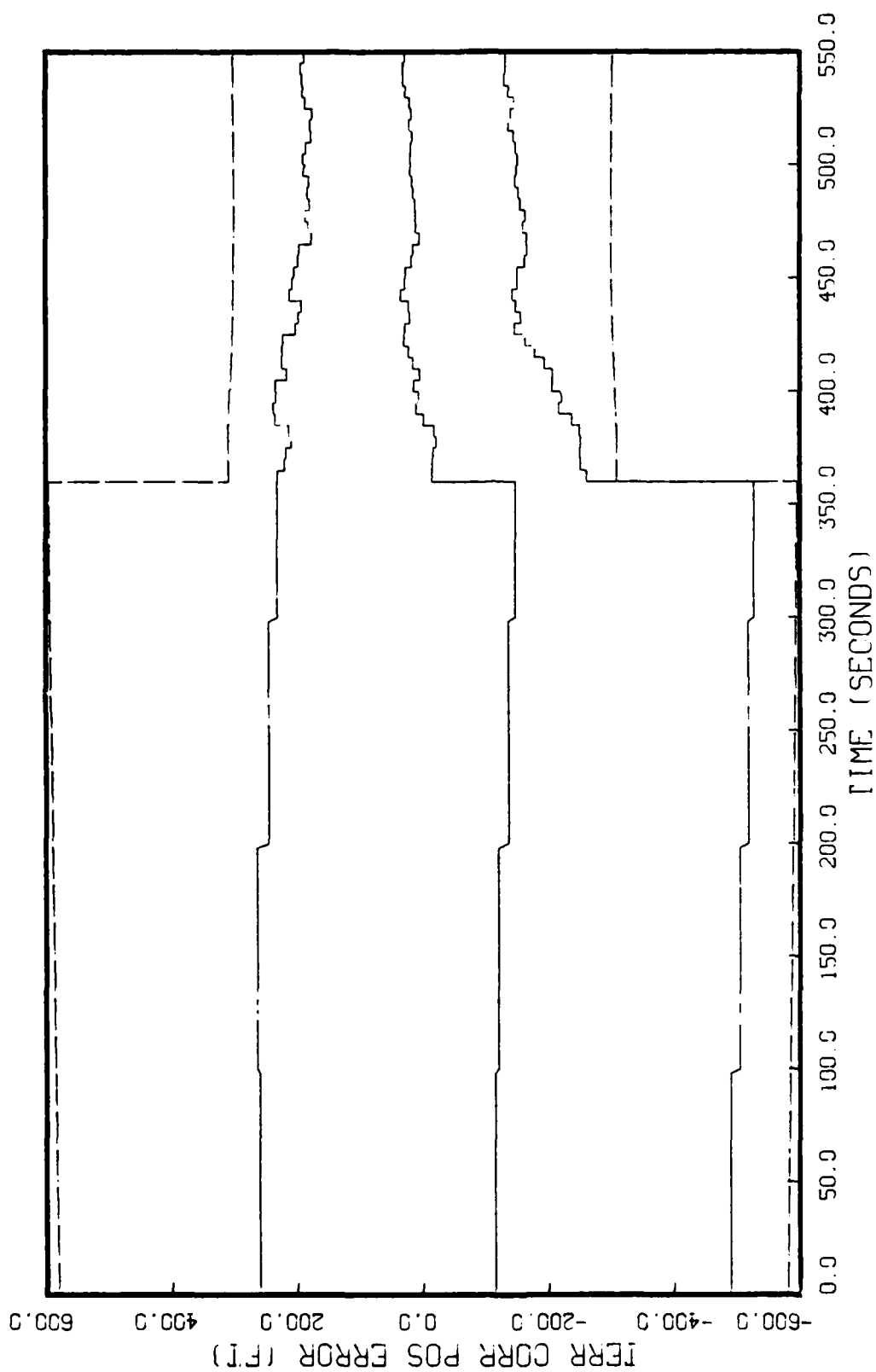


Fig. 3.24. East Terrain Correlator Position Error For Terrain Correlator Measurement

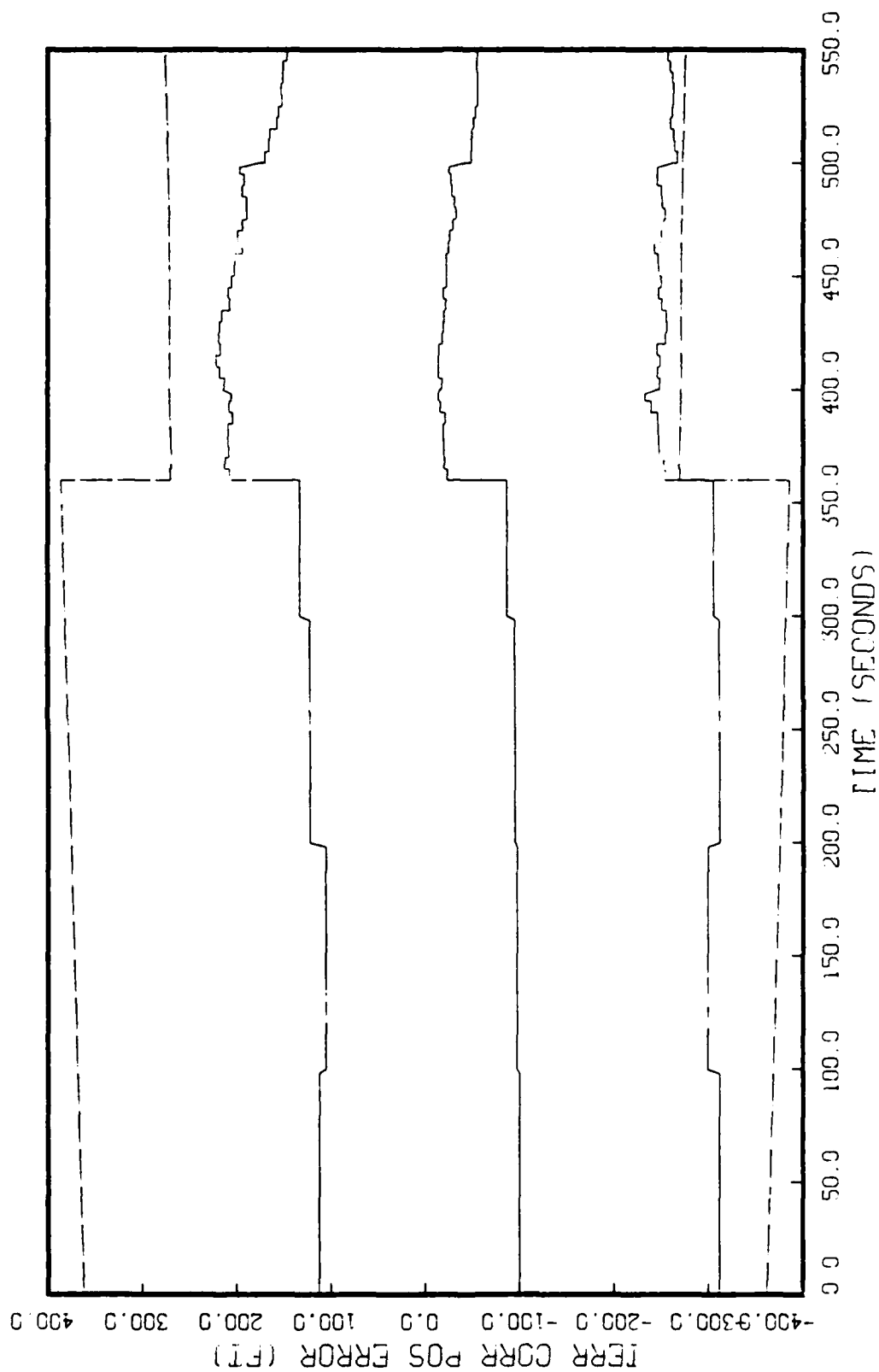


Fig. 3.25. North Terrain Correlator Position Error For Terrain Correlator Measurement

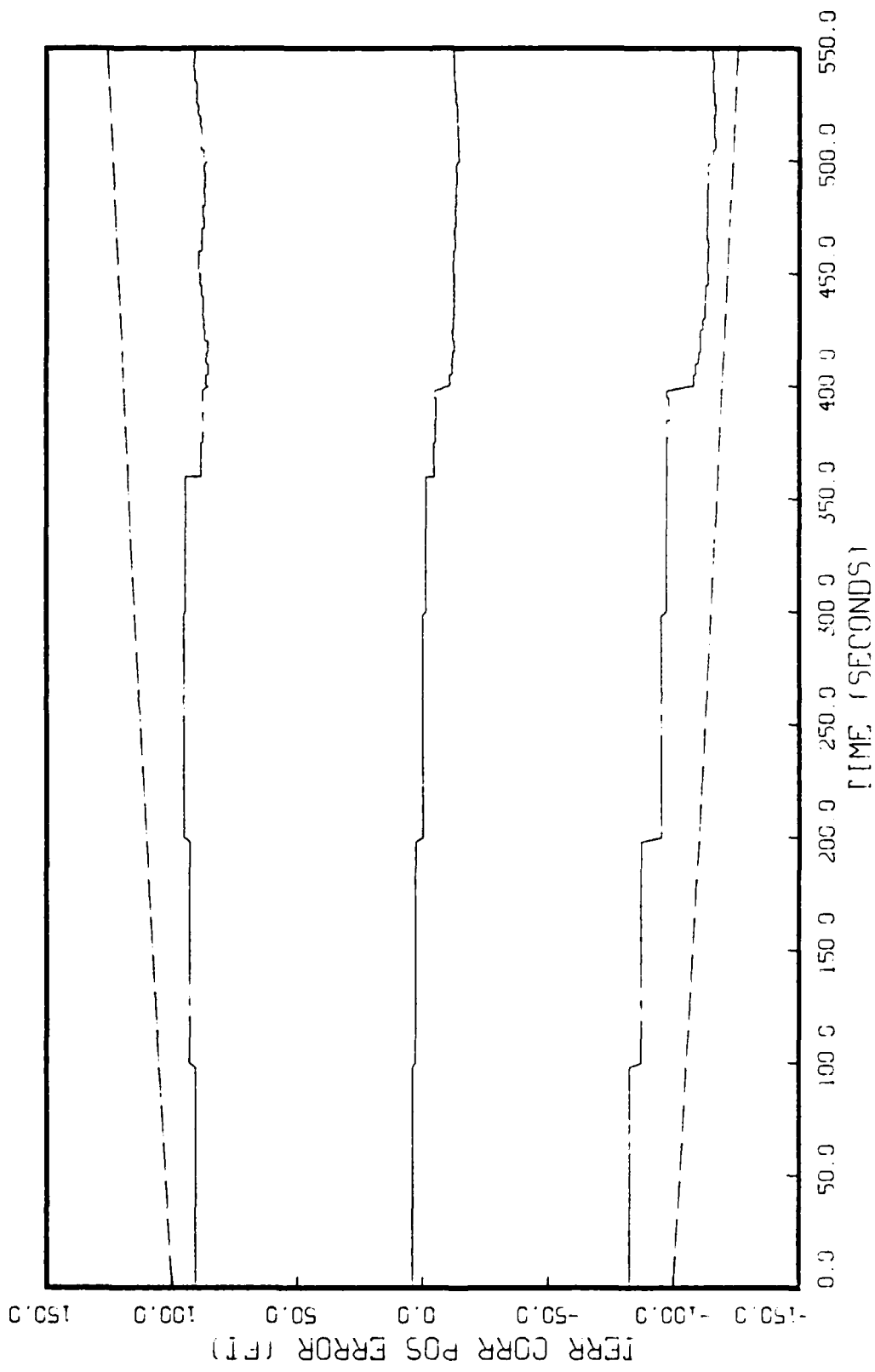


Fig. 3.26. Vertical Terrain Correlator Position Error For Terrain Correlator Measurement

#### IV. The FDI System

##### Background

The basis for many FDI systems lies in the generation of a filter model which represents some "real world" set of equations. The filter model is usually a scaled-down version of a larger, more inclusive and accurate "truth" model because of the necessity to conserve computer memory in an on-board computer. The most common form of filter model is usually a linear set of state equations. The linearization of the typically non-linear "real world" description has been performed about some nominal set of parameters which typify an acceptable operating condition. The formulation of the Kalman filter represents the best set of filter equations based on such a linear model. The prior statement is factual since the filter's performance is statistically better than any other type of linear filter construction, and it is superior to nonlinear forms as well if all uncertainties can be described as Gaussian processes.

In order to establish the quantities which are the essential inputs to the FDI system from the operational navigation Kalman filter, a brief description of the equations which are the basis for, and describe, this filter are essential. The system dynamics equation which describes any general state in the real world is assumed to be a linear stochastic equation of the form

$$x(k + 1) = \Phi(k) x(k) + B(k) u(k) + w(k) \quad (4-1)$$

where

$x(k)$  = real world description of  $x$  at time  $k$

$\Phi(k)$  = state transition matrix

$B(k)$  = input gain matrix

$u(k)$  = input quantities

$w(k)$  = zero-mean, white, Gaussian noise with statistics

$$E[w(k)] = 0 \quad E[w(k)^2] = Q(k) \quad (4-2)$$

The sensor equation for the filter which describes the measurement process is:

$$z(k) = H(k) x(k) + J(k) u(k) + v(k) \quad (4-3)$$

where

$z(k)$  = measurement of state  $x(k)$

$H(k)$  = measurement matrix

$J(k)$  = input gain matrix

$v(k)$  = a zero-mean, white, Gaussian noise process independent of  $w(k)$ , with statistics:

$$E[v(k)] = 0 \quad E[v(k)^2] = R(k) \quad (4-4)$$

If there are no failures in the system, the optimal Kalman filter state estimator is described by the following set of discrete equations:

$$\hat{x}(k + 1/k) = \Phi(k) \hat{x}(k/k) + B(k) u(k) \quad (4-5)$$

$$\hat{x}(k/k) = \hat{x}(k/k - 1) + K(k) \gamma(k) \quad (4-6)$$

$$\gamma(k) = z(k) - H(k) \hat{x}(k/k - 1) - J(k) u(k) \quad (4-7)$$

where  $\gamma$  is the zero-mean, Gaussian residual and the gain  $K(k)$  is calculated from:

$$P(k + 1/k) = \Phi(k) P(k/k) \Phi^T(k) + Q(k) \quad (4-8)$$

$$V(k) = H(k) P(k/k - 1) H^T(k) + R(k) \quad (4-9)$$

$$K(k) = P(k/k - 1) H^T(k) V^{-1}(k) \quad (4-10)$$

$$P(k/k) = P(k/k - 1) - K(k) H(k) P(k/k - 1) \quad (4-11)$$

where

$P(k/k - 1)$  is the estimation error covariance of state estimate  $\hat{x}(k/k - 1)$

$P(k/k)$  is the corresponding error covariance of  $\hat{x}(k/k)$

$V(k)$  is the covariance of  $\gamma(k)$

The above equations represent the "normal mode" filter (i.e., the filter is operating with no-failure parameters).

#### Failure Detection Concept

Sensor failure detection is concerned with the detection of changes in the system. As was stated in Chapter II, the failure of a sensor is usually manifested as an abrupt change in the  $H$  matrix, increases in measurement noise, or as biases in the measurement process equation.

All FDI logic is based on a comparison of actual system output quantities and some established values which represent either an acceptable value or a failure declaration bound. These reference values are usually predetermined based on preset constants, historical averages of output, related sensor output, or the outputs of dynamically related models (14:2). Outputs which are compared to these pre-established values are derived from actual measurements, state and parameter estimates based on these measurements, or various statistical measures such as variance or variance ratios.

The level of the malfunction caused by a particular failure, in effect, categorizes that failure. "Soft" faults result from small changes in the system characteristics and are interpreted as degraded system performance; however, the overall system performance does not change significantly. Examples of soft failures are increased sensor bias or measurement noise. Hard failures are large in magnitude and affect system performance significantly. Examples of such failures are computer hardware failure and gimbal lock. Combinations of hard and soft type failures are composite failures or "mid" failures (14:8).

As was previously stated, sensor faults are manifested in  $H$ , the measurement matrix, or in increased bias or measurement noise in the measurement process equation. Sensor failures reduce the observability of the system (as measured by eigenvalues of observability Gramian). This may

degrade mission effectiveness without any effect on controllability. An example would be radar failure which would cause poor navigation accuracy without affecting the closed-loop aircraft response.

#### Observability Criteria

Observability from a certain set of measurement devices can be determined mathematically. One observability test for instrumentation involves the  $\phi$  (state transition) matrix and the H (measurement) matrix. This test is described by the following equation:

$$O_s = \text{rank } [H^T, \phi^T H^T, (\phi^T)^2 H^T, \dots, (\phi^T)^{N-1} H^T] \quad (4-12)$$

where

$O_s$  represents the dimensionality of the observable subspace for all measurements represented in H. Any variation of  $O_s$  with changes in H indicates the effects of faults on the observable subspace. (Notes this test is only for time-invariant systems).

#### Detectability Criteria

Detectability refers to the ability to distinguish between no-failure and failed conditions based on measured output. Faults are detectable if the statistics of the output under failed conditions are statistically different from the no-failure outputs. Detectability of a faulty condition does not imply that one sensor fault can necessarily be distinguished from another.



### Fault Isolation

Fault isolatability refers to the FDI system's ability to distinguish, based on the output measurements, among the faulty conditions which may occur in the system. Any two faults can be distinguished from each other if they are statistically different from each other in their effect on sensor outputs.

### FDI Technique Review

There are three major components of an FDI approach:

- (1) Type of statistical technique used
- (2) Modeling requirements
- (3) Computer implementation

The statistical technique should provide an acceptable degree of detection and isolation delay, and acceptable false/missed alarm probabilities, yet be easy to implement. Modeling requirements are determined by the type of fault which must be detected and/or identified and the statistical techniques used. The computer implementation should consider the question of whether parallel processing is available. Parallel processing would be desirable as would the utilization of several simple steps rather than a few complex steps for software implementation.

### Stochastic Failure Detection

Deterministic methods fail to differentiate between random disturbances (noise) and true system faults.

Stochastic design methods, which model dynamic noise (generated by sensor's internal hardware and external environment), measurement noise (environmental effects), and modeling errors (usually incorporated into the appropriate noise strengths) are necessary modeling features to generate acceptable tradeoffs between missed/false alarms and detection delay.

Either a single Kalman filter or a bank of Kalman filters can be utilized for the fault detection/isolation process. In the single Kalman filter, the states and covariances are propagated under the no-failure condition. With this approach, the observed characteristics of either the filter measurement residuals or some other filter outputs are then used to detect and isolate failures. This technique was used in early developments by Mehra and Peschon (31) and was further redefined by Willsky, Deyst, and Crawford (50) and Willsky and Jones (49). The main idea of this approach is that the internally computed statistics of the Kalman Filter will be different from the true observed behavior of residuals or other variables if a fault occurs. Banks of Kalman filters were first proposed by Magill(21) and Lainiotis (19) and were applied by Montgomery (32) for redundancy management. The concept is basically two-fold; one Kalman filter is propagated for the no-failure condition and an additional Kalman filter is propagated for each of the failed states. Deckert and Deyst (11) compute the likelihood

ratios sequentially in what is referred to as a sequential probability ratio test (SPRT).

#### The SPRT

A typical SPRT is generated upon the basis of two hypotheses: the hypothesis of no-failure ( $H_0$ ) and failure ( $H_1$ ). The probability ratio is defined as:

$$\gamma_N(i) = \frac{p(Y_N(i)/H_0)}{p(Y_N(i)/H_1)} \quad (4-13a)$$

where

$N$  = the number of most recent measurements to be used (a moving window)

and the SPRT yields the decisions:

$$\begin{aligned} \gamma_N(i) > A &= H_0 \text{ is correct} \\ \gamma_N(i) < B &= H_1 \text{ is correct} \\ A \leq \gamma_N(i) \leq B &= \text{No decision} \end{aligned} \quad (4-13b)$$

The SPRT overcomes the problem of not being able to decrease the probability of false alarm and the probability of missed alarm simultaneously. This is accomplished by setting the threshold values  $A$  and  $B$  until the probabilities of missed and false alarm are minimized.

The SPRT has the following advantages and disadvantages (14):

### Advantages

- (1) If there are only a few simple hypotheses to test, SPRT is attractive.
- (2) Given acceptable probabilities of false and missed alarms the method will detect faults with minimal time delay, if the a priori distributions are known exactly.

### Disadvantages

- (1) Thresholds for probability of false and missed alarms are difficult to select because of the complex distribution functions.
- (2) To detect faults in minimal time, many SPRTs must be run each using data of different duration (i.e., soft faults require long duration and hard faults require short duration).
- (3) The number of SPRTs increase as the square of the number of hypotheses (very large if there are unknown parameters).

### Voting Systems

The process of fault detection and isolation using like sensors (3 or more) will not be addressed further in this thesis. Without system hardware redundancy being considered, the only possible application of voting for the system under consideration would be in gyro and accelerometer fault detection; however, this must be ruled out since the three gyros and accelerometers are mounted orthogonally by assumption. Because of the orthogonality, they do not measure any shared component of attitude or acceleration which would be a necessary requirement for voting. Note, there are nonorthogonal 4 and 6 gyro and/or accelerometer INSs which would allow such voting.

### FDI System Design

The purpose of this thesis is to find a suitable FDI system to incorporate with the aided navigation system. The FDI system must meet the aforementioned requirements of simplicity, accuracy, and speed. All of the process techniques which have been addressed to this point have advantages and disadvantages when measured against these requirements.

Based on this process review and the FDI requirements, innovations - based detection systems offer the greatest accuracy, constrained by the need for simplicity and speed (time from actual failure to declaration) (47:609).

Since a navigation system does not necessarily require the rapid detection/isolation accuracy that an aircraft flight control system requires for aircraft survival, a certain delay of time-to-failure declaration can be tolerated without endangering the aircraft or crew. This time-to-failure declaration allows the FDI system to recover in effect from harsh dynamical characteristics caused by harsh maneuvers. The occurrence of a harsh maneuver will cause gyro and accelerometer error states to grow at a significant rate due to rotational rates about the IMU axes. These error states could then, themselves, cause thresholds to be surpassed when no failure has occurred or, since they drive attitude and velocity error states, cause these states to incur violation of thresholds. Because of this, a time-to-

failure parameter would prevent inadvertent threshold violation. Consistent surpassing of thresholds would indicate failure whereas transient passage would not.

#### Failure Detection System

The failure detection system for this thesis will utilize likelihood function statistical testing. This technique is very simple to implement compared to various likelihood ratio tests. The likelihood ratio techniques addressed in this thesis require additional filter states to model failed conditions which can result in a large number of additional states. The likelihood function only utilizes information which is readily available from the Kalman filter as part of its no-failure measurement/update algorithms. This makes it attractive when measured against the desire of accuracy, speed, and ease of implementation. Moreover, likelihood ratios must be established for each hypothesized form of failure, and failures of a different form can go undetected.

The Kalman filter (designed for no-failure operation) generates outputs in the form of estimates of certain quantities in the system dynamics. When these values are compared to measured values of the same quantities, error signals (residuals) are generated. These residuals can then be utilized to determine if the system is operating normally or if a fault has occurred.

A likelihood function provides one way of making a statistical test for a failure. A time-history for the error signals being tracked is "windowed" to keep the likelihood function computationally tractable. In order to "window" the residuals, the N most recent values are examined to compare them to a statistical description (in effect, approximating statistics (ensemble average) with temporal averaging (N-step)) of their values assuming no-failure conditions. This value of N can be adjusted to maintain reasonable detection performance. Use of a single sample would not be advisable since single samples of large value could be expected due to harsh flight dynamics, large noise values at a given sample time, etc. This could generate a false alarm when no failure actually exists. On the other hand, too large a value of N could make the likelihood function "insensitive" to a change and no failure might be detected when a failure has actually occurred. Therefore, an (iterative) adjustment in "window" size is necessary during the design process to establish acceptable performance.

The formulation of the likelihood function begins with an expression for the joint probability density function for the N most recent residuals based on the past residuals:

$$p[e(i), e(i - 1), \dots, e(i - N + 1) / e(i - N), \dots, e(1)]$$

where  $e(i)$  is a residual value and  $p(x/y)$  is the conditional probability of the variable  $x$ , conditioned on the value of  $y$ .

The basis for this conditional density is found in estimation theory.

Baye's Rule for conditional density functions is given in the following equation:

$$p[a,b/c] = p[a/b,c] p[b/c] \quad (4-14)$$

Applying this equation to the residual conditional density function produces

$$\begin{aligned} p[e(i), e(i-1), \dots, e(i-N+1)/e(i-N), \dots, e(1)] \\ = p[e(i)/e(i-1), \dots, e(1)] \times \\ p[e(i-1), \dots, e(i-N+1)/e(i-N), \dots, e(1)] \quad (4-15) \end{aligned}$$

Applying Baye's Rule repeatedly to the last density function in Eq(4-15) produces

$$\begin{aligned} p[e(i), e(i-1), \dots, e(i-N+1)/e(i-N), \dots, e(1)] \\ = \prod_{j=i-N+1}^i p[e(j)/e(j-1), \dots, e(1)] \quad (4-16) \end{aligned}$$

This equation is then the product of the conditional densities of the N most recent residuals, each conditioned on the previous time-history of residuals. A likelihood function is then derived which is the natural logarithm of the derived conditional density as given by Eq(4-16):



$$LF_N(i) = \ln \{p[e(i), \dots, e(i-N+1)/e(i-N), \dots, e(1)]\}$$

$$= \sum_{j=i-N+1}^i \ln \{p[e(j)/e(j-1), \dots, e(1)]\} \quad (4-17)$$

Under the assumption that the residual sequence is a set of independent, zero-mean, Gaussian random variables, Eq(4-17) can be written as

$$LF_N(i) = \sum_{j=i-N+1}^i \ln \frac{1}{(2\pi)^{1/2} \sigma(j)} \exp\{(-1/2)e^2(j)/\sigma^2(j)\} \quad (4-18)$$

Note: the use of  $e$  in this development assumes that  $e$  is a scalar residual out of many possible residuals

where  $\sigma(j)$  is the filter estimated standard deviation of the  $j$ th sample from the formulation

$$\sigma^2(j) = \underline{h}^T(j) \underline{P}(j/j-1) \underline{h}(j) + R(j) \quad (4-20)$$

where

$\underline{h}^T$  = measurement matrix row

$\underline{P}^-$  = propagated filter covariance

$R$  = measurement noise variance

By substituting the  $N$  most recent residual values into Eq(4-19) the likelihood function for the observed data is:

$$LF_N(i) = (-N/2) \ln(2\pi) - \sum_{j=i-N+1}^i \ln \sigma(j) - 1/2 \sum_{j=i-N+1}^i [e^2(j)/\sigma^2(j)] \quad (4-21)$$

Since the residuals from the Kalman filter generate the likelihood function, then each of the densities described by Eq(4-17) is in fact a Gaussian density with the following statistics:

$$E[z(j)/e(j-1), \dots, e(1)] = \underline{h}^T(j) \underline{\hat{x}}(j/j-1) \quad (4-22)$$

where

$\underline{h}^T(j)$  is the measurement matrix row corresponding to the scalar residual under investigation

$\underline{\hat{x}}(j/j-1)$  is the state vector before measurement update

and the conditional variance

$$\begin{aligned} E\{e^2(j)/e(j-1), \dots, e(1)\} - E^2\{e(j)/e(j-1), \dots, e(1)\} \\ = \underline{h}^T(j) \underline{P}(j/j-1) \underline{h}(j) + R(j) \end{aligned} \quad (4-23)$$

where

$\underline{h}^T(j)$  is the measurement matrix row as given above

$\underline{P}(j/j-1)$  is the filter covariance before measurement update

$R(j)$  = measurement noise variance

For real-time likelihood function generation, the N most recent residuals and filter estimated covariances are used. As time progresses, the next residual and estimated covariance are brought in and the next likelihood function value is generated. As can be seen in Eq(4-21), if the squared residual becomes consistently larger than the

estimated variance, then the likelihood function will become more and more negative. A negative threshold level that the likelihood function should not surpass can then be determined (providing satisfactory performance). A failure is declared if the likelihood function becomes consistently more negative than this threshold. Another aspect to failure declaration is a time-to-failure-declaration parameter which minimizes false alarms by allowing temporary transient behavior (due to harsh maneuvers and other phenomena) to die out over the time-to-failure-declaration window. In a general sense, soft failures would be handled by tight thresholds plus a time-to-failure-declaration parameter and hard failures by a larger threshold only.

For this thesis, measurements are being made as shown in Table VIII.

Table VIII  
Measurement Processing

| External Aid       | # of measurements |
|--------------------|-------------------|
| Satellite Position | 3                 |
| Satellite Velocity | 3                 |
| Doppler Radar      | 3                 |
| Terrain Correlator | 3                 |

Each of the measurements produces a residual which is individually tracked (along with the estimated variance) by its own likelihood function. After the desired number of residuals and associated variances are stored, i.e., at time  $t_N$ , the likelihood function is initialized and likelihood function tracking can begin. In order to minimize computer loading and also track the likelihood functions, an approximated version of Eq(4-20) is employed:

$$LF_N^1(i) = \sum_{j=i-N+1}^i \{ (-1/2) [e^2(j) / \sigma^2(j)] \} \quad (4-24)$$

A failure can be declared if

$$LF_N^1(i) < -T \quad (4-25)$$

where

$LF_N^1(i)$  is the likelihood value

$T$  is a desired threshold (there may be more than one value, to detect both hard and soft failures)

Eq(4-24) can be rewritten to incorporate the threshold.

$$\sum_{j=i-N+1}^i [e^2(j) / \sigma^2(j)] > 2T \quad (4-26)$$

Initially, each of the measurement devices is run against the flight profile using a Monte Carlo process to generate a likelihood function baseline for normal (no failure) operation. Once the baseline likelihood function

has been identified for the measurement device, various failures (different magnitudes and devices) will be injected at a scheduled time to study their effect on the likelihood functions over the identical flight profile. When the likelihood function characteristics have been determined for the measurement processes, and appropriate thresholds for the no-failure case have been established, the characteristics of the failed conditions can then be exploited to establish the identification process.

The failures which will be modeled in this thesis are characteristic of real world faults. For instance, a gyro failure can be "soft", modeled to portray a gyro float leak; a "hard" failure can be used to simulate electrical failure or bearing failure. It is also useful at this point to distinguish between "hard-over" failures and hard failures (i.e., loss of signal content). A hard-over failure is characterized by an extremely large signal which is abnormal for the particular device. Mathematically, it could be modeled as:

$$z = Hx + v + b \quad (4-27)$$

where the value of  $H$  is much increased over the normal range of operation or a large magnitude bias  $b$  appears. Eq(4-27) can also be used to model a "hard" failure (loss of signal content) in which, in this scalar measurement case,  $H$  is set equal to zero and only measurement noise remains in the

scalar case. Simulations of both "soft" and "hard" faults will be performed (hard-over failures are not addressed). Soft failures of the various sensors will be accomplished by generating a one-sigma ramp contribution to the particular error state for the sensor being considered. This is mathematically expressed as

$$\dot{x} = \sigma_x \quad (4-28)$$

where

$x$  = sensor error state

$\sigma_x$  = ramp/slope chosen to be the initial condition of the bias error state per second.

Both "hard" failures and measurement noise increases can be modeled by using the measurement equation given by Eq(4-27). Hard failures for a particular sensor are modeled by simply setting the appropriate H matrix row elements equal to zero. The resulting measurement would then only have a measurement noise contribution from that particular sensor. Increases in the strength of measurement noise (see Eq(4-27)) for a particular sensor are representative of jamming or other external noise increases which mask the desired sensor signal. The effect of "hard-over" failures, modeled by the addition of a bias,  $b$ , as shown in Eq(4-27) will not be simulated in this thesis due to time constraints. Table IX gives a list of the various sensors, the type of fault, and its characterization.

Table IX  
Sensor Fault Classification

| Sensor Type              | Fault Modeled      | Classification |
|--------------------------|--------------------|----------------|
| gyro                     | float leak         | soft           |
| gyro                     | bearing failure    | hard           |
| accelerometer            | quantization fault | soft           |
| accelerometer            | pendulum lock      | hard           |
| satellite receiver clock | overheating        | soft           |
| satellite receiver clock | clock failure      | hard           |
| Doppler                  | frequency drift    | soft           |
| Doppler                  | beam failure       | hard           |
| Radar Altimeter          | gimballing errors  | soft           |
| Radar Altimeter          | beam failure       | hard           |
| Baro-Altimeter           | calibration drift  | soft           |
| Baro-Altimeter           | transducer failure | hard           |

Table X gives an example of how both gyro and accelerometer bias errors affect the dynamic motion states,  $x_1 - x_9$ , i.e., position errors, velocity errors, and tilts in the INS.  $x_{11}$ ,  $x_{12}$ , and  $x_{13}$  are gyro bias states.  $x_{23}$ ,  $x_{24}$ , and  $x_{25}$  are accelerometer bias states. The  $x$ 's in the table denote how the various states are coupled. It can be seen that gyro error states are direct drivers on the attitude

differential equations and accelerometer error states are drivers on the velocity differential equations. This infers that accelerometer failures should be noted earlier than a gyro failure for a velocity measurement since the accelerometer failure is one integration from velocity and a gyro failure is two integrations away. Of course, eventually such errors would corrupt all INS outputs. The structure of the measurement residuals has an impact on the detection of these faults. This aspect of identification will be addressed in the following chapter.

Table X  
Gyro and Accelerometer Error Tracking

| States         | x <sub>1</sub> | x <sub>2</sub> | x <sub>3</sub> | x <sub>4</sub> | x <sub>5</sub> | x <sub>6</sub> | x <sub>7</sub> | x <sub>8</sub> | x <sub>9</sub> | x <sub>11</sub> | x <sub>12</sub> | x <sub>13</sub> | x <sub>23</sub> | x <sub>24</sub> | x <sub>25</sub> |
|----------------|----------------|----------------|----------------|----------------|----------------|----------------|----------------|----------------|----------------|-----------------|-----------------|-----------------|-----------------|-----------------|-----------------|
| x <sub>1</sub> |                | x              | x              | x              |                |                |                |                |                |                 |                 |                 |                 |                 |                 |
| x <sub>2</sub> |                |                |                | x              | x              |                |                |                |                |                 |                 |                 |                 |                 |                 |
| x <sub>3</sub> |                |                | x              |                |                | x              |                |                |                |                 |                 |                 |                 |                 |                 |
| x <sub>4</sub> |                | x              | x              | x              | x              | x              |                | x              | x              |                 |                 |                 | x               | x               | x               |
| x <sub>5</sub> |                | x              | x              | x              | x              | x              | x              |                | x              |                 |                 |                 | x               | x               | x               |
| x <sub>6</sub> |                | x              | x              | x              | x              |                | x              | x              |                |                 |                 |                 | x               | x               | x               |
| x <sub>7</sub> |                |                | x              |                | x              |                |                | x              | x              | x               | x               | x               |                 |                 |                 |
| x <sub>8</sub> |                | x              | x              | x              |                |                | x              |                | x              | x               | x               | x               |                 |                 |                 |
| x <sub>9</sub> |                | x              | x              | x              |                |                | x              | x              |                | x               | x               | x               |                 |                 |                 |



The appropriate likelihood functions should react to these faults by having an increasingly negative value. Once the established threshold (whether soft or hard failure) has been surpassed, a failure is declared and the isolation/identification process begins.

#### The Isolation/Identification Process

The isolation/identification of a failed sensor is more time consuming than the failure detection process. The formulation of an isolation/identification process that is rapid, efficient, and as fault-free as possible, is the ultimate goal. Some of the statistical data which will be gathered during the failure process will aid the isolation/identification of a failed sensor. For instance, a gyro failure may affect only two of the three velocity error states initially, unlike the effects of any other failure, which may aid isolation/identification. If two unlike sensors (i.e., accelerometer and Doppler) affect identical states, then such information as time between any likelihood function threshold violations and magnitude may offer information which will aid the isolation/identification process. These various features, which should become evident during failure simulation, will be exploited if it is feasible.

The isolation/identification process to be implemented in this thesis will be based on information gathered during

the failure simulation. Each failure will have the following information gathered from it:

- (1) Which likelihood functions violated thresholds
- (2) The order of likelihood function threshold violation (time of failure)
- (3) Magnitude of likelihood functions (growth after failure declaration)
- (4) Magnitudes of other likelihood functions which may be large, but not past their thresholds.

With this information in hand, an isolation/identification algorithm will be developed, implemented, and tested. The actual formulation for the isolation/identification processor will appear in Chapter 5. It will be exercised against the same flight profile as was used for the failure simulation.

## V. FDI Analysis

### Simulation Overview

The formulation of an effective isolation/identification algorithm can rely on many characteristics of the likelihood function over the time duration of the residual tracking process. Certain characteristics of the likelihood function such as the time-of-failure declaration (with respect to the time of threshold passage of other likelihood functions for the same measurement process) after a failure is simulated, magnitude of the likelihood function value, and the rate of growth of the likelihood function due to the failure (i.e., the negative slope characteristics of the likelihood function after a simulated failure) can all aid the development of a suitable isolation algorithm for the particular application.

The initial data gathered for this isolation algorithm development consisted of the simulation of a specific set of failures (hard and soft) for each of the measurement processes (satellite, Doppler, and terrain correlator). The likelihood functions for each of the simulated failures were then analyzed for specific characteristics to establish a suitable basis for an isolation processor.

Tables XII thru XV, to be presented subsequently in this chapter, demonstrate the results achieved by the likelihood function detectors with magnitude singled out as the primary parameter for failure declaration. The failures were simulated in both benign (straight and level) flight and dynamic (hard

dive, jinking, turns, etc.) flight environments. Furthermore, time histories of actual likelihood functions are used to discern important characteristics to be used for failure detection and isolation. Chapter II, Table IV contains the flight profile which highlights the maneuver sequence. All such figures referenced in this chapter are located in the Appendix. The failure detection processor was simulated over a 550 second portion of the flight profile given in Chapter II (0 thru 550 seconds for the benign flight and 2300 thru 2850 seconds for the dynamic case).

As a result of the characteristics observed in the initial no-failure runs, the detection logic was not initialized for operation until 60 seconds after the measurement process had actually begun (for benign flight, the measurement process began at 2500 seconds). This delay was necessary to ensure that the filter transients had dissipated themselves and a reasonable steady-state condition had been achieved. The simulation times of interest are shown in Table XI.

Table XI

Simulation Times of Interest

| Type    | Start     | Initial Meas | Simulated Failure | Finish    |
|---------|-----------|--------------|-------------------|-----------|
| Benign  | 0 secs    | 360 secs     | 450 secs          | 550 secs  |
| Dynamic | 2300 secs | 2500 secs    | 2640 secs         | 2850 secs |

### No-Failure Likelihood Functions

The satellite measurement process consists of six measurements (3-position, 3 velocity). Each of the measurement processes is tracked by its own likelihood function processor. The thresholds shown in Tables XII and XIII list the maximum values for each likelihood function for the benign and dynamic cases, respectively. The N-step "window" for each of these likelihood functions, is set at 10. This value is justified based on the work of Maybeck (22). Fig.'s A.24 thru A.29 demonstrate the no-failure likelihood function plots for benign flight. Fig.'s A.38 thru A.43 demonstrate the no-failure likelihood function plots for dynamic flight.

The Doppler measurement process consists of three velocity measurements. Again, as in the satellite measurement process, each measurement is tracked by its own likelihood function. The "windows" for the likelihood functions are set at 10. Fig.'s A.44 thru A.46 are the likelihood function plots for the benign case and Fig.'s A.76 thru A.78 are the likelihood function plots for the dynamic case.

Terrain correlator processing consists of three position measurements. Three likelihood functions track this measurement process and are "windowed" at a sample size of 10 (same as previous cases). Fig.'s A.89 thru A.91 provide the likelihood function plots for the benign flight and Fig.'s A.92 thru A.94 apply to the dynamic case.

The threshold establishment for all measurement processes was selected by adding a value of minus one-tenth (-.1) to the

maximum values for the no-failure likelihood functions shown in the no-failure figures. This decision is primarily based on the small Monte Carlo sample size (10 samples) which was used in the simulations. By adding this value, a conservative threshold has, in fact, been proposed. Any simulated failures which have magnitudes beyond this value are then declared. Tighter thresholds would cause a greater sensitivity and generate false alarms. The false alarm/missed alarm trade off is an issue in itself.

#### Satellite Failure Detection (Benign)

Table XII, found later in this Chapter, lists the simulated failure results for the benign case. The tabulated results provide a significant insight into the failure characteristics of each of the simulated faults.

Soft gyro failures, (SGY1:x-axis, SGY2:y-axis, SGY3:z-axis) were not detectable in the benign case. This is attributable to the integrations that the soft gyro failures (these failures are simulated by one-sigma ramps for the particular gyro error state as discussed in Chapter IV) must pass through before affecting the velocity and position error states which are observable in the measurement process. The integration processes, in effect, filter out the failure effects before they can significantly influence the measurements. These soft gyro failures can then be classified as unobservable for this satellite measurement process with failure magnitude as the single detection parameter.

Hard gyro failures (modeled as 100-sigma jumps at the given failure time; this value was chosen to generate a reasonable time-rate-of-change for the failure growth (one order of magnitude) over the detection sample interval) are plotted in Fig.'s A.19 thru A.23. These failures are readily observable as can be seen in Table XII. A gyro 1 or 2 hard failure (HGY1, HGY2) is observable in measurements 4, 5, and 6 which are physically the 3 velocity error states. However, a gyro 3 hard failure is not detected by any of the measurements. Gyro 3 measures angularities about the Z platform (aircraft axis for strapdown) axis. This lack of gyro 3 sensitivity is a possible indication of the impact of the coordinate frame transformation for platform to navigation frame. Because of the direction cosine matrix transformation, the gyro 3 failure characteristics are lost in the transformation possibly due to the multiplication by a very small sine or cosine term or terms.

Soft accelerometer failures (SAC1: x-axis, SAC2: y-axis, SAC3: z-axis) (Fig.'s A.15 thru A.18) produce a more pronounced effect on the likelihood functions than those observed for soft gyro failures. SAC1 magnitude growth was observed in measurements 4 and 6, corresponding to east and vertical velocity error states, respectively. SAC2 growth is observed in measurements 4 and 5 (north velocity error state). A SAC3 failure was also detected by measurement 6. The increased observability of the soft accelerometer failure as compared to the soft gyro failure is due to the faster influence of the accelerometer

error states on the velocity error states (i.e., gyro failures must pass through attitude error states before affecting the velocity error states, whereas, accelerometer errors states affect the velocity error states directly).

Hard accelerometer failures (HAC1, HAC2, HAC3) (Fig.'s A.7 thru A.14) are also observable in more measurements and are of greater magnitude than gyro failures (a function of the error state equation coupling).

Soft and hard satellite failures were observed in measurements 4, 5, and 6, respectively. Soft satellite failures (SSATF) (Fig.'s A.4 thru A.6) do not appear in measurements 4, 5, or 6 since no direct coupling occurs in the states that affect these measurements. The hard satellite failures (HSATF) (Fig.'s A.1 thru A.3) produced results that are somewhat contrary to the expected results (soft failures affected measurements 1, 2, and 3 and thus, one would expect hard failures to have even more impact on these measurements). The explanation of these results is attributable to the way the hard failures are modeled. These hard failures are simulated by zeroing the satellite error states in the measurement equation (this technique for modeling is discussed in Chapter IV). These errors are small compared to the other measurement states and are quickly compensated for by the filter. These soft failures are one-sigma ramps continuously applied to the error states and cannot be compensated for by the filter, thus producing large residuals and eventual likelihood function growth.



Table XII

Satellite Likelihood Function Failure Statistics for Benign Flight

| Simulated Failure | LF#1  |      | LF#2   |      | LF#3   |      | LF#4   |      | LF#5   |      | LF#6    |      |
|-------------------|-------|------|--------|------|--------|------|--------|------|--------|------|---------|------|
|                   | Mag   | Time | Mag    | Time | Mag    | Time | Mag    | Time | Mag    | Time | Mag     | Time |
| No Fail           | -1.96 | 470  | -4.39  | 485  | -6.46  | 500  | -6.93  | 490  | -4.93  | 490  | -9.54   | 495  |
| SGY1              | -1.96 | 470  | -4.39  | 485  | -6.46  | 500  | -6.93  | 490  | -4.93  | 490  | -9.54   | 495  |
| SGY2              | -1.96 | 470  | -4.39  | 485  | -6.46  | 500  | -6.95  | 490  | -4.93  | 490  | -9.54   | 495  |
| SGY3              | -1.96 | 470  | -4.39  | 485  | -6.46  | 500  | -6.93  | 490  | -4.93  | 490  | -9.54   | 495  |
| HGY1              | -1.98 | 510  | -4.4   | 475  | -6.46  | 500  | -6.95* | 480  | -5.67* | 470  | -9.58*  | 495  |
| HGY2              | -1.97 | 470  | -4.4   | 485  | -6.50  | 500  | -9.48* | 480  | -5.32* | 470  | -10.5*  | 485  |
| HGY3              | -1.96 | 470  | -4.39  | 485  | -6.46  | 500  | -6.93  | 490  | -4.93  | 490  | -9.54   | 495  |
| SAC1              | -1.97 | 470  | -4.39  | 485  | -6.47  | 500  | -7.78* | 490  | -4.88  | 470  | -9.86*  | 495  |
| SAC2              | -1.97 | 470  | -4.37  | 475  | -6.46  | 500  | -6.99* | 480  | -5.09* | 480  | -9.54   | 495  |
| SAC3              | -1.96 | 470  | -4.39  | 485  | -6.47  | 500  | -6.93  | 500  | -4.85  | 490  | -9.87*  | 485  |
| HAC1              | -1.98 | 470  | -4.39  | 480  | -6.48  | 500  | -7.91* | 480  | -5.59* | 470  | -10.39* | 485  |
| HAC2              | -1.97 | 470  | -4.33  | 475  | -6.47  | 500  | -9.39* | 480  | -8.58* | 480  | -9.51   | 485  |
| HAC3              | -2.0  | 510  | -4.37  | 475  | -6.91* | 500  | -7.52* | 480  | -4.99* | 470  | -13.29* | 475  |
| SSATF             | -2.18 | 470  | -4.64* | 475  | -6.83* | 500  | -6.92  | 490  | -4.93  | 490  | -9.55   | 495  |
| HSATF             | -1.96 | 470  | -4.39  | 485  | -6.37  | 500  | -7.14* | 470  | -6.37* | 470  | -10.34* | 475  |

\* indicates initial failure value after threshold

### Satellite Failure Detection (Dynamic)

The dynamic simulation for the satellite measurement process produced results for the likelihood functions that were surprising. As can be seen by Table XIII (found later in this chapter), the likelihood functions were generally insensitive to both hard and soft failures. In the dynamic simulation, the failures were initialized at 2640 seconds. During this period of time, the aircraft is performing vertical dives, jinking, and climbing maneuvers; it could well be the case that these failures are being masked due to the rapid changes in the direction cosine matrix for platform to navigation frame transformations. The cosine and sine terms in this matrix are of rapidly changing angles which most likely results in minimizing a large failure. This is a practical explanation for gyro and accelerometer failures, but what about the change in behavior of the satellite failures?

The soft satellite failure (SSATF) produced the same measurement failures, but the dynamic case produced failures that were of greater magnitude than the benign case. However, the time to failure detections is much longer for the dynamic case (See Fig.'s A.30 thru A.32). One could surmise that the dynamic case is less sensitive to the soft satellite failure; it is harder to distinguish failure effects from dynamic effects in a harsh dynamic setting than in a benign case.

Hard satellite failures were unobservable in the dynamic case. The hard satellite failure has the same explanation as

Table XIII

Satellite Likelihood Function Failure Statistics For Dynamic Flight

| Simulated Failure | LF#1   |      | LF#2   |      | LF#3   |      | LF#4   |      | LF#5   |      | LF#6   |      |
|-------------------|--------|------|--------|------|--------|------|--------|------|--------|------|--------|------|
|                   | Mag    | Time | Mag    | Time | Mag    | Time | Mag    | Time | Mag    | Time | Mag    | Time |
| No Fail           | -2.84  | 2620 | -7.52  | 2635 | -5.39  | 2680 | -8.01  | 2620 | -5.58  | 2625 | -5.11  | 2635 |
| SGY1              | -2.84  | 2620 | -7.52  | 2635 | -5.39  | 2680 | -8.01  | 2620 | -5.58  | 2625 | -5.11  | 2635 |
| SGY2              | -2.84  | 2620 | -7.52  | 2635 | -5.39  | 2680 | -8.01  | 2620 | -5.58  | 2625 | -5.11  | 2635 |
| SGY3              | -2.84  | 2620 | -7.52  | 2635 | -5.35  | 2680 | -8.01  | 2620 | -5.58  | 2625 | -5.11  | 2635 |
| HGY1              | -2.84  | 2620 | -7.52  | 2635 | -5.39  | 2680 | -8.01  | 2620 | -5.58  | 2625 | -5.11  | 2635 |
| HGY2              | -2.84  | 2620 | -7.52  | 2635 | -5.39  | 2680 | -8.01  | 2620 | -5.58  | 2625 | -5.11  | 2635 |
| HGY3              | -2.84  | 2620 | -7.52  | 2635 | -5.39  | 2680 | -8.01  | 2620 | -5.58  | 2625 | -5.11  | 2635 |
| SAC1              | -2.84  | 2620 | -7.52  | 2635 | -5.39  | 2680 | -8.01  | 2620 | -5.58  | 2625 | -5.11  | 2635 |
| SAC2              | -2.84  | 2620 | -7.52  | 2635 | -5.39  | 2680 | -8.63* | 2725 | -5.58  | 2625 | -5.11  | 2635 |
| SAC3              | -2.84  | 2620 | -7.52  | 2635 | -5.39  | 2680 | -8.01  | 2725 | -5.58  | 2625 | -5.11  | 2635 |
| HAC1              | -2.84  | 2620 | -7.52  | 2635 | -5.39  | 2680 | -8.44* | 2700 | -5.60* | 2675 | -5.11  | 2635 |
| HAC2              | -2.84  | 2620 | -7.52  | 2635 | -5.39  | 2680 | -9.69* | 2685 | -5.58  | 2675 | -5.11  | 2635 |
| HAC3              | -2.84  | 2620 | -7.52  | 2635 | -5.46* | 2680 | -8.01  | 2685 | -5.58  | 2675 | -5.22* | 2670 |
| SSATPF            | -4.06* | 2675 | -8.59* | 2695 | -7.35* | 2740 | -8.01  | 2685 | -5.58  | 2675 | -5.11  | 2635 |
| HSATP             | -2.84  | 2620 | -7.52  | 2635 | -5.43  | 2680 | -8.01  | 2685 | -5.58  | 2675 | -5.11  | 2635 |

\* indicates initial failure value after threshold

given for the benign case (i.e., small magnitude of failure compared to the other measurement states). The velocity error states are being rapidly perturbed by the harsh maneuvers which most likely causes their values in the measurement process to "overshadow" the hard failures and, in essence, make the failure unobservable.

Hard accelerometer failures (HAC1, HAC2, HAC3) were detected in all measurements. However, the number of measurements which were excited by the failure represents a significant reduction compared to the benign case. Fig.'s A.35 thru A.36 provide the likelihood function plots for these failures.

The decreased measurement sensitivity was also observed for the soft accelerometer failure (SAC1, SAC2, SAC3). Fig. A.37 shows the tracking of SAC2 failure in measurement process 4.

#### Doppler Failure Detection (Benign)

The results for Doppler likelihood function failures detection are shown in Table XIV which is found later in this chapter. The Doppler measurement process was utilized to determine (through likelihood function testing) what effect that hard and soft gyro, accelerometer, and Doppler failures have on the likelihood functions. Further, this was done to establish what characteristics of these failures could be exploited for isolation and identification processing. The dynamic flight results will be discussed after the benign results. Measurement 7 corresponds to the east velocity error state,

measurement 8 corresponds to the north velocity error state and measurement 9 corresponds to the vertical velocity error state.

Soft gyro failures (SGY1, SGY2, SGY3) were not observable in the likelihood functions. The explanation of this condition is the same as given in the satellite measurement process.

Hard gyro failures (HGY1, HGY2, HGY3) were detected in two of the simulated cases. A HGY1 failure was detected in measurements 7 and 8 (See Fig.'s A.47 and A.48). A HGY2 failure was detected in measurements 7 and 8, also (See Fig.'s A.49 and A.50). A HGY3 failure was not detected by any of the measurement processes. A HGY3 failure would not be expected to be observable in a benign flight since no vertical rate changes are taking place. This is an observability situation which would drastically affect the INS once the vertical channel becomes excited by a maneuver. Refer to Chapter IV for a discussion of failure types (soft, hard, hard-over).

Soft accelerometer failures (SAC1, SAC2, SAC3) were detected in two of the simulated cases. A SAC1 failure was detected in measurement processes 7 and 8 (See Fig.'s A.53 and A.54). A SAC 3 failure was not observed by any of the likelihood functions. Again, the unobservable nature of the SAC3 failure is due to the benign flight environment which does not perturb the vertical states. If the sensor error states had been used explicitly in the measurement process then drastic effects would have been noted.

Hard accelerometer failures (HAC1, HAC2, HAC3) followed the same pattern as the soft accelerometer failures except for

the HAC3 failure (See Fig.'s A.55 and A.56). The HAC3 failure was detected by measurement processes 7 and 9 (See Fig.'s A.57 and A.58).

A soft Doppler failure (SDOP) was detected by all three measurements (See Fig.'s A.59 thru A.61). A hard Doppler failure (HDOP) was only detected by measurement process 9 (See Fig. A.62). This is most likely due to the rapid recovery of the measurement process from the zeroing of the particular H matrix entry for the Doppler error state.

#### Doppler Failure Detection (Dynamic)

The dynamic flight simulation for Doppler failures showed a tremendous lack of sensitivity for various failures that were observable in the benign case. The only failures that produced observable values were the following: hard accelerometer failures; HAC1 (See Fig.'s A.71 and A.72), HAC2 (See Fig.'s A.67 and A.68), and HAC3 (See Fig.'s A.69 and A.70); soft accelerometer failures, SAC1 and SAC2 (See Fig.'s A.64 thru A.66); soft and hard Doppler errors, SDOP (Fig.'s A.64 thru A.66) and HDOP (See Fig. A.63). The only tractable explanation for this lack of sensitivity is the fact that both soft and hard failures (except for HDOP) were injected through that state differential equations. These errors must first be transformed through a direction cosine matrix which carries the error states from the platform frame to the navigation frame. Because of the harsh maneuvers during this time frame, certain angles of the coordinate frame transformation become both extremely large and extremely small. When these angles become arguments for cosines and sines, the failures can be significantly reduced

Table IV

Doppler Likelihood Function Failure Statistics for Design And Dynamic(+) Flight

| Simulated Failure | LF#7  |      | LF#8  |      | LF#9  |      | LF#76 |      | LF#83  |      | LF#93 |      |
|-------------------|-------|------|-------|------|-------|------|-------|------|--------|------|-------|------|
|                   | Mag   | Time | Mag   | Time | Mag   | Time | Mag   | Time | Mag    | Time | Mag   | Time |
| No Fail           | -4.66 | 515  | -5.62 | 515  | -6.79 | 475  | -5.67 | 2640 | -4.16  | 2735 | -7.22 | 2725 |
| SGY1              | -4.65 | 515  | -5.62 | 515  | -6.79 | 475  | -5.67 | 2640 | -4.15  | 2735 | -7.25 | 2725 |
| SGY2              | -4.67 | 515  | -5.62 | 515  | -6.79 | 475  | -5.67 | 2640 | -4.17  | 2735 | -7.22 | 2725 |
| SGY3              | -4.66 | 515  | -5.62 | 515  | -6.79 | 475  | -5.67 | 2640 | -4.16  | 2735 | -7.23 | 2725 |
| HGY1              | *     | 490  | -6.87 | 495  | -6.79 | 475  | -5.67 | 2640 | -4.14  | 2735 | -7.28 | 2725 |
| HGY2              | *     | 485  | -6.84 | 495  | -6.79 | 475  | -5.67 | 2640 | -4.19  | 2735 | -7.22 | 2725 |
| HGY3              | -4.64 | 515  | -5.63 | 515  | -6.79 | 475  | -5.67 | 2640 | -4.16  | 2735 | -7.23 | 2725 |
| SAC1              | -5.73 | 515  | -5.84 | 515  | -6.79 | 475  | -5.67 | 2640 | -5.44* | 2735 | -7.29 | 2725 |
| SAC2              | -5.73 | 515  | -5.94 | 500  | -6.79 | 475  | -5.67 | 2640 | -4.44  | 2735 | -7.03 | 2725 |
| SAC3              | -4.66 | 515  | -5.62 | 500  | -6.76 | 475  | -5.67 | 2640 | -4.15  | 2735 | -7.1  | 2725 |
| HAC1              | -5.98 | 485  | -8.79 | 515  | -6.76 | 475  | -6.71 | 2705 | -4.2   | 2675 | *     | 2725 |
| HAC2              | -6.06 | 485  | -5.77 | 475  | -6.79 | 475  | -5.70 | 2675 | -4.52  | 2695 | -7.02 | 2725 |
| HAC3              | -4.69 | 515  | -5.61 | 500  | -7.52 | 475  | -5.67 | 2640 | -4.33  | 2735 | -8.07 | 2685 |
| SDOP              | -9.35 | 475  | -8.61 | 470  | -6.79 | 475  | -6.08 | 2675 | -8.08  | 2655 | -7.88 | 2680 |
| HDOP              | -4.54 | 515  | -5.38 | 515  | -7.02 | 455  | -5.67 | 2675 | -4.34  | 2690 | -7.22 | 2725 |

\* indicates initial failure value after threshold

and hard to distinguish, resulting in missed failures.

The explanation for HDOP is related to the higher no-failure dynamic likelihood function magnitude for the vertical measure and lower value for measurement 8 which make the failure detection sensitivity for measurement 8 greater than for measurement 9.

#### Terrain Correlator Failure Detection (Benign)

The terrain correlator measurement process results are shown in Table XV which appears later. Both benign and dynamic results are given in this table. The discussion initially deals with the benign case. Dynamic results will be discussed at the end of this section. Measurements 10, 11, and 12 correspond to the east position error state, north position error state, and vertical position error states, respectively.

Soft gyro failures (SGY1, SGY2, SGY3) did not change the likelihood function values from the no-failure condition. This is consistent with the findings for both the satellite and Doppler results and the same explanation is proposed for this case.

Hard gyro failure (HGY1, HGY2, HGY3) were not detected for any of the cases. This is consistent with the satellite position measurements and the conditions for this unobservable behavior are explained in the satellite position.

Soft accelerometer failures (SAC1, SAC2, SAC3) were basically only observable in measurement 10 (See Fig.'s A.79 and A.86). Their magnitude (related to the no-failure condition) is not a significant increase. A failure declaration for these failures would require extremely tight thresholds. One could state that these failures are slightly observable.

Hard accelerometer failures (HAC1, HAC2, HAC3) produced



significant changes in the likelihood functions for all 3 measurements. A HAC1 failure was observable in measurements 10 and 11 (See Fig.'s A.87 and A.88). A HAC2 failure was observable in measurements 10 and 11 ( See Fig.'s A.84 and A.85). A HAC3 failure was detected in measurement 12 (See Fig. A.82). When compared to the satellite position results, a greater sensitivity was seen in HAC1, HAC2, and HAC3 failures for the terrain correlator. The exact reason for this greater sensitivity is not clear. It is possible that the filter tuning for the satellite position measurement process requires additional effort. Filter tuning will be discussed in the Chapter VI, Recommendations.

A hard radar-altimeter failure (HRAF) was found in measurement process 3 (See Fig. A. 80). Again, this is what was expected. The magnitude of this failure was significant and rapid detection of this type of failure should occur.

A hard baro-accelerometer failure (HBAF) was highly observable in measurement 3 (See Fig. A.83). The failure magnitude should make the detection processor react quickly.

#### Terrain Correlator Failure Detection (Dynamic)

The dynamic flight results shown in Table XV, demonstrate a different type of behavior than that which was seen in both the satellite and Doppler measurements. Satellite and Doppler dynamic results demonstrated a tremendous decrease in failure sensitivity compared to the benign case results, which was attributed to coordinate frame transformation conditions. The terrain correlator dynamic flight results show a "redistribution" of the failure magnitudes. However, one has to hypothe-

size the same explanation for this condition since the "re-distribution" could only take place through a direction cosine matrix transformation.

Both soft and hard gyro failures were not observed. This is consistent with the results noted for the satellite position measurements.

Soft accelerometer failures (SAC1, SAC2, SAC3) were found in measurement process 10 (See Fig.'s A.95 and A.96). Again the coordinate frame transformation is assumed to be responsible.

Hard accelerometer failures (HAC1, HAC2, HAC3) had mixed results. A HAC1 failure was detected in measurements 10 and 11 (See Fig.'s A.97 and A.98). A HAC2 failure was found in measurement 10 (See Fig. A.99). A HAC3 failure was observed in measurement 10 (See Fig. A.100). Again, the strong coupling into measurement process 10 is consistent with the other dynamic results.

A soft radar-altimeter failure (SRAF) was detected in measurement process 12 (See Fig. A.103). This failure induced increase in likelihood function magnitude was extremely small.

A hard radar-altimeter failure (HRAF) was observable in measurement 12 (See Fig. A.104). The measurement 12 results were expected since this failure was injected through the vertical measurement process.

A hard baro-altimeter failure (HBAF) was detected by measurement process 12 (See Fig. A.105). The strong magnitude of the failure seen in measurement 12 was expected for the same

Table XV  
Terrain Correlator Likelihood Function For Design And Dynamic(3) Flight

| Simulated Failure | LF#10  |      | LF#11 |      | LF#12   |      | LF#100 |       | LF#110 |       | LF#120 |       |
|-------------------|--------|------|-------|------|---------|------|--------|-------|--------|-------|--------|-------|
|                   | Mag    | Time | Mag   | Time | Mag     | Time | Mag    | Time  | Mag    | Time  | Mag    | Time  |
| No Fail           | -5.44  | 505. | -2.32 | 500. | -6.15   | 475. | -5.99  | 2745. | -4.25  | 2655. | -6.7   | 2610. |
| SGY1              | -5.44  | 505. | -2.32 | 500. | -6.15   | 475. | -5.99  | 2715. | -4.25  | 2655. | -6.7   | 2610. |
| SGY2              | -5.44  | 505. | -2.32 | 500. | -6.15   | 475. | -5.78  | 2720. | -4.25  | 2655. | -6.7   | 2610. |
| SGY3              | -5.44  | 505. | -2.32 | 500. | -6.15   | 475. | -5.79  | 2720. | -4.25  | 2655. | -6.7   | 2610. |
| HGY1              | -5.43  | 505. | -2.32 | 500. | -6.15   | 475. | -5.96  | 2715. | -4.25  | 2655. | -6.7   | 2610. |
| HGY2              | -5.45  | 505. | -2.32 | 500. | -6.15   | 475. | -5.98  | 2715. | -4.25  | 2655. | -6.7   | 2610. |
| HGY3              | -5.44  | 505. | -2.32 | 500. | -6.15   | 475. | -5.80  | 2720. | -4.25  | 2655. | -6.7   | 2610. |
| SAC1              | -5.62* | 495. | -2.28 | 500. | -6.15   | 475. | -6.58* | 2715. | -4.25  | 2655. | -6.7   | 2610. |
| SAC2              | -5.62* | 495. | -2.39 | 495. | -6.15   | 475. | -6.58  | 2715. | -4.25  | 2655. | -6.7   | 2610. |
| SAC3              | -5.44  | 505. | -2.32 | 500. | -6.13   | 475. | -6.01  | 2715. | -4.25  | 2655. | -6.7   | 2610. |
| HAC1              | -6.98  | 495. | -2.69 | 505. | -6.15   | 475. | -6.36  | 2715. | -5.14  | 2725. | -6.7   | 2610. |
| HAC2              | -7.02  | 495. | -2.42 | 475. | -6.15   | 475. | -9.89  | 2715. | -4.26  | 2725. | -6.7   | 2610. |
| HAC3              | -5.44  | 505. | -2.32 | 500. | -7.33   | 515. | -6.13  | 2715. | -4.26  | 2725. | -6.77  | 2690. |
| GRAP              | -5.44  | 505. | -2.32 | 500. | -6.48   | 475. | -6.00  | 2715. | -4.26  | 2655. | -6.77  | 2610. |
| HKAP              | -5.44  | 505. | -2.32 | 495. | -45.00* | 460. | -6.02  | 2715. | -4.26  | 2655. | -46.37 | 2650. |
| HBAF              | -5.44  | 505. | -2.32 | 495. | -15.47* | 460. | -6.01  | 2715. | -4.26  | 2655. | -46.37 | 2650. |

\* indicates initial failure value after threshold

reason given for the hard radar-altimeter failure.

#### Another Detection Approach

The results discussed for satellite, Doppler, and terrain correlator measurement failure detection demonstrated a significant lack of sensitivity utilizing failure magnitude as the sole condition for failure declaration. The use of thresholds (magnitude limits) for failure declaration needs to be complemented by some other form of "trigger" which monitors another characteristic of the likelihood function. The two failure detectors working together should improve the detection process. Evaluation of the likelihood functions for the various measurement processes offered a possible parameter which could be utilized. Under failed conditions, likelihood functions for observable failures demonstrate a negative value increase (i.e., magnitude increase). However, these increases may be unobserved because the use of a conservative threshold will not detect the failure. This "negative increase" characteristic of the failure can be exploited. Additionally, one could also use tighter threshold with time-to-failure declaration.

A negative slope detector with variable sample size can be developed which slides along the likelihood function. This slope detector functions by working with the N-step likelihood function "window" to observe the negative growth of the likelihood function. The slope detector is thus an M-step "window" in which the likelihood function operates. The equation for the likelihood function is given in Eq. 4-24. The slope de-

tector takes each N-step likelihood function value and compares it to the next likelihood function value. If the next value is more negative than the preceeding value, the next likelihood function value is tested. This process continues until such time as the preestablished Mth-step has been reached (at which time a failure is declared), or, if a sample fails the test, the M-step process is reinitialized from this negative sample. The sensitivity (window size) can be established based on the no-failure flight characteristics. Once this is done, a failure should be declared if the M-step window found M samples in which each successive sample was more negative than the preceeding sample or samples.

This additional detection will be exercised against the same flight profiles as the magnitude detector in a stand alone fashion. Once this has been done, the results of threshold testing and the slope detector will be combined to determine their joint capability.

#### No-Failure Slope Detection

The establishment of the suitable "window" size for the slope detector was based on finding the sensitivity point (point at which no failures are declared under no-failure conditions) for each of the likelihood functions for both benign and dynamic flight. Exercising each of the measurement processes over the same flight profiles (same likelihood function results), the slope detectors were tuned to be insensitive to the slope characteristics for no-failure operation. The end results of this tuning produced the following "windows" for

the slope detector:

- 1.) Satellite (Benign) 4
- 2.) Satellite (Dynamic) 7
- 3.) Doppler (Benign) 6
- 4.) Doppler (Dynamic) 7
- 5.) Terr Corr (Benign) 6
- 6.) Terr Corr (Dynamic) 6

#### Satellite Slope Failure Detection (Benign)

Tables XVI and XVII, found later in this chapter, contain the results of the failure simulations for this measurement sequence. The most significant impact of this failure detection process is found in the hard accelerometer failures and soft satellite failures. A lesser capability is found for soft accelerometer failures.

#### Satellite Slope Failure Detection (Dynamic)

Tables XVI and XVIII demonstrate a reduced detection capability when compared to the benign slope detection capability. However, when this information is added to the simple threshold test, additional failure information has been made available.

#### Doppler Slope Failure Detection (Benign)

Tables XVI and XIX provide the information for this measurement sequence. As can be seen in Table XVI, there is very little information to make a distinction between failures with slope detection as the sole test. Table XIX provided the sequence for a particular failure and does provide insight as to which failure is identifiable dependent on the time of fail-

ure declaration.

#### Doppler Slope Failure Detection (Dynamic)

The results for this test are provided in Tables XVI and XX which are found later in this chapter. The information shown in Table XVI demonstrates a greater sensitivity to failures than the benign case. Table XX reveals that this failure information should contribute significantly to the decision process.

#### Terrain Correlator Slope Failure Detection (Benign)

A small failure detection capability is found in Tables XVI and XXI. The only failures which were detectable with this technique were hard accelerometer failures. Table XXI provides the time-of-failure sequence for these failures.

#### Terrain Correlator Slope Failure Detection (Dynamic)

A significant change from the benign case is noted in Tables XVI and XXII. The detection capability diminished for the hard accelerometer failures but improved for soft accelerometer failures.

#### Slope Detection Analysis

This technique has demonstrated a notable contribution to the failure declaration decision process. Especially in the dynamic case, a significant improvement in failure detection was achieved. The most notable class of failure was hard accelerometer failures. Soft accelerometer failures also gained additional information for failure isolation. It can be surmised that the combination of these results with those achieved by simple threshold establishment should offer a more divers-

Table XVI

## Slope Failure Detection Results

| Failure Simulated | Satellite Sequence |         | Doppler Sequence |         | Terrain Correlator Sequence |         |
|-------------------|--------------------|---------|------------------|---------|-----------------------------|---------|
|                   | Benign             | Dynamic | Benign           | Dynamic | Benign                      | Dynamic |
| SGY1              | NF                 | NF      | NF               | NF      | NF                          | NF      |
| SGY2              | NF                 | NF      | NF               | NF      | NF                          | NF      |
| SGY3              | NF                 | NF      | NF               | NF      | NF                          | NF      |
| HGY1              | NF                 | NF      | NF               | NF      | NF                          | NF      |
| HGY2              | NF                 | NF      | NF               | NF      | NF                          | NF      |
| HGY3              | NF                 | NF      | NF               | NF      | NF                          | NF      |
| SAC1              | 5                  | NF      | 8                | 7       | NF                          | 11,10   |
| SAC2              | 5,4                | 5       | NF               | 7       | NF                          | 11,10   |
| SAC3              | NF                 | NF      | NF               | NF      | NF                          | NF      |
| HAC1              | 4,6,3,5            | 4,2     | 8                | 9,8,7   | 10                          | 11,12   |
| HAC2              | 6,4,<br>5,3,2      | 2,5     | 8,7              | 9,8     | 10,11                       | NF      |
| HAC3              | 6,4,<br>5,3,2      | 2,5,6   | 9                | NF      | 12,11                       | 10      |
| SSATF             | 6,2,1,3            | 1,2,3,4 | N/A              | N/A     | N/A                         | N/A     |
| HSATF             | 5                  | NF      | N/A              | N/A     | N/A                         | N/A     |
| SDOP              | N/A                | N/A     | 8                | 8,7,9   | N/A                         | N/A     |
| HDOP              | N/A                | N/A     | NF               | 9,7     | N/A                         | N/A     |
| SRAF              | N/A                | N/A     | N/A              | N/A     | NF                          | NF      |
| HRAF              | N/A                | N/A     | N/A              | N/A     | NF                          | NF      |
| HBAF              | N/A                | N/A     | N/A              | N/A     | NF                          | NF      |



Table XVII

Slope Failure Sequence For Satellite Likelihood Functions (Benign Flight)

| Failure Simulated | LF# | Time | LF# | Time | LF# | Time | LF# | Time | LF# | Time |
|-------------------|-----|------|-----|------|-----|------|-----|------|-----|------|
| SAC1              | 5   | 540  | --  | --   | --  | --   | --  | --   | --  | --   |
| SAC2              | 5   | 500  | 4   | 530  | --  | --   | --  | --   | --  | --   |
| HAC1              | 4   | 485  | 6   | 495  | 3   | 495  | 5   | 510  | --  | --   |
| HAC2              | 6   | 485  | 4   | 485  | 5   | 490  | 3   | 495  | 2   | 545  |
| HAC3              | 6   | 485  | 4   | 490  | 5   | 510  | 3   | 530  | 2   | 540  |
| SSATF             | 6   | 485  | 2   | 485  | 1   | 500  | 3   | 530  | --  | --   |
| HSATF             | 5   | 525  | --  | --   | --  | --   | --  | --   | --  | --   |

Table XVIII

Slope Failure Sequence For Satellite Likelihood Functions (Dynamic Flight)

| Failure Simulated | LF# | Time | LF# | Time | LF# | Time | LF# | Time | LF# | Time |
|-------------------|-----|------|-----|------|-----|------|-----|------|-----|------|
| SAC2              | 5   | 2765 | --  | --   | --  | --   | --  | --   | --  | --   |
| HAC1              | 4   | 2700 | 2   | 2710 | --  | --   | --  | --   | --  | --   |
| HAC2              | 2   | 2710 | 5   | 2795 | --  | --   | --  | --   | --  | --   |
| HAC3              | 2   | 2710 | 5   | 2710 | 6   | 2780 | --  | --   | --  | --   |
| SSATF             | 1   | 2680 | 2   | 2710 | 3   | 2755 | 4   | 2845 | --  | --   |

Table XIX

Slope Failure Sequence For Doppler  
Likelihood Functions (Benign Flight)

| Failure<br>Simulation | LF# | Time | LF# | Time |
|-----------------------|-----|------|-----|------|
| SAC1                  | 8   | 535  | --  | --   |
| HAC1                  | 8   | 525  | --  | --   |
| HAC2                  | 8   | 495  | 7   | 515  |
| HAC3                  | 9   | 525  | --  | --   |
| SDOP                  | 7   | 495  | 8   | 500  |

Table XX

Slope Failure Sequence For Doppler  
Likelihood Functions (Dynamic Flight)

| Failure<br>Simulated | LF# | Time | LF# | Time | LF# | Time |
|----------------------|-----|------|-----|------|-----|------|
| SAC1                 | 7   | 2815 | --  | --   | --  | --   |
| SAC2                 | 7   | 2830 | --  | --   | --  | --   |
| HAC1                 | 9   | 2690 | 8   | 2700 | 7   | 2780 |
| HAC2                 | 9   | 2690 | 8   | 2695 | --  | --   |
| SDOP                 | 8   | 2675 | 7   | 2815 | 9   | 2825 |
| HDOP                 | 9   | 2760 | 7   | 2765 | --  | --   |

Table XXI

Slope Failure Sequence For Terrain Correlator  
Likelihood Functions (Benign Flight)

| Failure<br>Simulated | LF# | Time | LF# | Time |
|----------------------|-----|------|-----|------|
| HAC1                 | 10  | 535  | --  | --   |
| HAC2                 | 10  | 535  | 11  | 540  |
| HAC3                 | 12  | 520  | 11  | 545  |

Table XXII

Slope Failure Sequence For Terrain Correlator  
Likelihood Functions (Dynamic Flight)

| Failure<br>Simulated | LF# | Time | LF# | Time |
|----------------------|-----|------|-----|------|
| SAC1                 | 11  | 2815 | 10  | 2845 |
| SAC2                 | 11  | 2820 | 10  | 2835 |
| HAC1                 | 11  | 2720 | 12  | 2725 |
| HAC3                 | 10  | 2765 | --  | --   |

ified failure isolation algorithm. This failure information for the joint detection logic is given in Tables XXIII thru XXIX.

#### The FDI Detection Processor

The failure detection capability for each of the measurement processes is shown in Tables XXIII thru XXIX. The information derived from these tables will be utilized to develop a suitable isolation/identification algorithm and software implementation. The significant aspect of this complete detection processor will be the reliance on both simple threshold and slope detection failure sequence for a decision. For instance, as noted in Tables XXIII and XXIV a HAC1 failure during satellite measurement (benign flight) would result in the following sequence for each detection method:

| <u>Threshold</u> | <u>Slope</u> |
|------------------|--------------|
| 5-470 sec        | 4-490 sec    |
| 4-480 sec        | 6-495 sec    |
| 6-485 sec        | 3-510 sec    |
|                  | 5-520 sec    |

As can be seen from this data, four additional votes are available from the slope detector to, in effect, enhance the failure decision process. This same argument can be repeated for all Table XXIII entries where both simple threshold and slope detection logic have generated a measurement failure sequence for a particular fault. The pattern for each type of failure would hopefully generate a simple decision set. One point that

should be made is, the hard failure of an INS sensor (gyro or accelerometer) dictates a failed INS. Therefore, the simple logic of declaring an INS failure vs. a specific INS component is justified. In some cases (soft failures) the isolation to a specific gyro or accelerometer could allow the sensor to continue to operate if the additional error from the soft failure could be compensated for in the filter structure (e.g., increasing the measurement noise strength, R).

For external aiding devices, the same argument as given in the previous paragraph holds. This simplifies the isolation process where the desire for simplicity is a key issue.

The isolation capability of the processor demonstrate a diversified decision table which decreases the ambiguities and increases the probability of a correct isolation.

Table XXIV demonstrates a significant isolation capability for the satellite benign case with the only ambiguities noted for the hard gyro failure isolation. However, once a hard gyro failure of any kind has been noted, the INS has failed so isolation to a specific sensor is not necessarily important. Table XXV contains the information for the satellite dynamic case. Although this is a significant reduction in capability, the isolation process for those failures that were detectable had an enhanced failure isolation capability vs. a single test of either type.

Table XXVI contains the information for the benign Doppler case. As can be seen from the table, ambiguity exists for the hard gyro failure isolation capability. All other failures

are distinct from each other. Table XXVII provides the data for the dynamic Doppler detection isolation capability. Again, there is an ambiguity; however, this time it is for the soft accelerometer failures. If one is willing to use a time-to-failure declaration algorithm, then this ambiguity can be removed. All other failures generated distinct failure sequences.

Table XXVII demonstrates a severe ambiguity problem for the terrain correlator benign case. Ambiguities exist in both soft accelerometer failures, soft and hard radar altimeter failures and hard baro-altimeter failures. The only way to begin to overcome this problem would be a failure growth rate test or some other form of test to isolate the failures based on a single measurement failure. Table XXIX which provides information for the dynamic terrain correlator case, demonstrates ambiguity problems, also. Soft accelerometer failures, hard radar-altimeter failures, and hard baro-altimeter failures had ambiguity problems. Again, some form of time-to-failure parameter or growth rate test would aid the isolation capability.

Table XXIII summarizes the combined failure detection capability for this FDI processor. As demonstrated by this table, all soft gyro failures (SGY1, SGY2, SGY3) were undetected by the measurement processes (LF#1 thru LF#12); therefore, some other failure detection methodology must be employed to discern failures of this type. Hard gyro failures (HGY1, HGY2) were detectable by LF#4 thru LF#8 for the benign

case. As seen in Tables XXIV and XXVI, HGY1 and HGY2 failures were ambiguous in the particular failure sequence; however, the use of a time-between-failure test (e.g., the failure time between LF#7 and LF#8) could remove this ambiguity. No hard gyro failures were observed in the dynamic case. Table XXIII also demonstrates the fact that there are no ambiguities for soft accelerometer failures (SAC1, SAC2, SAC3) in the benign case. A SAC1 failure is discernable from a SAC2 failure because LF#6 detects a SAC2 failure but does not detect the SAC1 failure. In the dynamic case, this same argument holds except LF#5 detects a SAC2 failure but does not detect a SAC1 failure. Hard accelerometer failures (HAC1, HAC2, HAC3) did not produce any ambiguity problems for either the benign or dynamic case. This is evidenced by the results shown in Table XXIII and further refined by Tables XXIV thru XXIX. The remaining failure types shown in Table XXIII will not be addressed since they are aiding device peculiar.

In summary, this analysis indicated an enhanced decision capability for the total (threshold and slope) FDI system. However, ambiguity problems exist that need to be addressed.

Table XXIII

## Combined Failure Detection Capability

| Simulated Failure | Satellite Detection    |                    | Doppler Detection |                  | Terrain Correlator Detection |                  |
|-------------------|------------------------|--------------------|-------------------|------------------|------------------------------|------------------|
|                   | Benign                 | Dynamic            | Benign            | Dynamic          | Benign                       | Dynamic          |
| SGY1              | +NF<br>*NF             | +NF<br>*NF         | +NF<br>*NF        | +NF<br>*NF       | +NF<br>*NF                   | +NF<br>*NF       |
| SGY2              | +NF<br>*NF             | +NF<br>*NF         | +NF<br>*NF        | +NF<br>*NF       | +NF<br>*NF                   | +NF<br>*NF       |
| SGY3              | +NF<br>*NF             | +NF<br>*NF         | +NF<br>*NF        | +NF<br>*NF       | +NF<br>*NF                   | +NF<br>*NF       |
| HGY1              | +4,5,6<br>*NF          | +NF<br>*NF         | +7,8<br>*NF       | +NF<br>*NF       | +NF<br>*NF                   | +NF<br>*NF       |
| HGY2              | +4,5,6<br>*NF          | +NF<br>*NF         | +7,8<br>*NF       | +NF<br>*NF       | +NF<br>*NF                   | +NF<br>*NF       |
| HGY3              | +NF<br>*NF             | +NF<br>*NF         | +NF<br>*NF        | +NF<br>*NF       | +NF<br>*NF                   | +NF<br>*NF       |
| SAC1              | +4,6<br>*5             | +NF<br>*NF         | +7,8<br>*8        | +8<br>*7         | +10<br>*NF                   | +10<br>*11,10    |
| SAC2              | +4,5<br>*5,4           | +4<br>*5           | +7,8<br>*NF       | +8<br>*7         | +10<br>*NF                   | +10<br>*11,10    |
| SAC3              | +6<br>*NF              | +NF<br>*NF         | +NF<br>*NF        | +NF<br>*NF       | +NF<br>*NF                   | +NF<br>*NF       |
| HAC1              | +4,5,6<br>*4,6,3,5     | +4,5<br>*4,2       | +7,8<br>*8        | +7,9<br>*9,8,7   | +10,11<br>*10                | +10,11<br>*11,12 |
| HAC2              | +4,5<br>*6,4,5,3,2     | +4<br>*2,5         | +7,8<br>*8,7      | +7,8<br>*9,8     | +10,11<br>*10,11             | +10<br>*NF       |
| HAC3              | +3,4,5,6<br>*6,4,3,5,2 | +3,6<br>*2,5,6     | +7,9<br>*9        | +8,9<br>*NF      | +12<br>*12,11                | +10<br>*10       |
| SSATF             | +1,2,3<br>*6,2,1,3     | +1,2,3<br>*1,2,3,4 | N/A               | N/A              | N/A                          | N/A              |
| HSATF             | +4,5,6<br>*5           | +NF<br>*NF         | N/A               | N/A              | N/A                          | N/A              |
| SDOP              | N/A                    | N/A                | +7,8,9<br>*8      | +7,8,9<br>*8,7,9 | N/A                          | N/A              |
| HDOP              | N/A                    | N/A                | +9<br>*NF         | +8<br>*9,7       | N/A                          | N/A              |
| SRAF              | N/A                    | N/A                | N/A               | N/A              | +12<br>*NF                   | +12<br>*NF       |
| HRAF              | N/A                    | N/A                | N/A               | N/A              | +12<br>*NF                   | +12<br>*NF       |
| HBAF              | N/A                    | N/A                | N/A               | N/A              | +12<br>*NF                   | +12<br>*NF       |

+ magnitude threshold violation; \* slope failure declaration



Table XXIV  
Combined Failure Isolation Capability For Satellite  
Likelihood Functions (Benign Flight)

| Failure<br>Simulated | Failure Sequence (+=Threshold *=-Slope) |     |     |     |     |     |     |     |     |
|----------------------|---|-----|-----|-----|-----|-----|-----|-----|-----|
|                      | #1                                      | #2  | #3  | #4  | #5  | #6  | #7  | #8  | #9  |
| HGY1                 | LF                                      | 5+  | 4+  | --  | --  | --  | --  | --  | --  |
|                      | Time                                    | 470 | 480 | 495 | --  | --  | --  | --  | --  |
| HGY2                 | LF                                      | 5+  | 4+  | --  | --  | --  | --  | --  | --  |
|                      | Time                                    | 470 | 480 | 485 | --  | --  | --  | --  | --  |
| SAC1                 | LF                                      | 4+  | 6+  | --  | --  | --  | --  | --  | --  |
|                      | Time                                    | 490 | 495 | 540 | --  | --  | --  | --  | --  |
| SAC2                 | LF                                      | 4+  | 5+  | 4*  | --  | --  | --  | --  | --  |
|                      | Time                                    | 480 | 480 | 500 | 530 | --  | --  | --  | --  |
| SAC3                 | LF                                      | 6+  | --  | --  | --  | --  | --  | --  | --  |
|                      | Time                                    | 485 | --  | --  | --  | --  | --  | --  | --  |
| HAC1                 | LF                                      | 5+  | 4+  | 4*  | 6*  | 3*  | 5*  | --  | --  |
|                      | Time                                    | 470 | 480 | 485 | 485 | 495 | 510 | --  | --  |
| HAC2                 | LF                                      | 4+  | 5+  | 6*  | 5*  | 3*  | 2*  | --  | --  |
|                      | Time                                    | 480 | 480 | 485 | 485 | 490 | 545 | --  | --  |
| HAC3                 | LF                                      | 5+  | 6+  | 4+  | 4*  | 3+  | 5*  | 3*  | 2*  |
|                      | Time                                    | 470 | 475 | 480 | 485 | 490 | 510 | 530 | 540 |
| SSATP                | LF                                      | 1+  | 2+  | 2*  | 1*  | 3+  | 3*  | --  | --  |
|                      | Time                                    | 470 | 475 | 485 | 485 | 500 | 530 | --  | --  |
| HSATP                | LF                                      | 4+  | 5+  | 6+  | 5*  | --  | --  | --  | --  |
|                      | Time                                    | 470 | 470 | 475 | 525 | --  | --  | --  | --  |

Table XXV  
Combined Failure Isolation Capability for Satellite  
Likelihood Functions (Dynamic Flight)

| Failure<br>Simulated | Failure Sequence (+ = Threshold, * = Slope) |      |      |      |      |      |      |
|----------------------|---|------|------|------|------|------|------|
|                      | #1  | #2   | #3   | #4   | #5   | #6   | #7   |
| SAC2                 | LF  | 4+   | 5*   | --   | --   | --   | --   |
|                      | Time  | 2725 | 2765 | --   | --   | --   | --   |
| HAC1                 | LF  | 5+   | 4+   | 2*   | --   | --   | --   |
|                      | Time  | 2675 | 2700 | 2700 | 2710 | --   | --   |
| HAC2                 | LF  | 4+   | 2*   | 5*   | --   | --   | --   |
|                      | Time  | 2685 | 2710 | 2795 | --   | --   | --   |
| HAC3                 | LF  | 6+   | 3+   | 2*   | 5*   | 6*   | --   |
|                      | Time  | 2670 | 2680 | 2710 | 2710 | 2780 | --   |
| SSATF                | LF  | 1+   | 1*   | 2+   | 2*   | 3*   | 4*   |
|                      | Time  | 2675 | 2680 | 2695 | 2710 | 2740 | 2755 |
|                      |   |      |      |      |      |      | 2845 |

Table XXVI

Combined Failure Isolation Capability Doppler  
Likelihood Functions (Benign Flight)

| Failure<br>Simulated | Failure Sequence +=Threshold, *=Clope |     |        |     |
|----------------------|---------------------------------------|-----|--------|-----|
|                      | #1                                    | #2  | #3     | #4  |
| HGY1                 | LF                                    | 7+  | 8+     | --  |
|                      | Time                                  | 490 | 495    | --  |
| HGY2                 | LF                                    | 7+  | 8+     | --  |
|                      | Time                                  | 485 | 495    | --  |
| SAC1                 | LF                                    | 7+  | 8+     | 8*  |
|                      | Time                                  | 515 | 515    | 535 |
| SAC2                 | LF                                    | 8+  | 7+     | --  |
|                      | Time                                  | 500 | 515    | --  |
| HAC1                 | LF                                    | 7+  | 8+     | 8*  |
|                      | Time                                  | 485 | 515    | 525 |
| HAC2                 | LF                                    | 8+  | 7+     | 8*  |
|                      | Time                                  | 475 | 485    | 495 |
| HAC3                 | LF                                    | 9+  | 7+     | 9*  |
|                      | Time                                  | 475 | 515    | 525 |
| SDOP                 | LF                                    | 8+  | 7+, 9+ | 7*  |
|                      | Time                                  | 470 | 475    | 495 |
| HDOP                 | LF                                    | 7+  | --     | --  |
|                      | Time                                  | 455 | --     | --  |

Table XXVII  
Combined Failure Isolation Capability For  
Doppler Likelihood Function  
(Dynamic Flight)

| Failure<br>Simulated | Failure Sequence (+=Threshold *-Slope) |      |      |      |      |      |
|----------------------|--|------|------|------|------|------|
|                      | #1                                     | #2   | #3   | #4   | #5   | #6   |
| SAC1                 | LF                                     | 7*   | --   | --   | --   | --   |
|                      | Time                                   | 2735 | --   | --   | --   | --   |
| SAC2                 | LF                                     | 8+   | --   | --   | --   | --   |
|                      | Time                                   | 2735 | --   | --   | --   | --   |
| HAC1                 | LF                                     | 9*   | 7+   | 9+   | 7*   | --   |
|                      | Time                                   | 2690 | 2705 | 2725 | 2780 | --   |
| HAC2                 | LF                                     | 7+   | 8+   | 8*   | --   | --   |
|                      | Time                                   | 2675 | 2690 | 2695 | --   | --   |
| HAC3                 | LF                                     | 9+   | --   | --   | --   | --   |
|                      | Time                                   | 2685 | --   | --   | --   | --   |
| SDOP                 | LF                                     | 8+   | 8*   | 9+   | 7*   | 9*   |
|                      | Time                                   | 2655 | 2675 | 2680 | 2815 | 2825 |
| HDOP                 | LF                                     | 8+   | 7*   | --   | --   | --   |
|                      | Time                                   | 2690 | 2765 | --   | --   | --   |

Table XXVIII  
Combined Failure Isolation Capability For Terrain  
Correlator Likelihood Functions  
(Benign Flight)

| Failure<br>Simulated | Failure Sequence (+=Threshold *=Slope) |     |     |     |
|----------------------|--|-----|-----|-----|
|                      | #1                                     | #2  | #3  | #4  |
| SAC1                 | 10+                                    | --  | --  | --  |
|                      | 495                                    | --  | --  | --  |
| SAC2                 | 10+                                    | --  | --  | --  |
|                      | 495                                    | --  | --  | --  |
| HAC1                 | 10+                                    | 11+ | 12* | --  |
|                      | 495                                    | 505 | 535 | --  |
| HAC2                 | 11+                                    | 10+ | 10* | 11* |
|                      | 475                                    | 495 | 535 | 540 |
| HAC3                 | 12+                                    | 12* | 11* | --  |
|                      | 515                                    | 520 | 545 | --  |
| SRAF                 | 12+                                    | --  | --  | --  |
|                      | 475                                    | --  | --  | --  |
| HRAF                 | 12+                                    | --  | --  | --  |
|                      | 460                                    | --  | --  | --  |
| HBAF                 | 12+                                    | --  | --  | --  |
|                      | 460                                    | --  | --  | --  |

Table XXIX  
Combined Failure Detection Capability For Terrain  
Correlator Likelihood Functions  
(Dynamic Flight)

| Failure<br>Simulated | Failure Sequence (+Threshold *-Slope) |      |      |      |      |
|----------------------|---------------------------------------|------|------|------|------|
|                      |                                       | #1   | #2   | #3   | #4   |
| SAC1                 | LF                                    | 10+  | 11*  | 10*  | --   |
|                      | Time                                  | 2715 | 2815 | 2845 | --   |
| SAC2                 | LF                                    | 10+  | 11*  | 10*  | --   |
|                      | Time                                  | 2715 | 2820 | 2835 | --   |
| HAC1                 | LF                                    | 10+  | 11*  | 11+  | 12*  |
|                      | Time                                  | 2715 | 2720 | 2725 | 2725 |
| HAC2                 | LF                                    | 10+  | --   | --   | --   |
|                      | Time                                  | 2715 | --   | --   | --   |
| HAC3                 | LF                                    | 10+  | 10*  | --   | --   |
|                      | Time                                  | 2715 | 2765 | --   | --   |
| HRAF                 | LF                                    | 12+  | --   | --   | --   |
|                      | Time                                  | 2650 | --   | --   | --   |
| HBAF                 | LF                                    | 12+  | --   | --   | --   |
|                      | Time                                  | 2650 | --   | --   | --   |

## VI. Conclusions And Recommendations

### Conclusions

This thesis has dealt with the development of a suitable filter model and failure detection/identification (FDI) processor for and adaptive tactical navigation (ATN) system model. A thorough review of the present FDI techniques was conducted and, based on this information, an innovations-based approach was selected. A likelihood function residual monitoring methodology was developed for the measurement processes. Based on the characteristics of the observed likelihood function values, a suitable failure detection algorithm was developed. The observed failure "signature" due to an introduced soft or hard failure was then tabulated to establish the basis for an isolation processor.

The performance of the FDI processor provided a baseline insight into its limitations and capabilities. The processor, as it is presently implemented, lacks sensitivity to gyro failures. This is due to the number of integrations between the injected failure and the error state which is present in the explicit measurement equation. The use of both simple threshold settings and the slope detection methodology in the failure detection processor provided generally acceptable results. Suggestions for areas of future consideration with respect to FDI methodology will be made in the Recommendation section.

The filter model which was developed for this thesis

resulted in a 26-state representation for a 52-state "truth" model. The proper tuning of this filter presented some problems due to the model reduction for certain sensors. The establishment of suitable values for the dynamic driving noise strength,  $Q$ , and the measurement noise strength,  $R$ , warranted the addition of pseudonoises to the position error states of the INS to prevent divergence. The addition of this pseudo-noise provided satisfactory performance but better performance may be achieved by readjustment of dynamic noise strengths for other filter states.

The software development has now reached the point where the isolation/identification algorithm can be implemented.

#### Recommendations

The following recommendations are being made to improve the overall performance of the FDI system and provide more insight into the FDI methodology.

- 1.) The state reduction for the filter model results in the addition of noise to compensate for unmodeled error states for various sensors. Further sensitivity studies should be conducted to determine what practical changes may be necessary to provide a filter that indeed contain the states needed for proper operation. The evaluation of the present filter suggests there may be unmodeled states which affect the filter performance (especially in a dynamic flight environment).



- 2.) The present failure detector is based on simple threshold surpassing and slope detecting criteria. Other innovations-based detection schemes are available which could be augmented with the existing detection structure to establish a lower rate of missed and/or false alarms, etc. One such technique which was addressed in Chapter I is the generalized likelihood ratio (GLR). This method can be implemented easily since the quantities are already available in the existing detection software. Also, one could utilize tighter thresholds with time-to-failure declaration plus looser thresholds with immediate declaration for tracking soft and hard failures, respectively. Another method could utilize additional filters for detection only. These filters are not updated N-sample periods to enhance their failure sensitivity. Further, one could implement a multiple model filter in which specific failures are explicitly modeled in the filter structure.
- 3.) Further "tuning" needs to be accomplished on the detection thresholds to develop a desirable trade off between false and missed alarms. As part of this "tuning" process, the detection window size, N, should be evaluated and adjusted to maximize the sensitivity of the likelihood function, but constrained by the need to prevent trivial (no-

failure) singularly large residuals from generating false alarms.

- 4.) The window adjustment for the slope detector also has a sensitivity which must be adjusted to minimize the false alarms/missed alarms. This adjustment should also be considered for failure detection enhancement. Also, some form of algorithm could be developed for adaptive window sizing based on the dynamic environment. This in essence allows sensitivity adjustment for failure detection.
- 5.) The Monte Carlo process should be based on a larger number of samples to generate statistics which are more accurately representative of true performance. The reason that only 10 samples were used for this research was due to time constraints. Increasing the number of Monte Carlo runs will undoubtedly require a retuning of the filter which will even carry over to the threshold settings for the likelihood functions. This retuning was previously addressed in (3).

### Appendix: Likelihood Function Plots

This appendix contains the plotted results for the various failures which were simulated. The information gathered from these plots support the discussion presented in Chapter V.

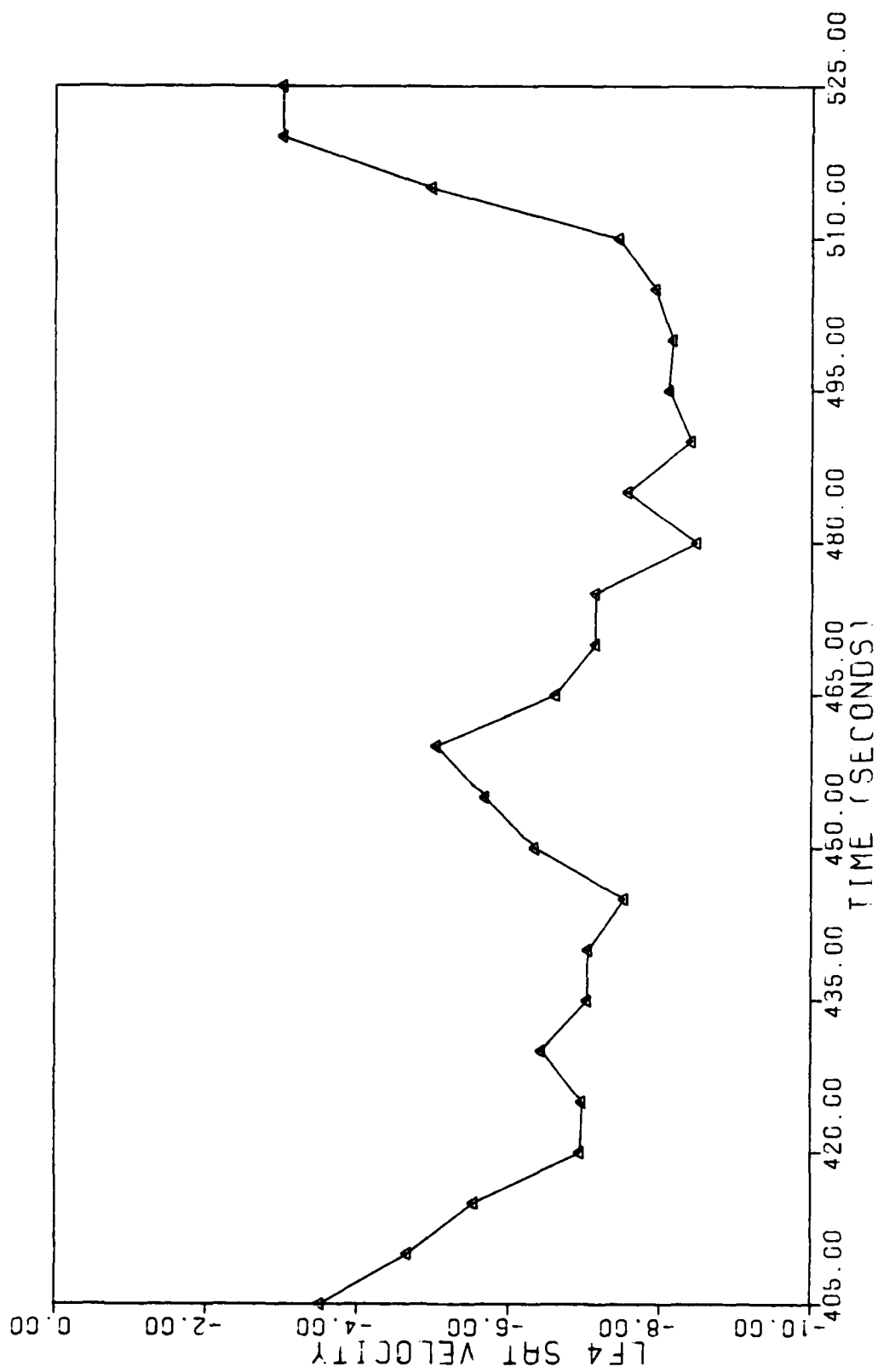


Fig. A.1. Hard Satellite Receiver Failure- - Satellite Velocity Measurement #4- - Benign Flight

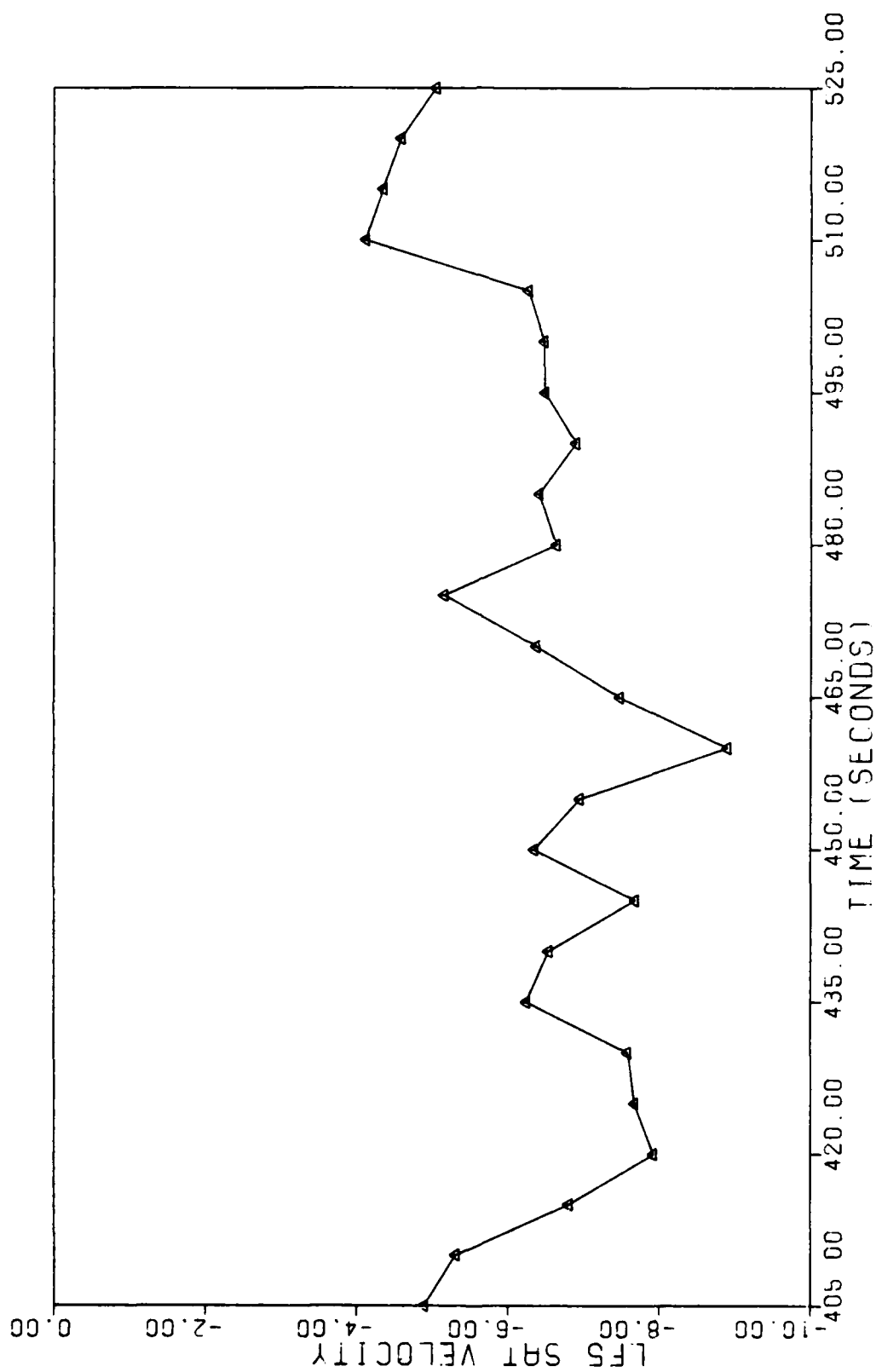


Fig. A.2. Hard Satellite Receiver Failure--Satellite Velocity Measurement #5--Benign Flight

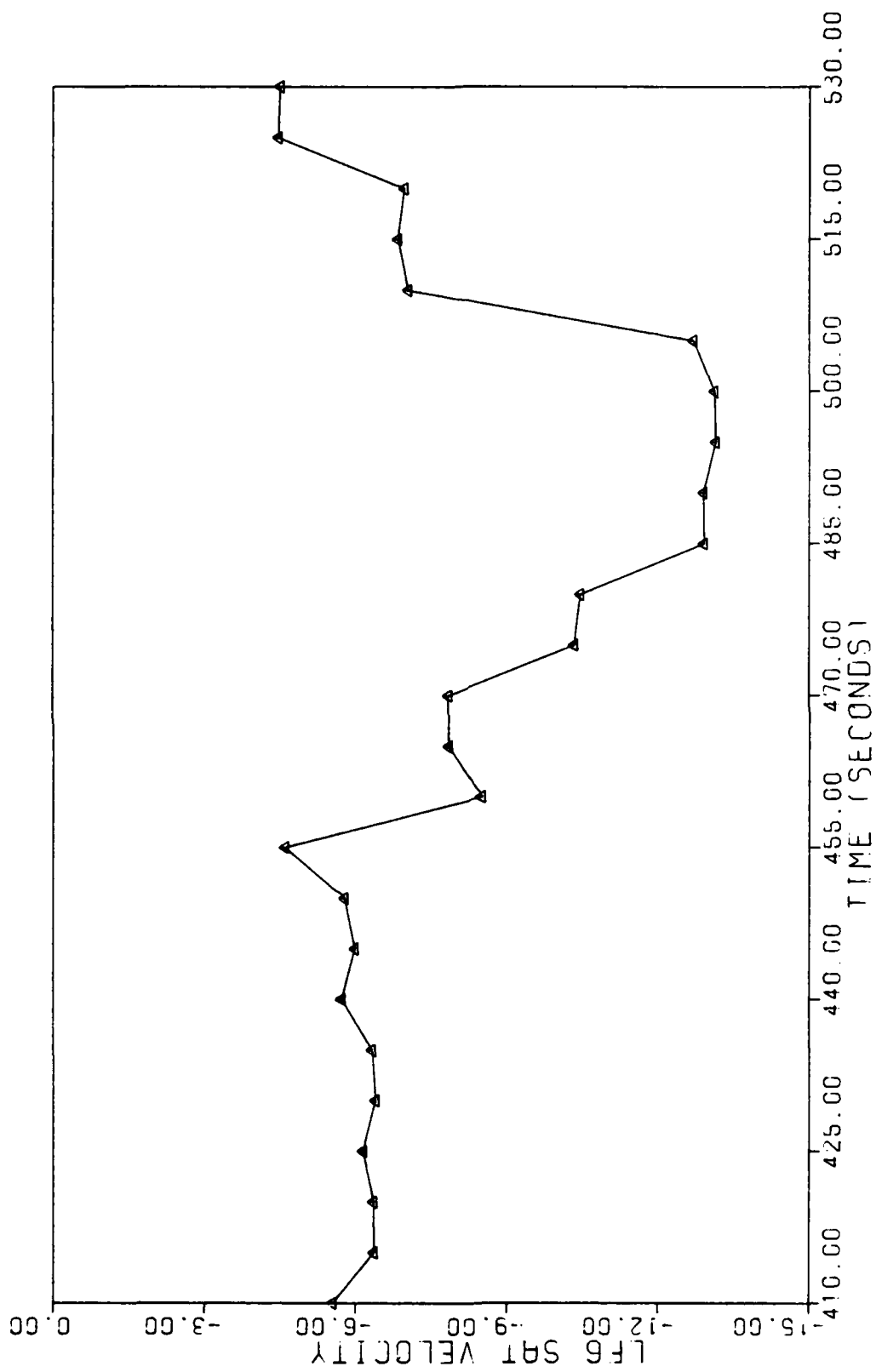


Fig. A.3. Hard Satellite Receiver Failure--Satellite Velocity Measurement #6--Benign Flight

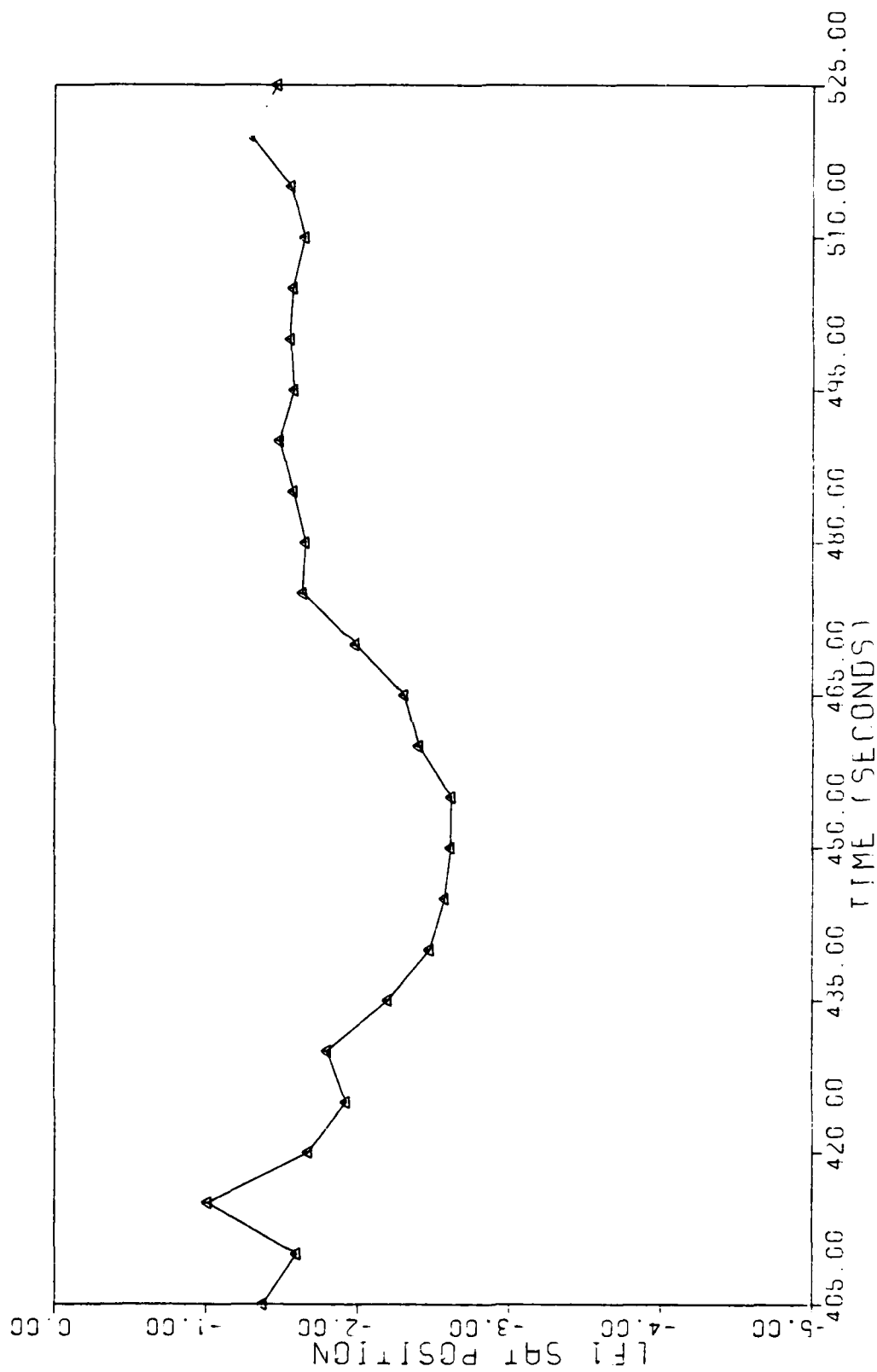


Fig. A.4. Soft Satellite Failure--Satellite Position Measurement #1--Benign Flight

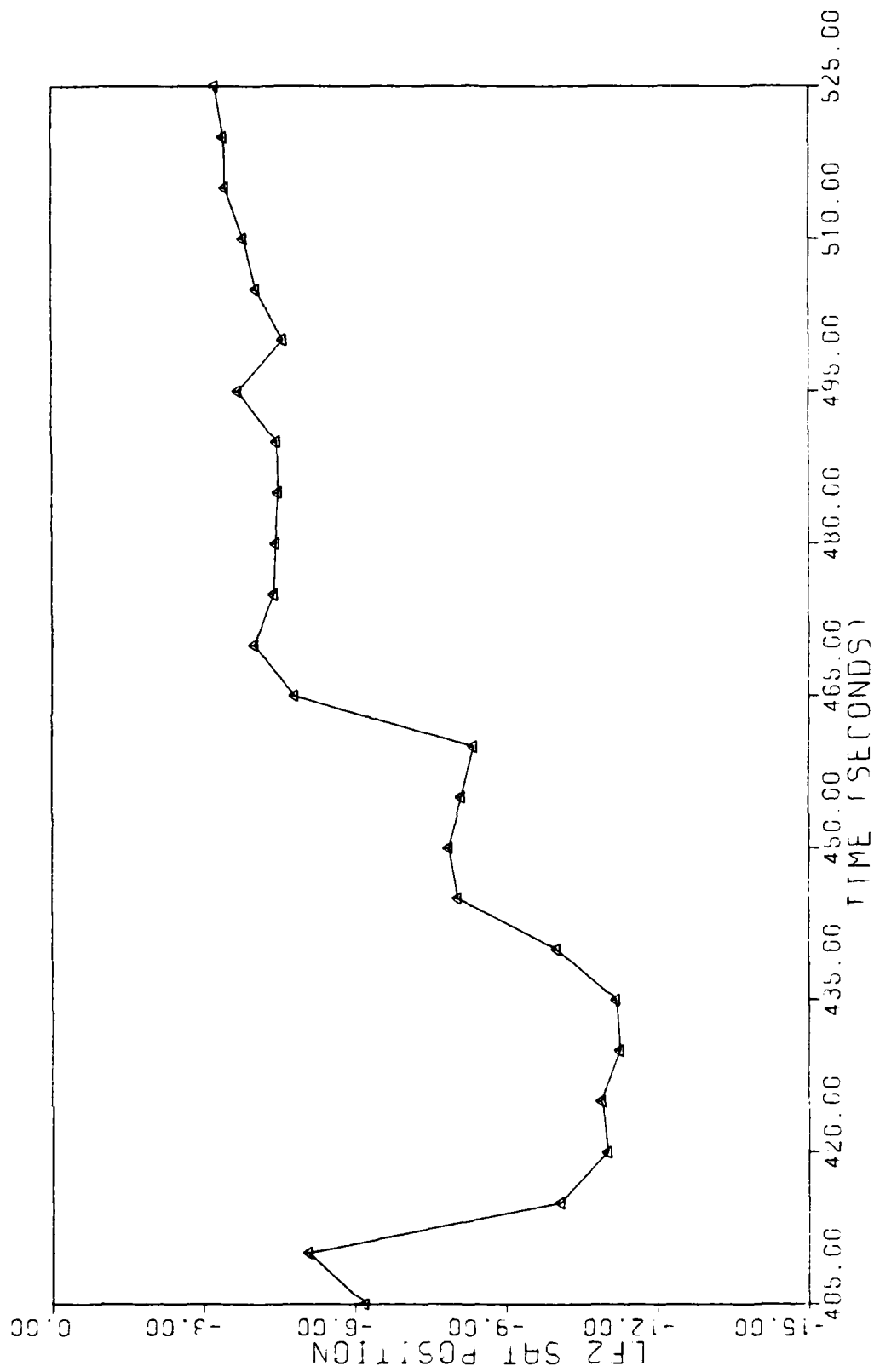


Fig. A.5. Soft Satellite Failure--Satellite Position Measurement #2--Benign Flight



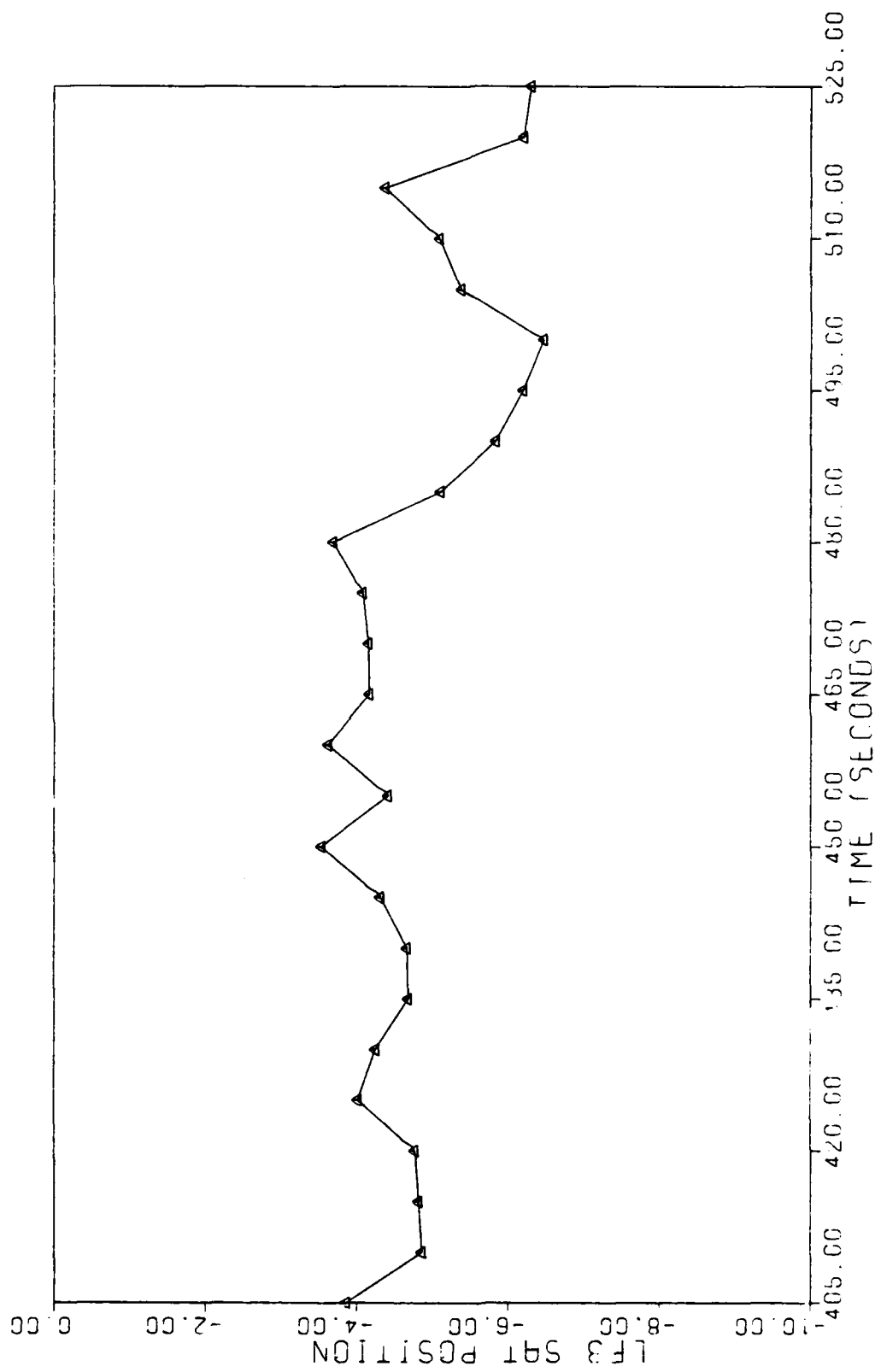


Fig. A.6. Soft Satellite Failure--Satellite Measurement #3--Benign Flight

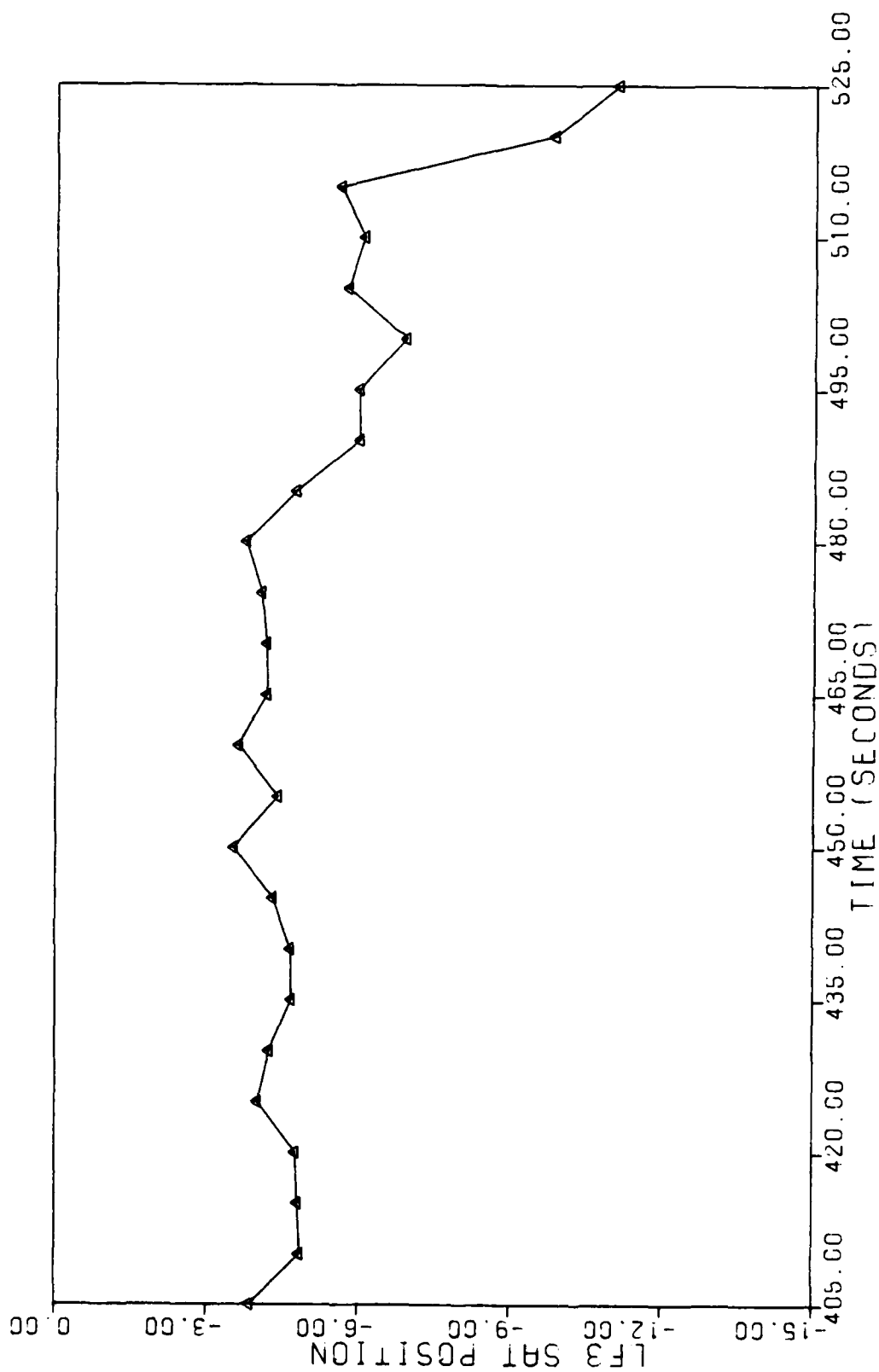


fig. A.7. Hard Accelerometer 3 Failure--Satellite Position Measurement #3--Benign Flight

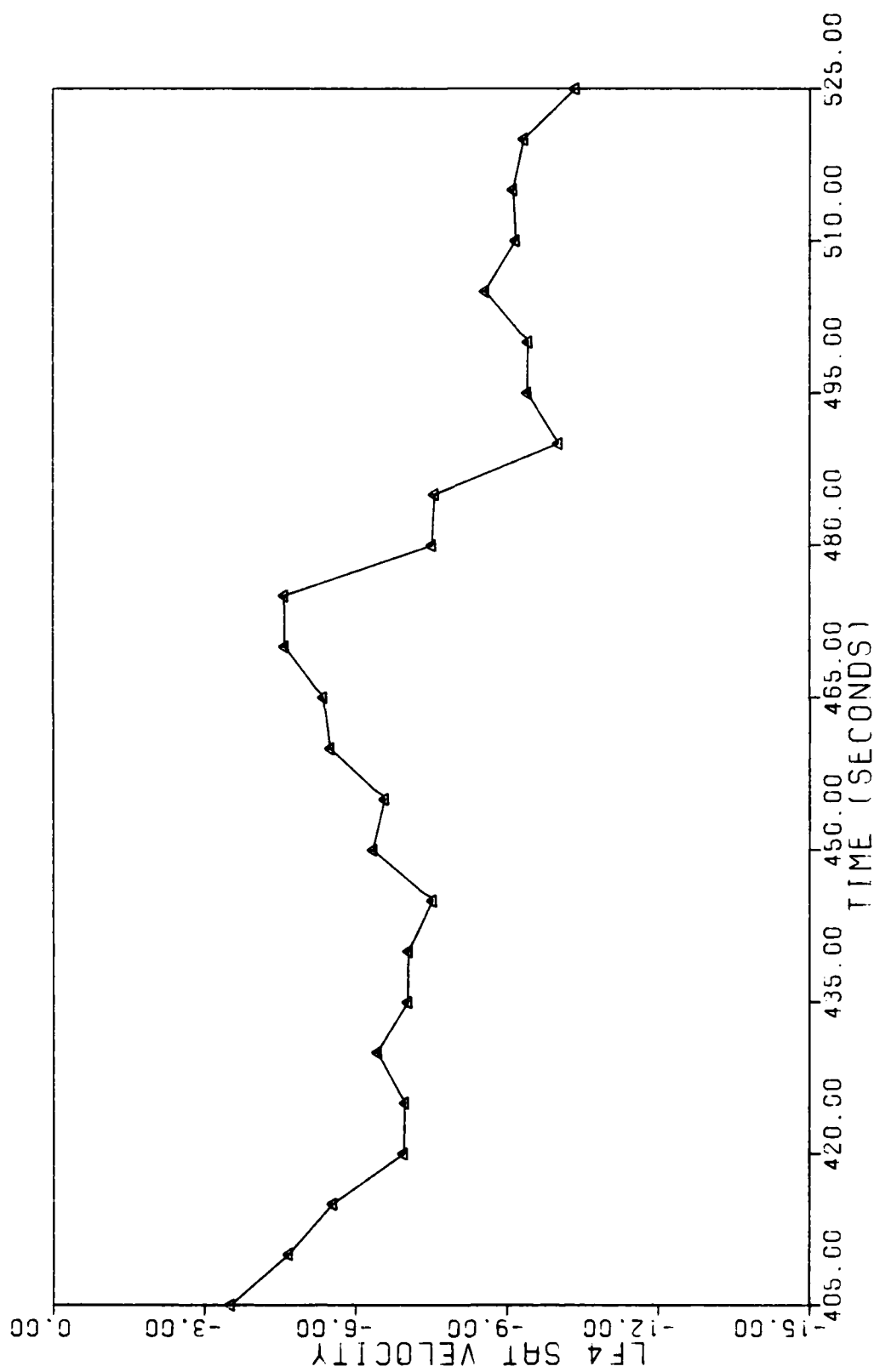


Fig. A.8. Hard Accelerometer 3 Failure--Satellite Velocity Measurement #4--Benign Flight

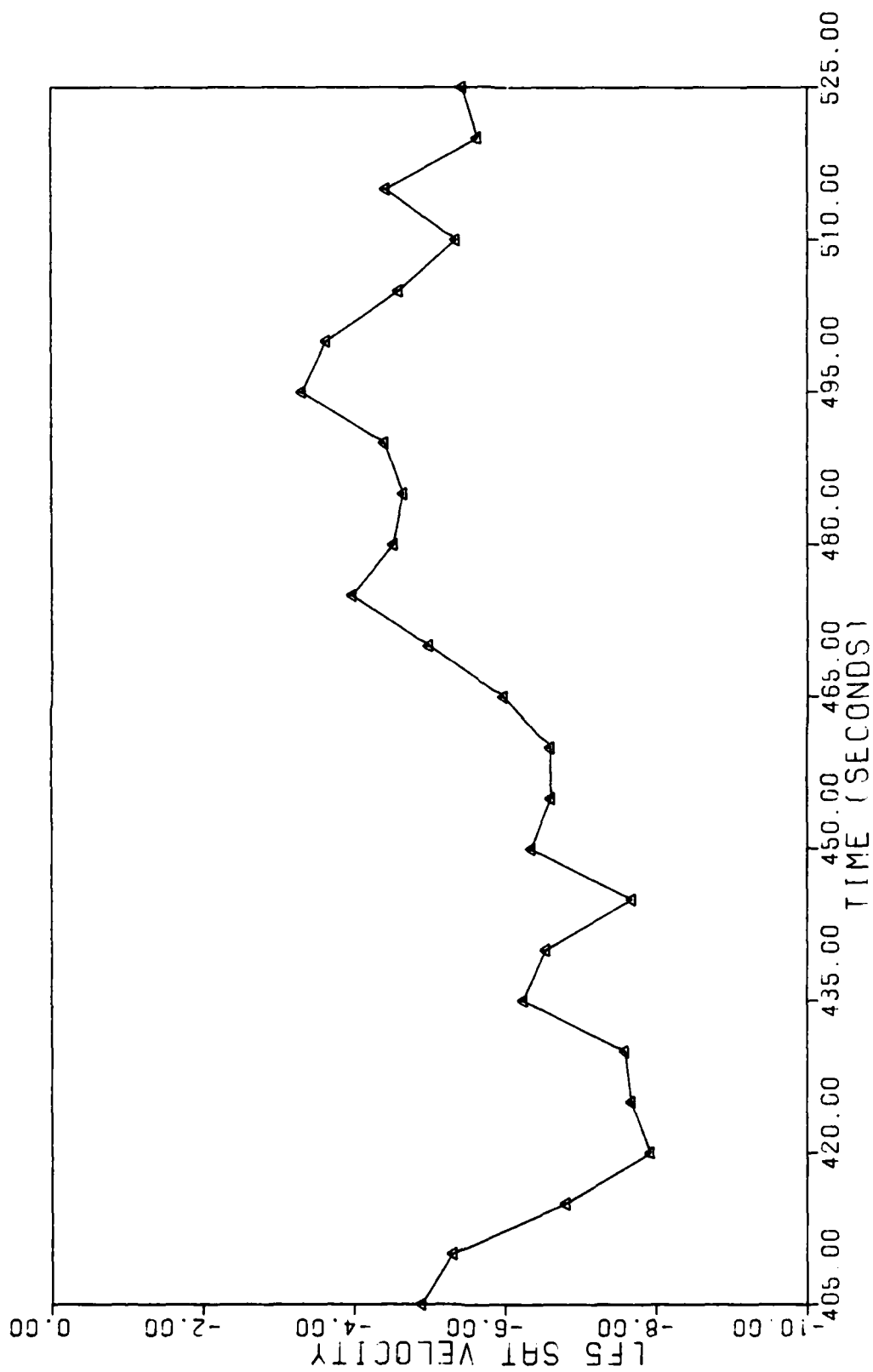


Fig. A.9. Hard Accelerometer 3 Failure--Satellite Velocity Measurement #5--Benign Flight

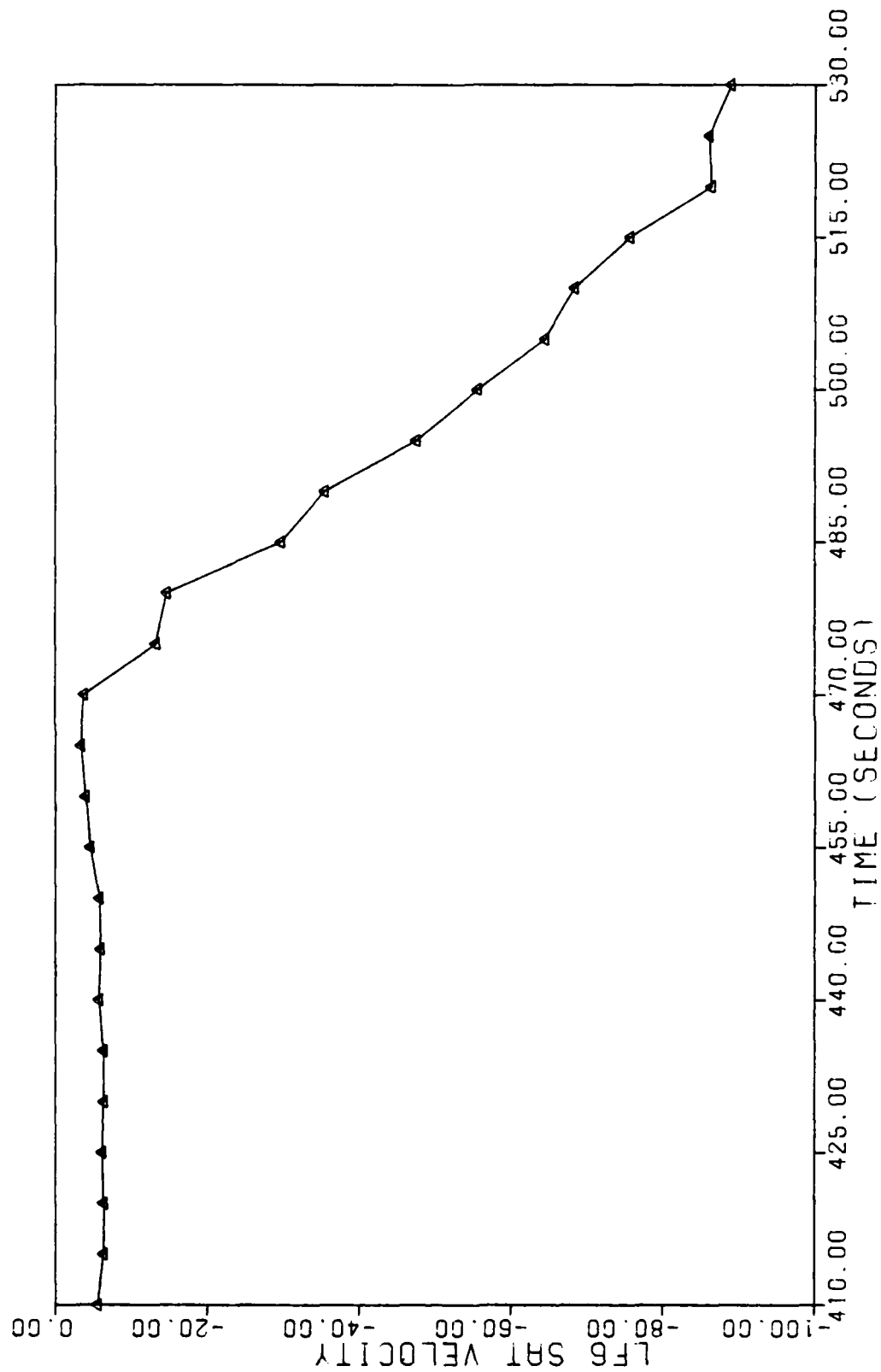
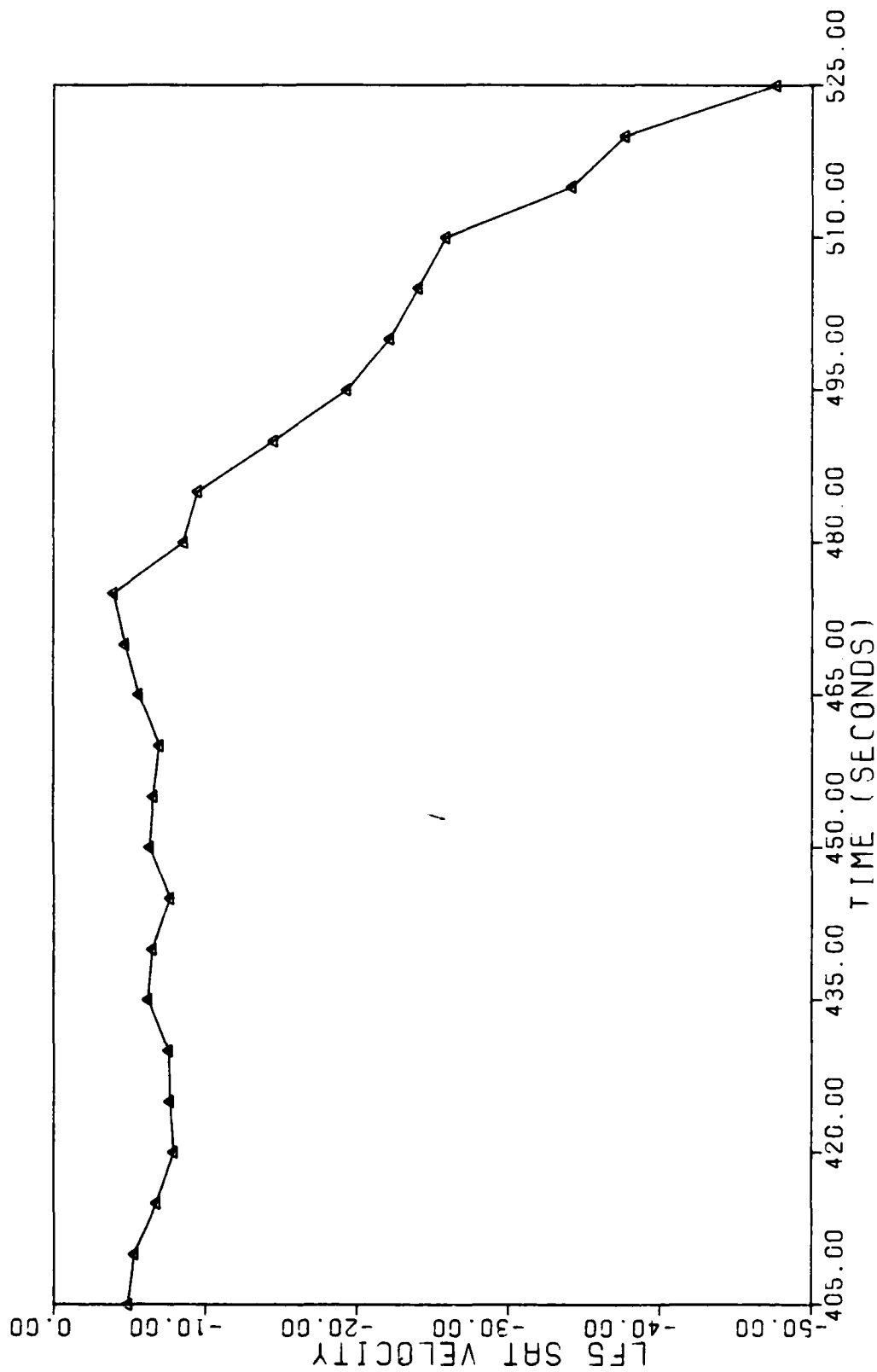


Fig. A.10. Hard Accelerometer 3 Failure--Satellite Velocity Measurement #6--Benign Flight



Ref. A.11. Hard Accelerometer 2 Failure--Satellite Velocity Measurement #5--Benign Flight

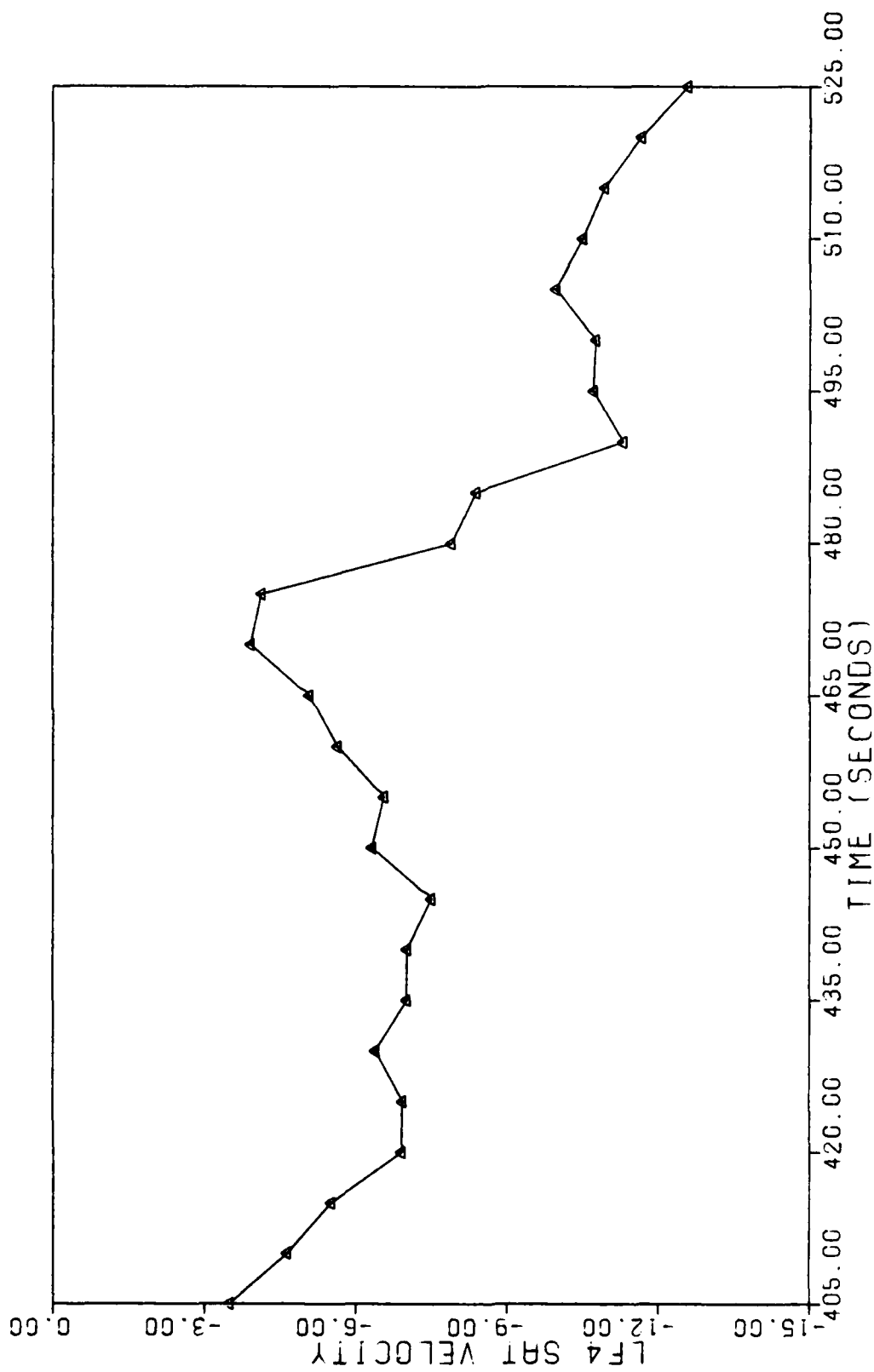


Fig. A.12. Hard Accelerometer 1 Failure--Satellite Velocity Measurement #4--Benign Flight

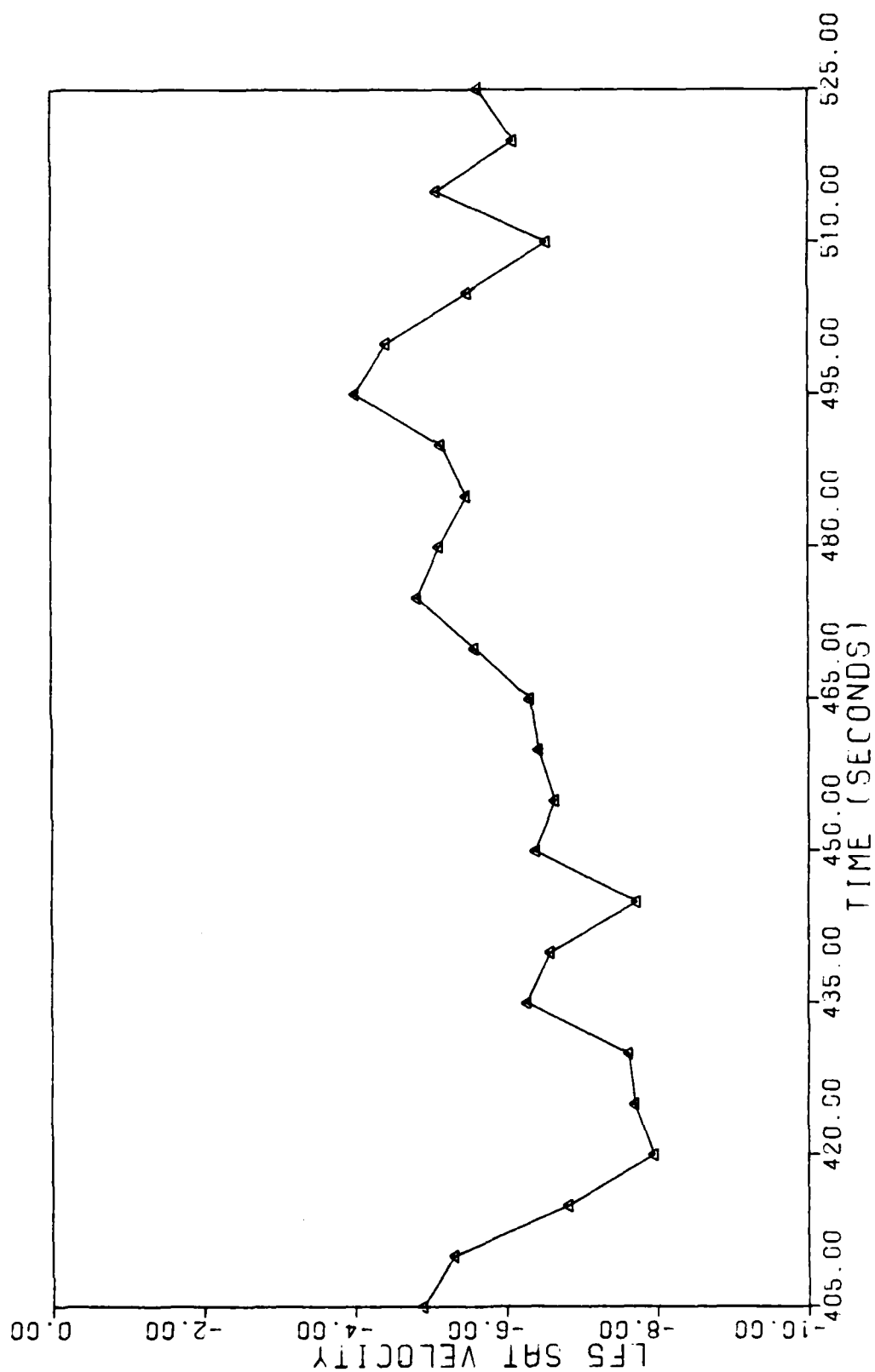


Fig. A.13. Hard Accelerometer 1 Failure--Satellite Velocity Measurement #5--Benign Flight



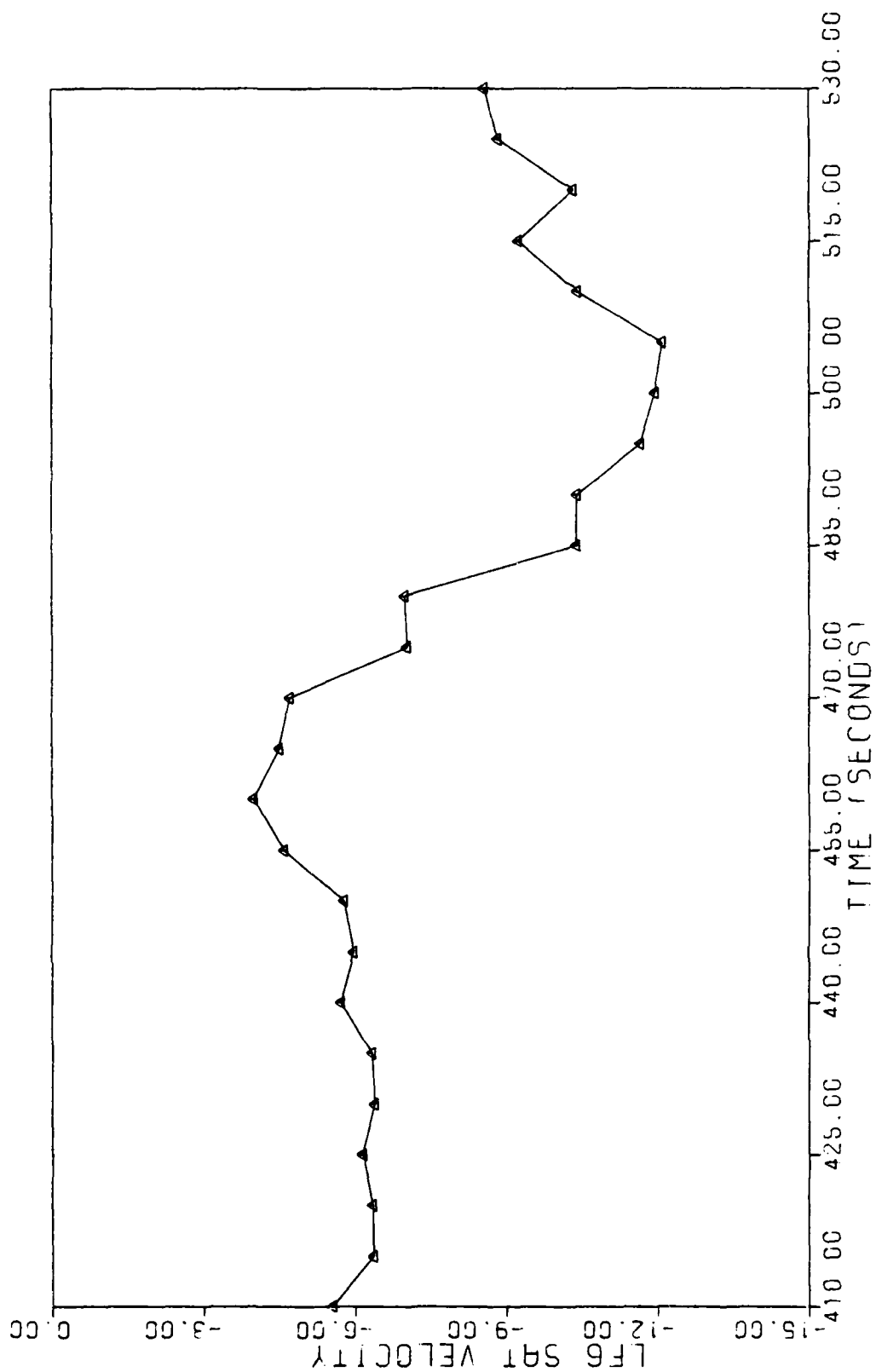


Fig. A.14. Hard Accelerometer 1 Failure--Satellite Velocity Measurement #6--Benign Flight

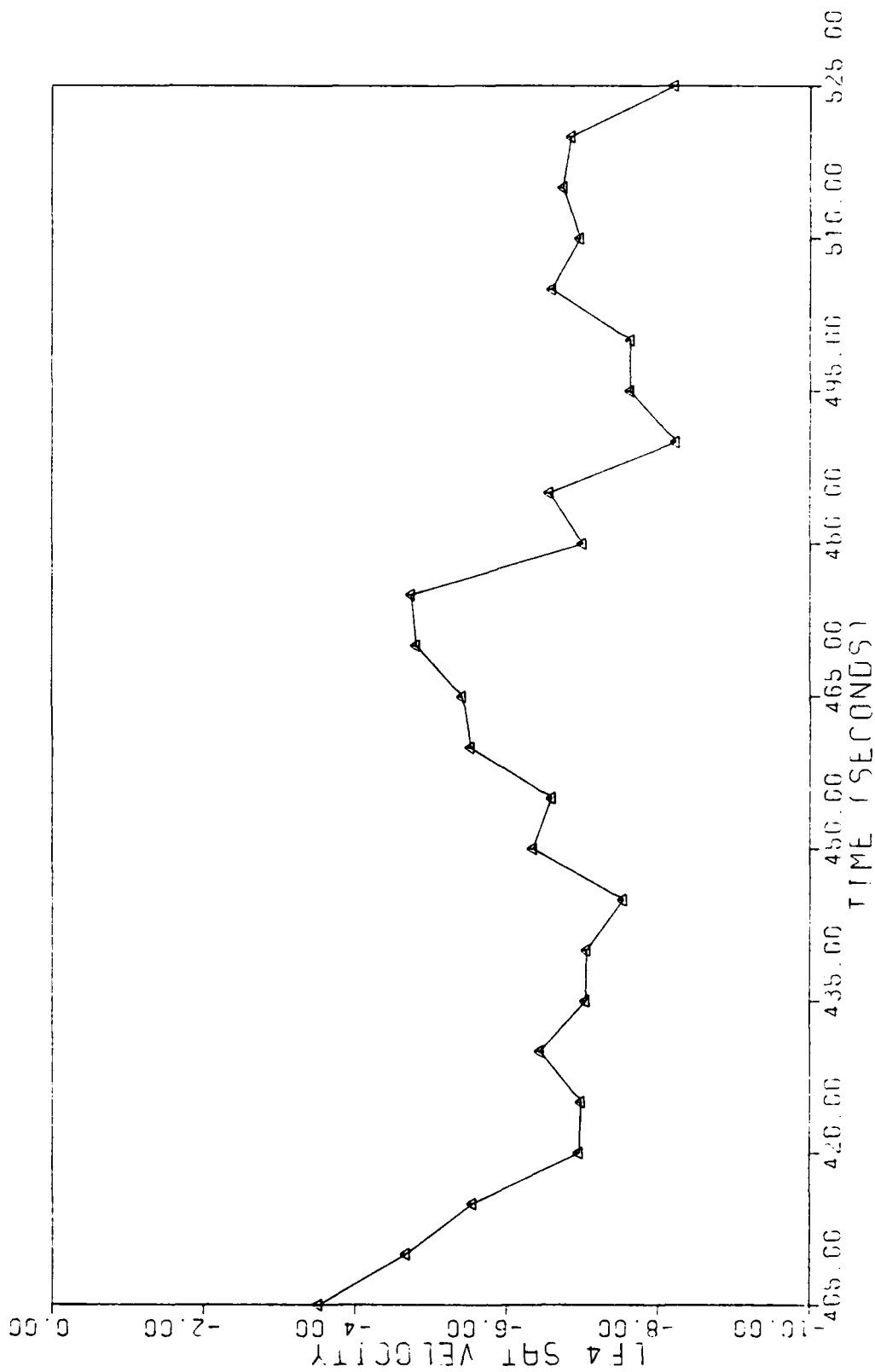


Fig. A.15. Soft Accelerometer 2 Failure--Satellite Velocity Measurement #4--Benign Flight

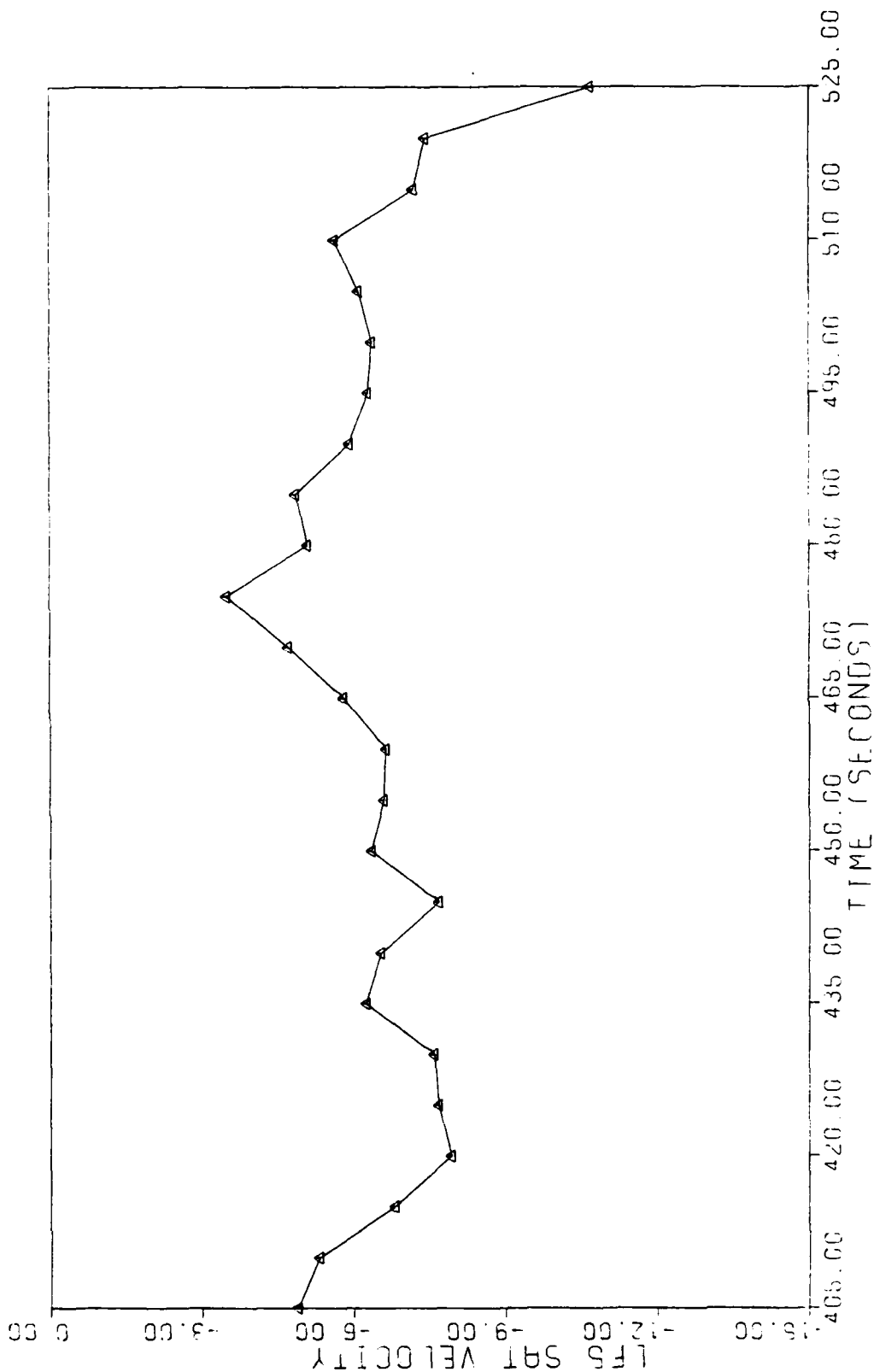


Fig. A.16. Soft Accelerometer 2 Failure--Satellite Velocity Measurement #5--Benign Flight

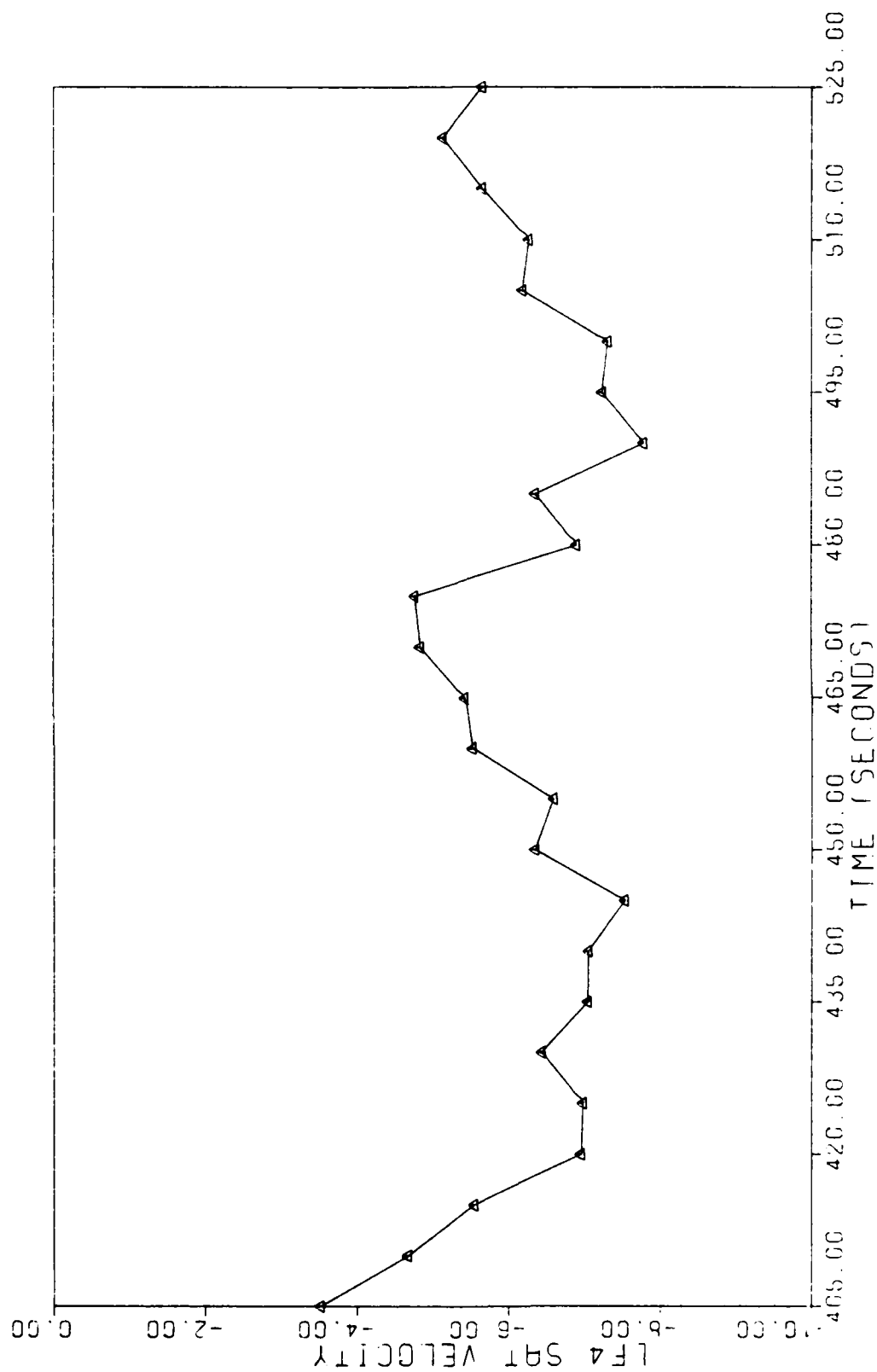


Fig. A.17. Soft Accelerometer 1 Failure--Satellite Velocity Measurement #4--Benign Flight

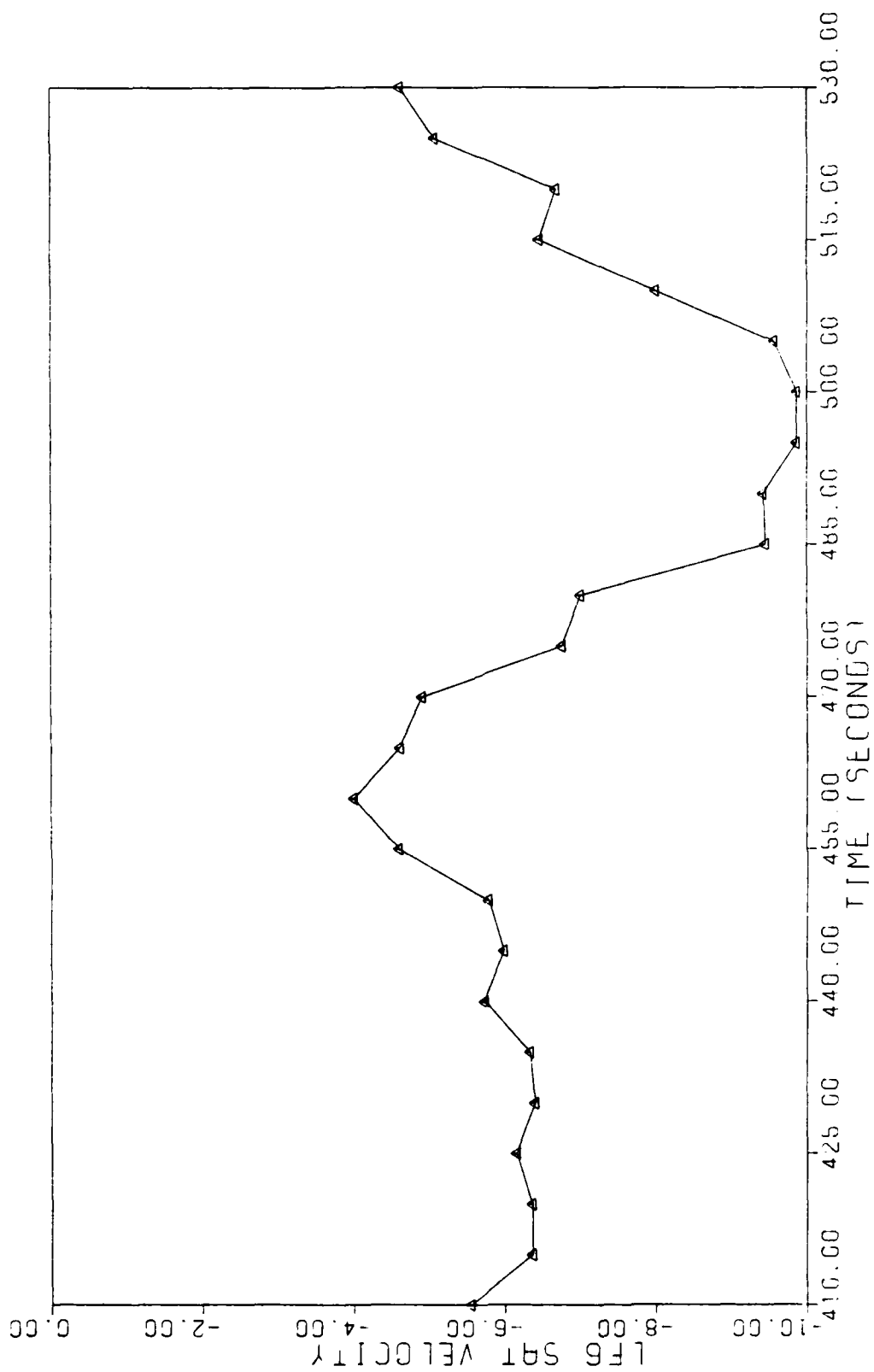


Fig. A.18. Soft Accelerometer 1 Failure--Satellite Velocity Measurement #6--Benign Flight

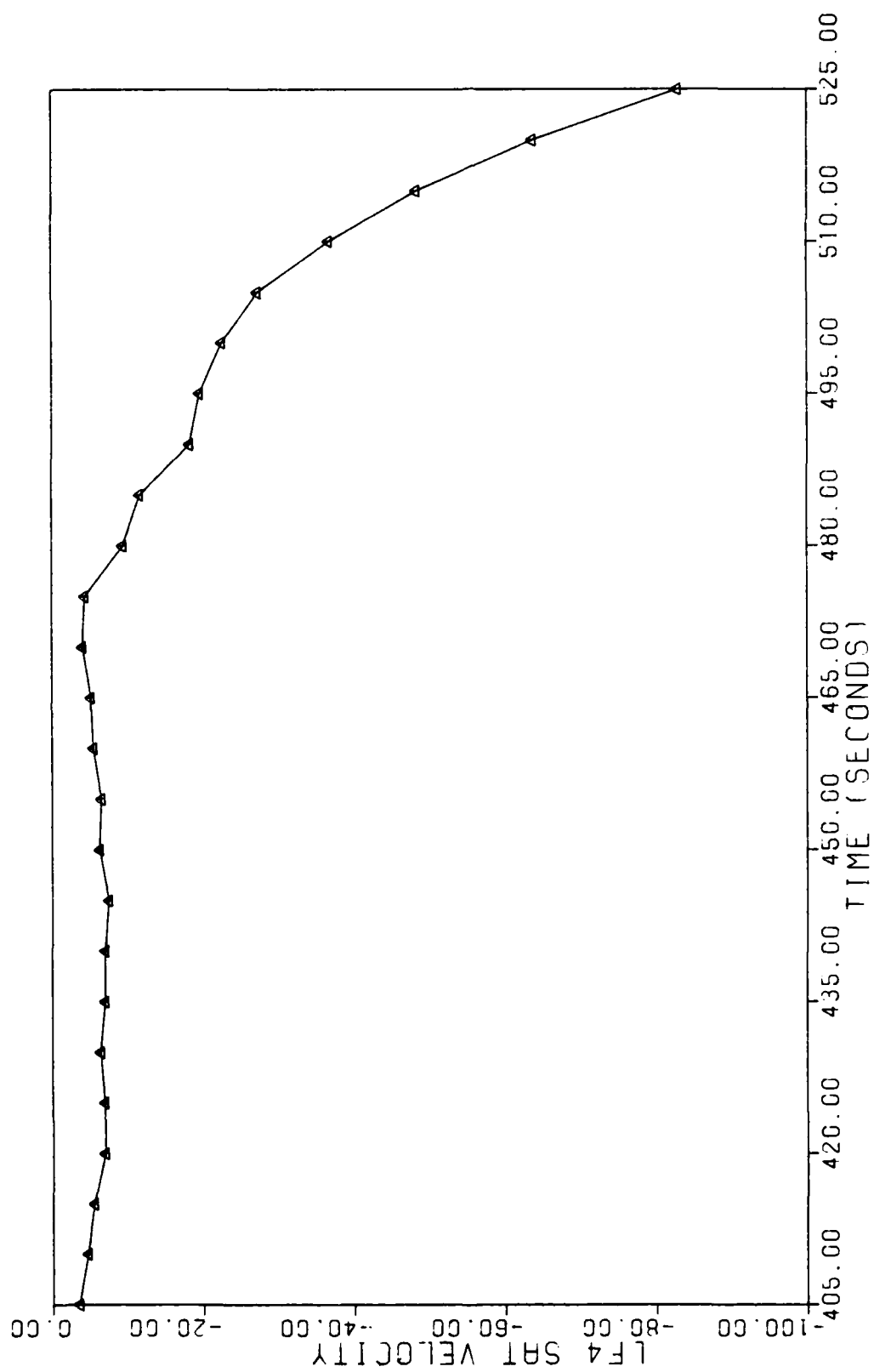


fig. A.19. Hard Gyro 2 Failure--Satellite Velocity Measurement #4--Benign Flight

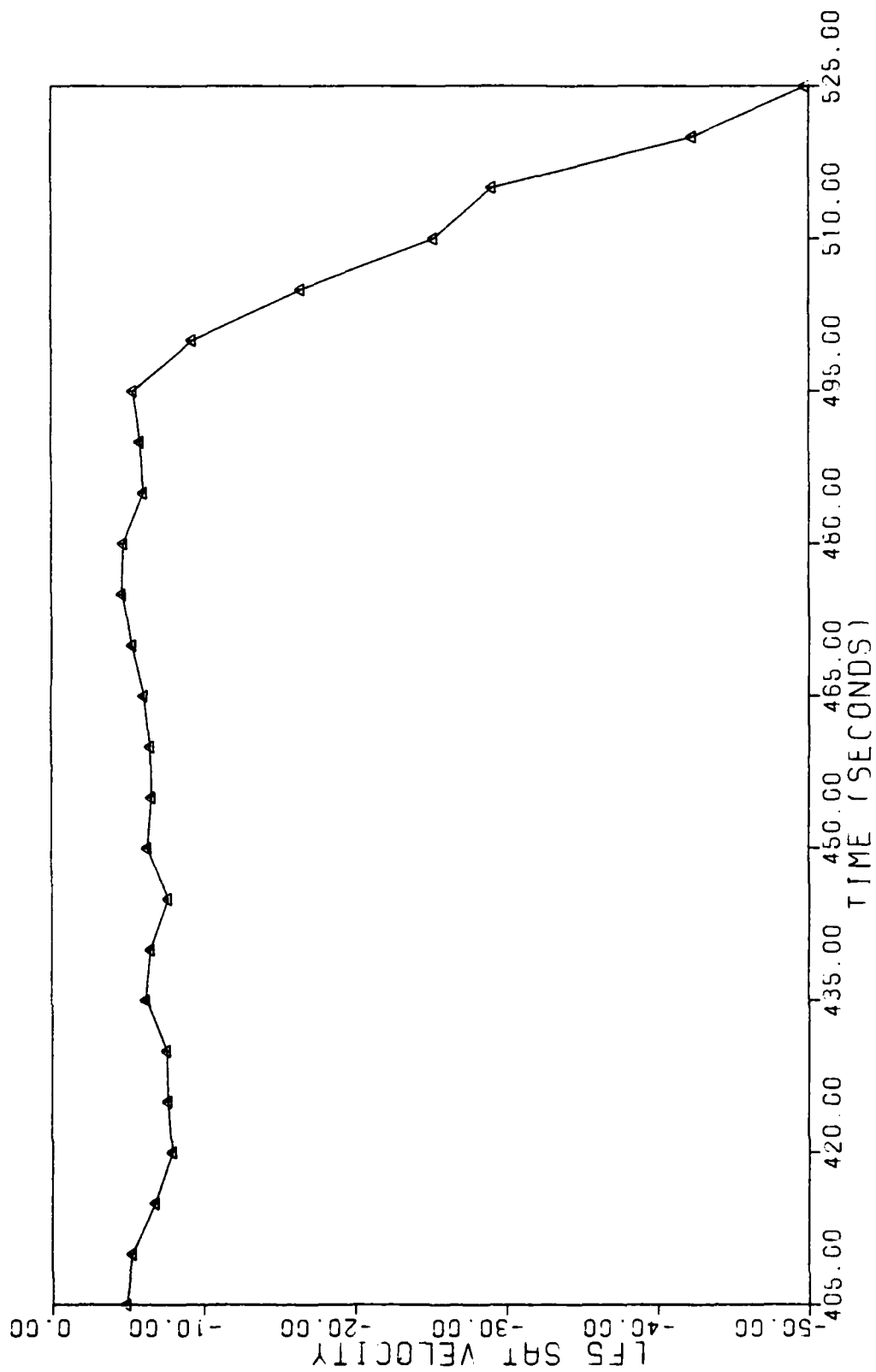


Fig. A.20. Hard Gyro 2 Failure--Satellite Velocity Measurement #5--Benign Flight

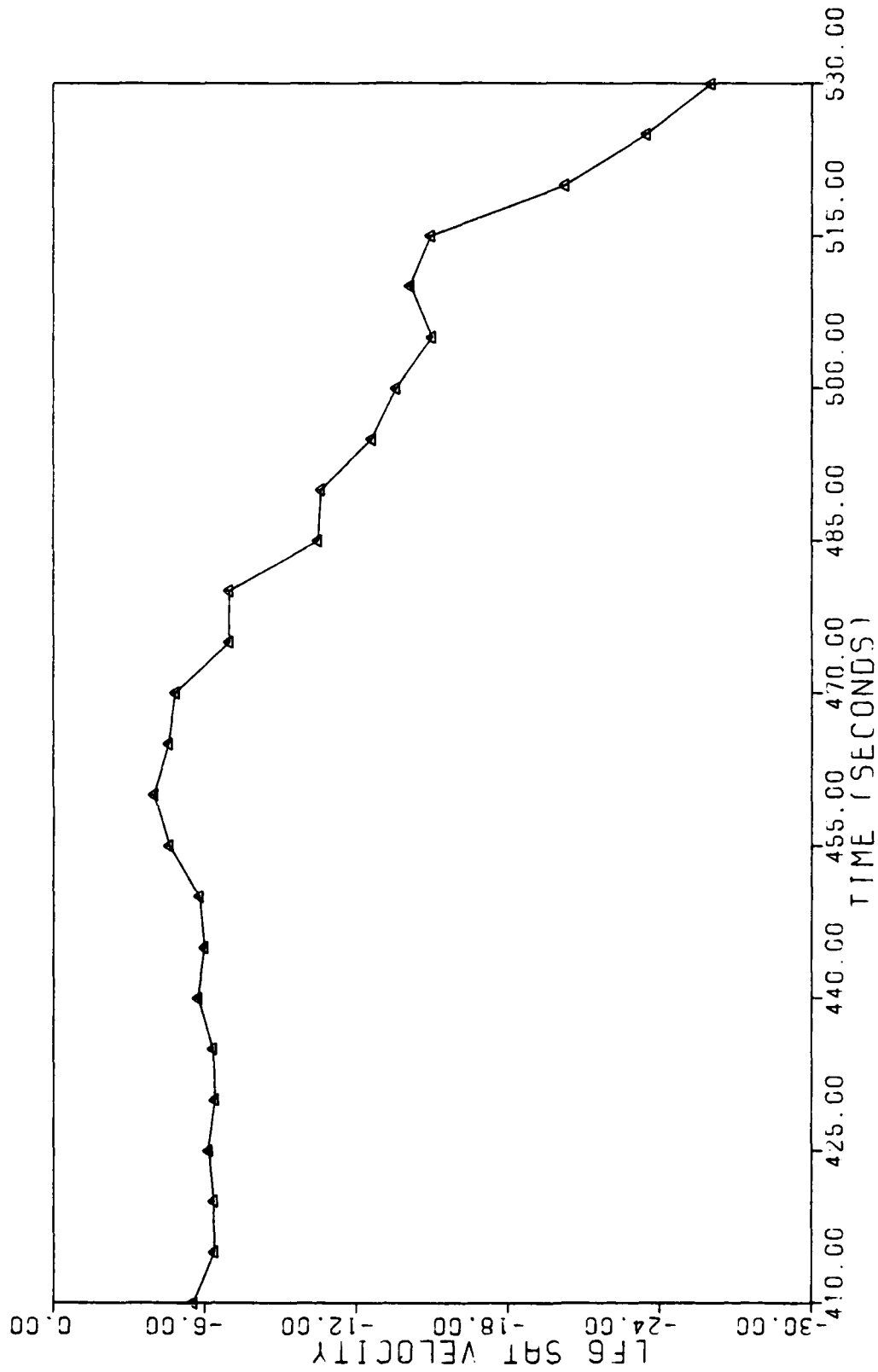


Fig. A.21. Hard Gyro 2 Failure--Satellite Velocity Measurement #6--Benign Flight



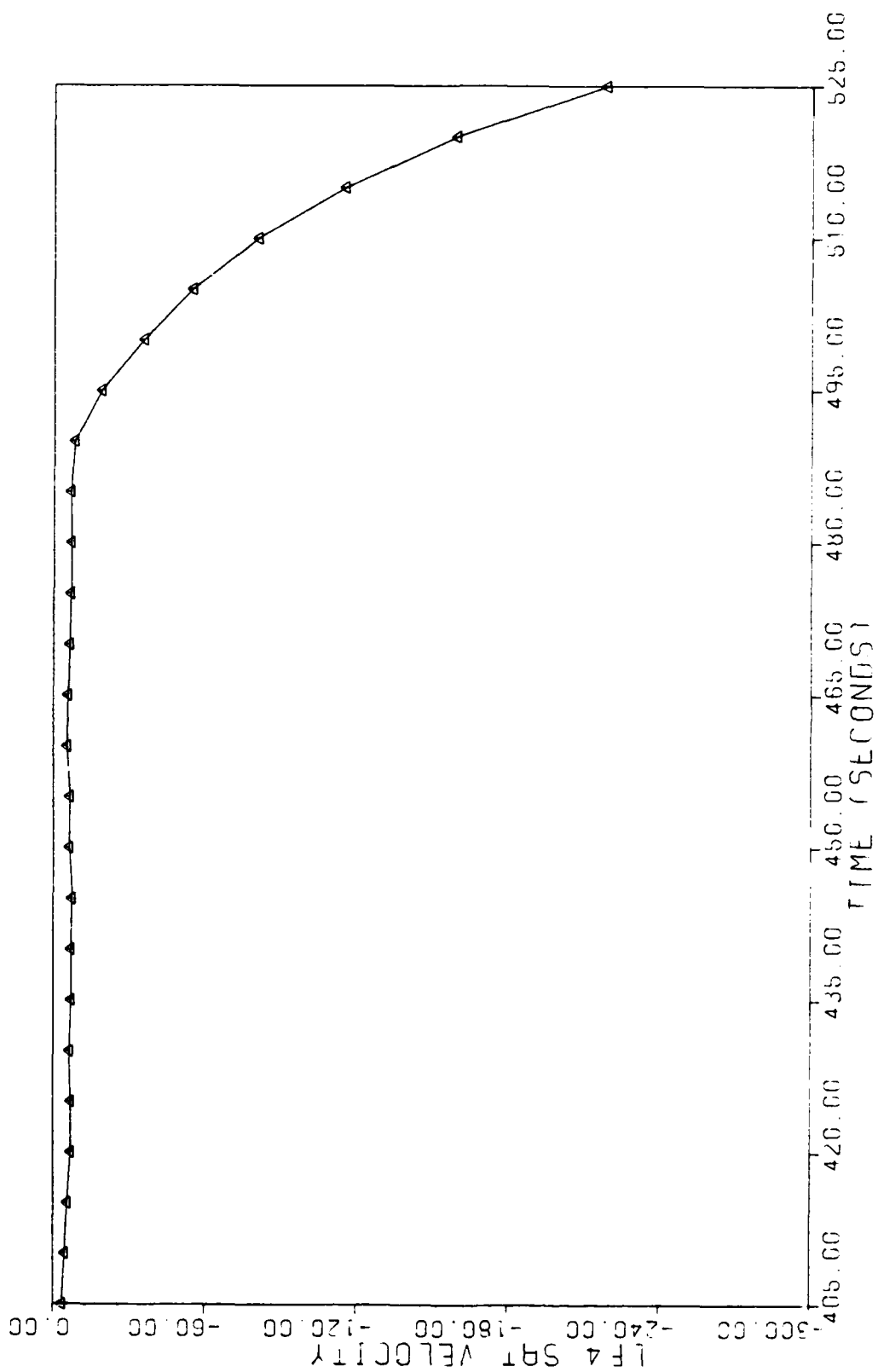


Fig. A.22. Hard Gyro 1 Failure--Satellite Velocity Measurement #4--Benign Flight

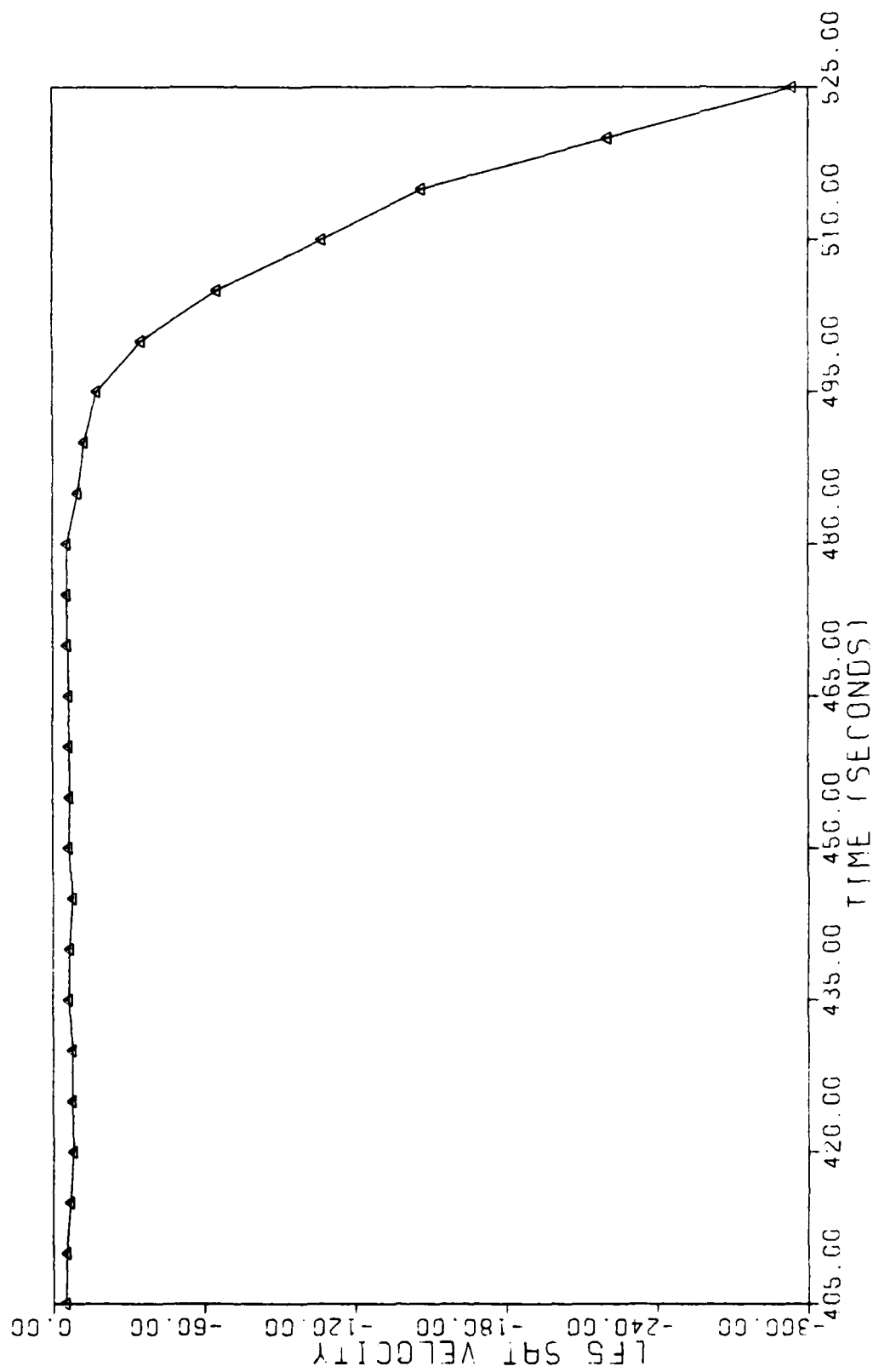


Fig. A.23. Hard Gyro 1 Failure--Satellite Velocity Measurement #6--Benign Flight

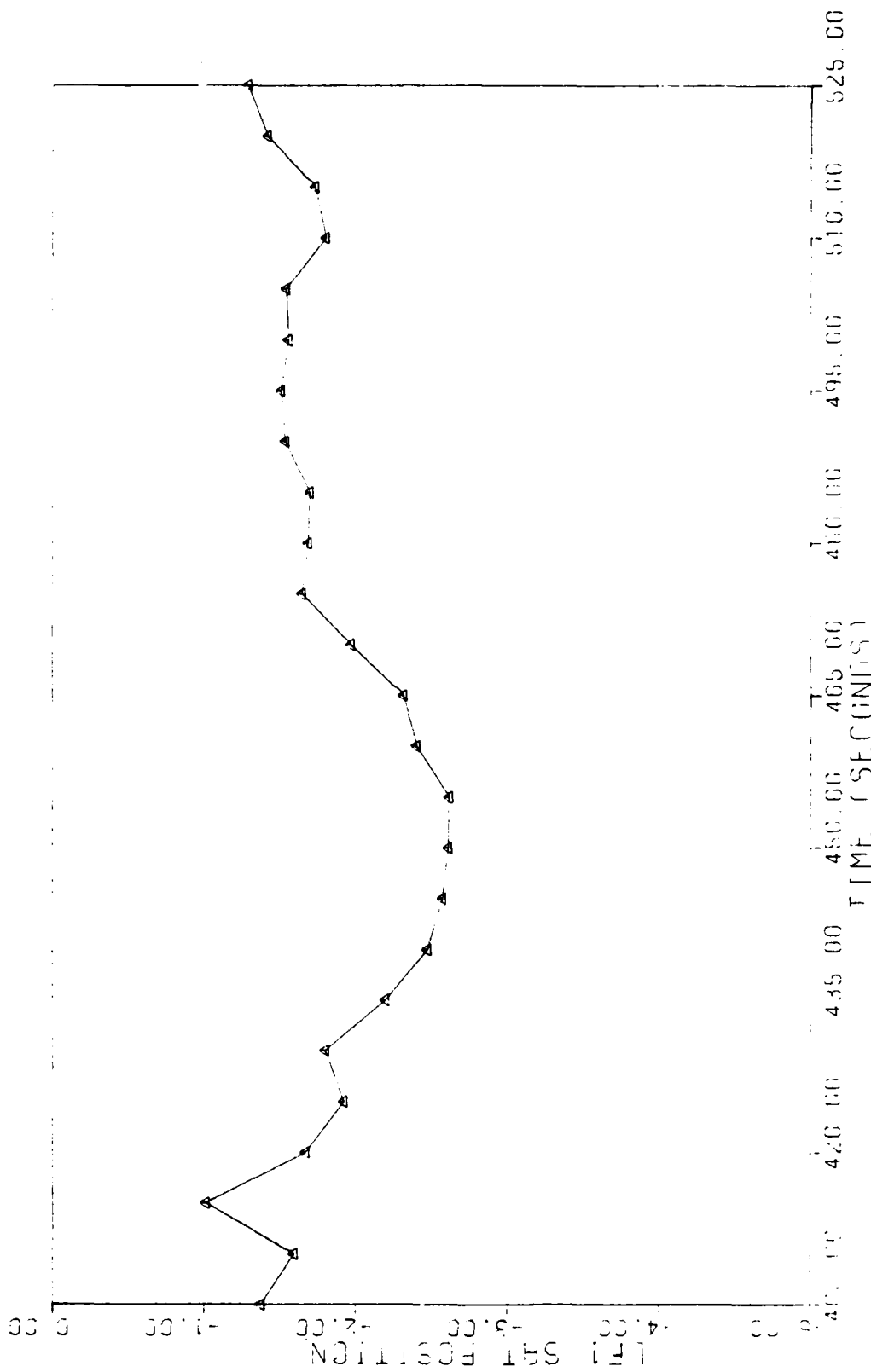


FIG. A.24. No Failure Condition--Satellite Position Measurement #1--Benign Flight

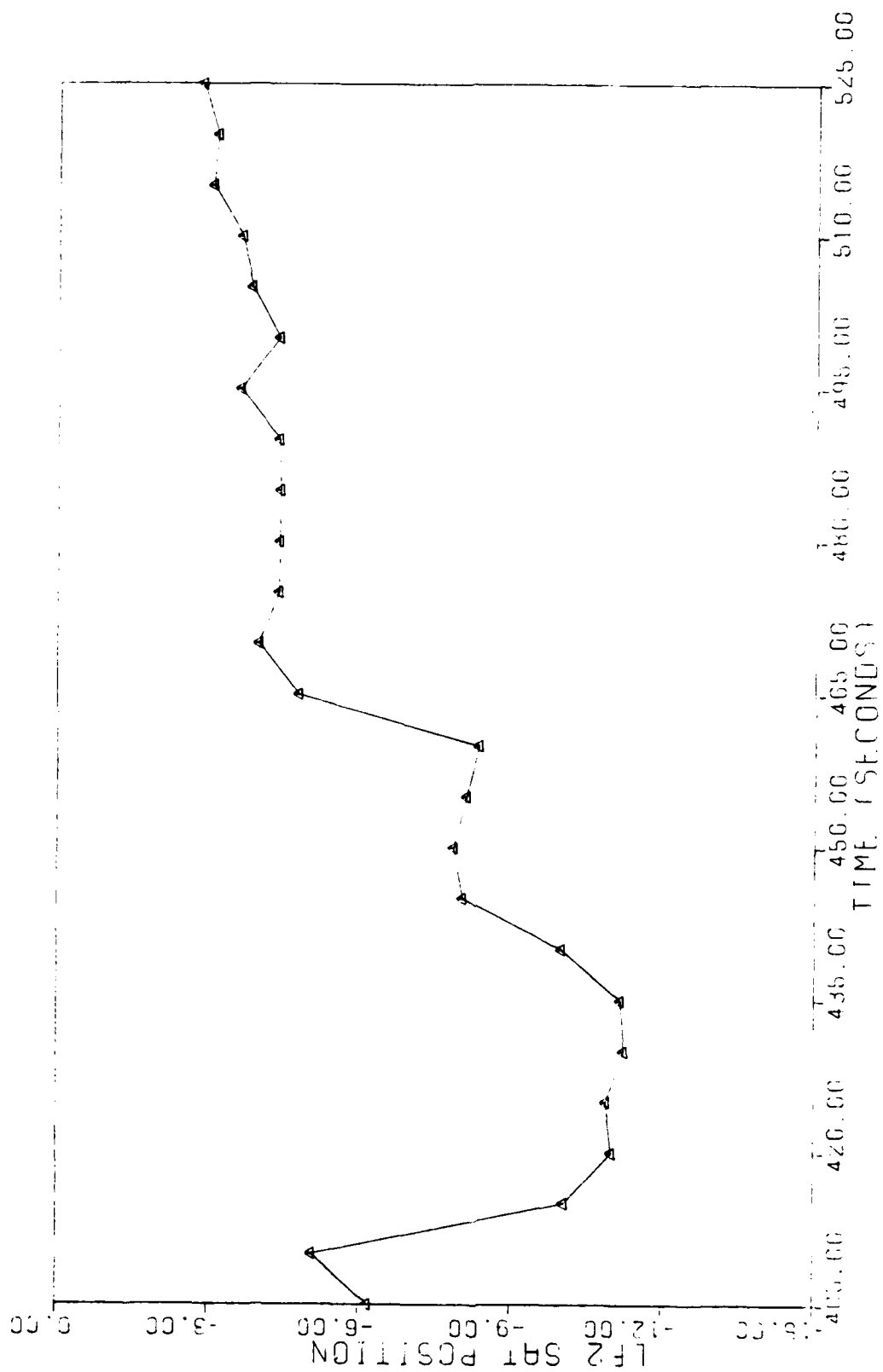


FIG. A.25. No Failure Condition--Satellite Position Measurement #2--Benign Flight

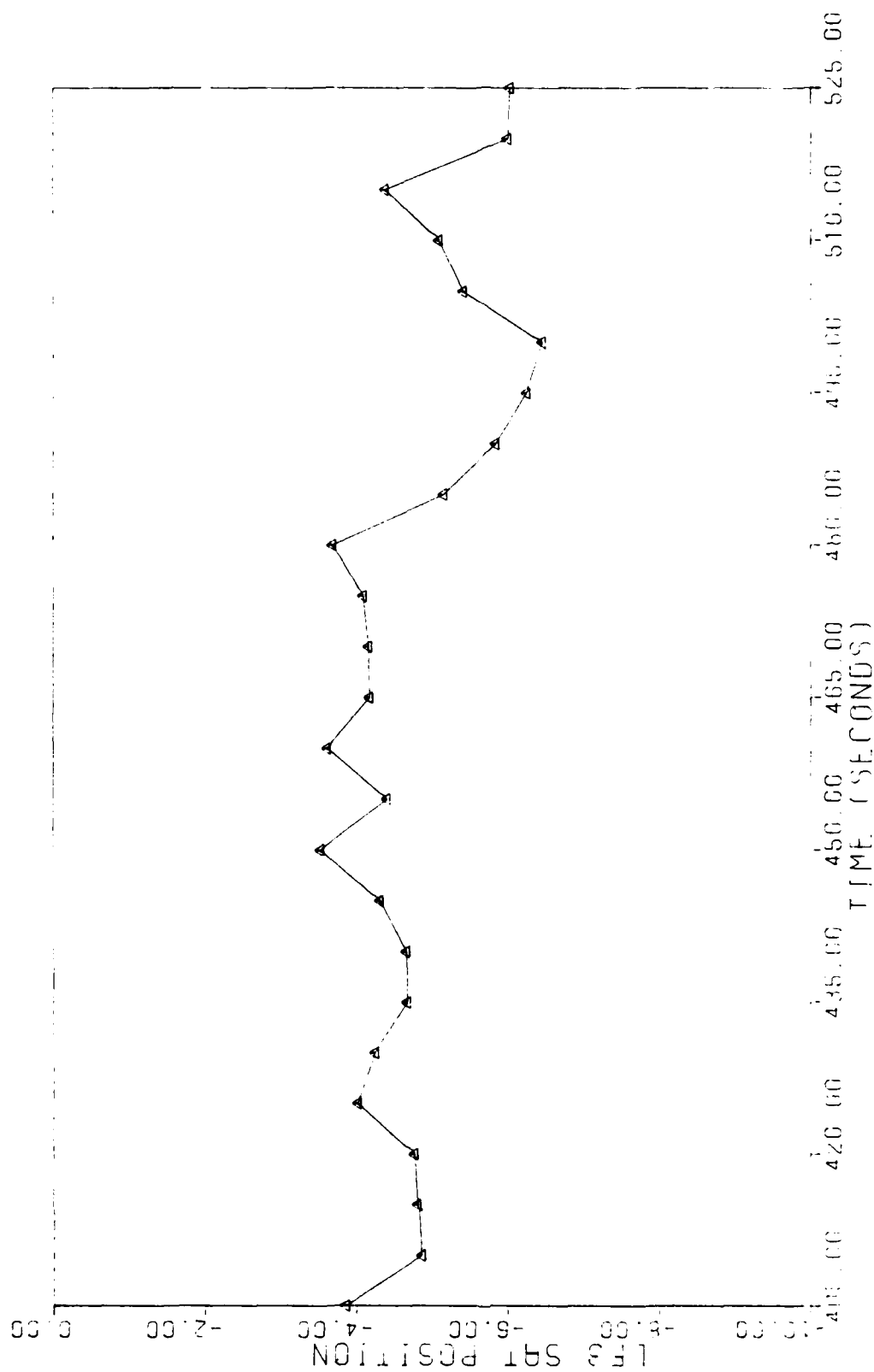


Fig. A.26. No Failure Condition--Satellite Position Measurement #3--Benign Flight

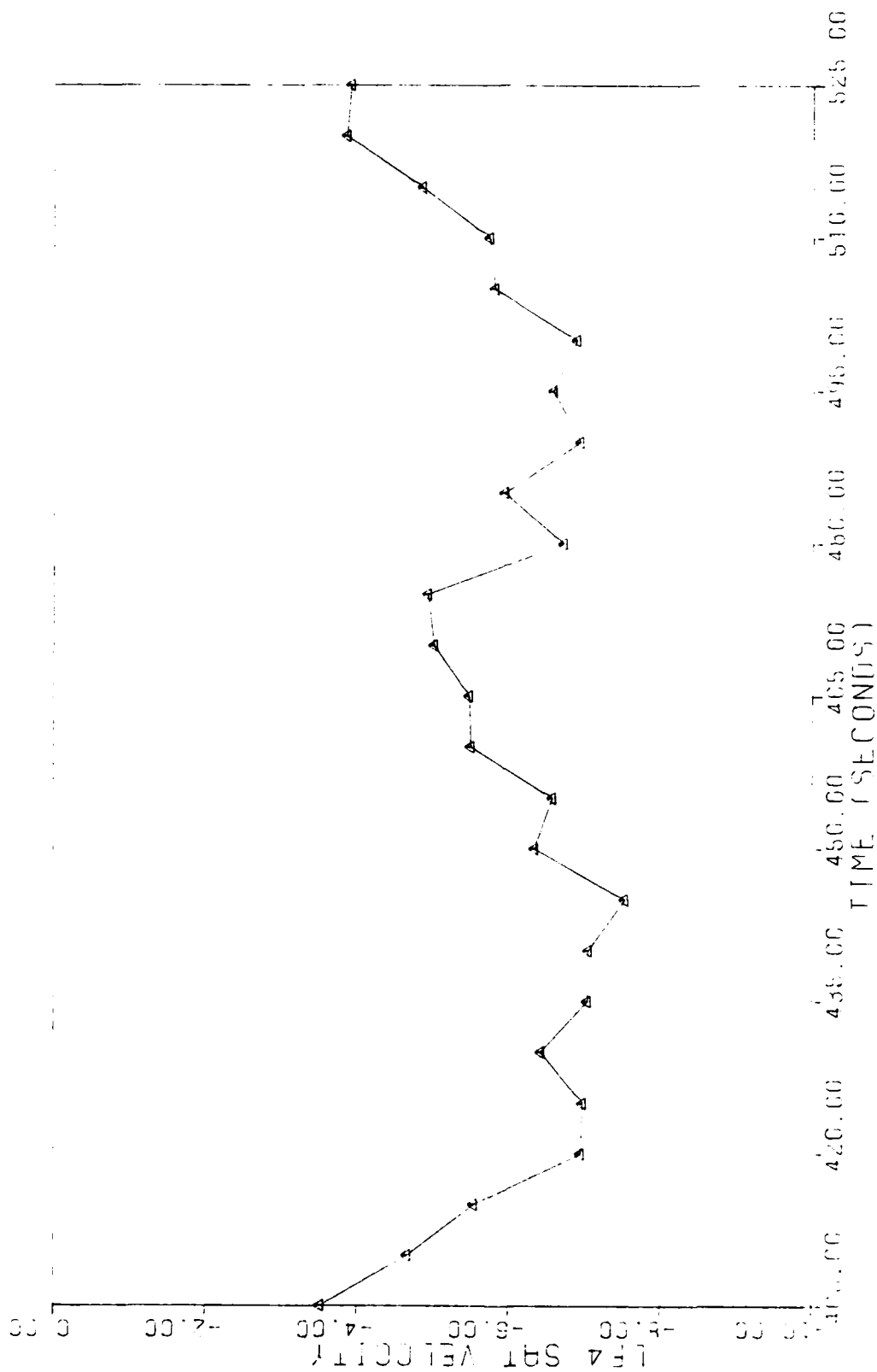


FIG. A.27. No Failure Condition--Satellite Velocity Measurement #4--Benign Flight

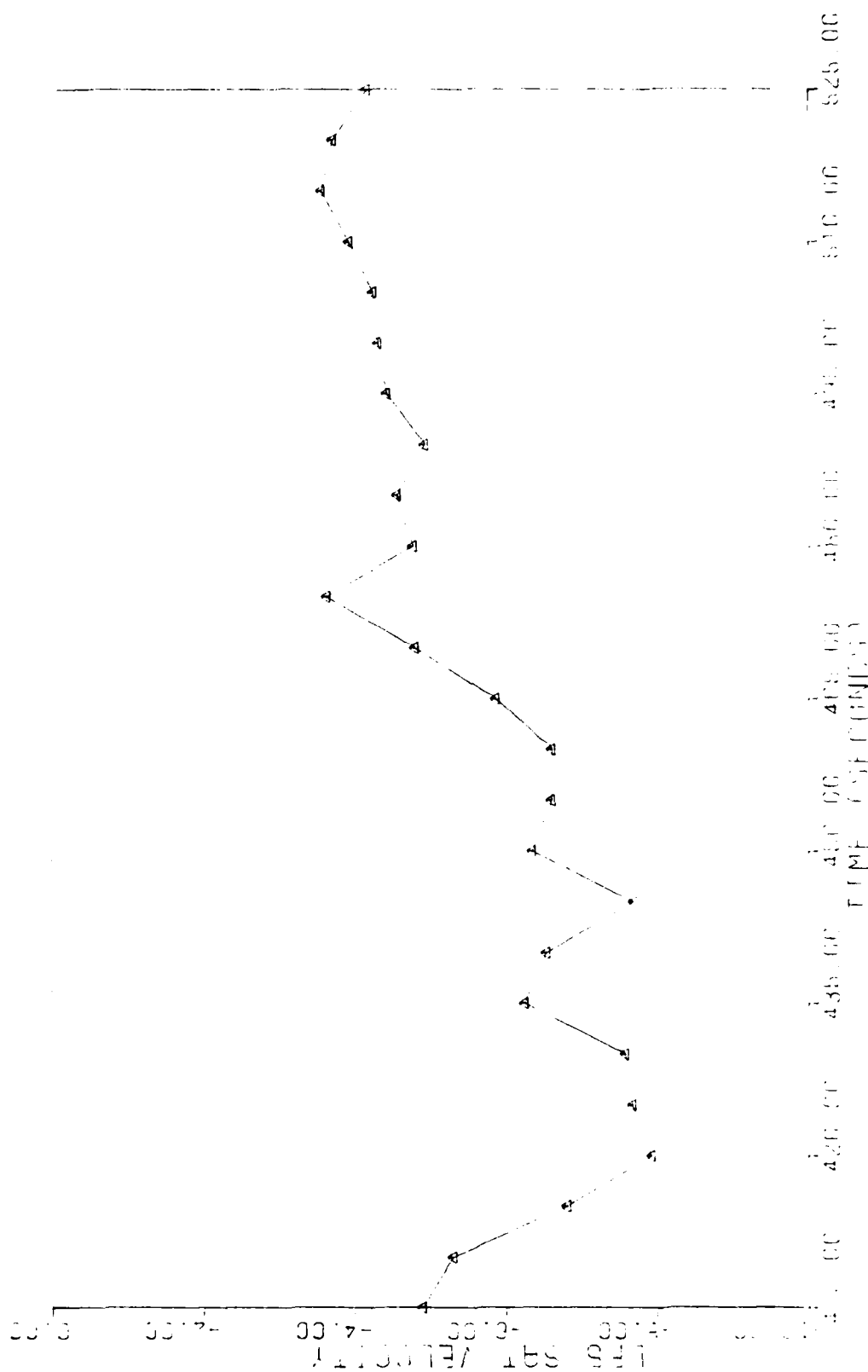


Fig. A.28. No Failure Condition--Satellite Velocity Measurement #5--Benign Flight

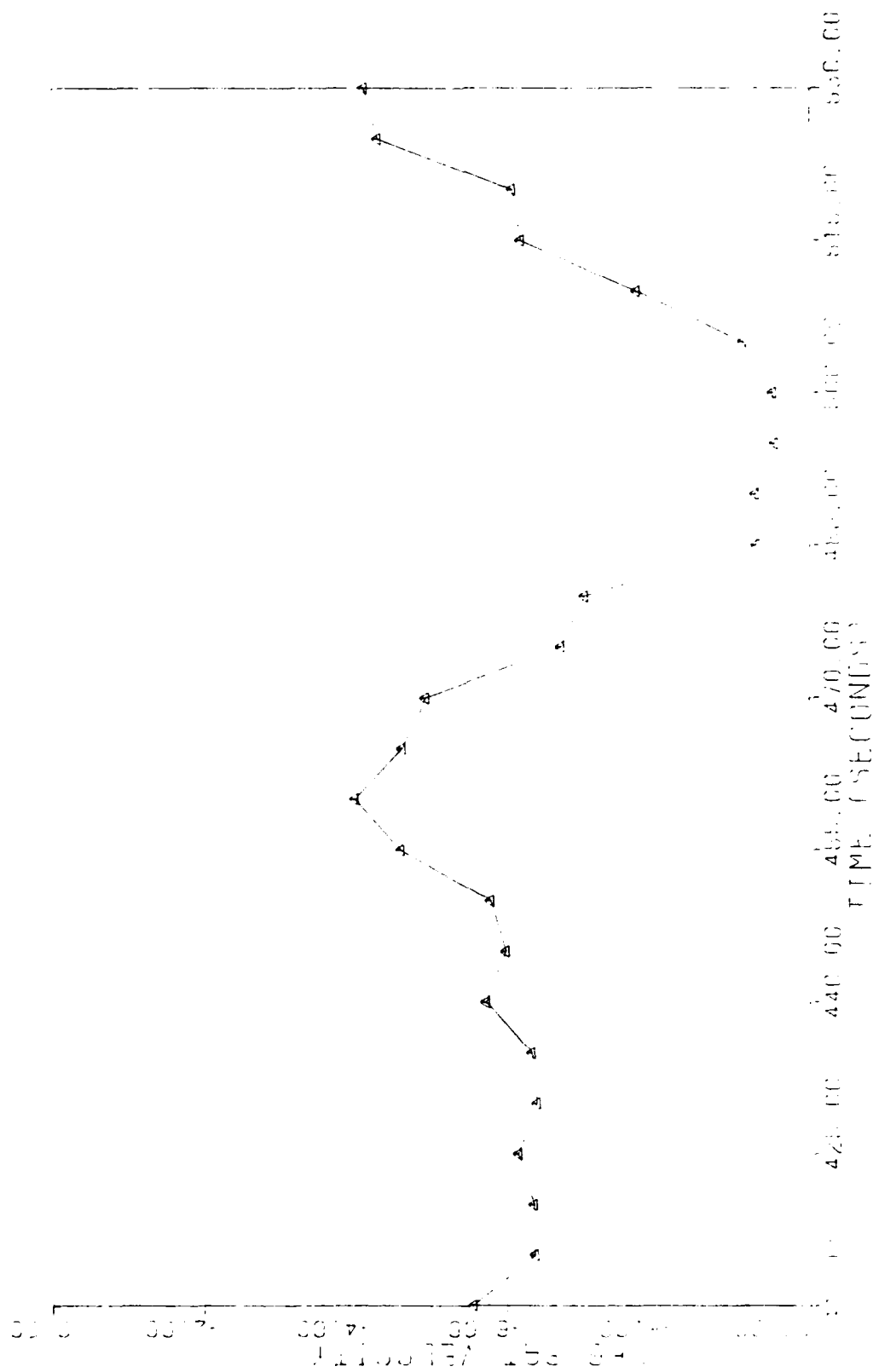


Fig. A.29. No Failure Condition--Satellite Velocity Measurement #5--Benign Flight



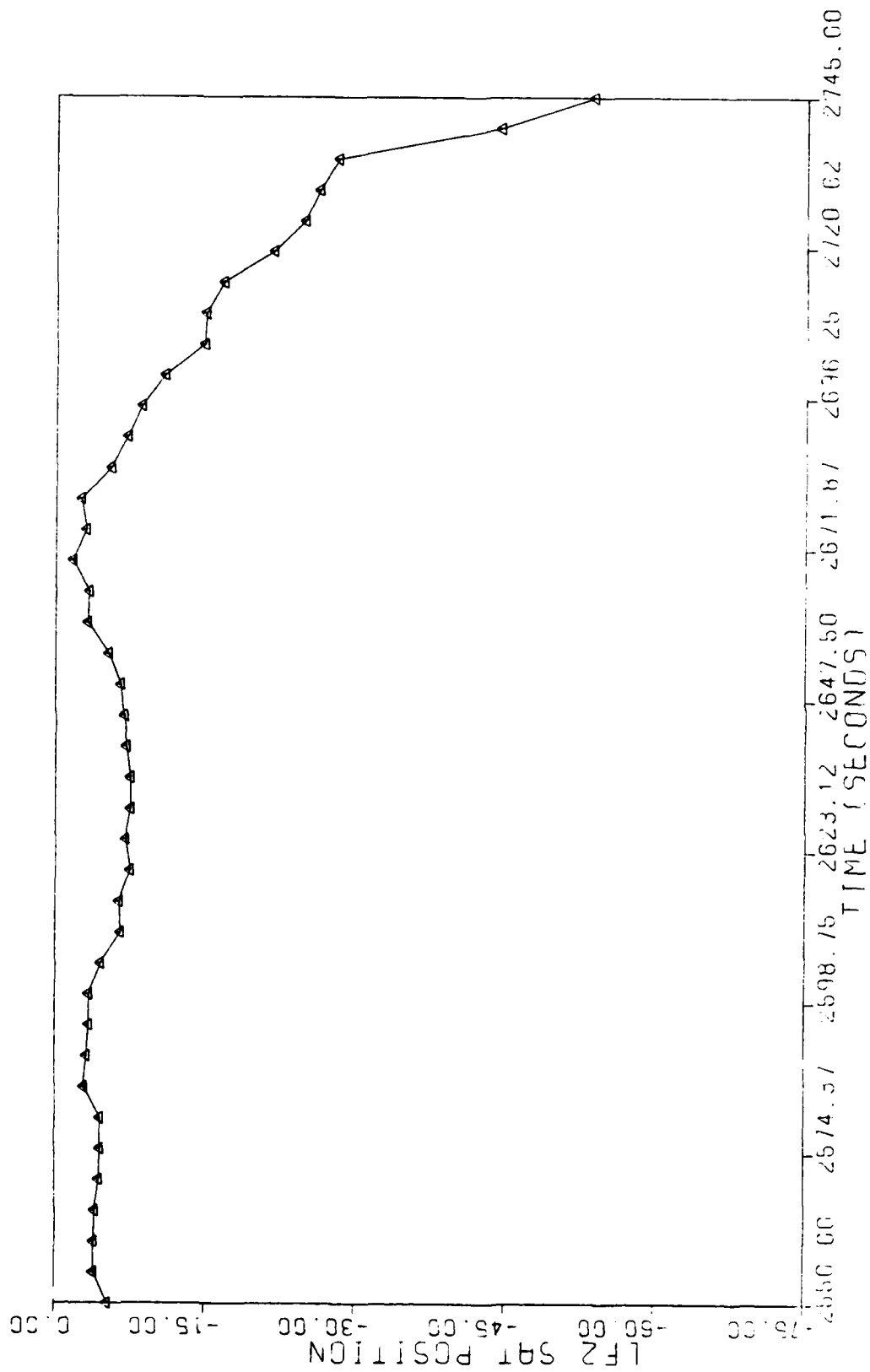


Fig. A.30. Soft Satellite Failure--Satellite Position Measurement #2--Dynamic Flight

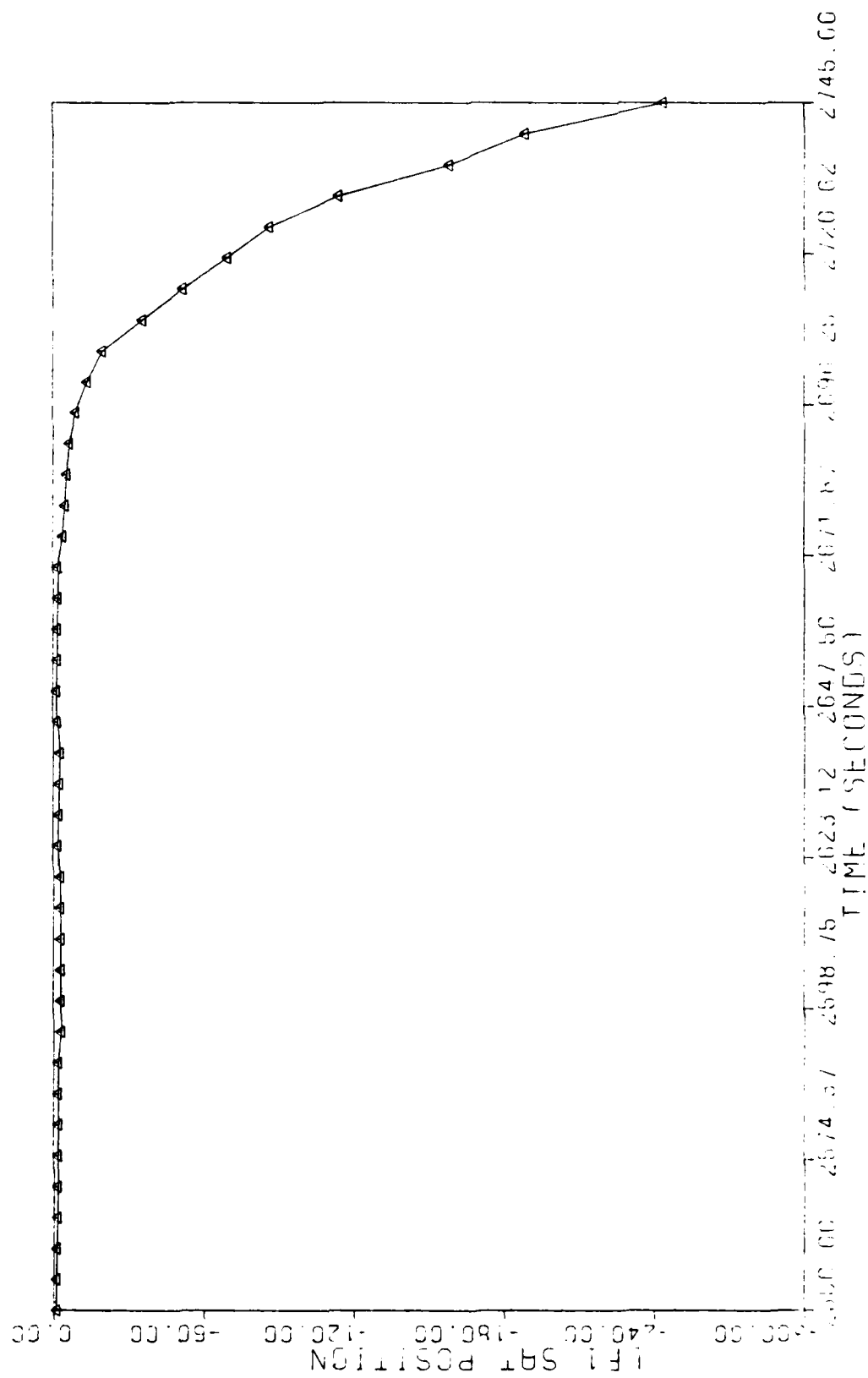


Fig. A.31. Soft Satellite Failure--Satellite Position Measurement #1--Dynamic Flight

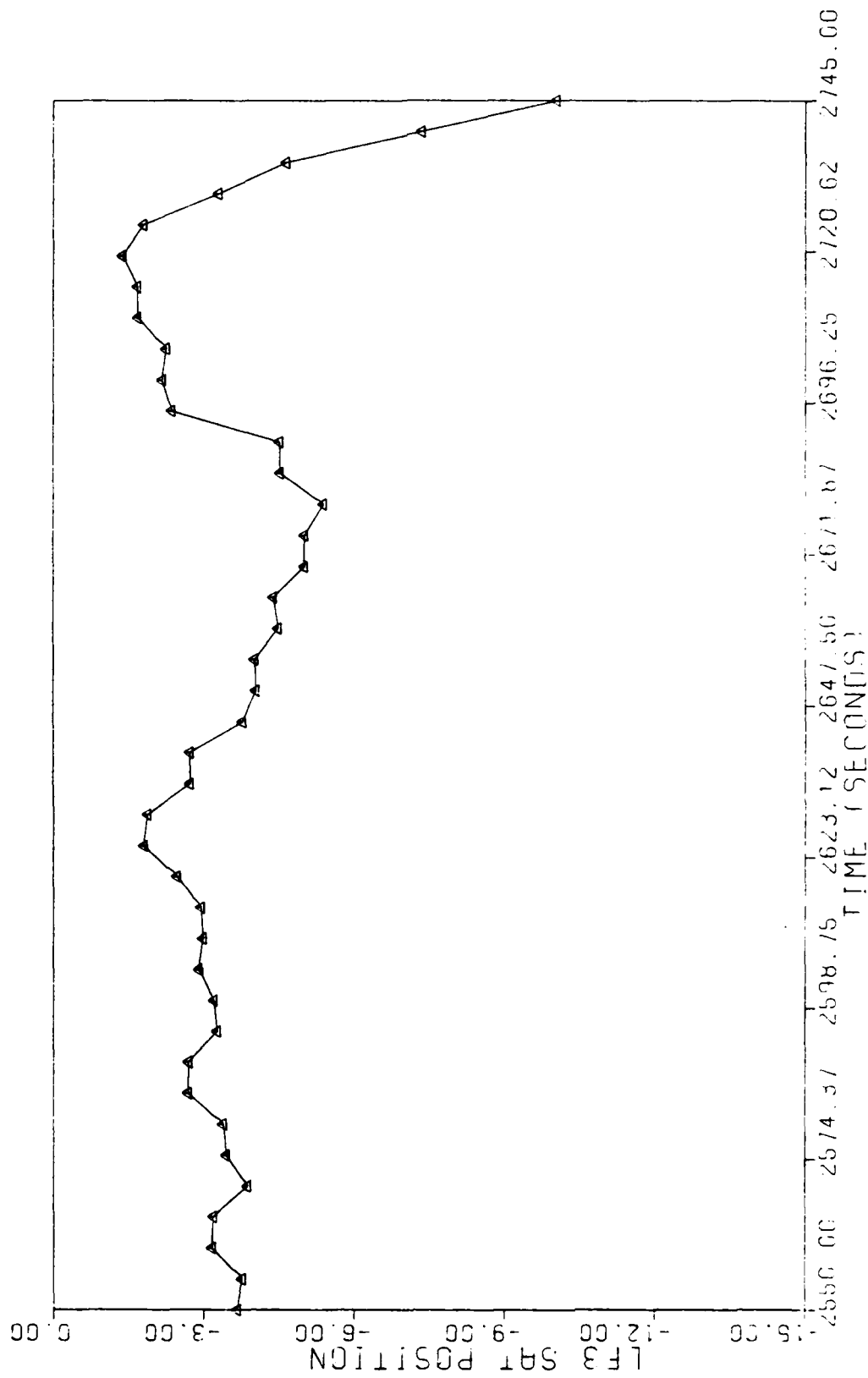


Fig. A.32. Soft Satellite Failure--Satellite Position Measurement #3--Dynamic Flight

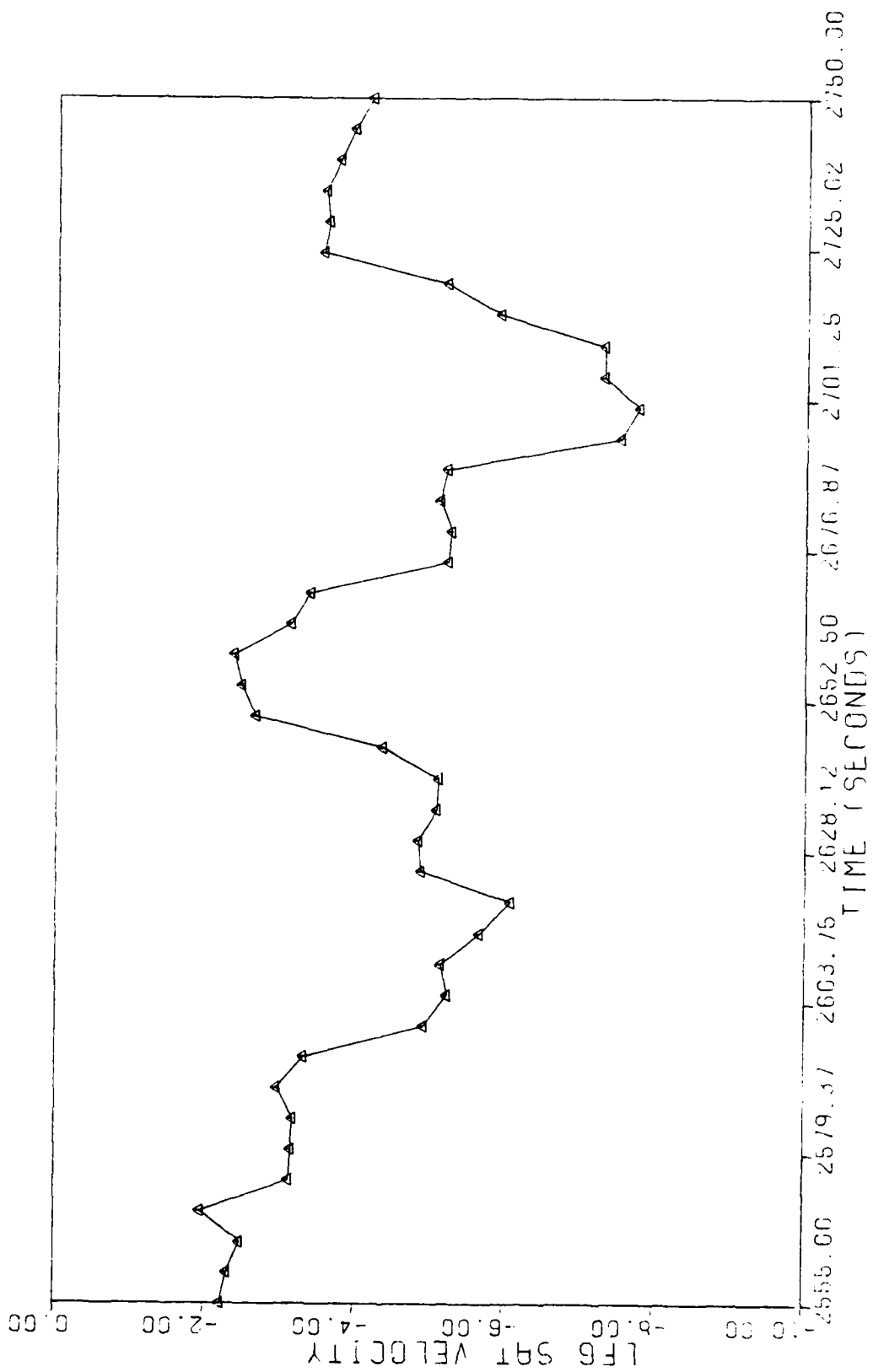


FIG. A.33. Hard Accelerometer 3 Failure--Satellite Velocity Measurement #6--Dynamic Flight

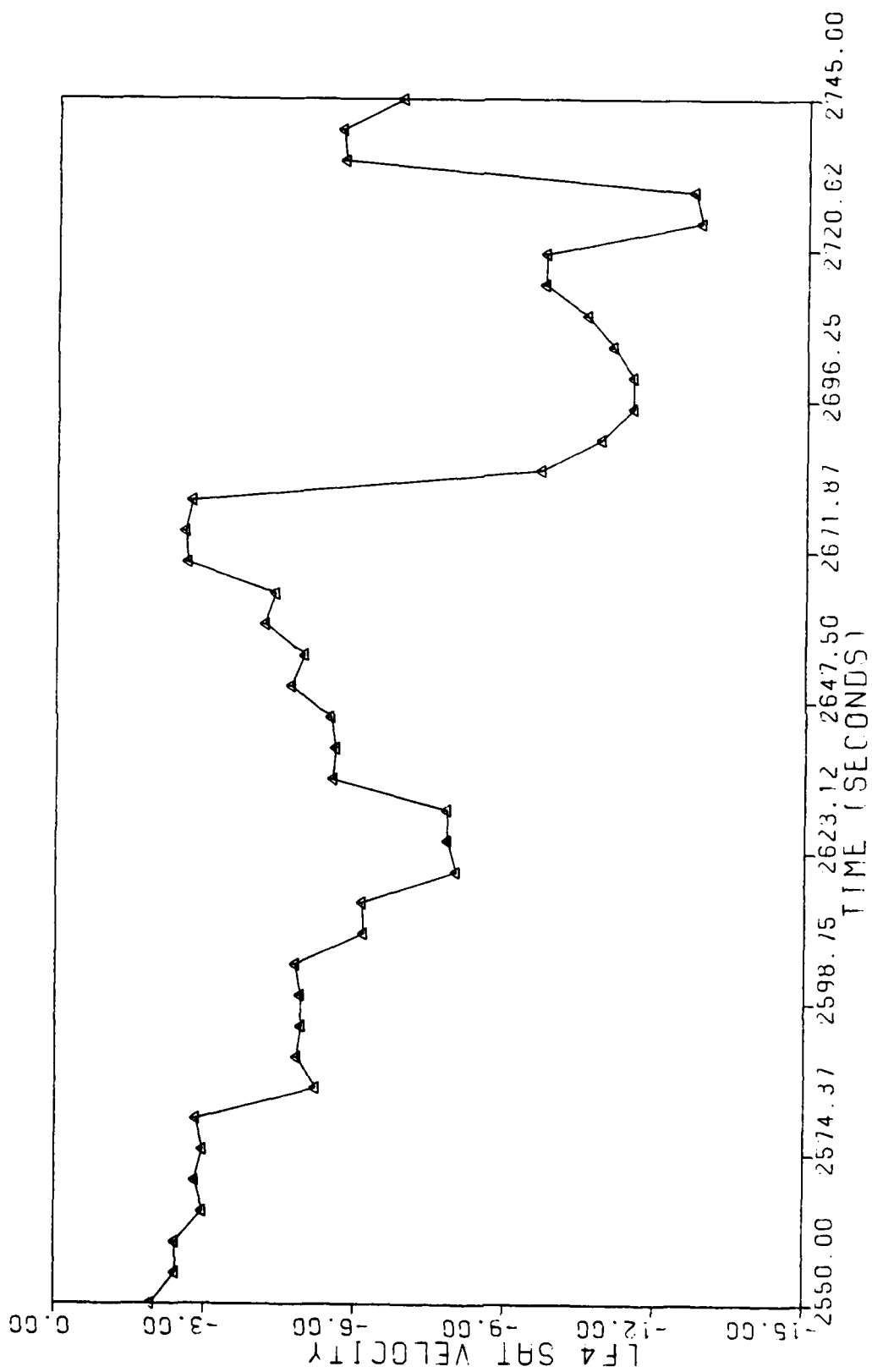


Fig. A.34. Hard Accelerometer 2 Failure--Satellite Velocity Measurement #4--Dynamic Flight

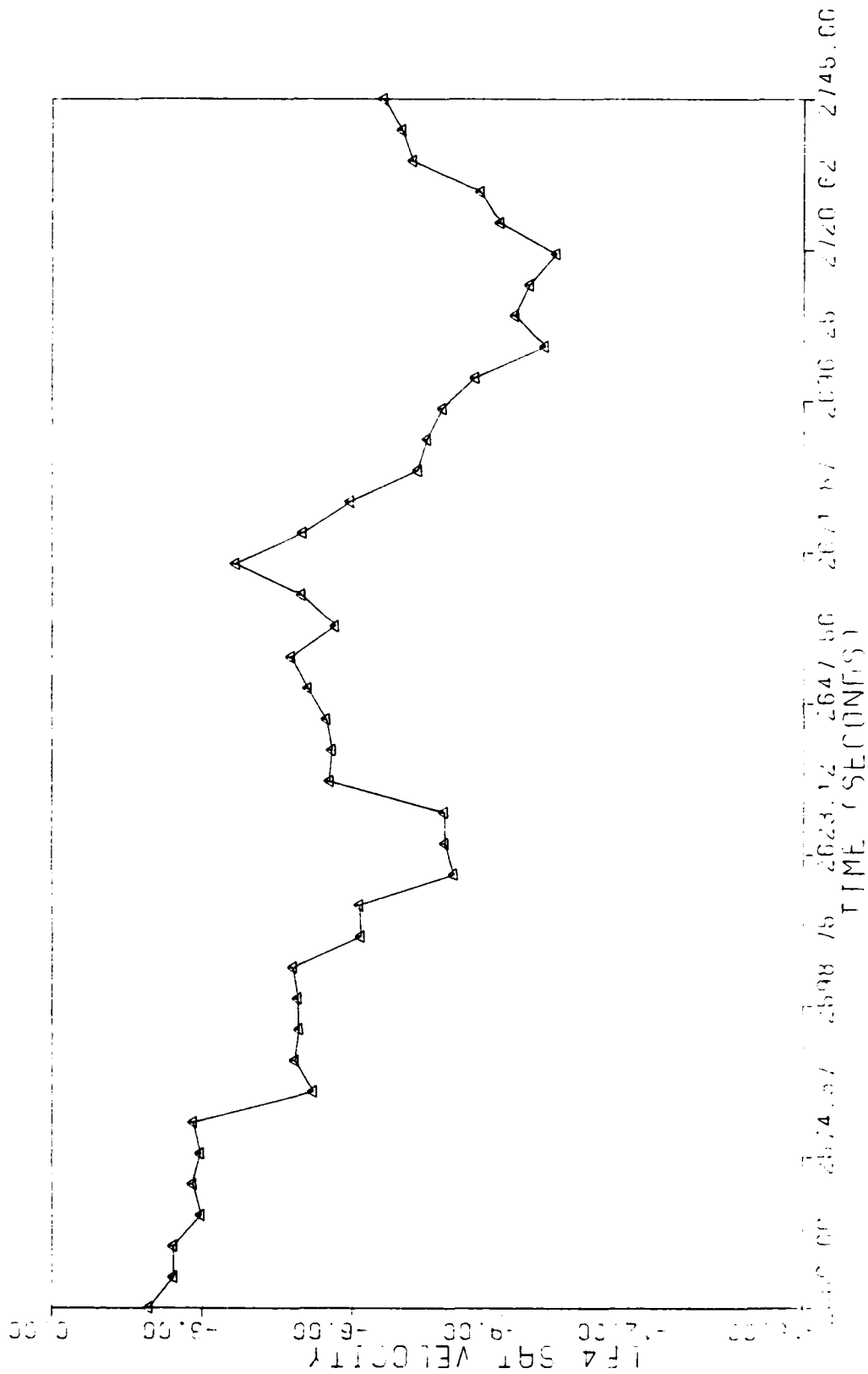


Fig. A.35. Hard Accelerometer 1 Failure--Satellite Velocity Measurement #4--Dynamic Flight

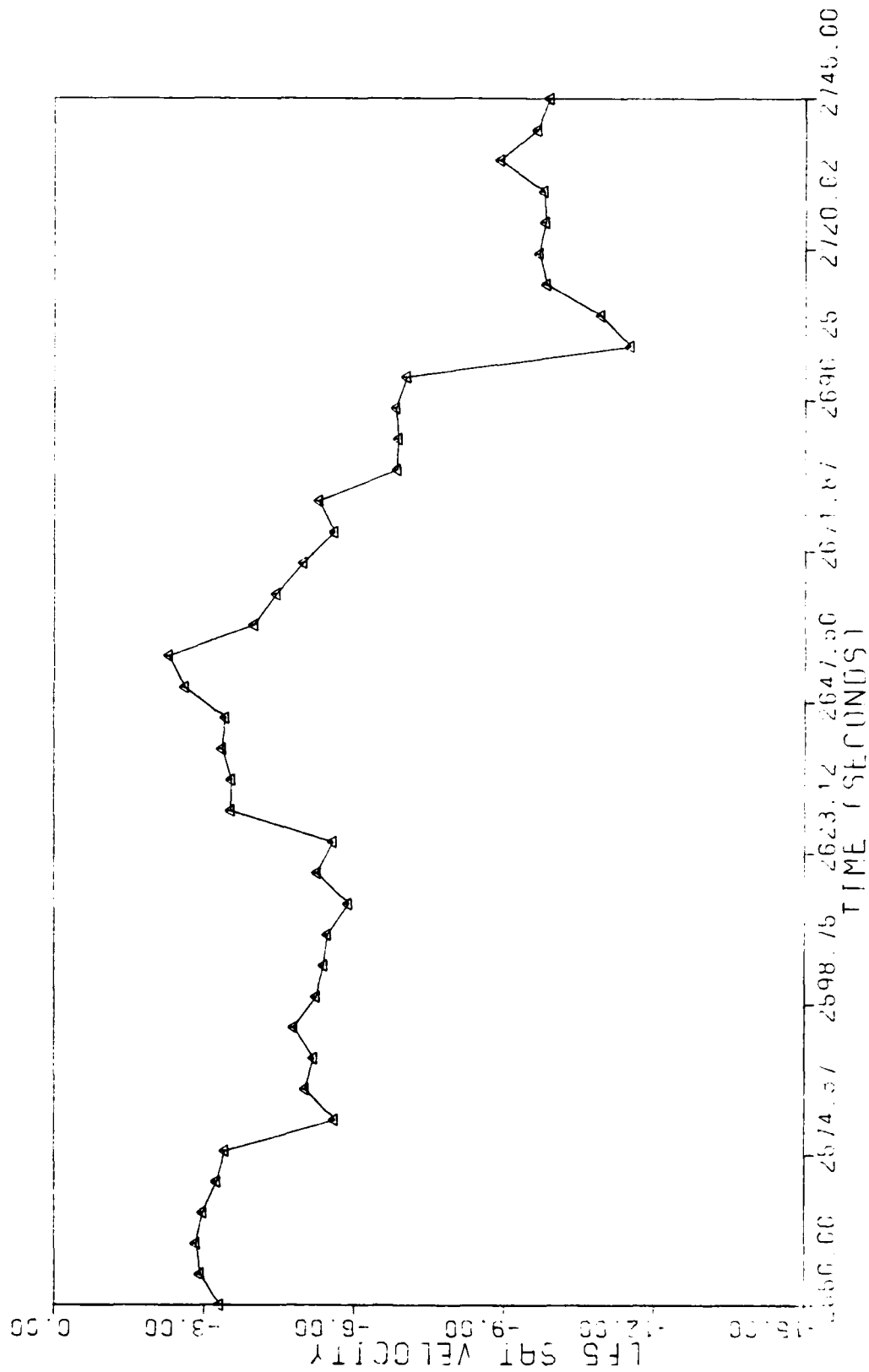
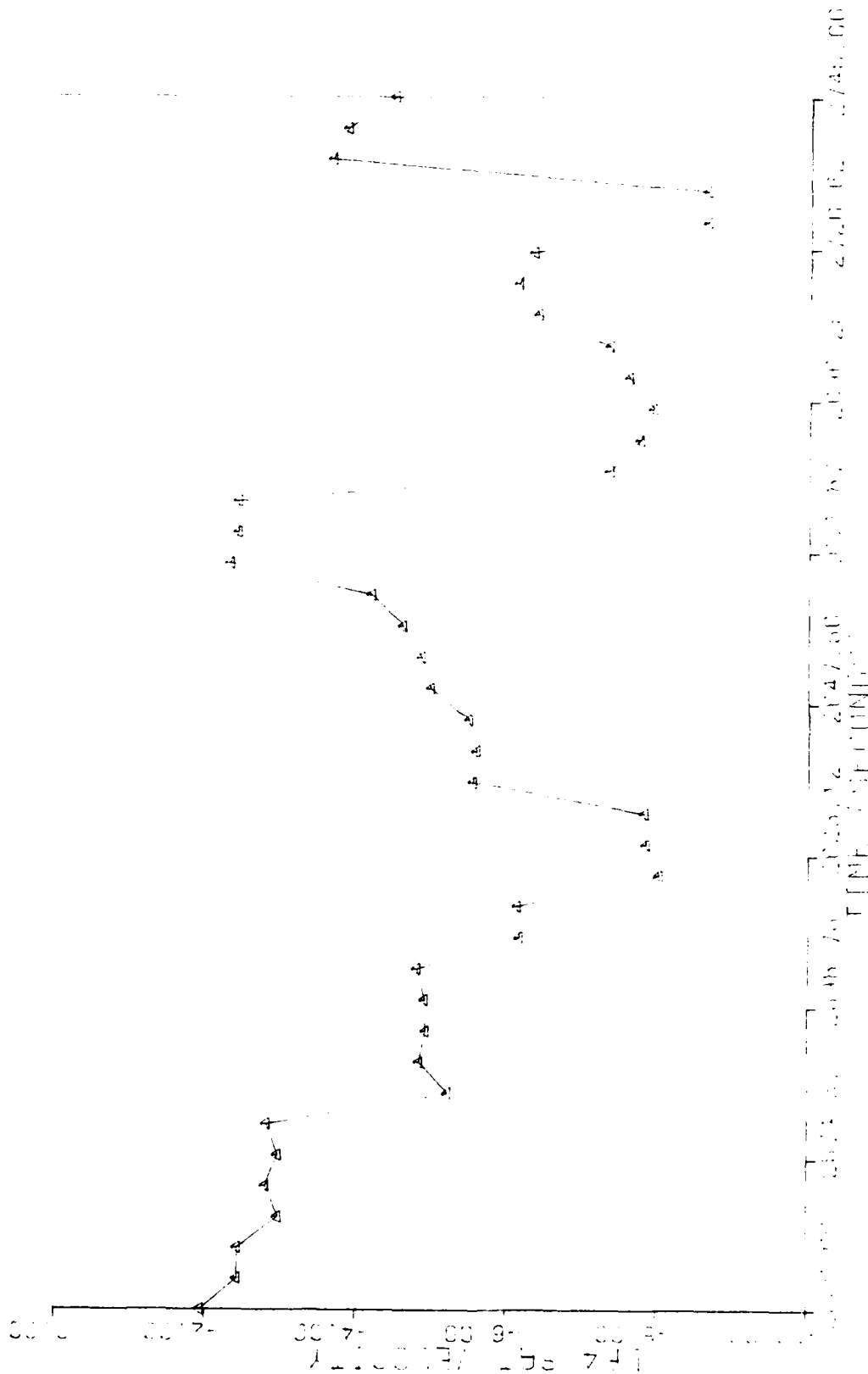


Fig. A.36. Hard Accelerometer 1 Failure--Satellite Velocity Measurement #5--Dynamic Flight



Ref. A.37. Soft Accelerometer 2 Failure--Satellite Velocity Measurement #4--Dynamic Flight



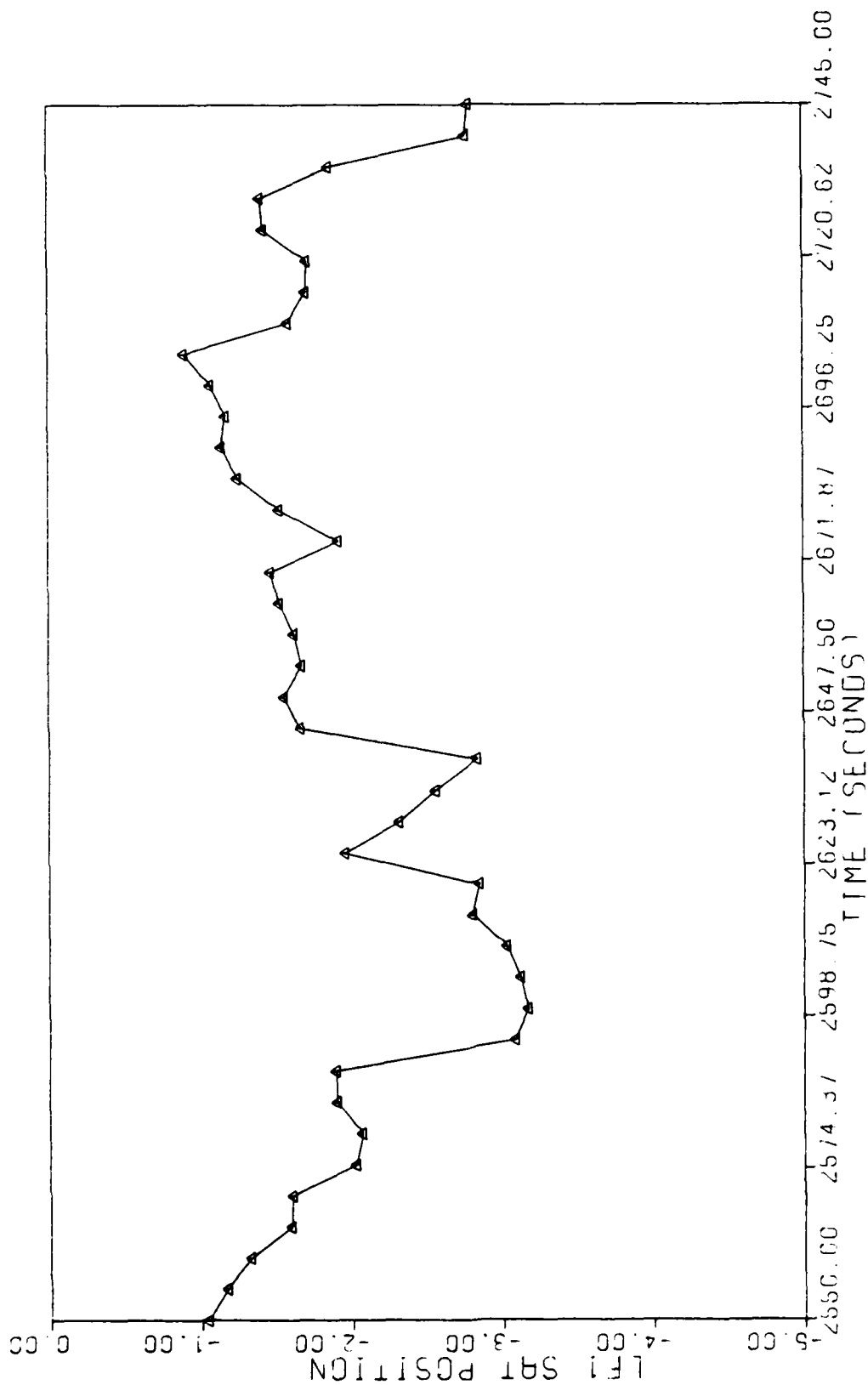


Fig. A.38. No Failure Condition--Satellite Position Measurement #1--Dynamic Flight

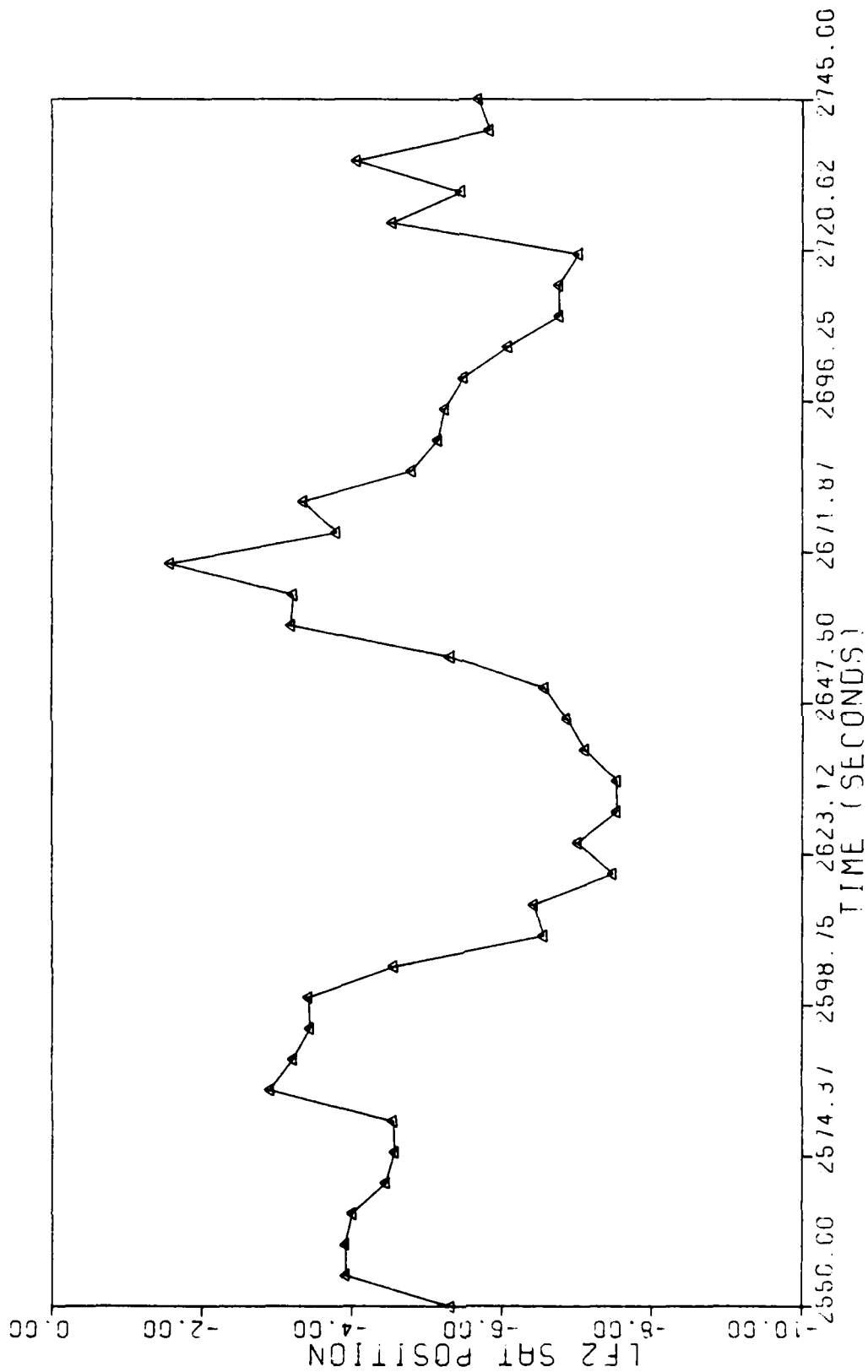


Fig. A.39. No Failure Condition--Satellite Position Measurement #2--Dynamic Flight

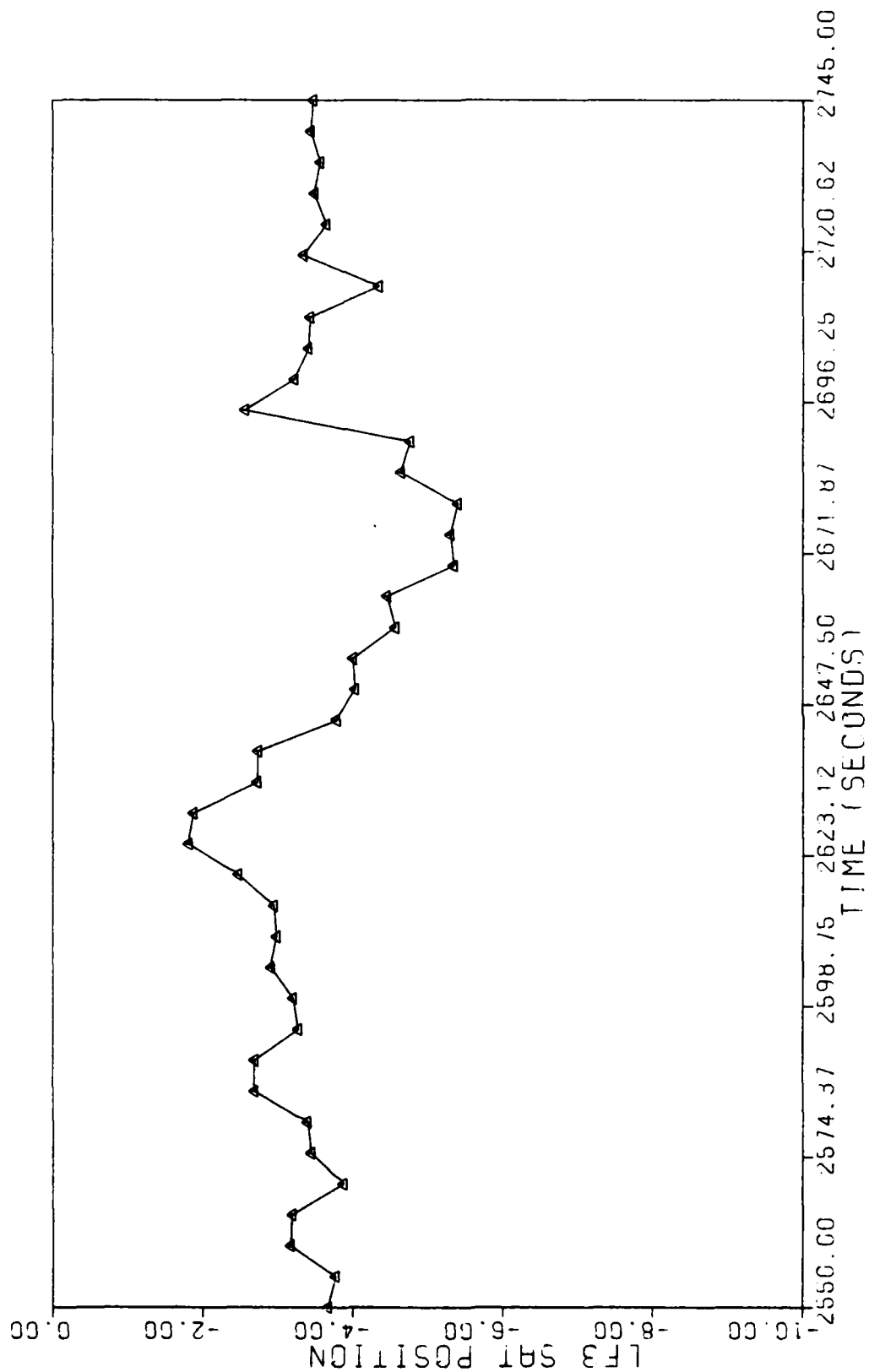


Fig. A.40. No Failure Condition--Satellite Position Measurement #3--Dynamic Flight

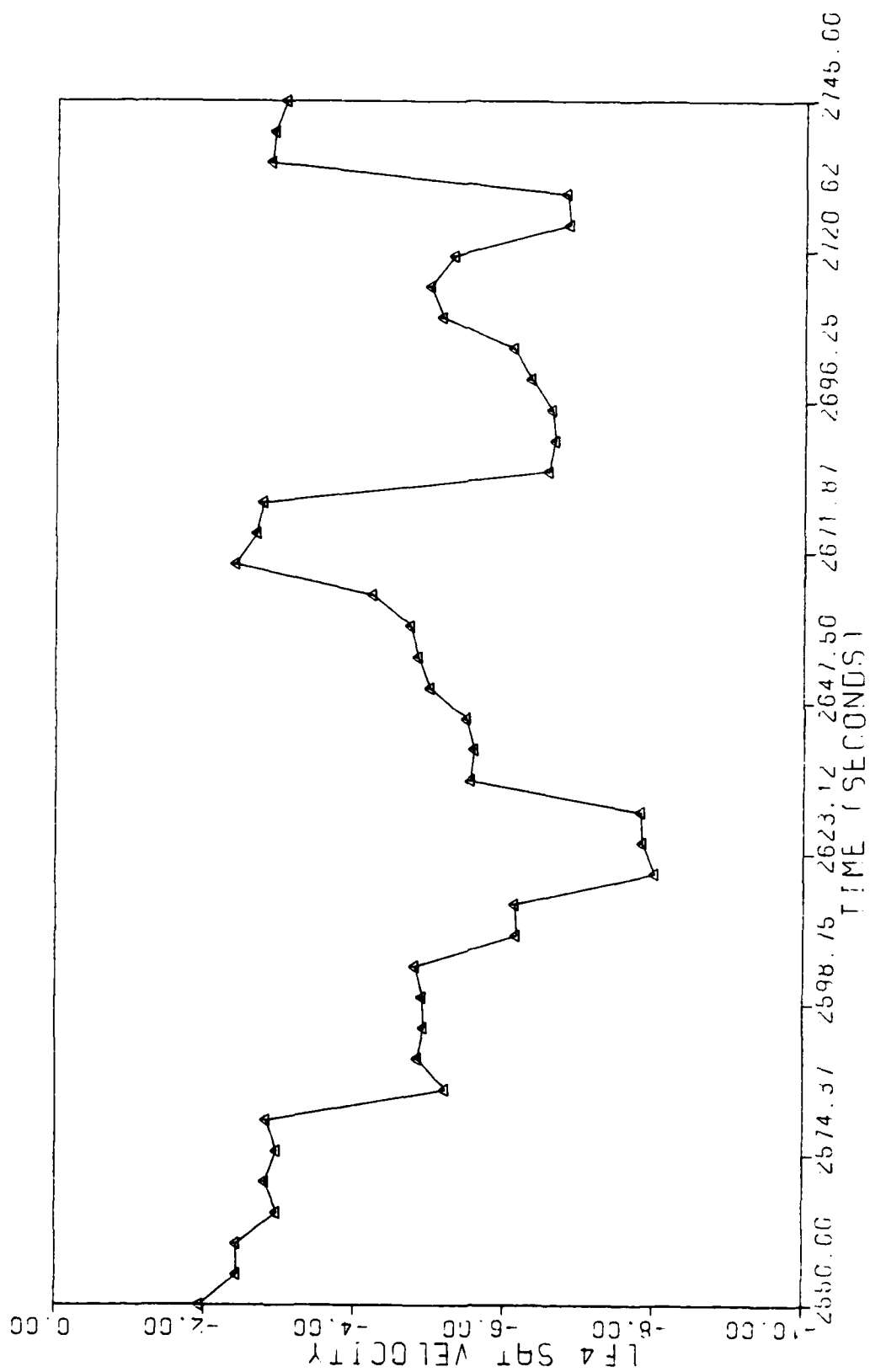


Fig. A.41. No Failure Condition--Satellite Velocity Measurement #4--Dynamic Flight

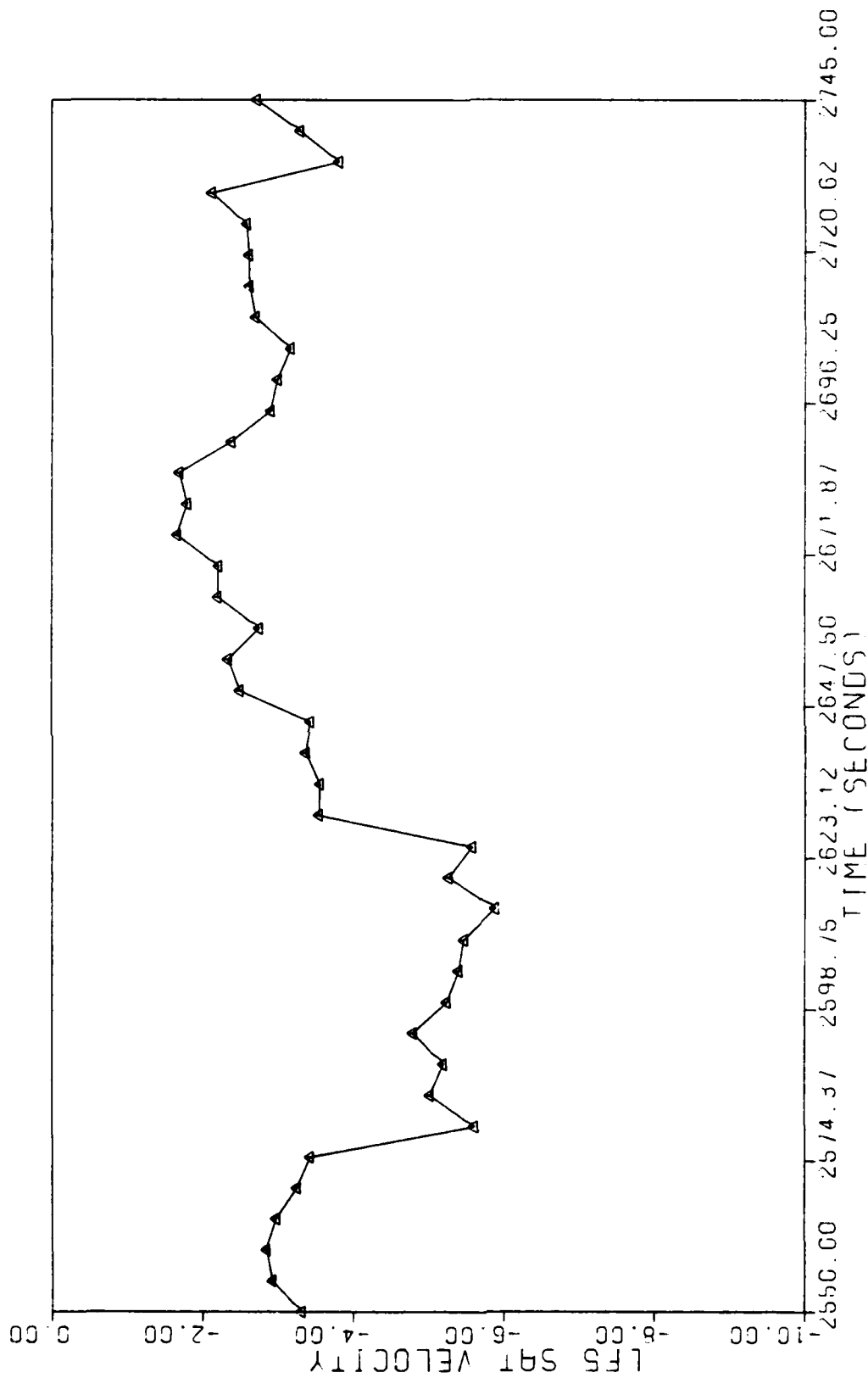


Fig. A.42. No Failure Condition--Satellite Velocity Measurement #5--Dynamic Flight

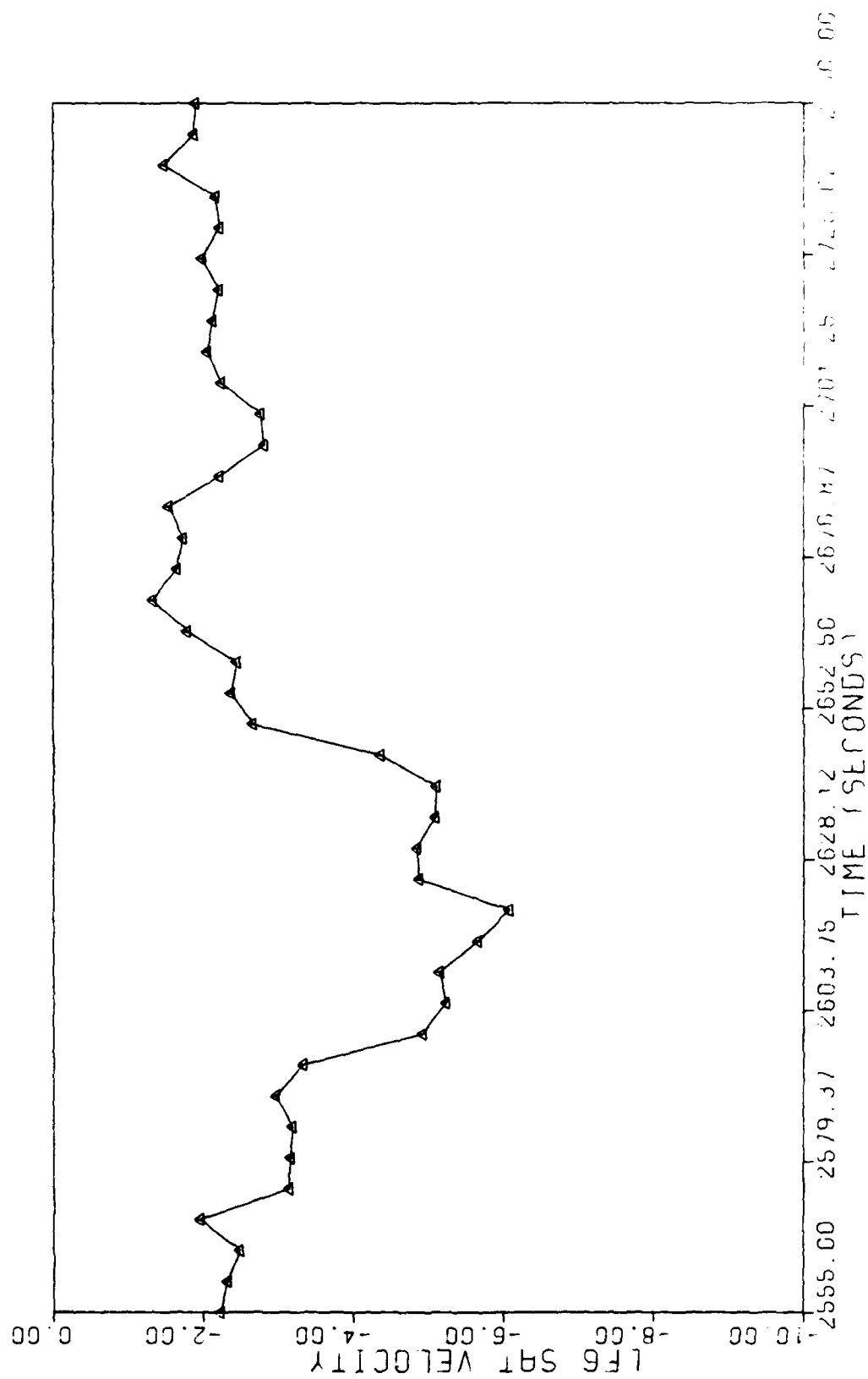


Fig. A.43. No Failure Condition--Satellite Velocity Measurement #6--Dynamic Flight

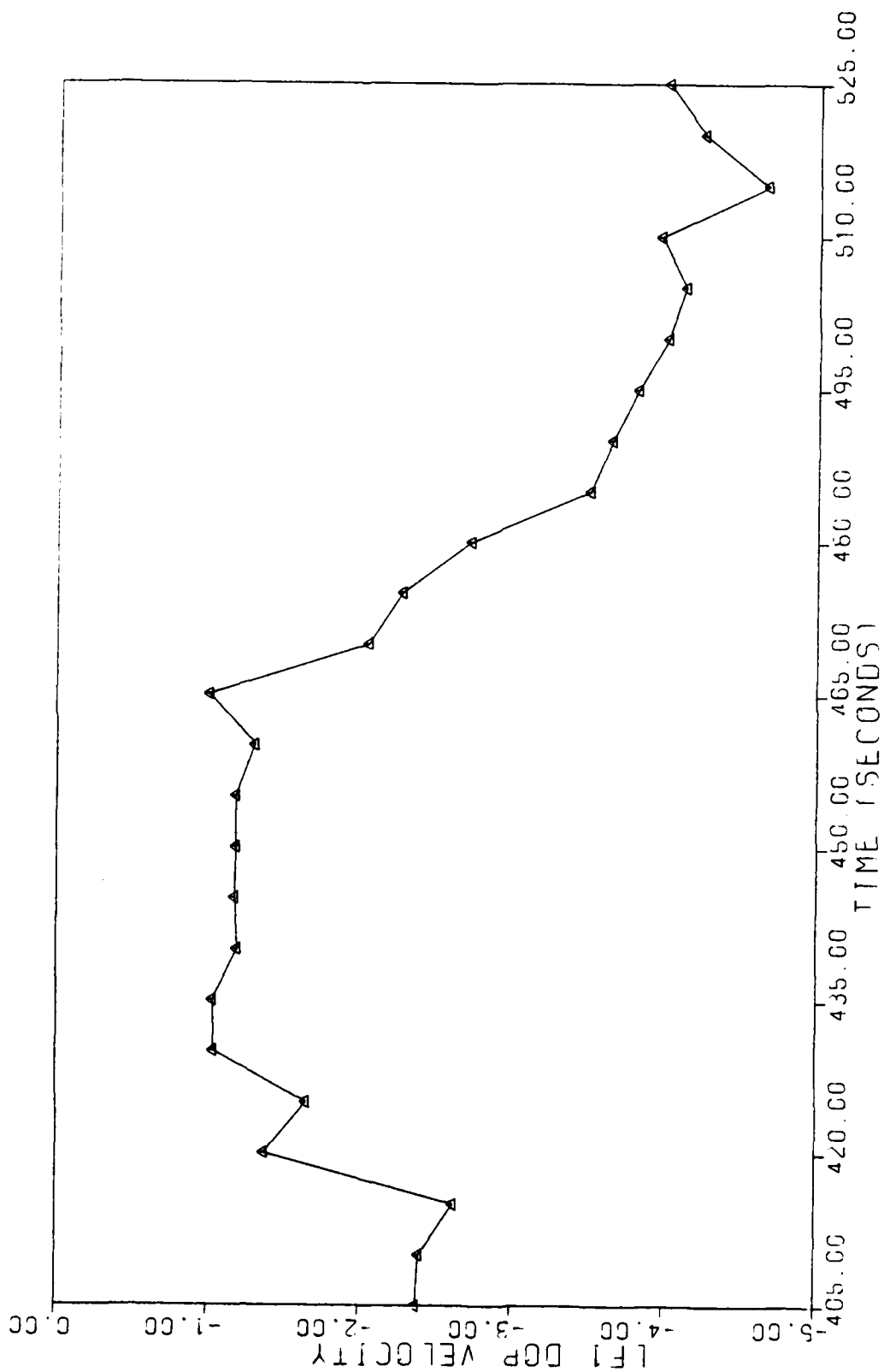


Fig. A-44. No Failure Condition--Doppler Velocity Measurement #1--Design Flight

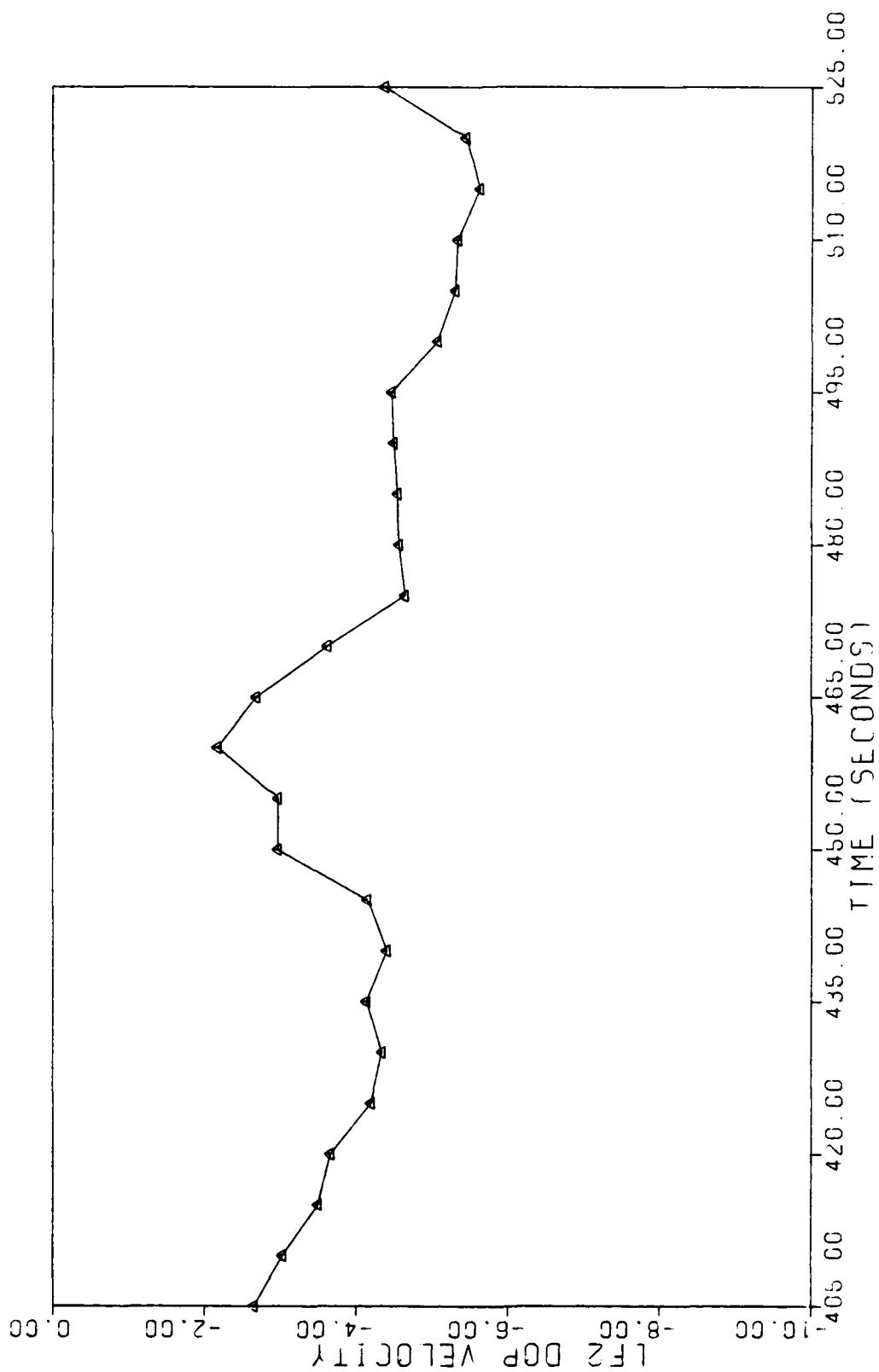


Fig. A.45. No Failure Condition--Doppler Velocity Measurement #2--Benign Flight



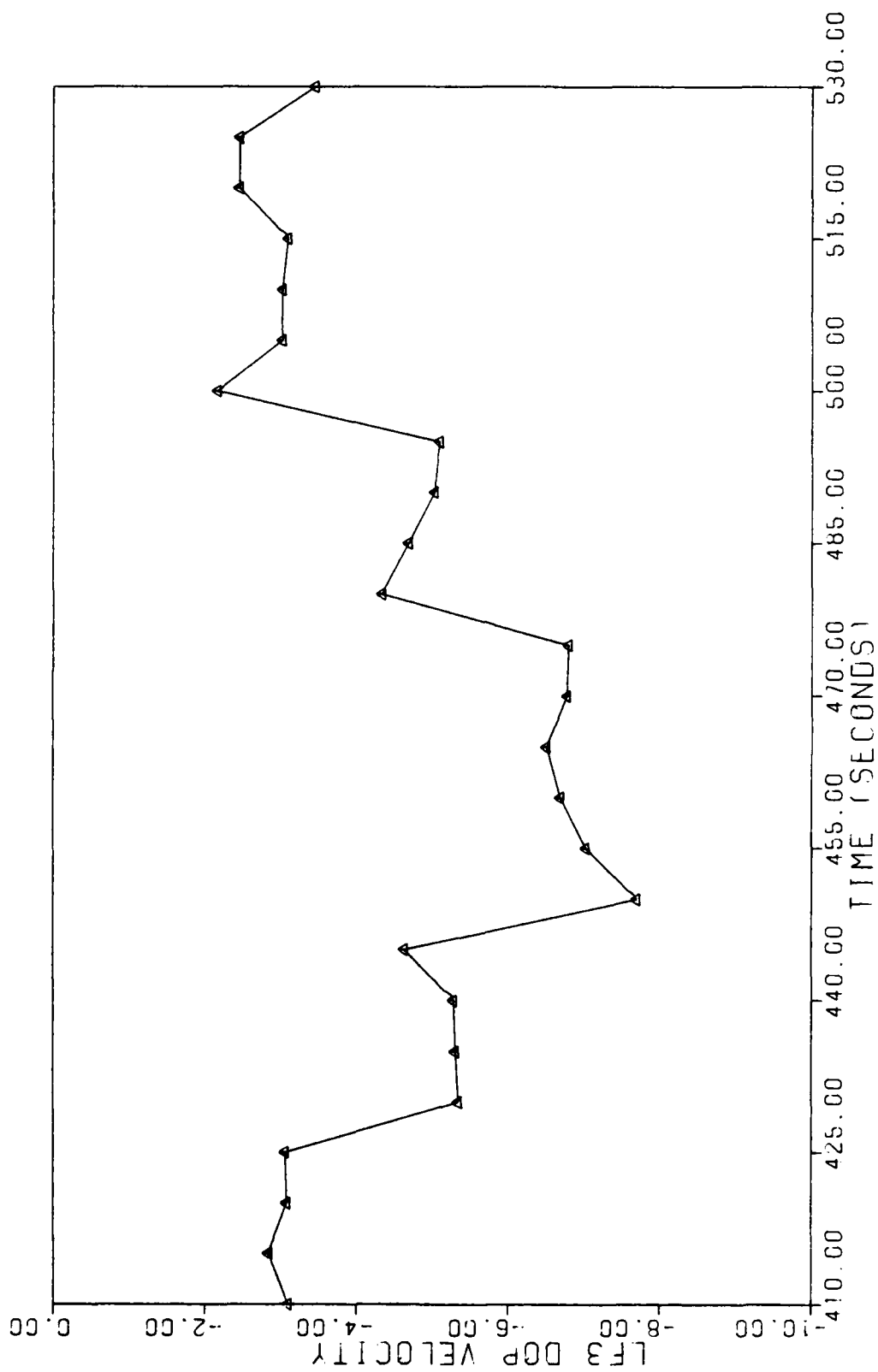


Fig. A.46. No Failure Condition--Doppler Velocity Measurement #3--Benign Flight

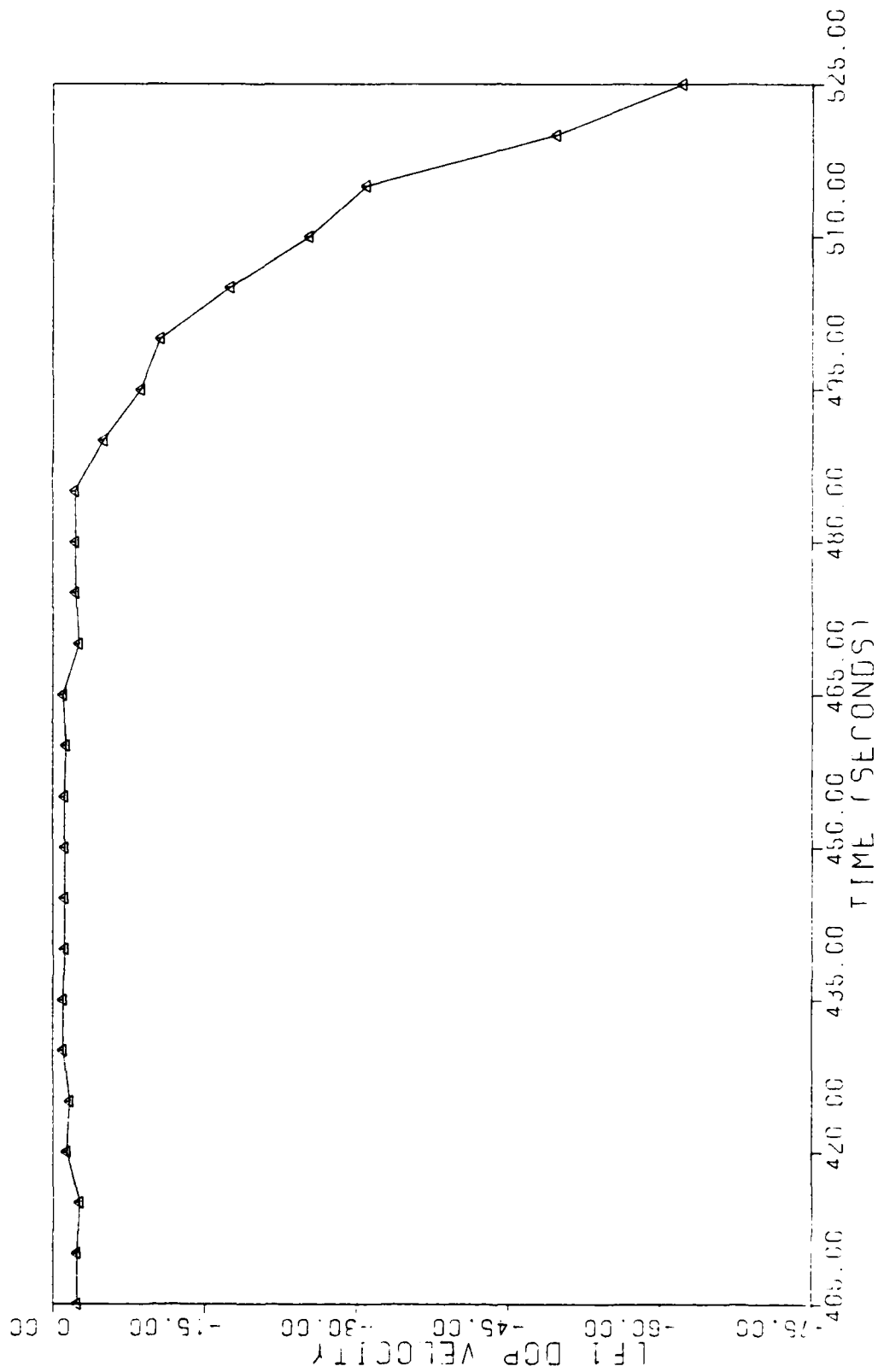


Fig. A.47. Hard Gyr, 1 Failure--Doppler Velocity Measurement #1--Benign Flight

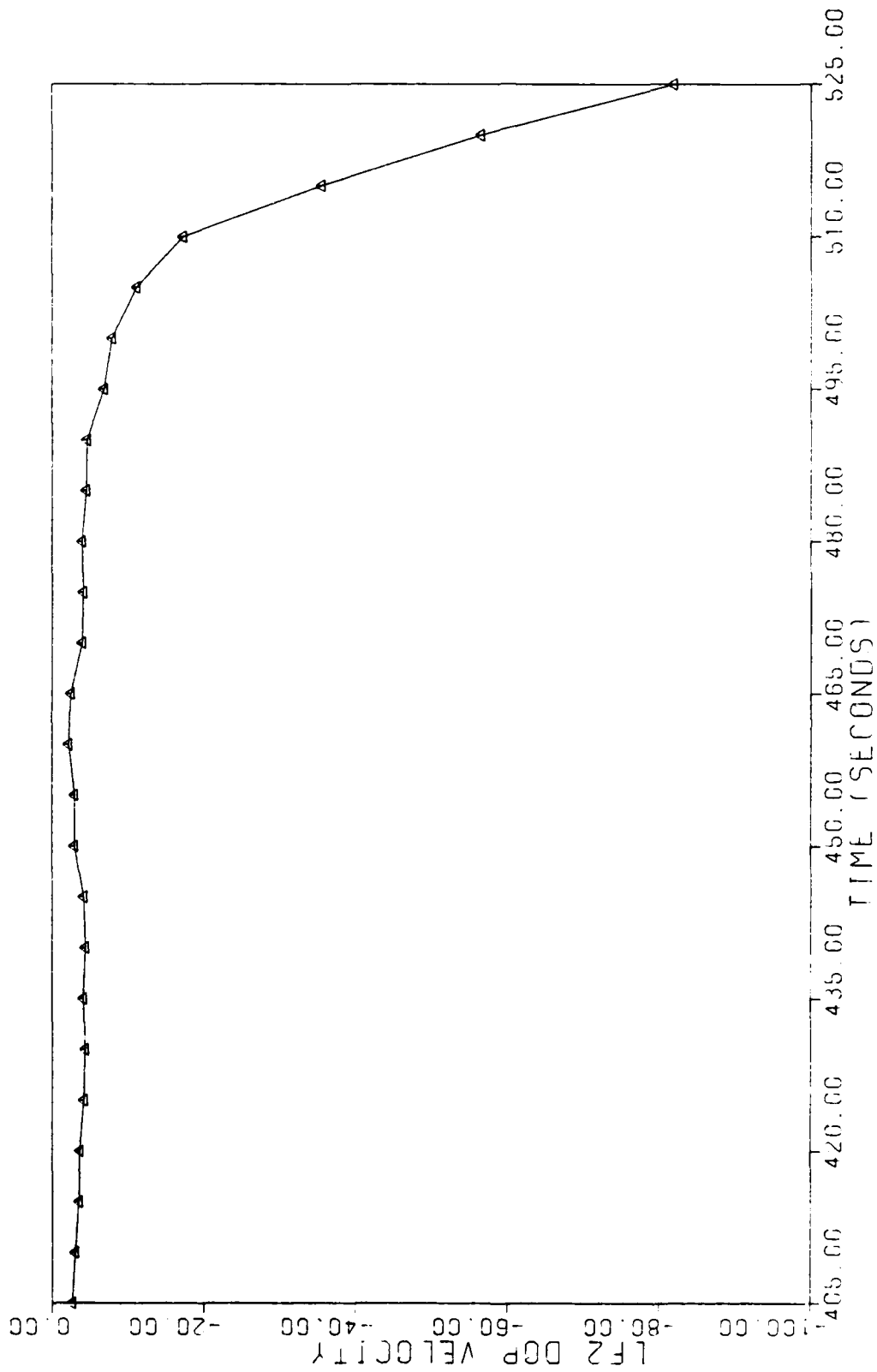


Fig. A.48. Hard Gyro 1 Failure--Doppler Velocity Measurement #2--Benign Flight

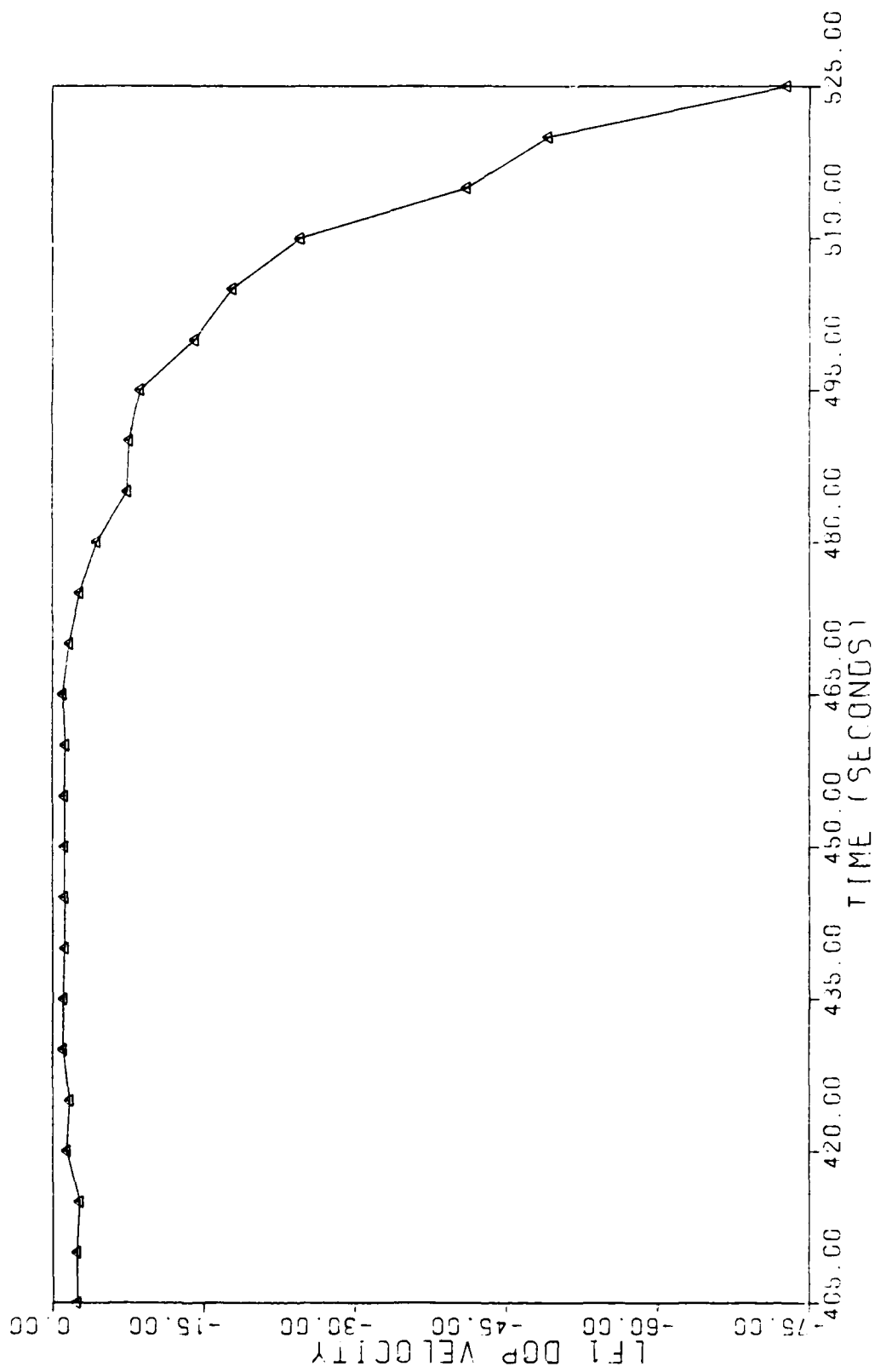


Fig. A.49. Hard Gyro 2 Failure--Doppler Velocity Measurement #1--Benign Flight

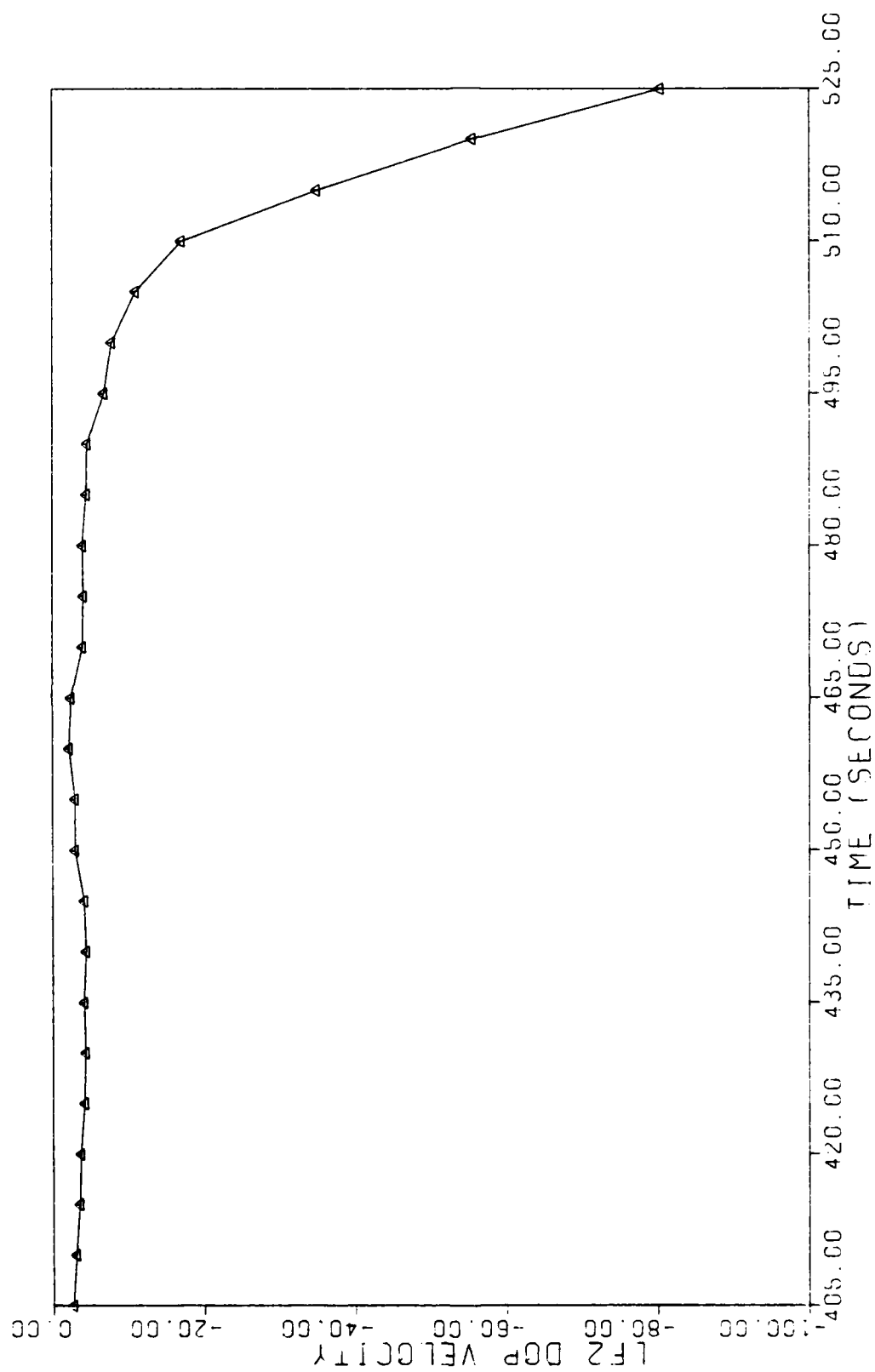


Fig. A.50. Hard Gyro 2 Failure--Doppler Velocity Measurement #2--Benign Flight

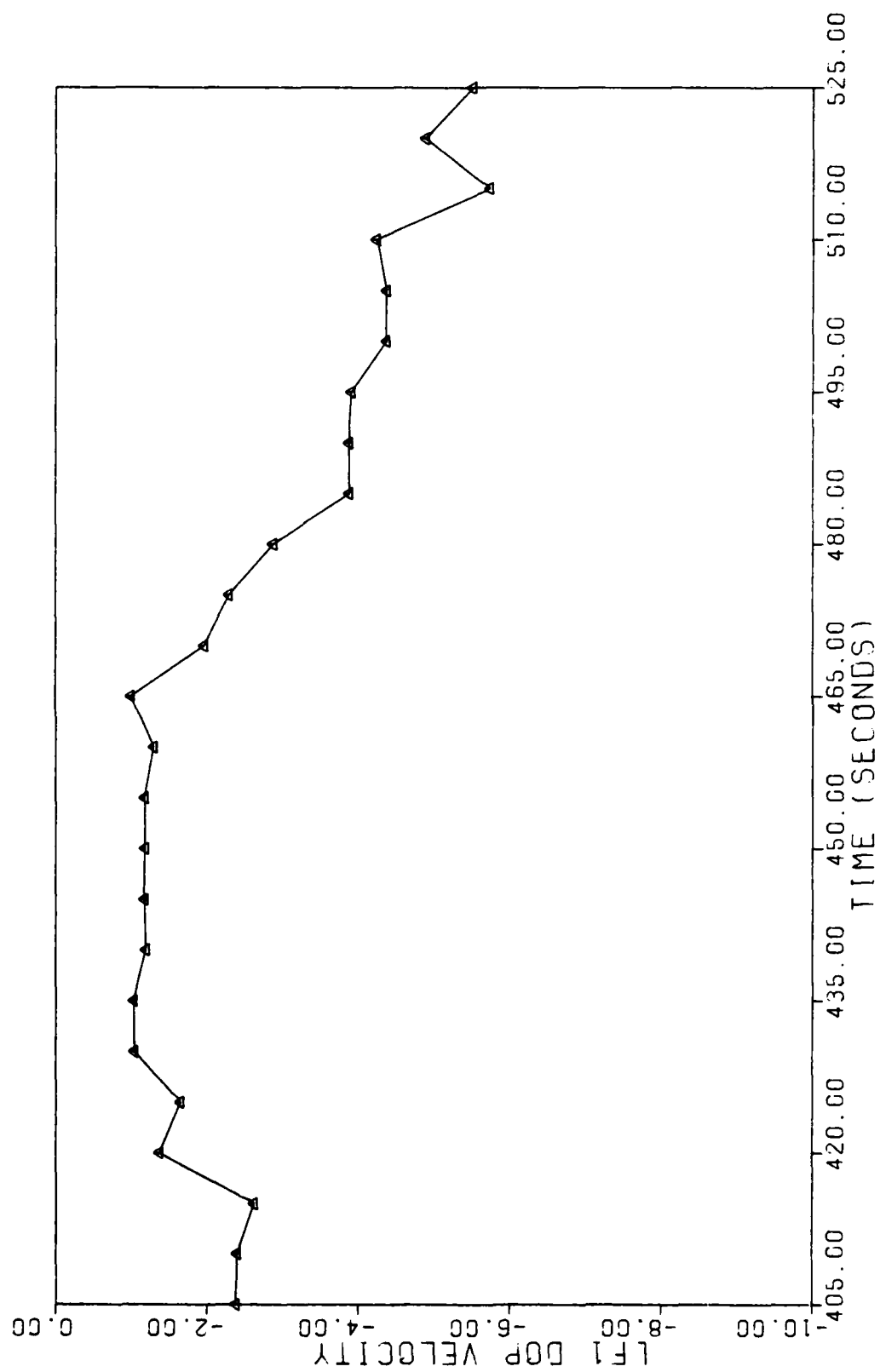


Fig. A.51. Soft Accelerometer 1 Failure--Doppler Velocity Measurement #1--Benign Flight

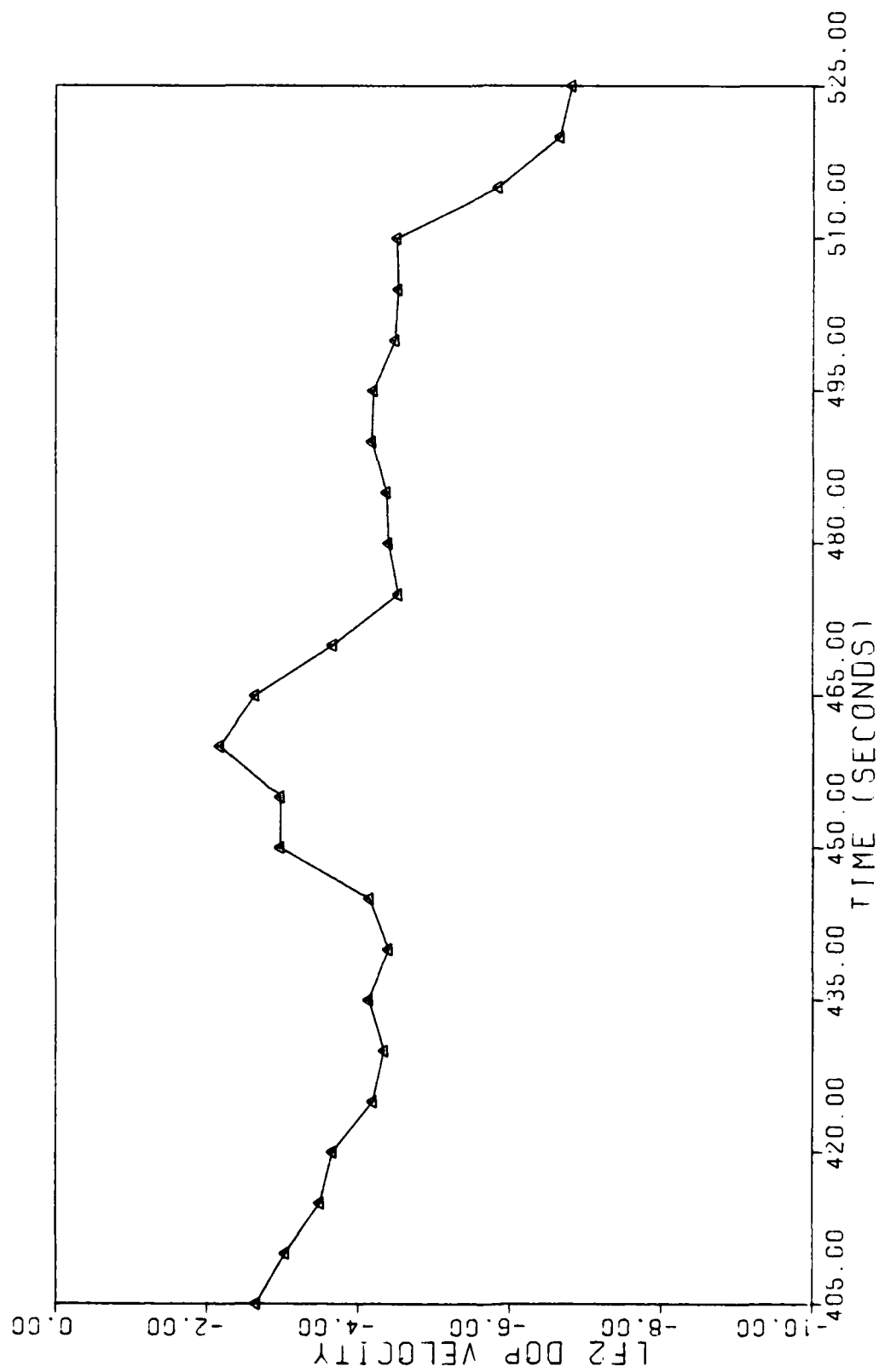


Fig. A.52. Soft Accelerometer 1 Failure--Doppler Velocity Measurement #2--Benign Flight

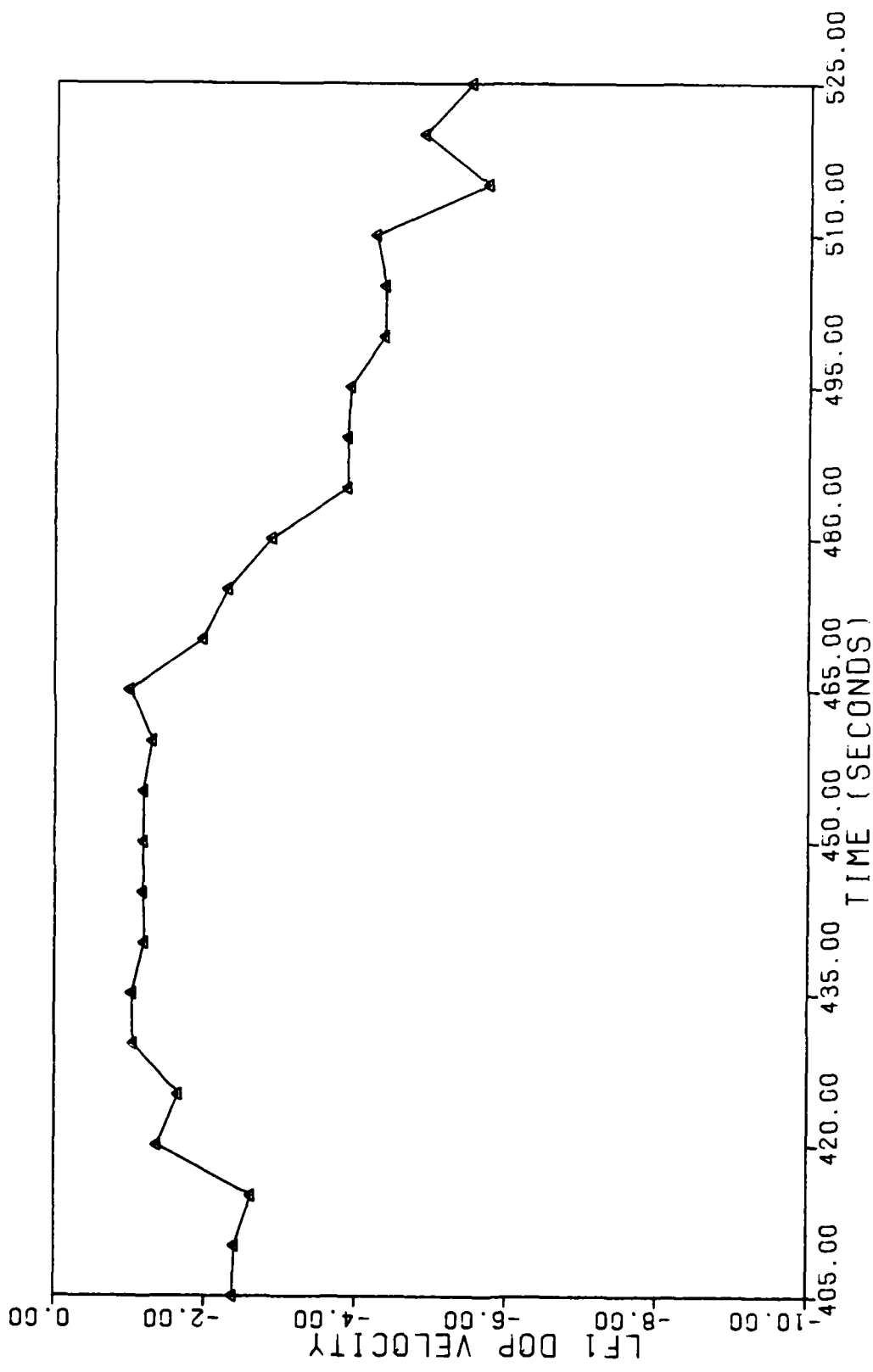


Fig. A.53. Soft Accelerometer 2 Failure--Doppler Velocity Measurement #1--Benign Flight



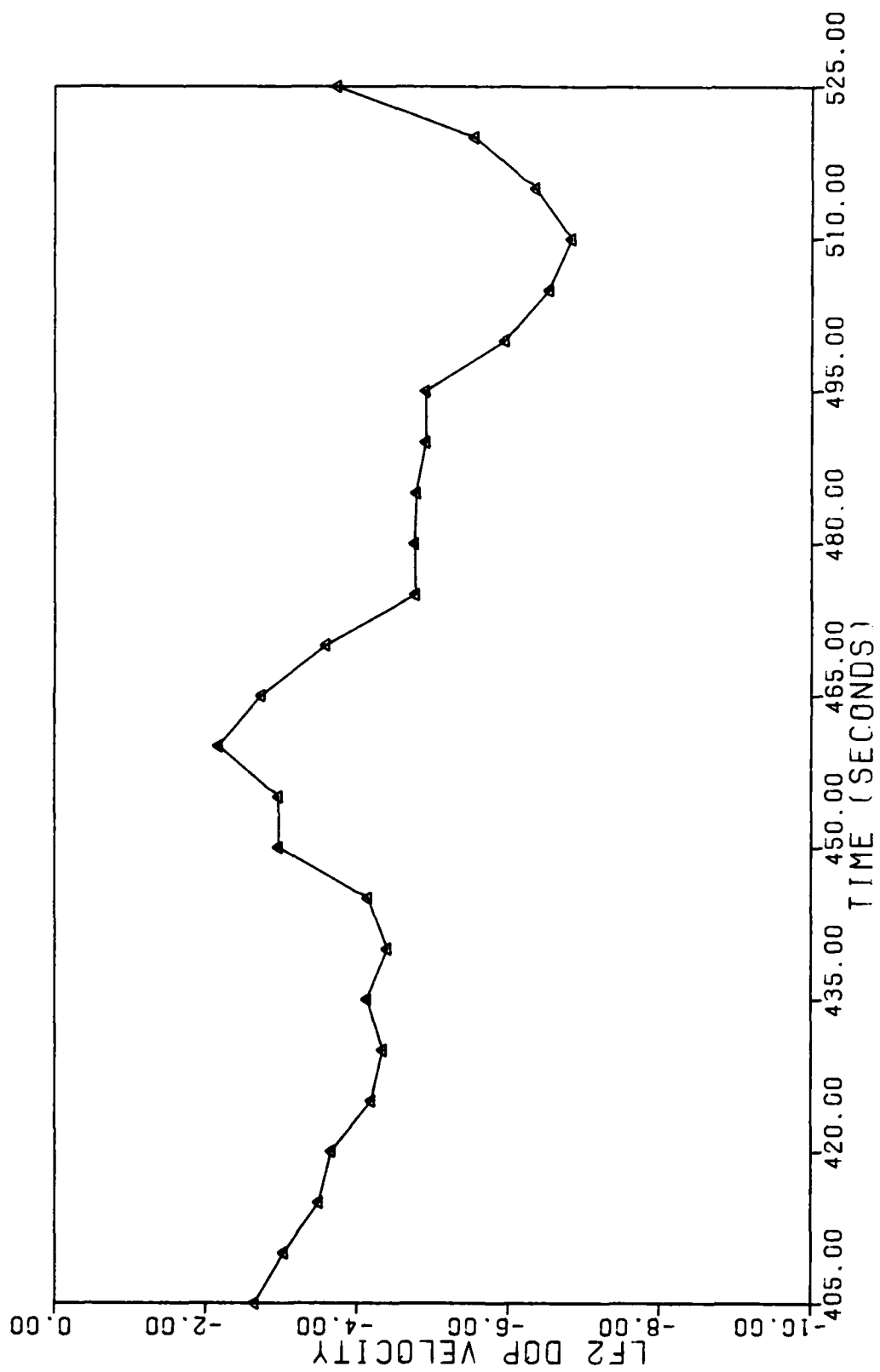


Fig. A.54. Soft Accelerometer 2 Failure--Doppler Velocity Measurement #2--Benign Flight

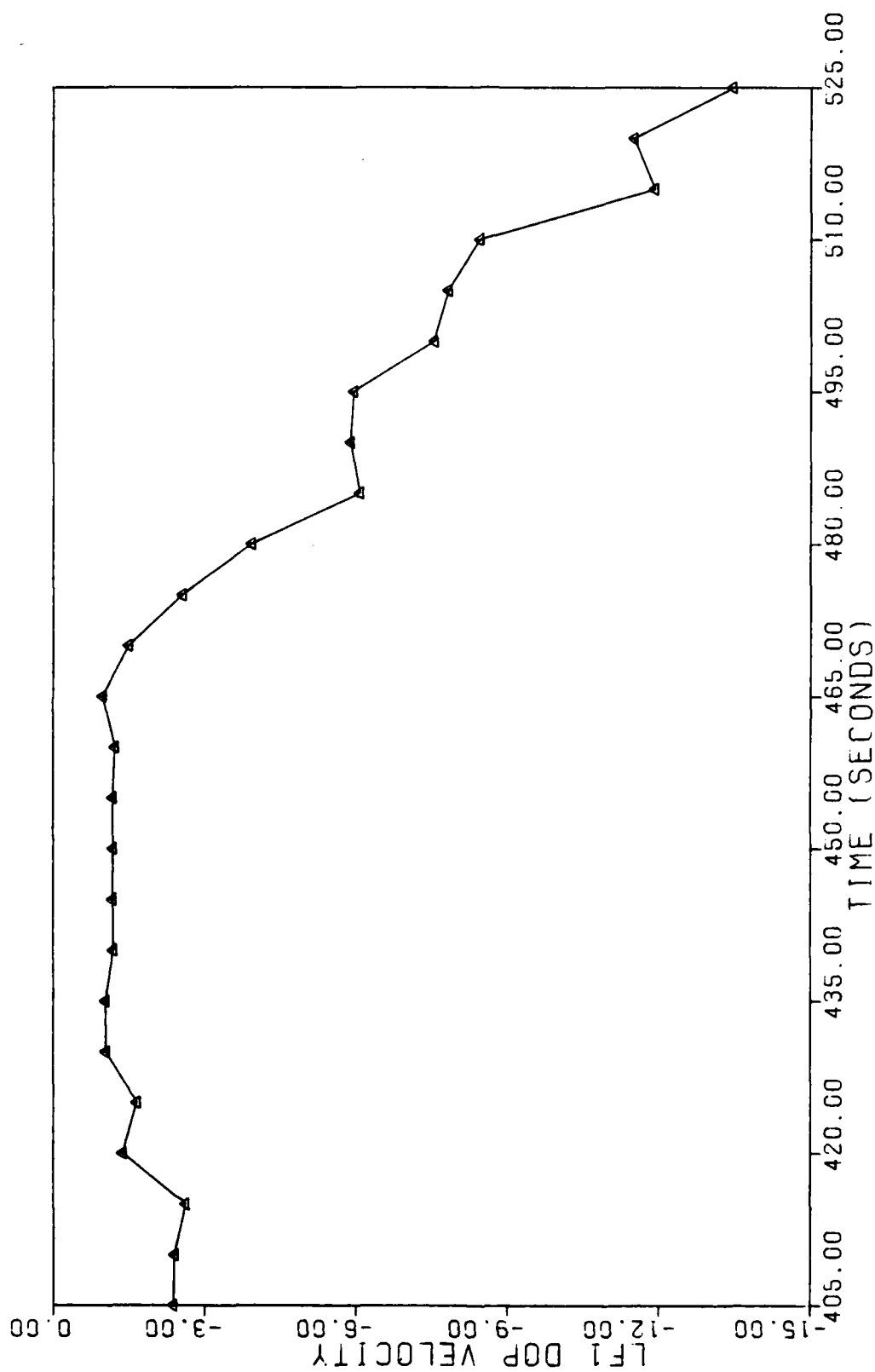


Fig. A.55. Hard Accelerometer 2 Failure--Doppler Velocity Measurement #1--Benign Flight

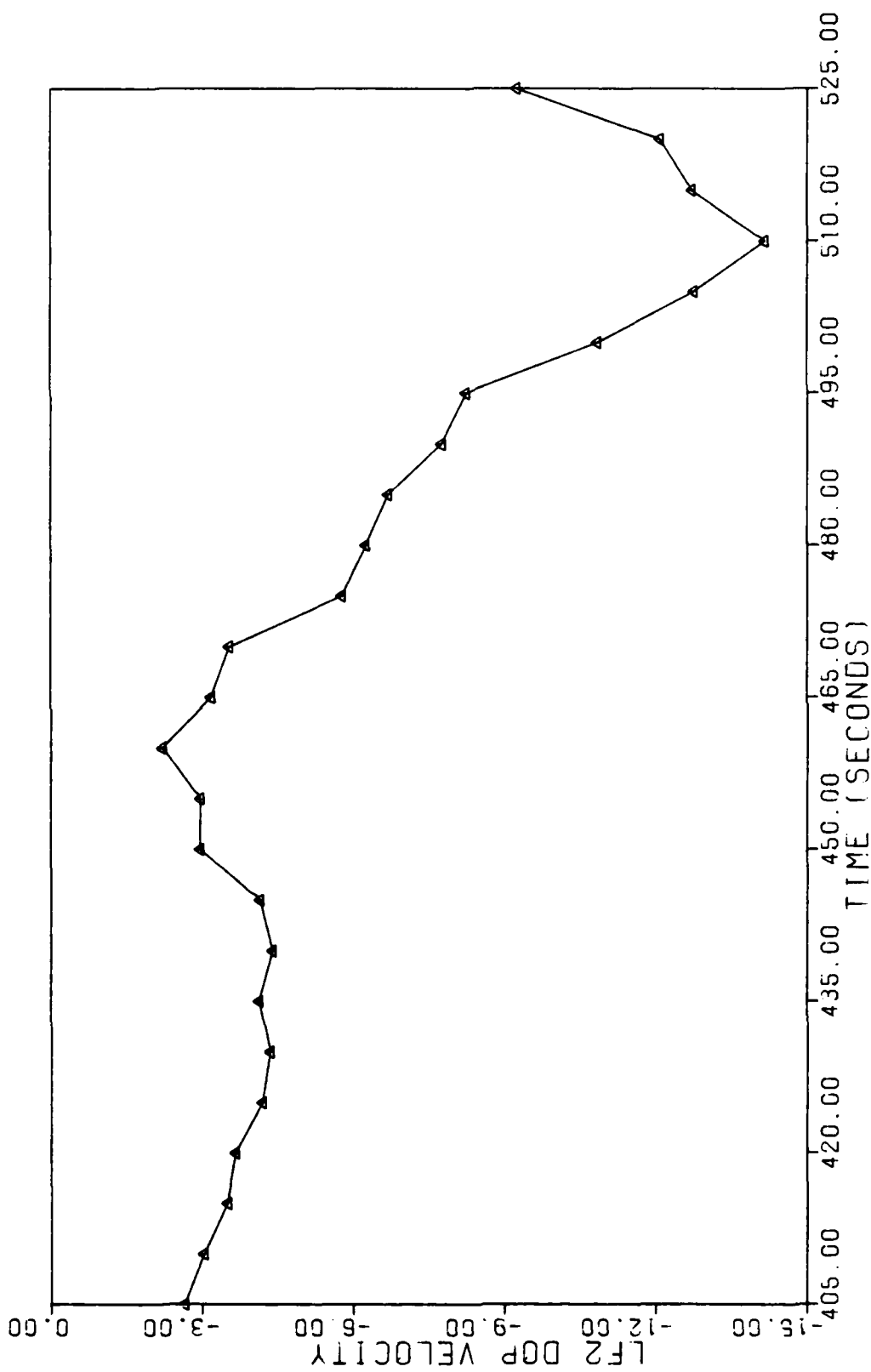


Fig. A.56. Hard Accelerometer 2 Failure--Doppler Velocity Measurement #2--Benign Flight

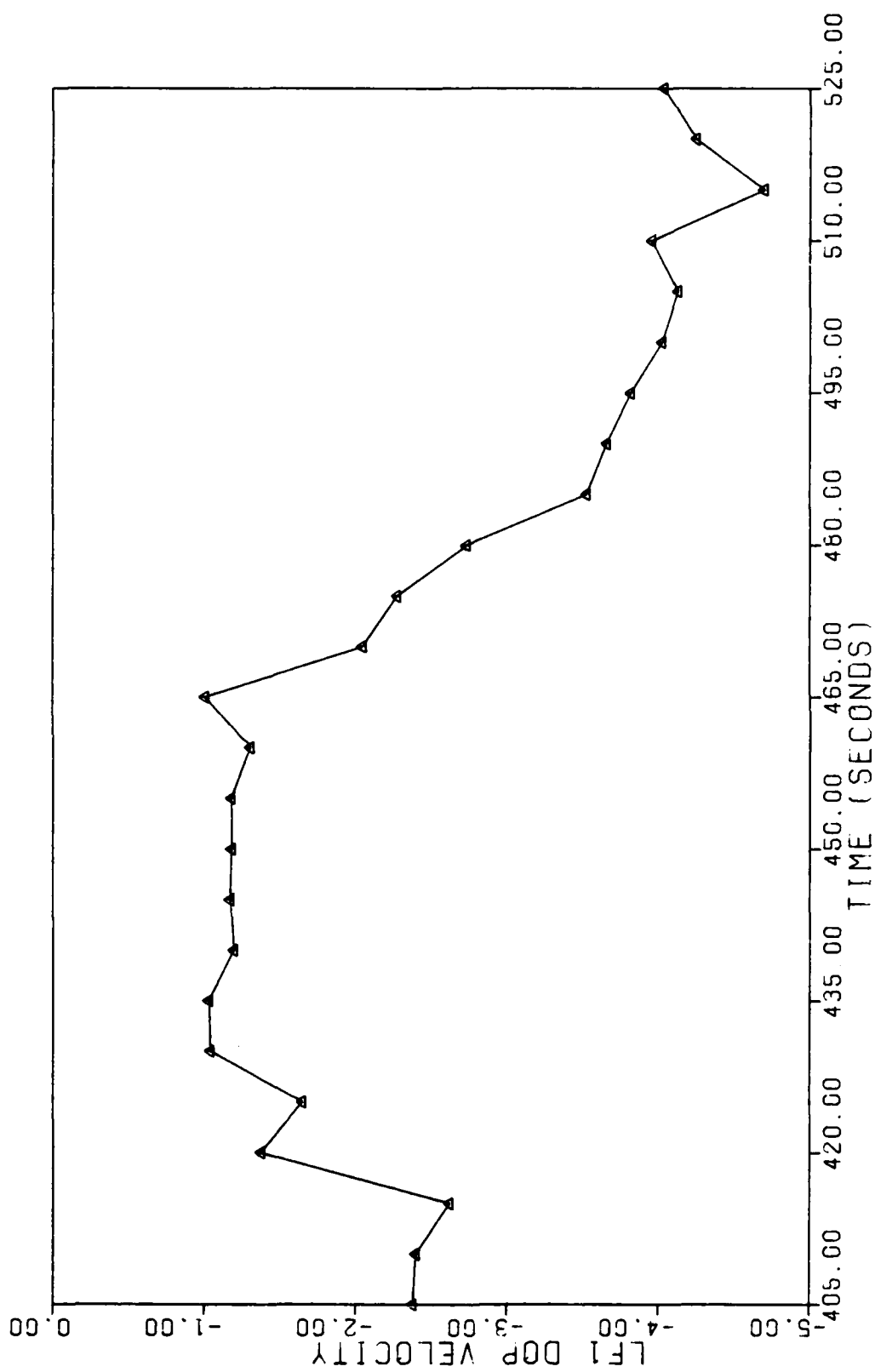


Fig. A.57. Hard Accelerometer 3 Failure--Doppler Velocity Measurement #1--Benign Flight

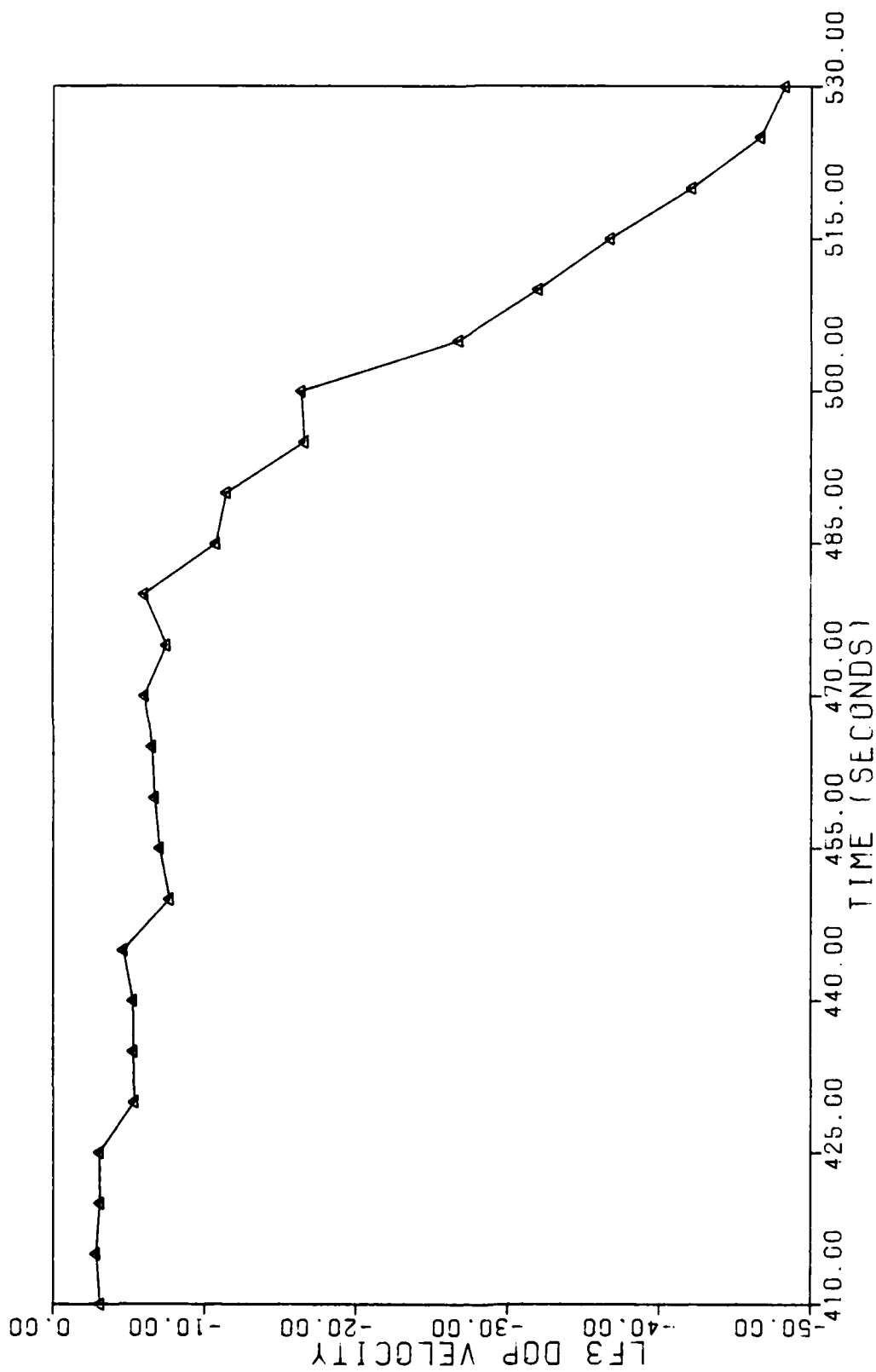


Fig. A.58. Hard Accelerometer 3 Failure--Doppler Velocity Measurement #3--Benign Flight

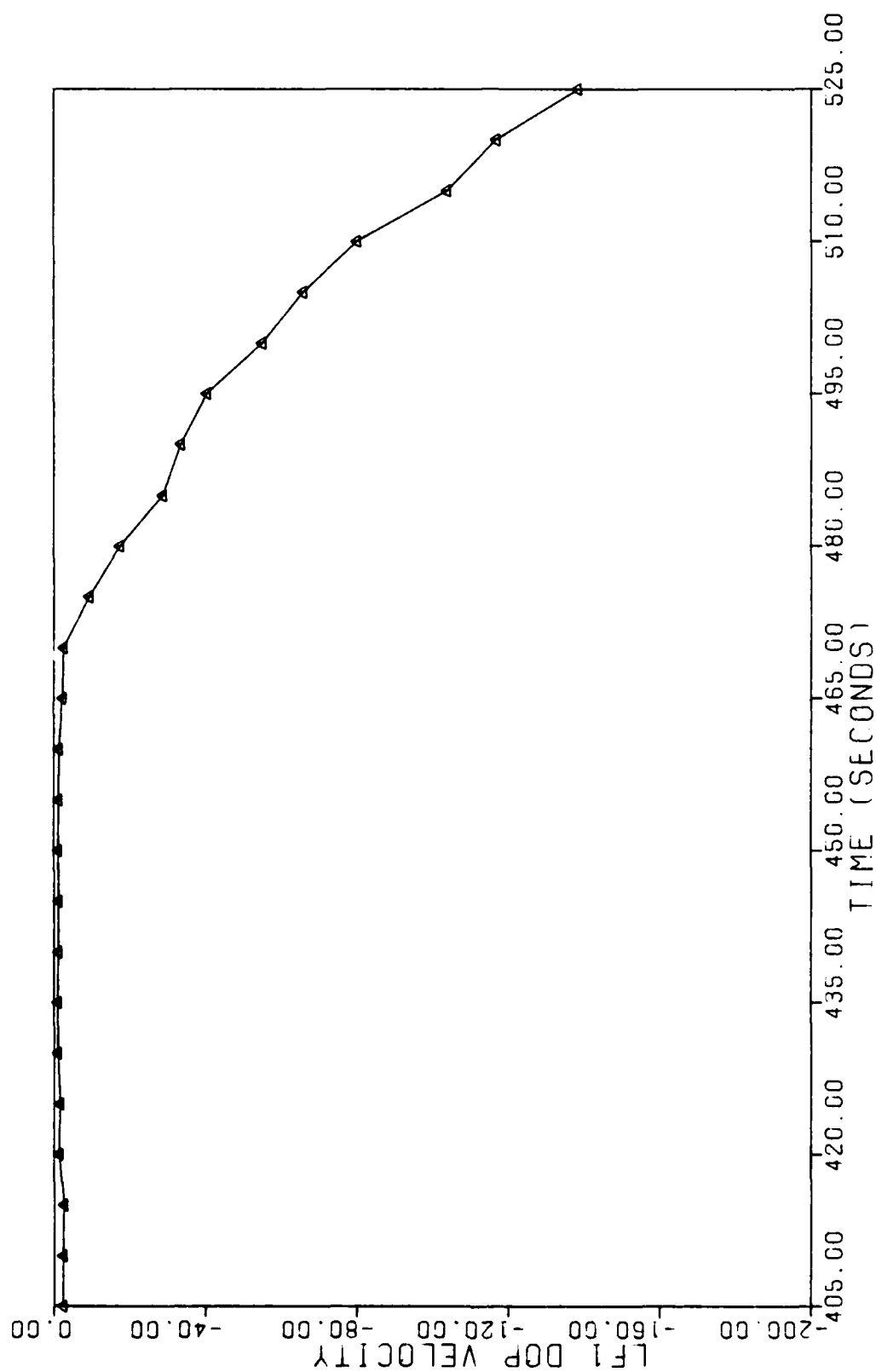


Fig. A.59. Soft Doppler Failure--Doppler Velocity Measurement #1--Benign Flight

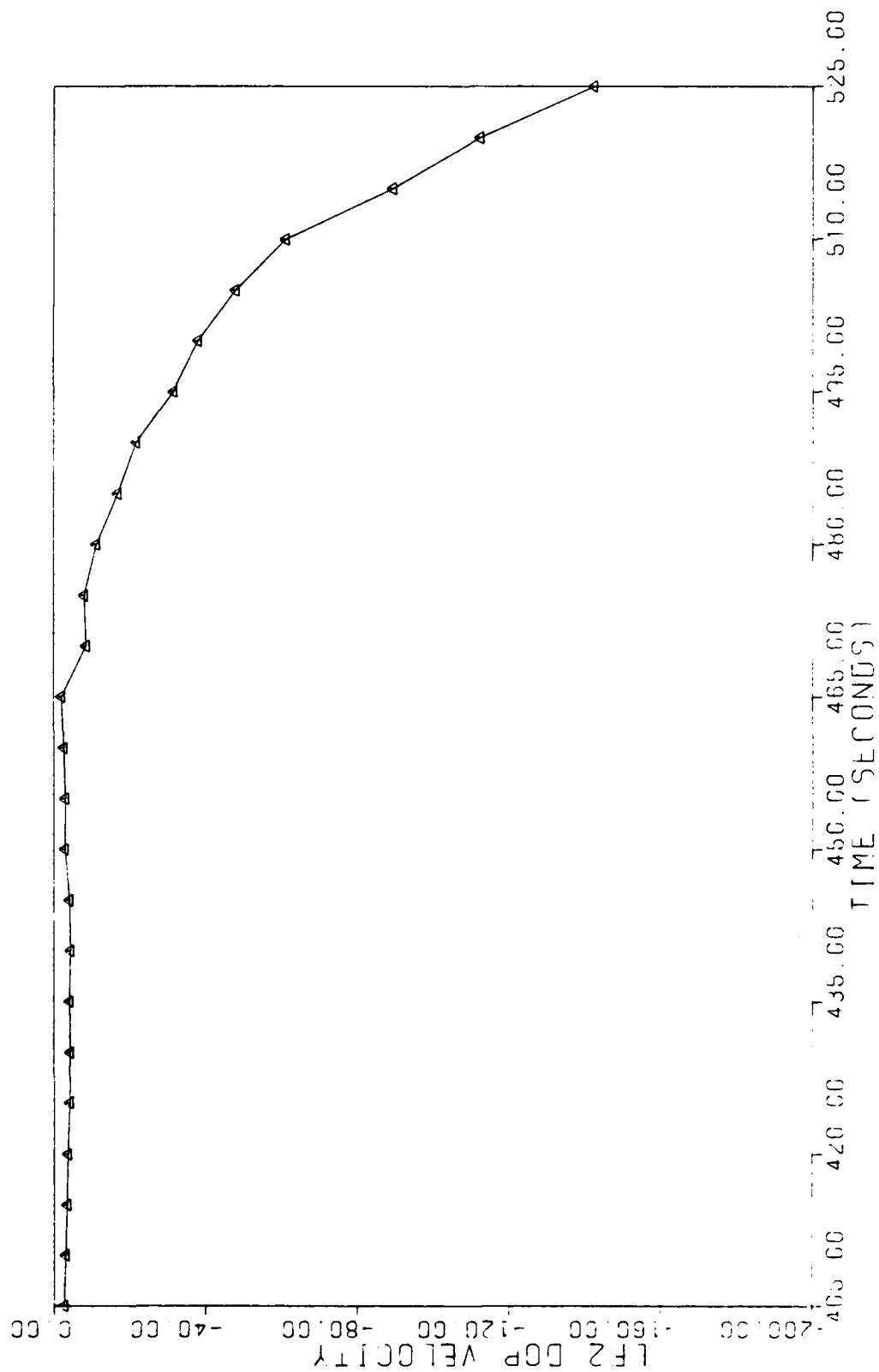


Fig. A.60. Soft Doppler Failure--Doppler Velocity Measurement #2--Benign Flight

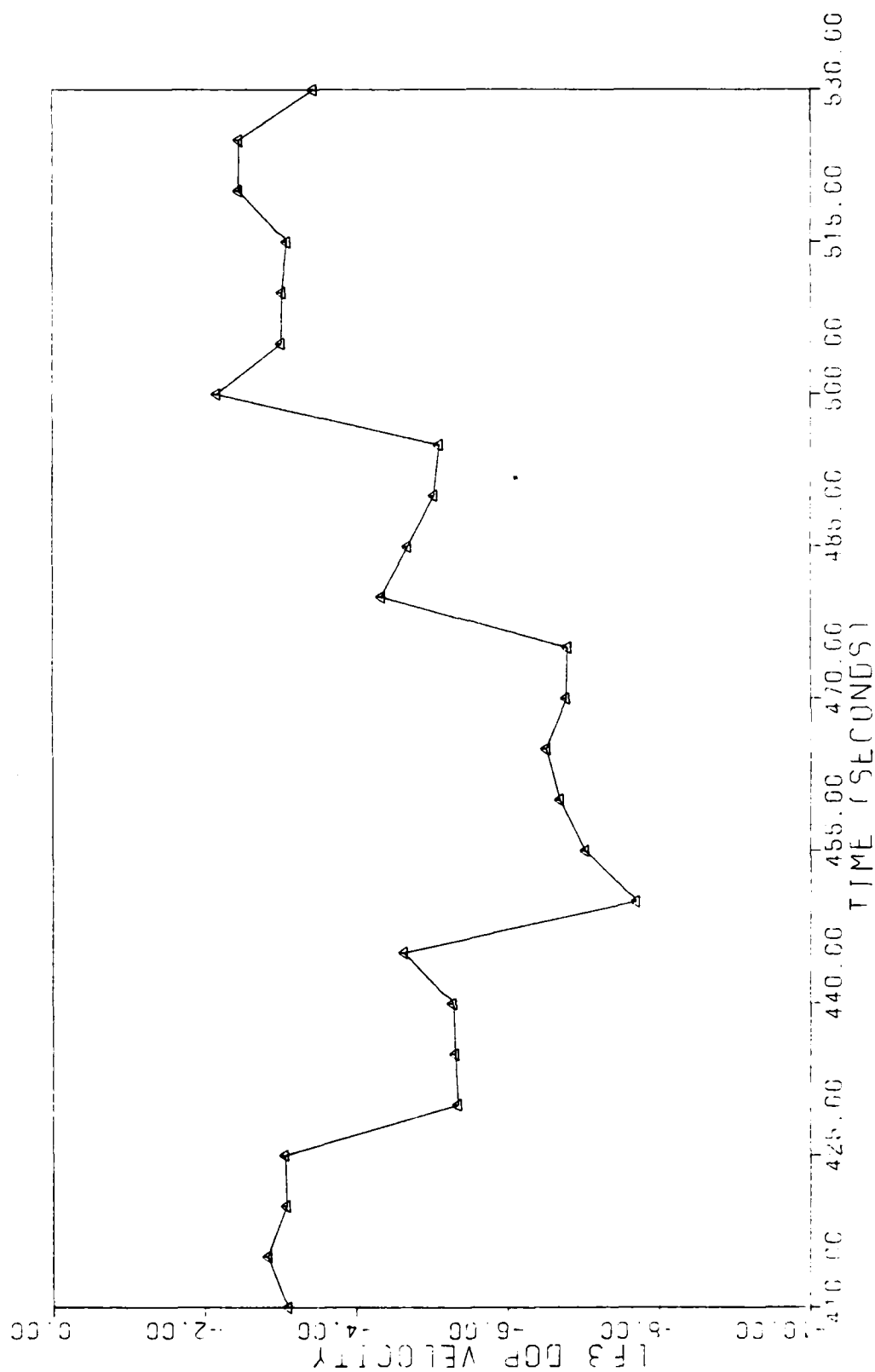


Fig. A.61. Soft Doppler Failure--Doppler Velocity Measurement #3--Benign Flight



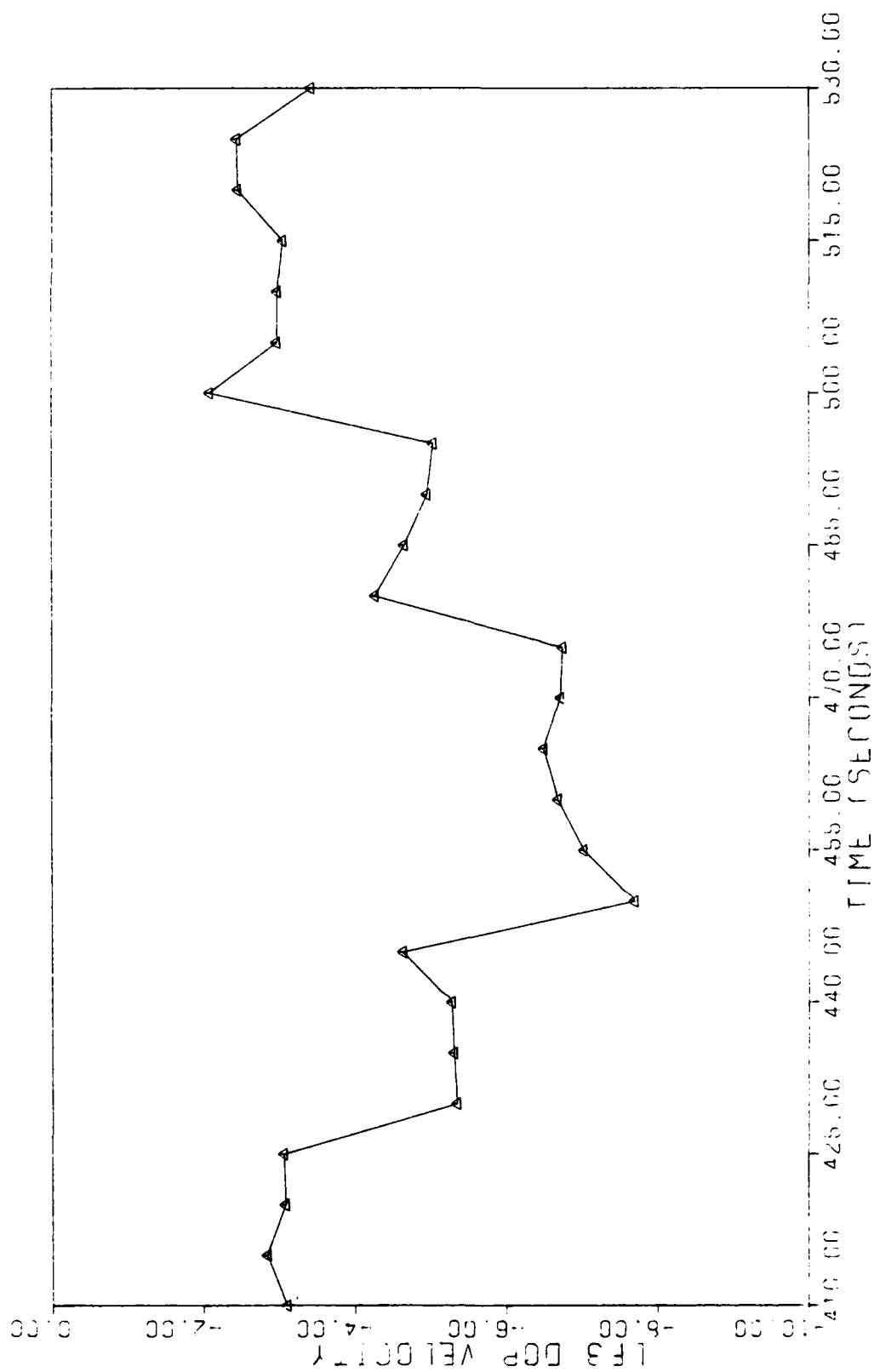


Fig. A.62. Harrier Doppler Failure--Doppler Velocity Measurement #3--Design Flight

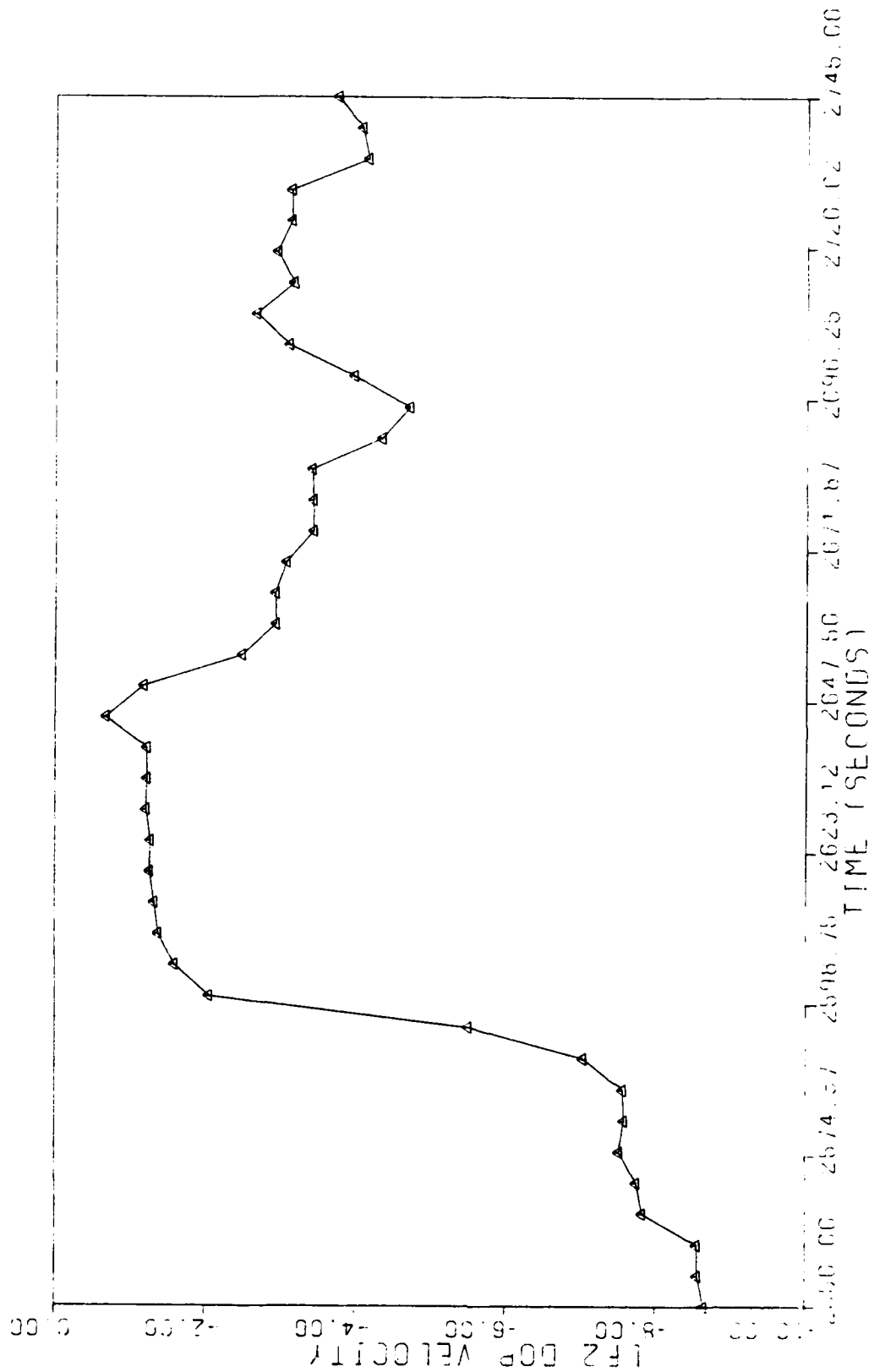


Fig. A.63. Hard Doppler Failure--Doppler Velocity Measurement #2--Dynamic Flight

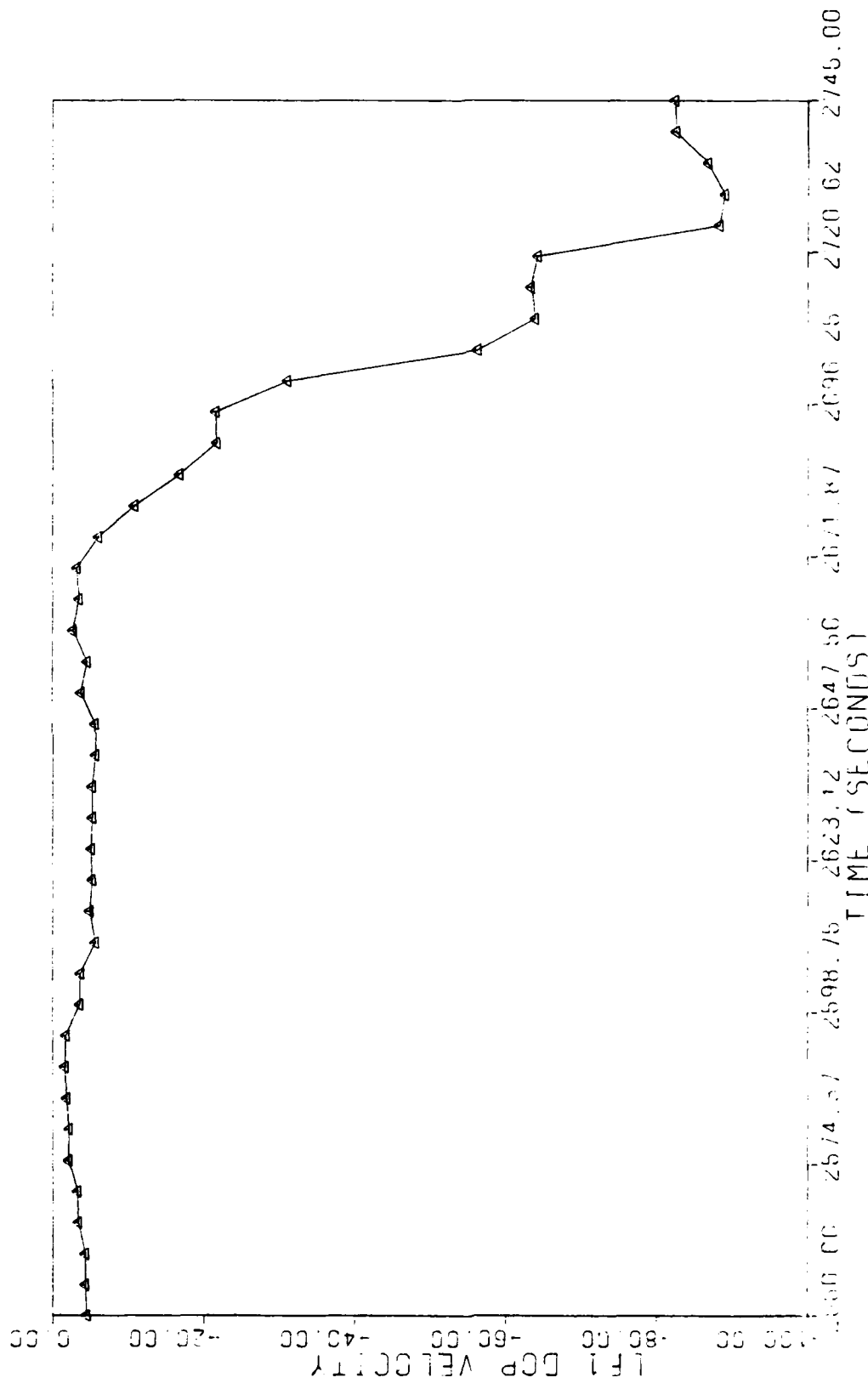


Fig. A.64. Soft Doppler Failure--Doppler Velocity Measurement #1--Dynamic Flight

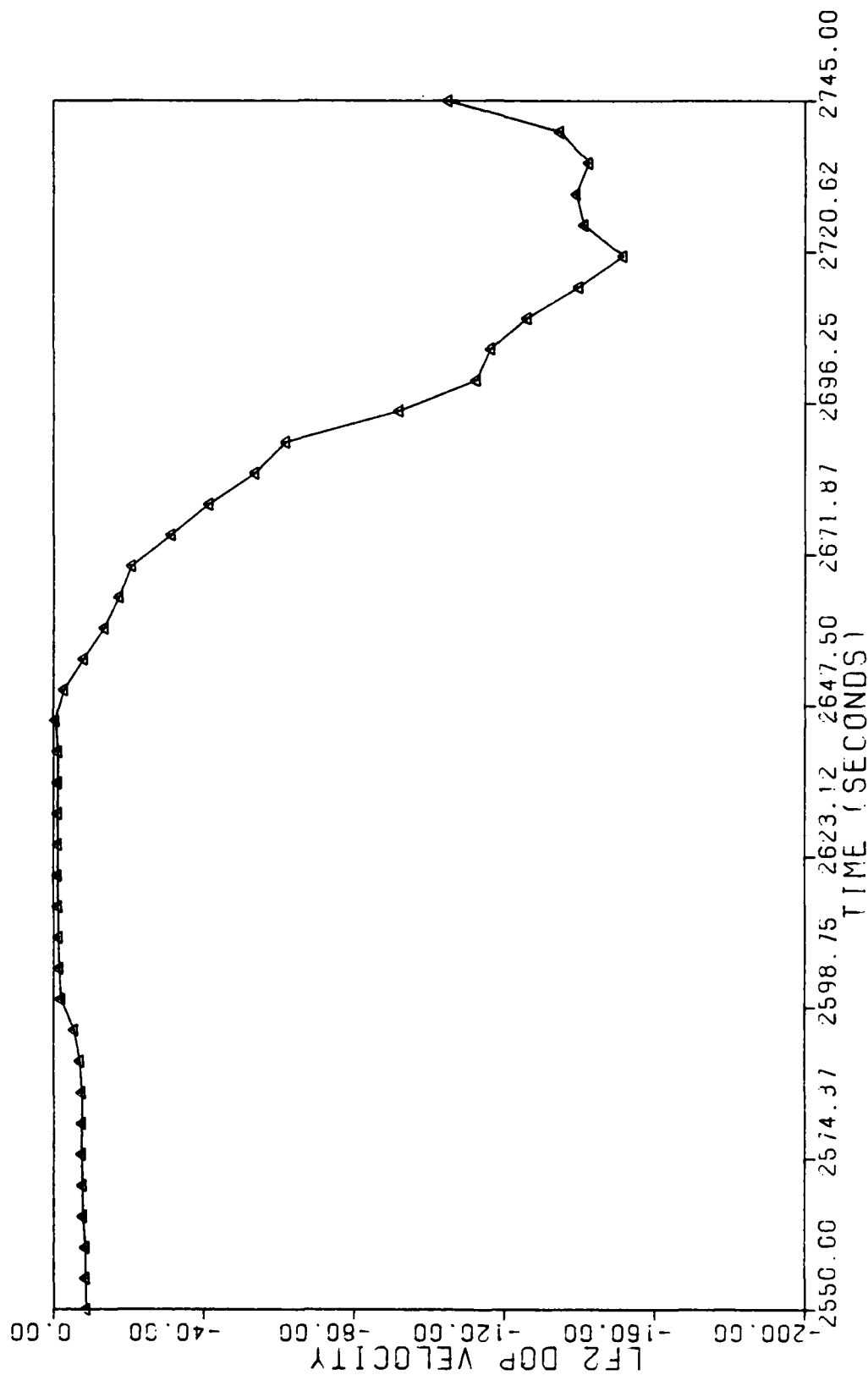


Fig. A.65. Soft Doppler Failure--Doppler Velocity Measurement #2--Dynamic Flight

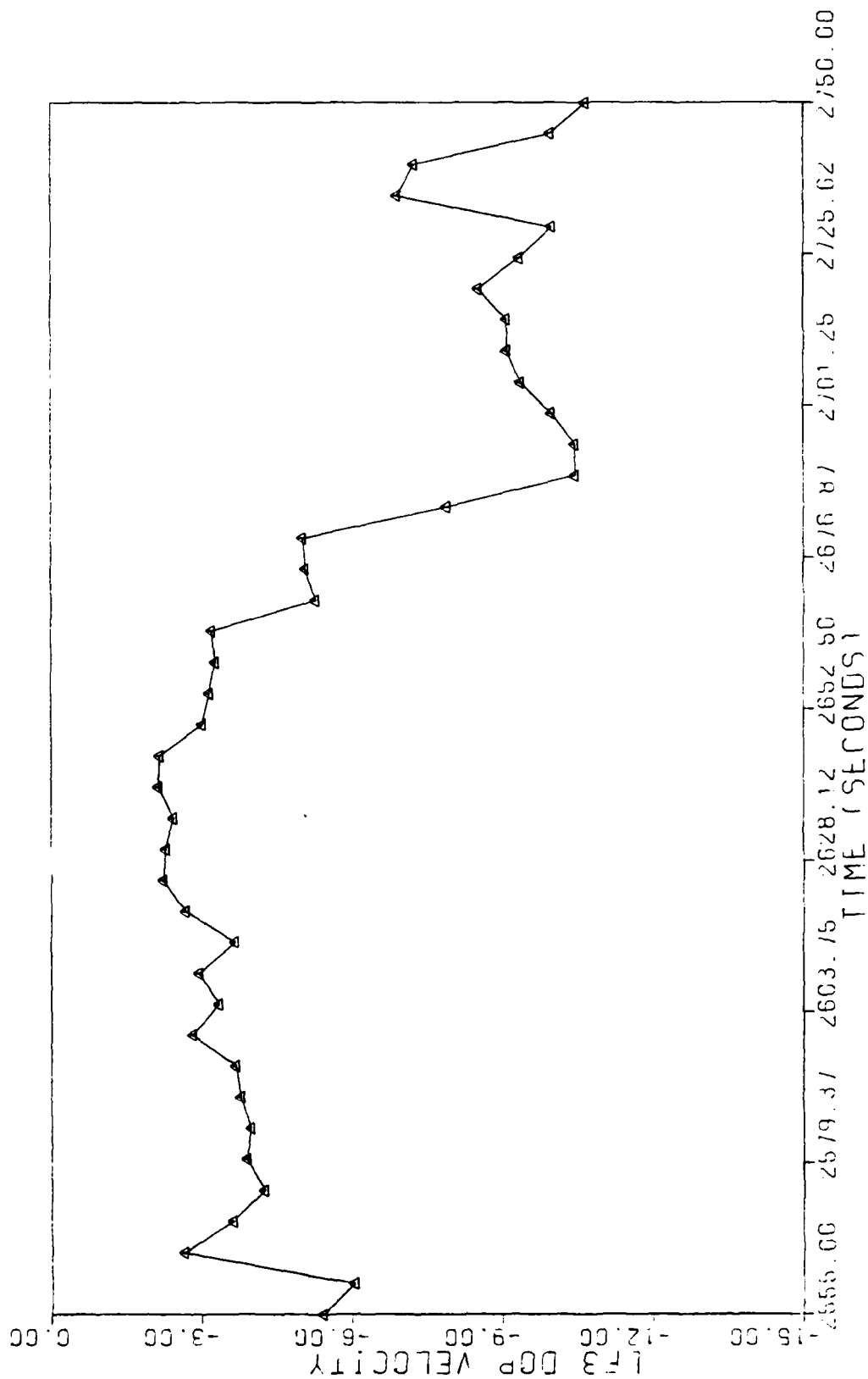


Fig. A.66. Soft Doppler Failure--Doppler Velocity Measurement #3--Dynamic Flight

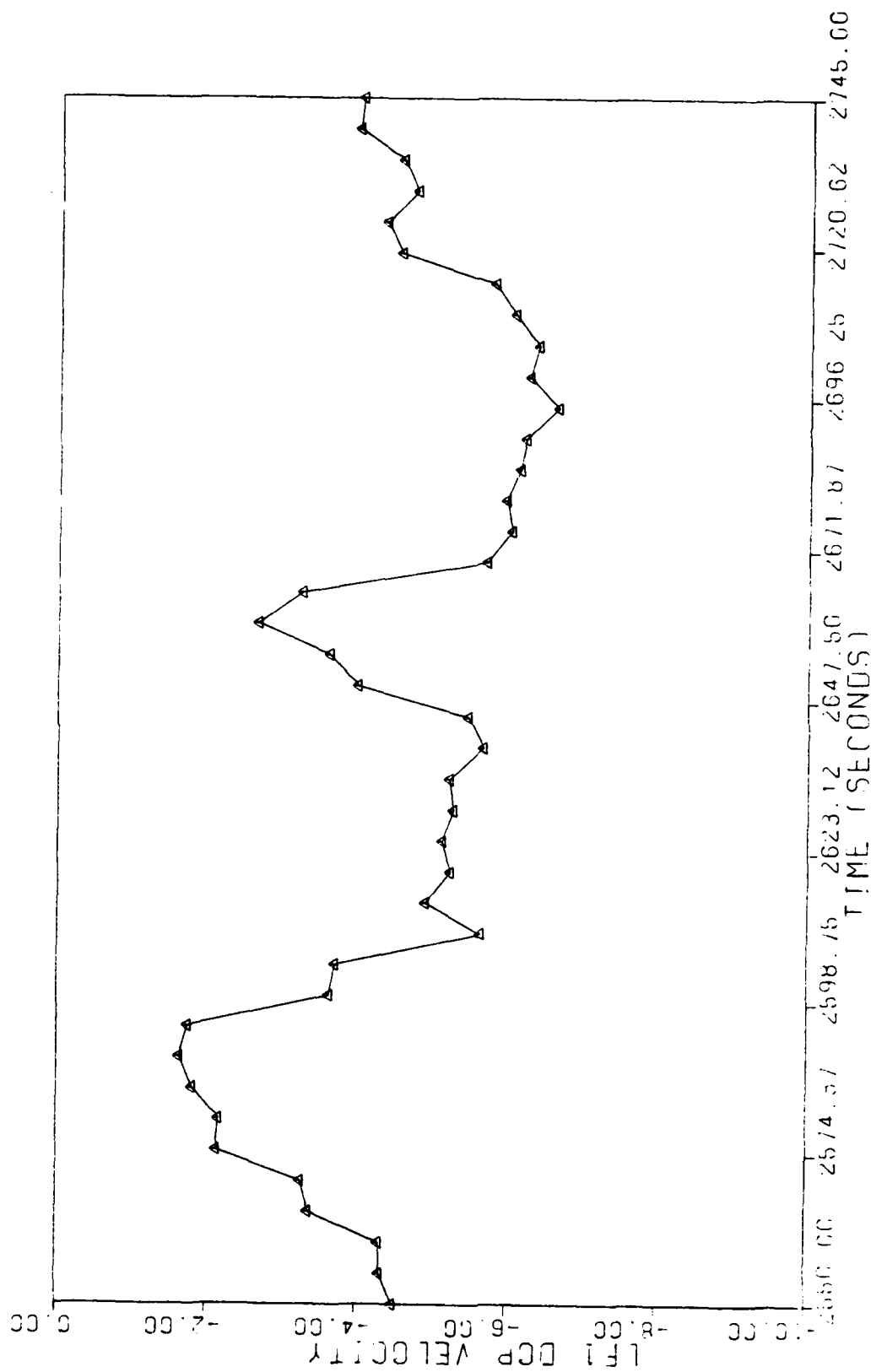


Fig. A.67. Hard Accelerometer 2 Failure--Doppler Velocity Measurement #1--Dynamic Flight

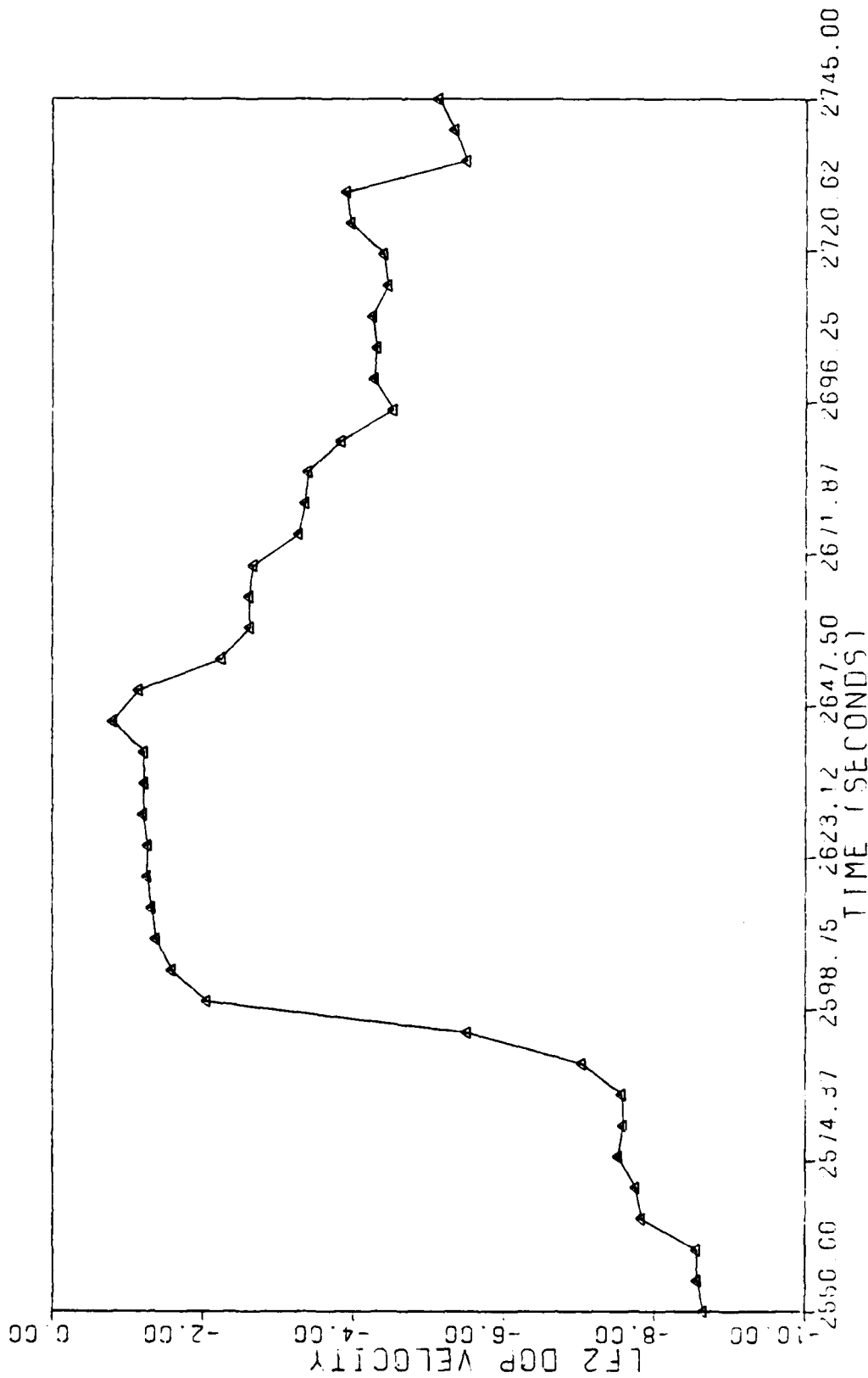


Fig. A.68. Hard Accelerometer 2 Failure--Doppler Velocity Measurement #2--Dynamic Flight

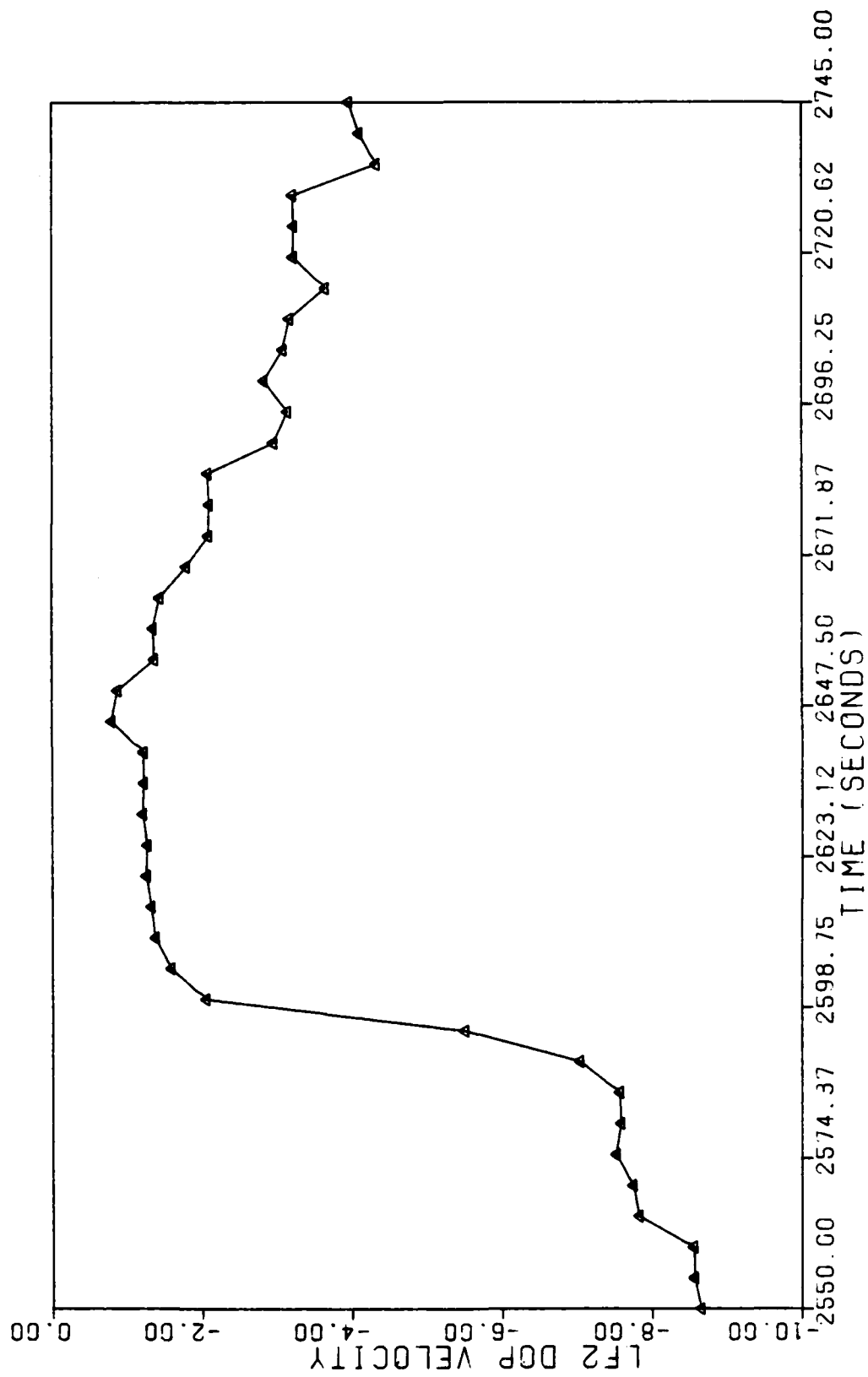


Fig. A.69. Hard Accelerometer 3 Failure--Doppler Velocity Measurement #2--Dynamic Flight



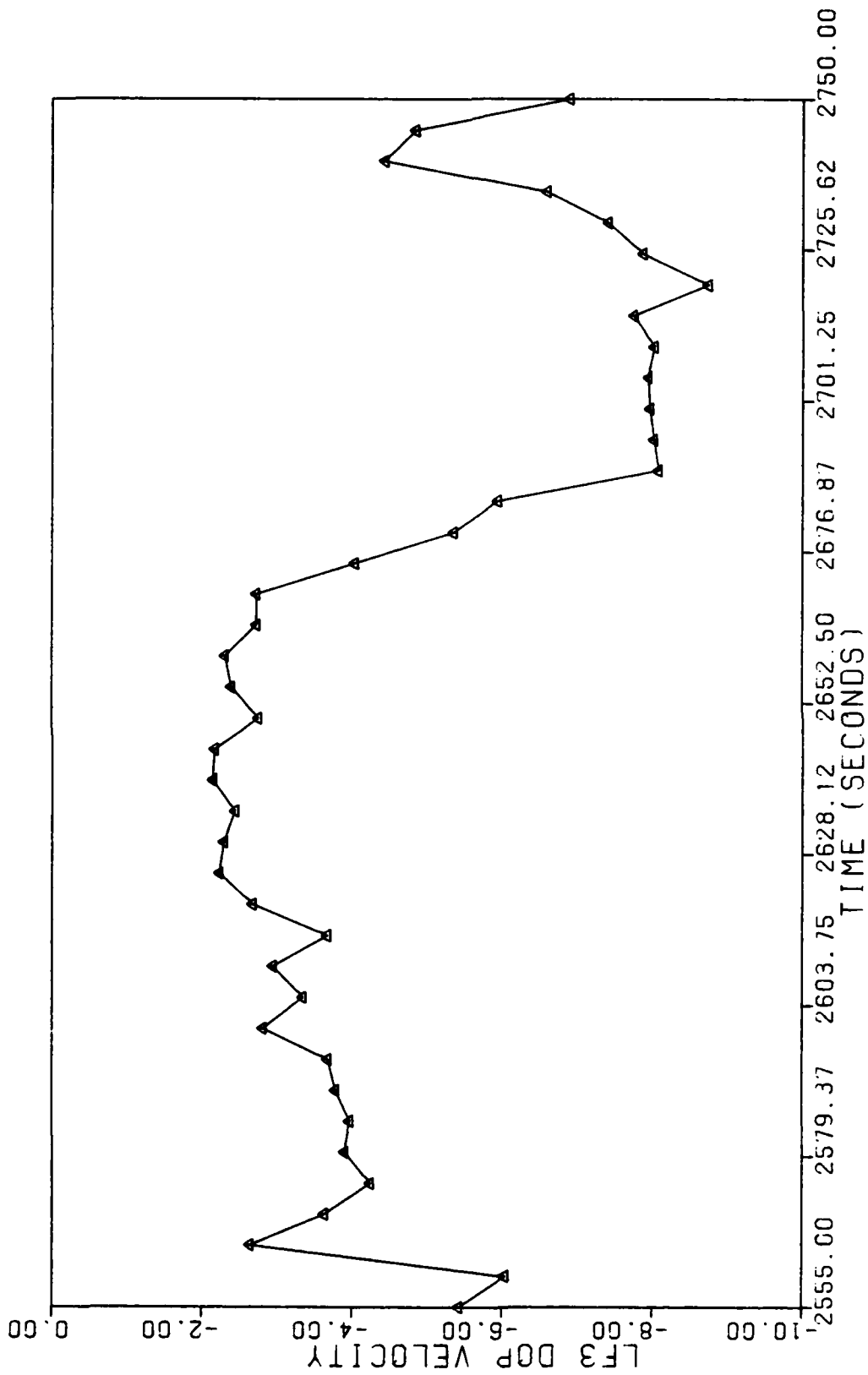


Fig. A.70. Hard Accelerometer 3 Failure--Doppler Velocity Measurement #3--Dynamic Flight

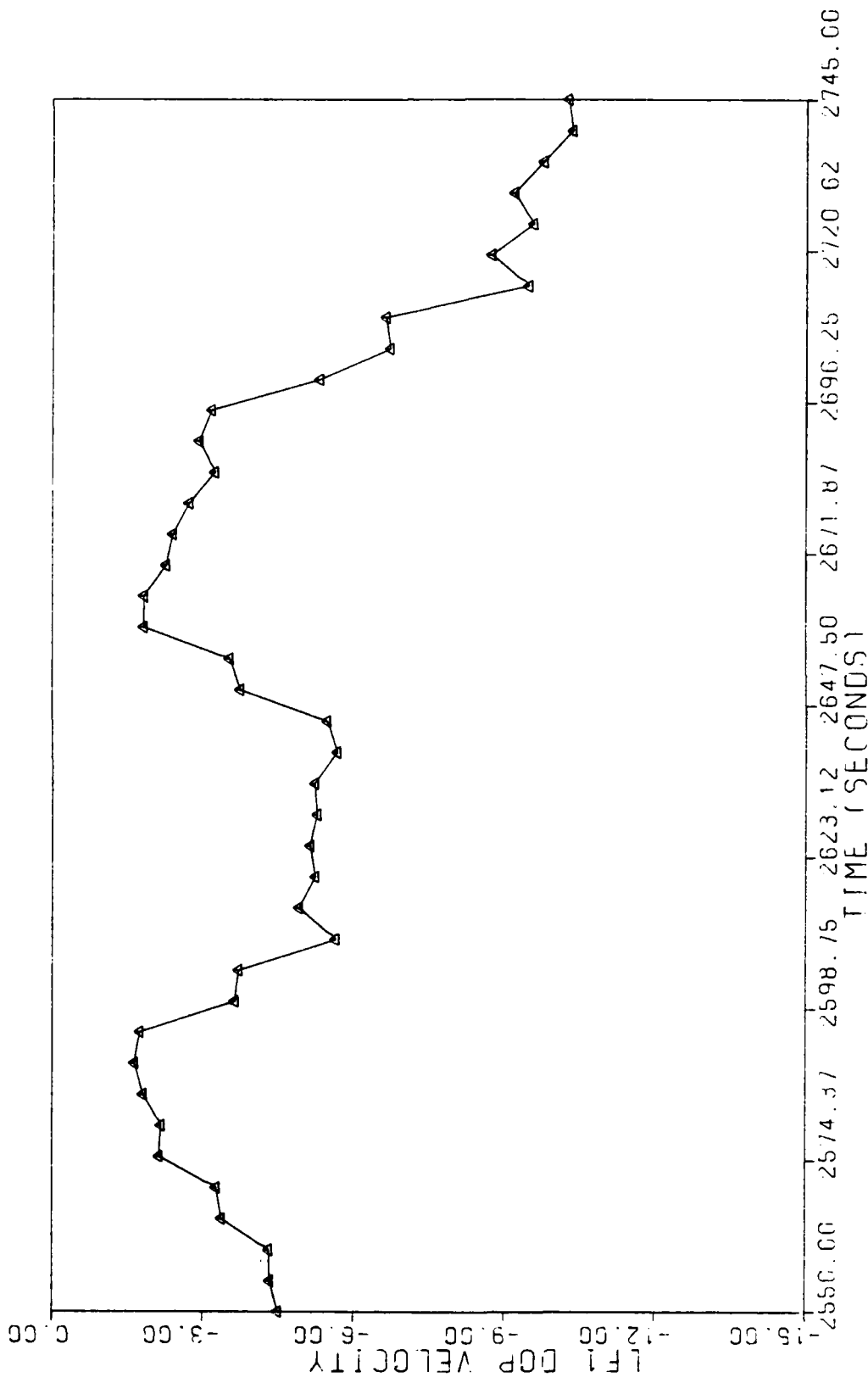


Fig. A.71. Hard Accelerometer 1 Failure--Doppler Velocity Measurement #1--Dynamic Flight

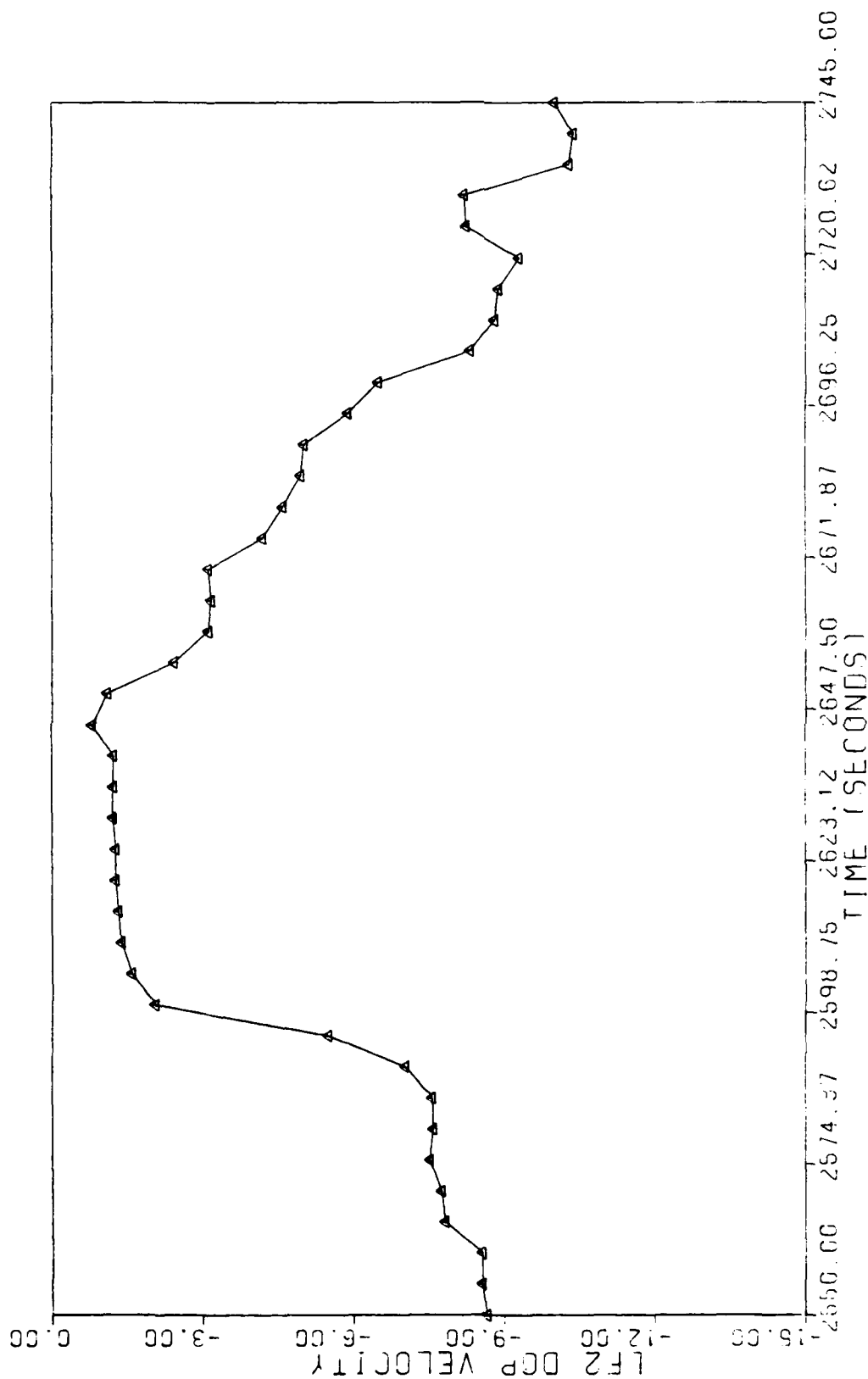


Fig. A.72. Hard Accelerometer 1 Failure--Doppler Velocity Measurement #2--Dynamic Flight

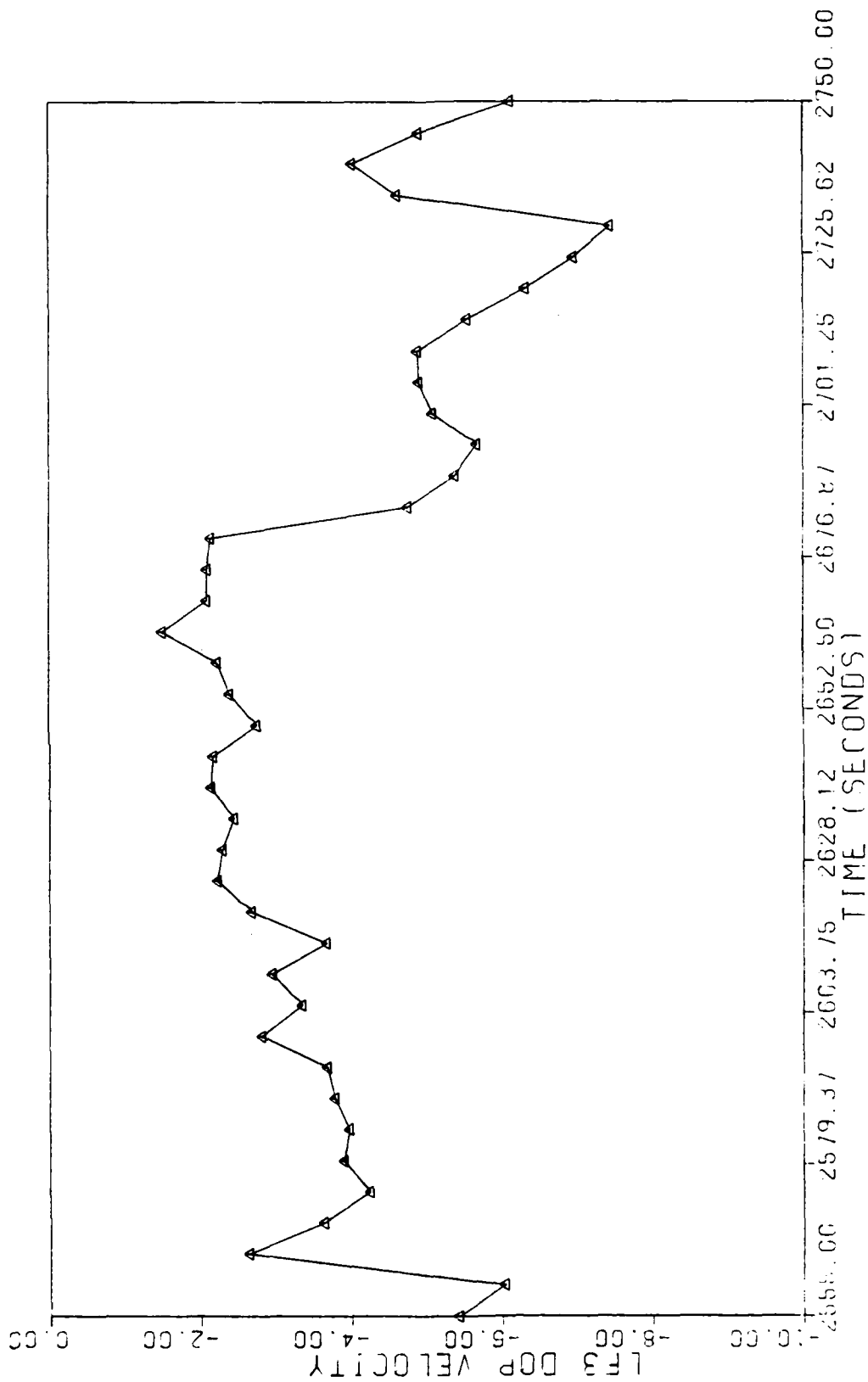


Fig. A.73. Hard Accelerometer 1 Failure--Doppler Velocity Measurement #3--Dynamic Flight

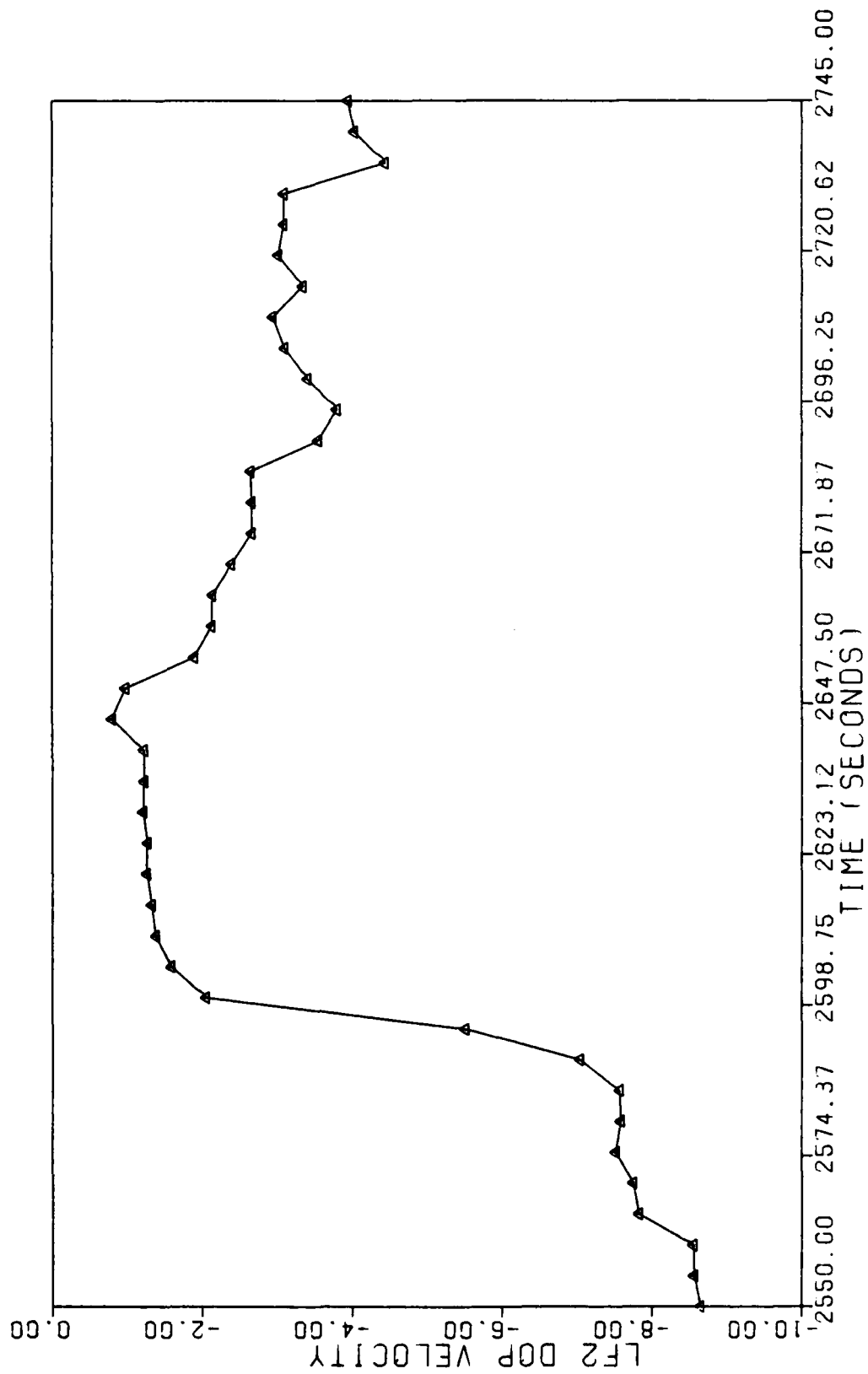


Fig. A.74. Soft Accelerometer 2 Failure--Doppler Velocity Measurement #2--Dynamic Flight

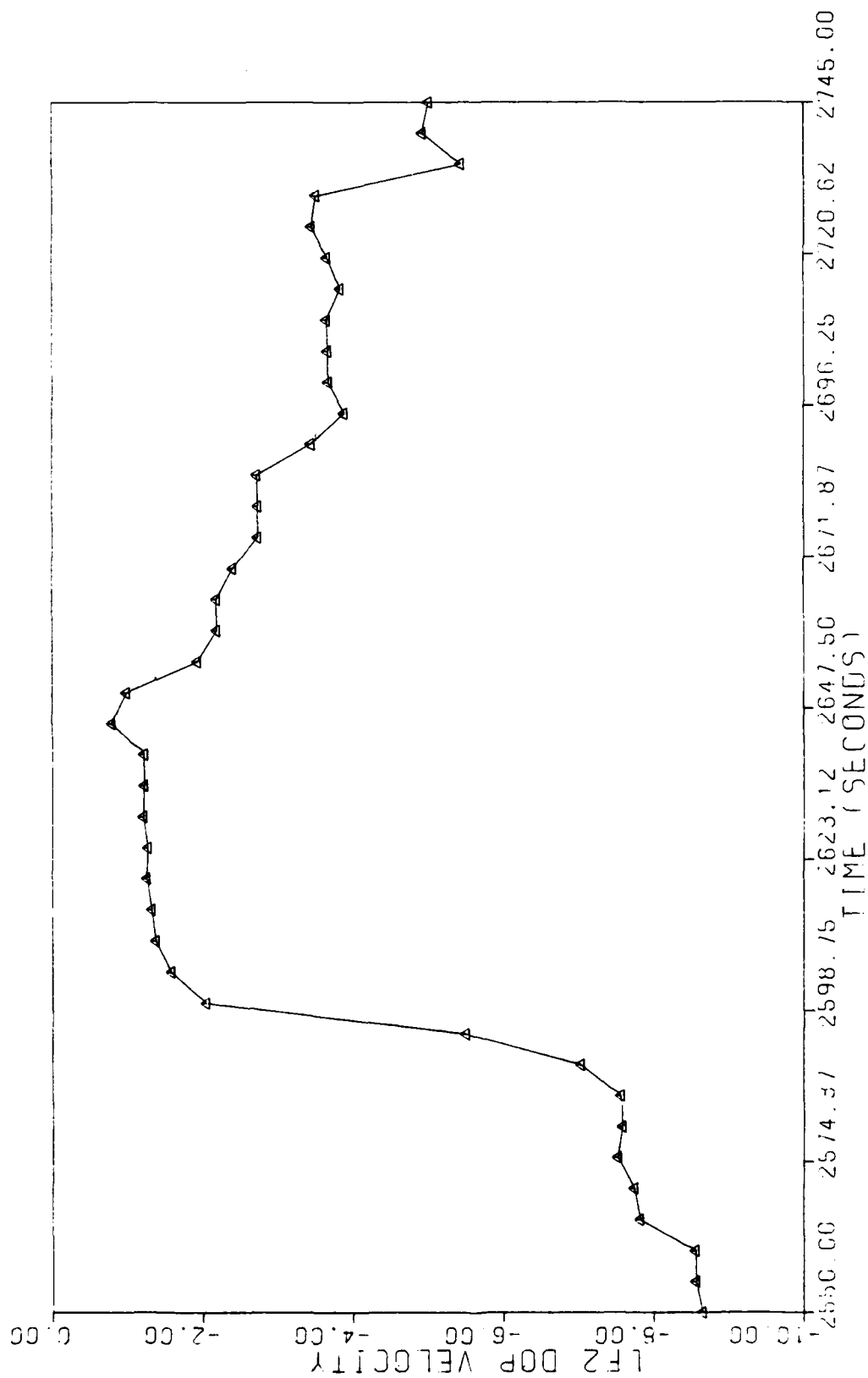


Fig. A.75. Soft Accelerometer 1 Failure--Doppler Velocity Measurement #2--Dynamic Flight

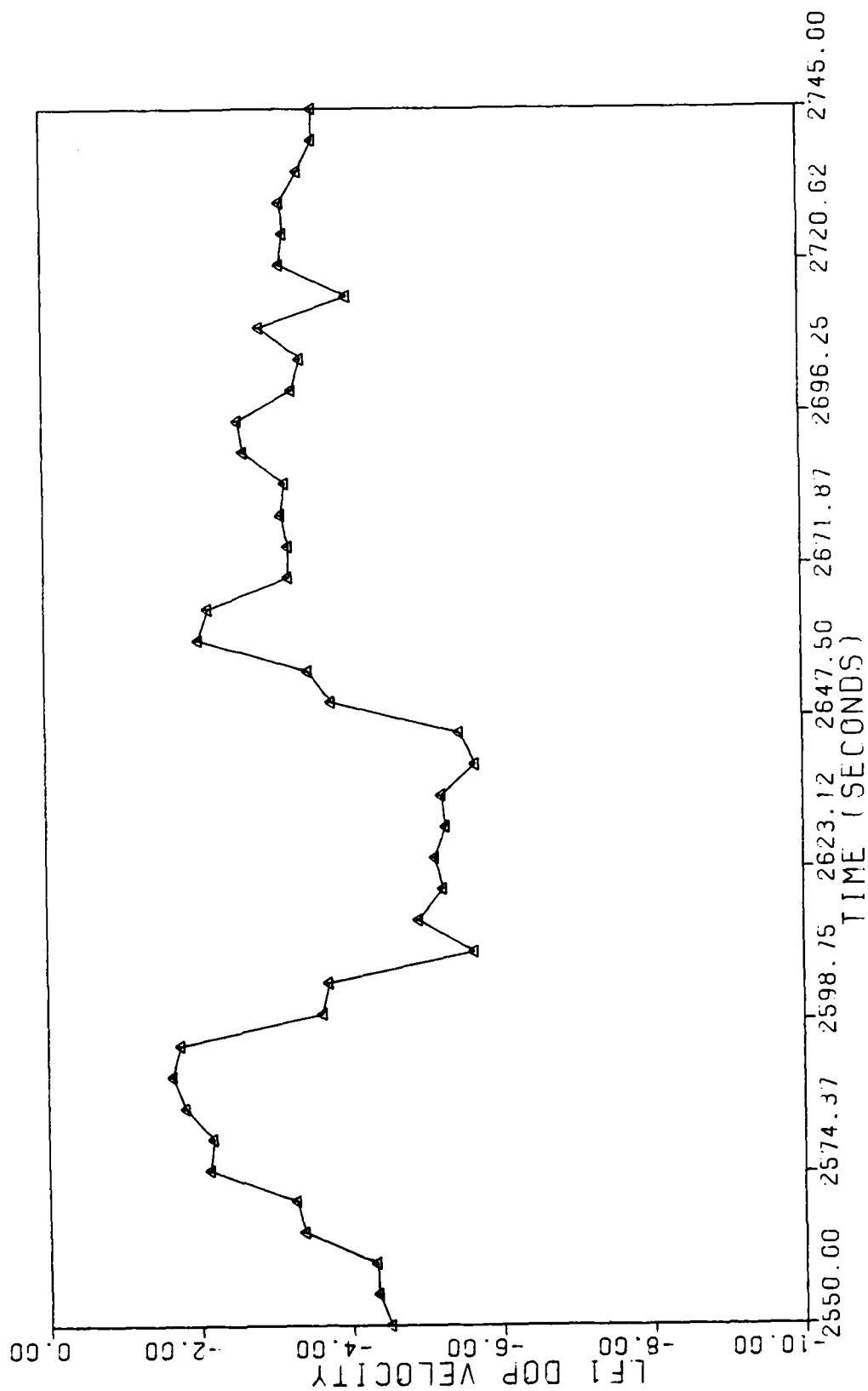


Fig. A.76. No Failure Condition--Doppler Velocity Measurement #1--Dynamic Flight

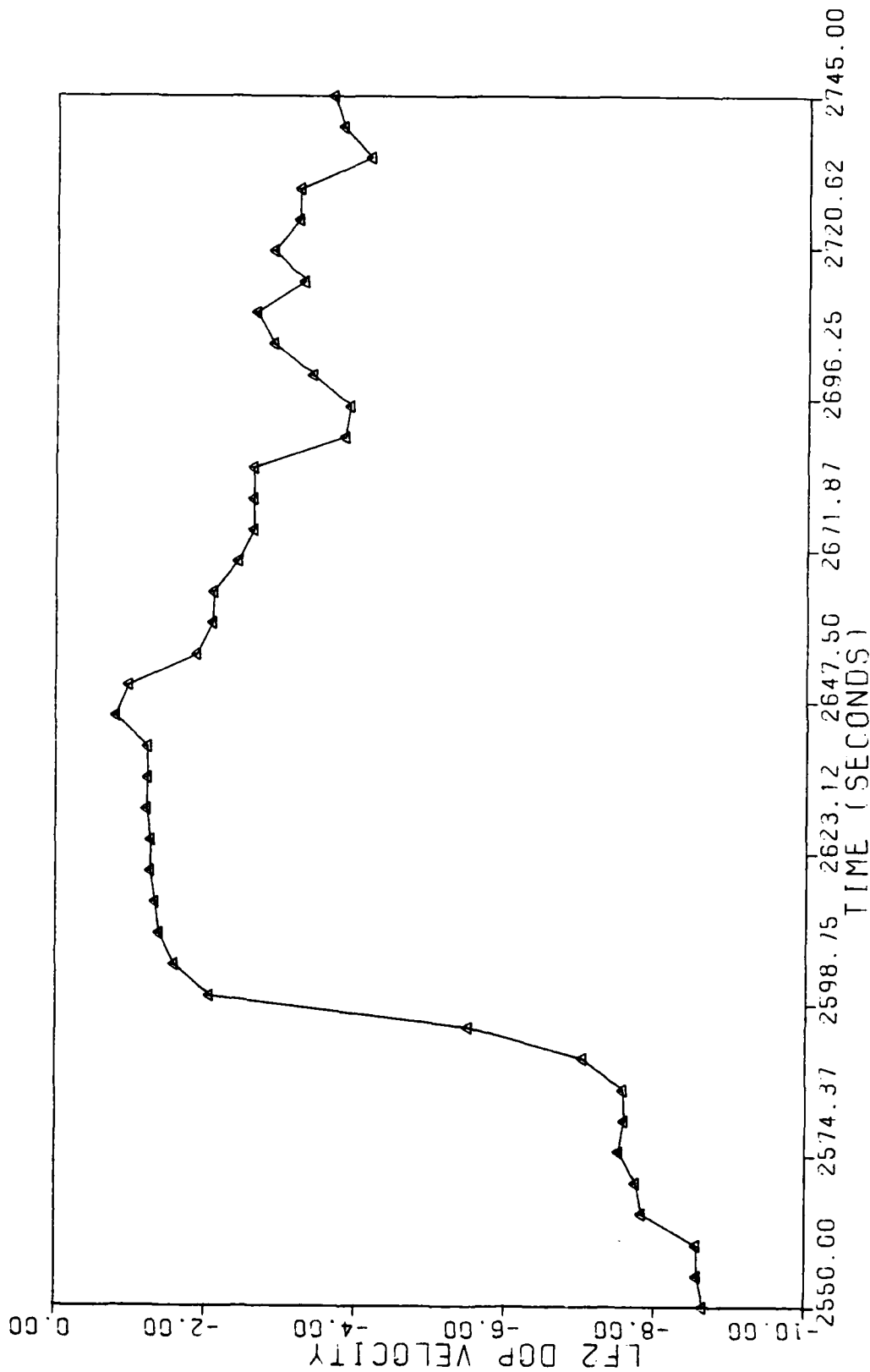


Fig. A.77. No Failure Condition--Doppler Velocity Measurement #2--Dynamic Flight



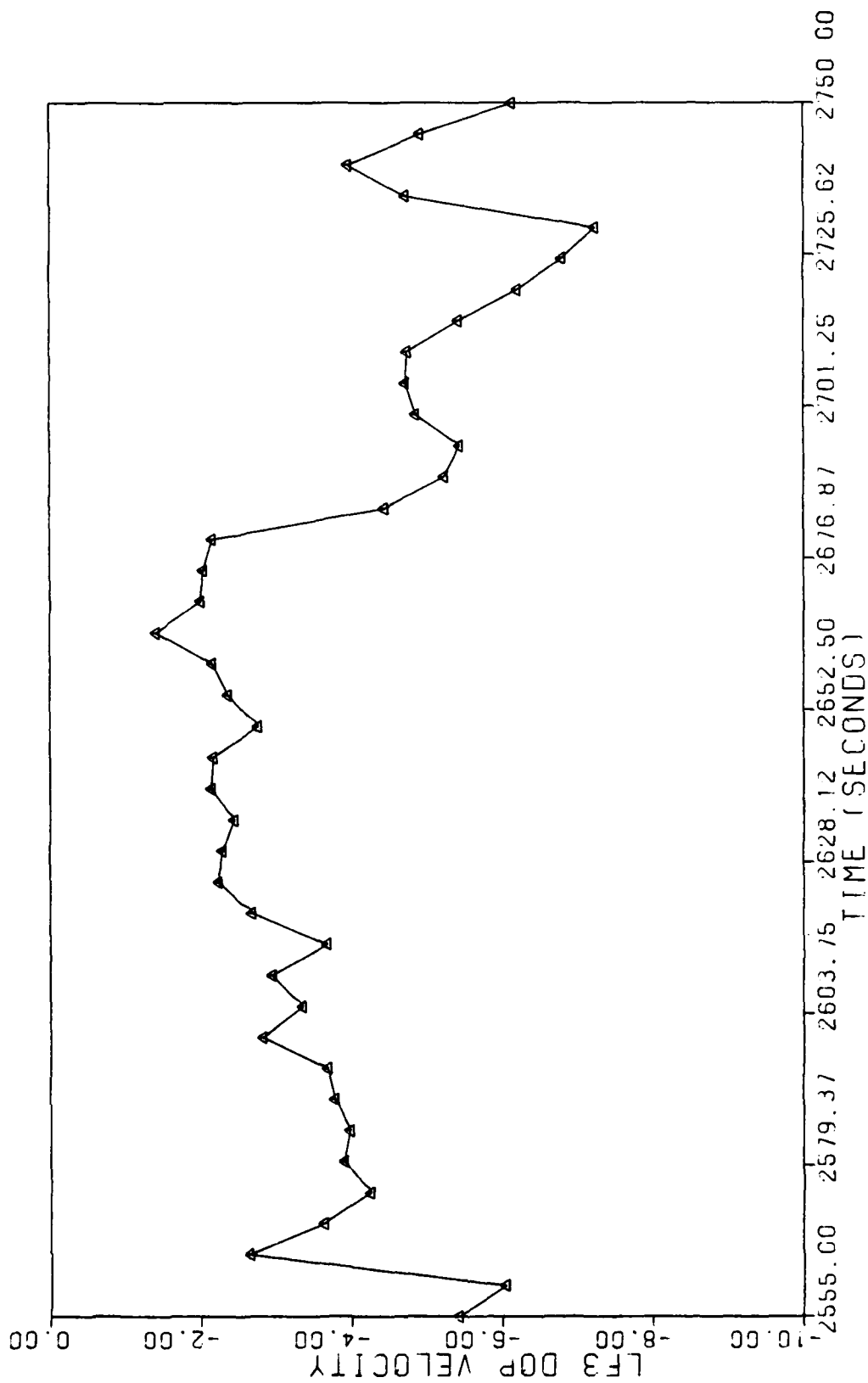


Fig. A.78. No Failure Condition--Doppler Velocity Measurement #3--Dynamic Flight

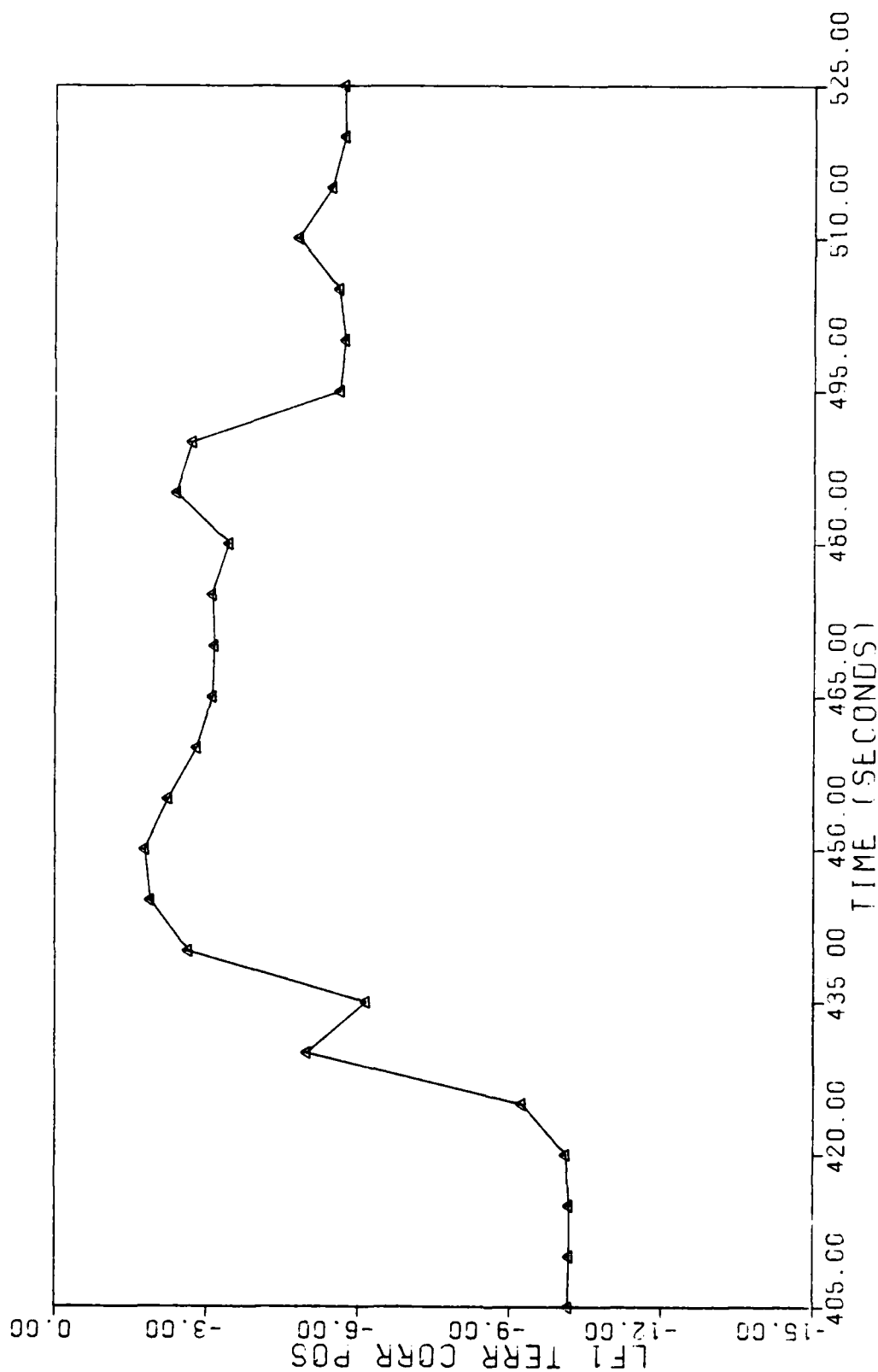


Fig. A.79. Soft Accelerometer 1 Failure--Terrain Correlator Position Measurement #1--Benign Flight

A-80

Copy available to DTIC does not  
permit fully legible reproduction

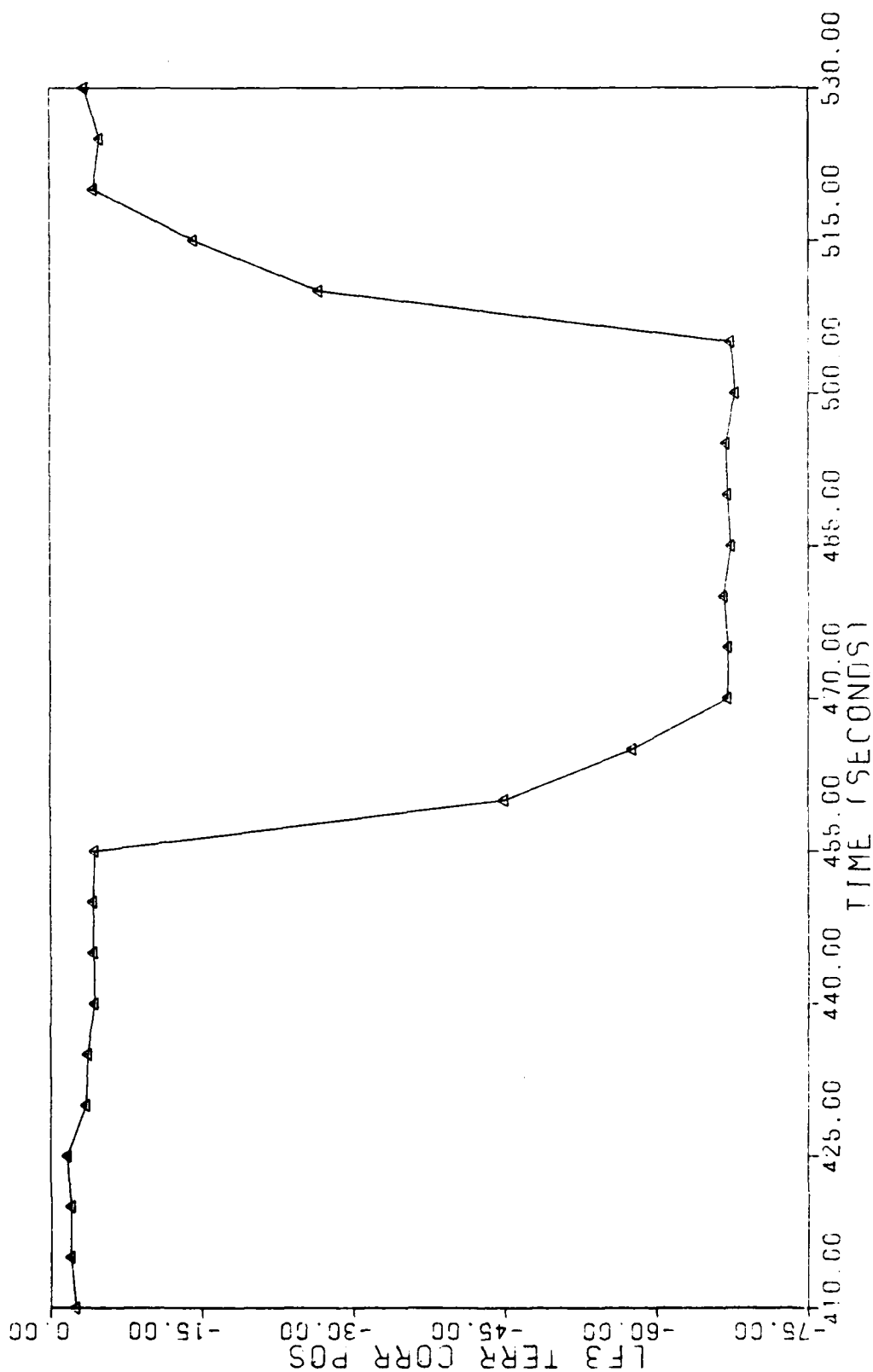


Fig. A.80. Hard Radar Altimeter Failure--Terrain Correlator Measurement #3--Benign Flight

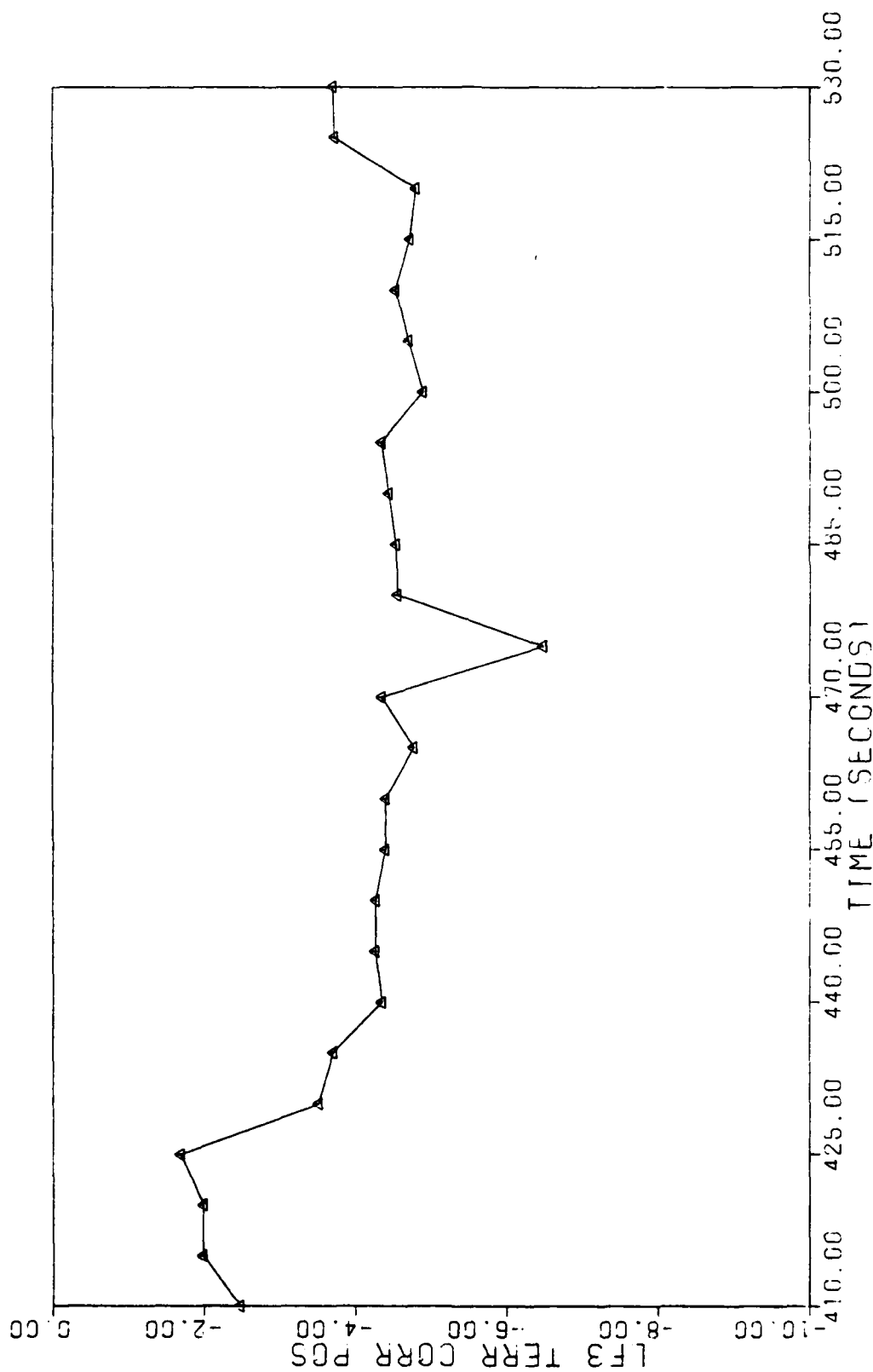


FIG. A.81. Soft Radar Altimeter Failure--Terrain Correlator Measurement #3--Benign Flight

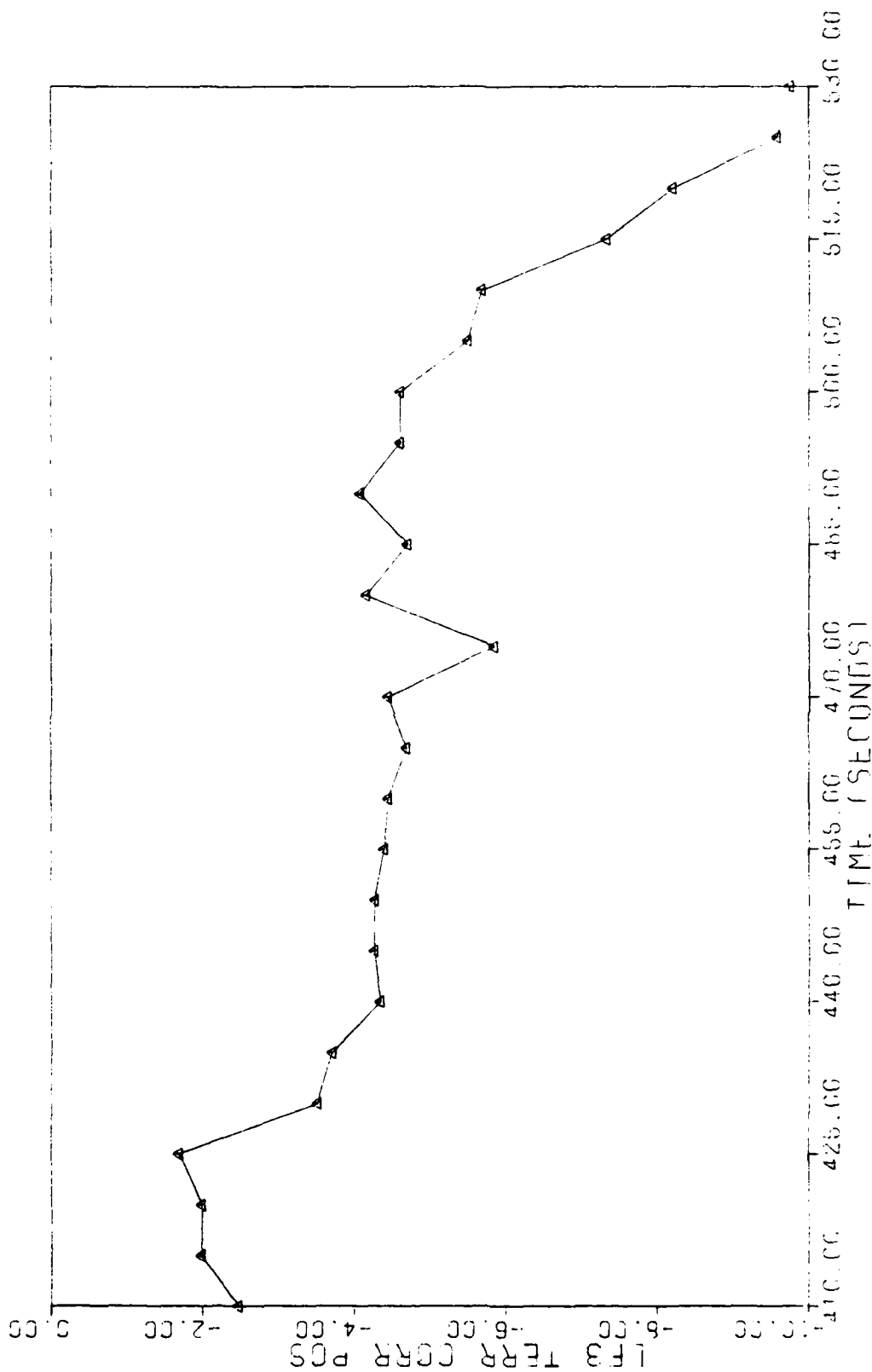


Fig. A.82. Hard Accelerometer 3 Failure--Terrain Correlator Measurement #3--Benign Flight

A-83

Copy available to DTIC does not permit full length reproduction

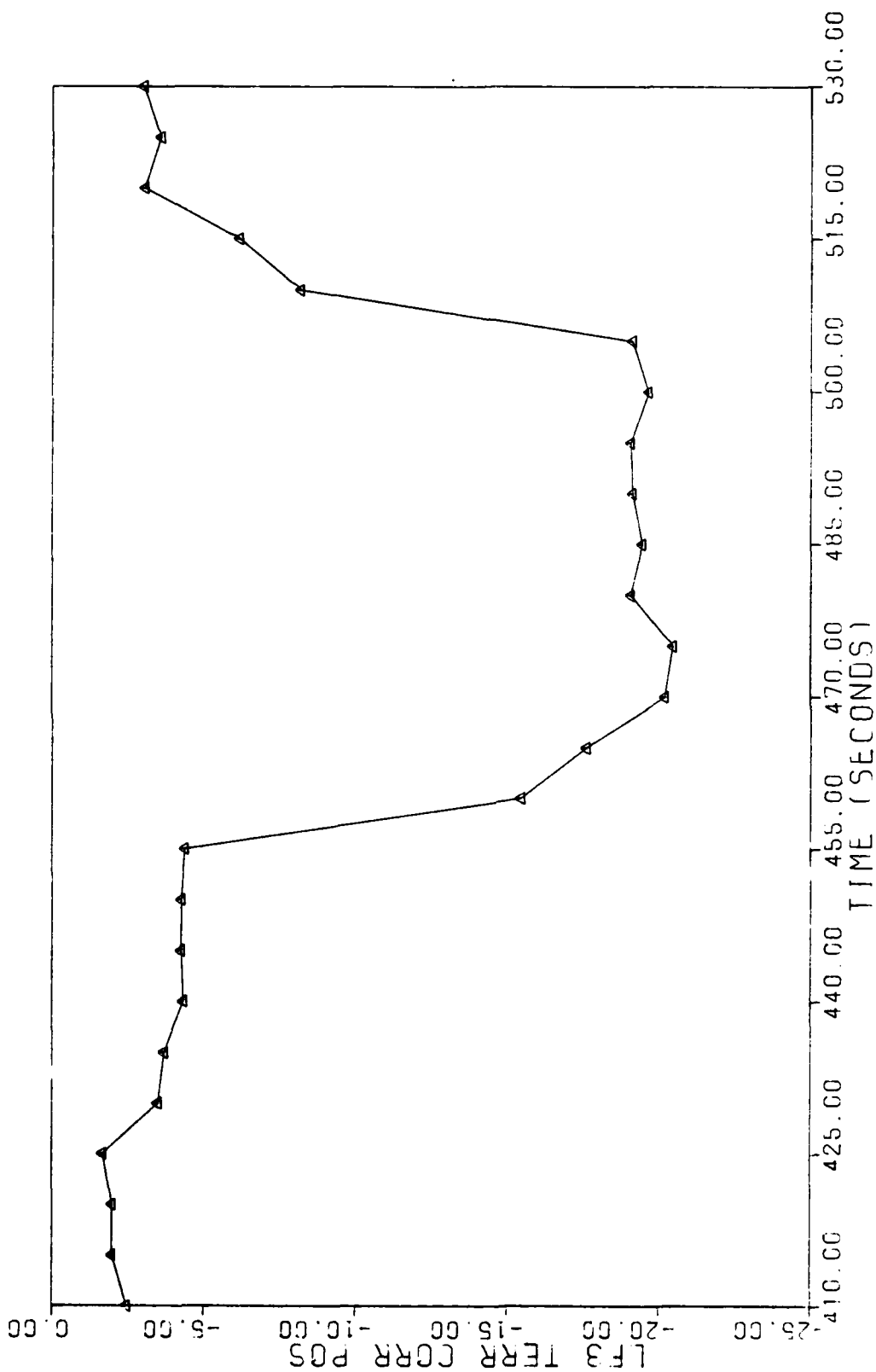


Fig. A.83. Hard Baro-altimeter Failure--Terrain Correlator Measurement #3--Benign Flight

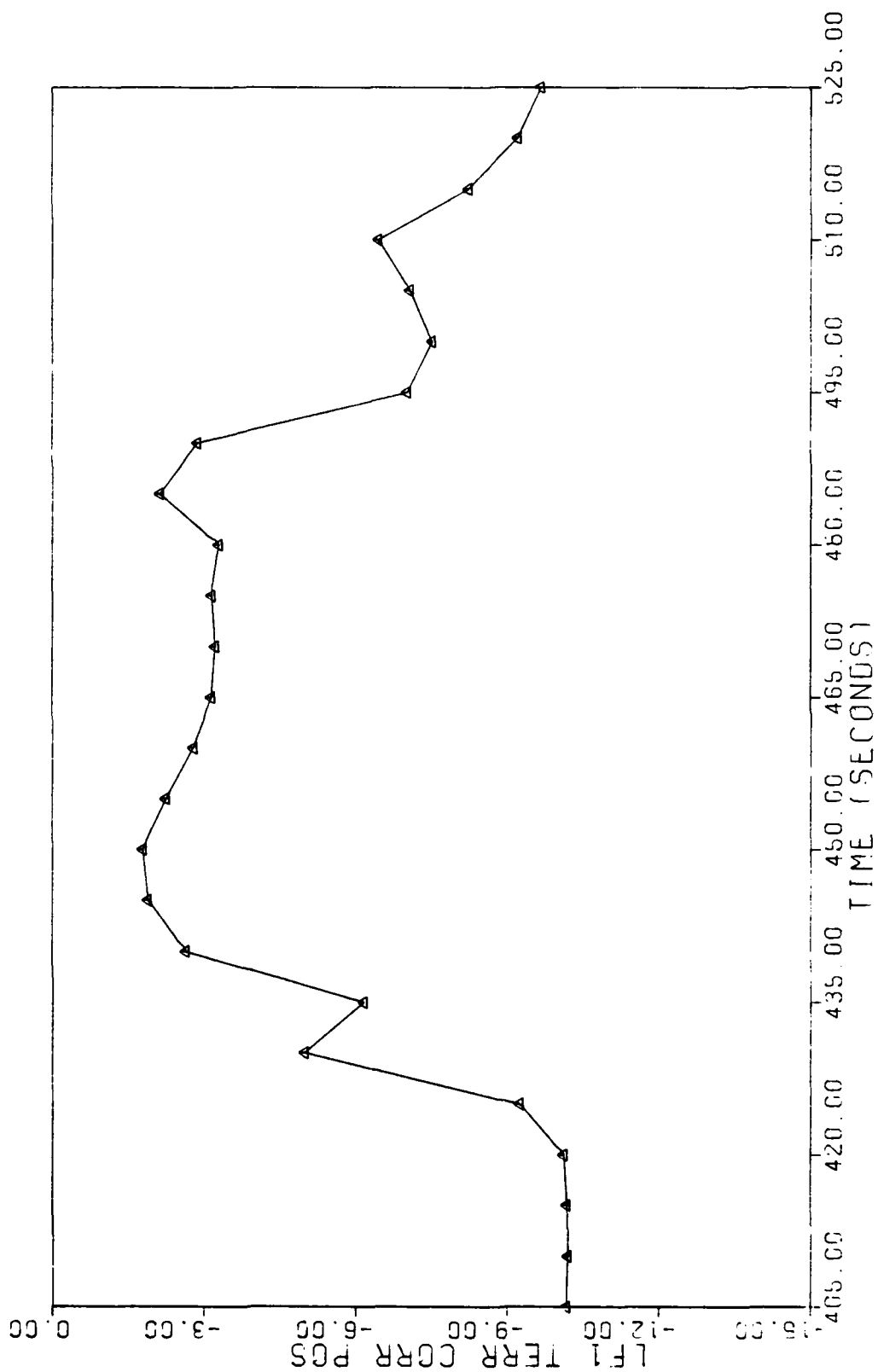


Fig. A.84. Hard Accelerometer 2 Failure--Terrain Correlator Measurement #1--Benign Flight

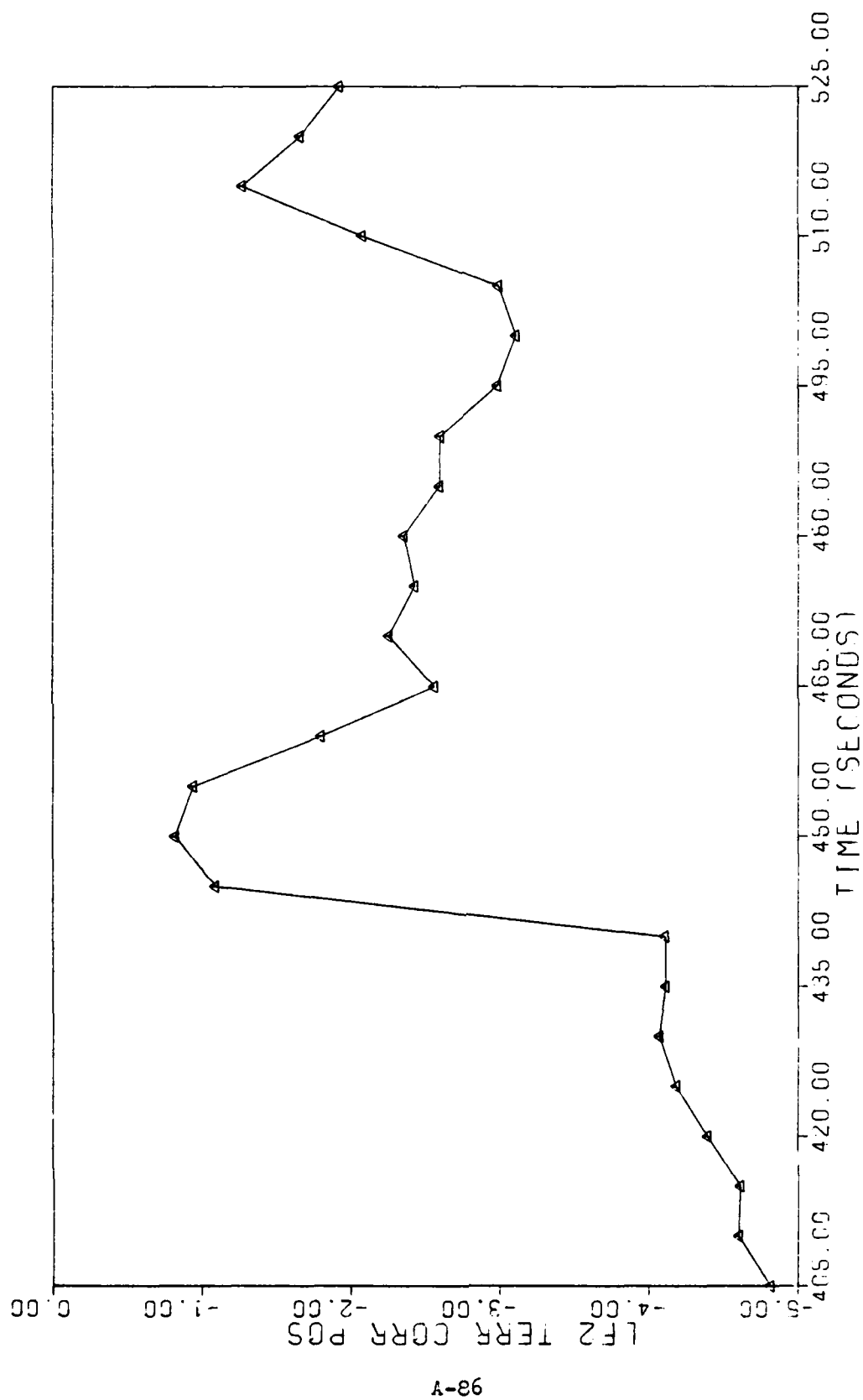


Fig. A.85. Hard Accelerometer 2 Failure--Terrain Correlator Measurement #2--Benign Flight



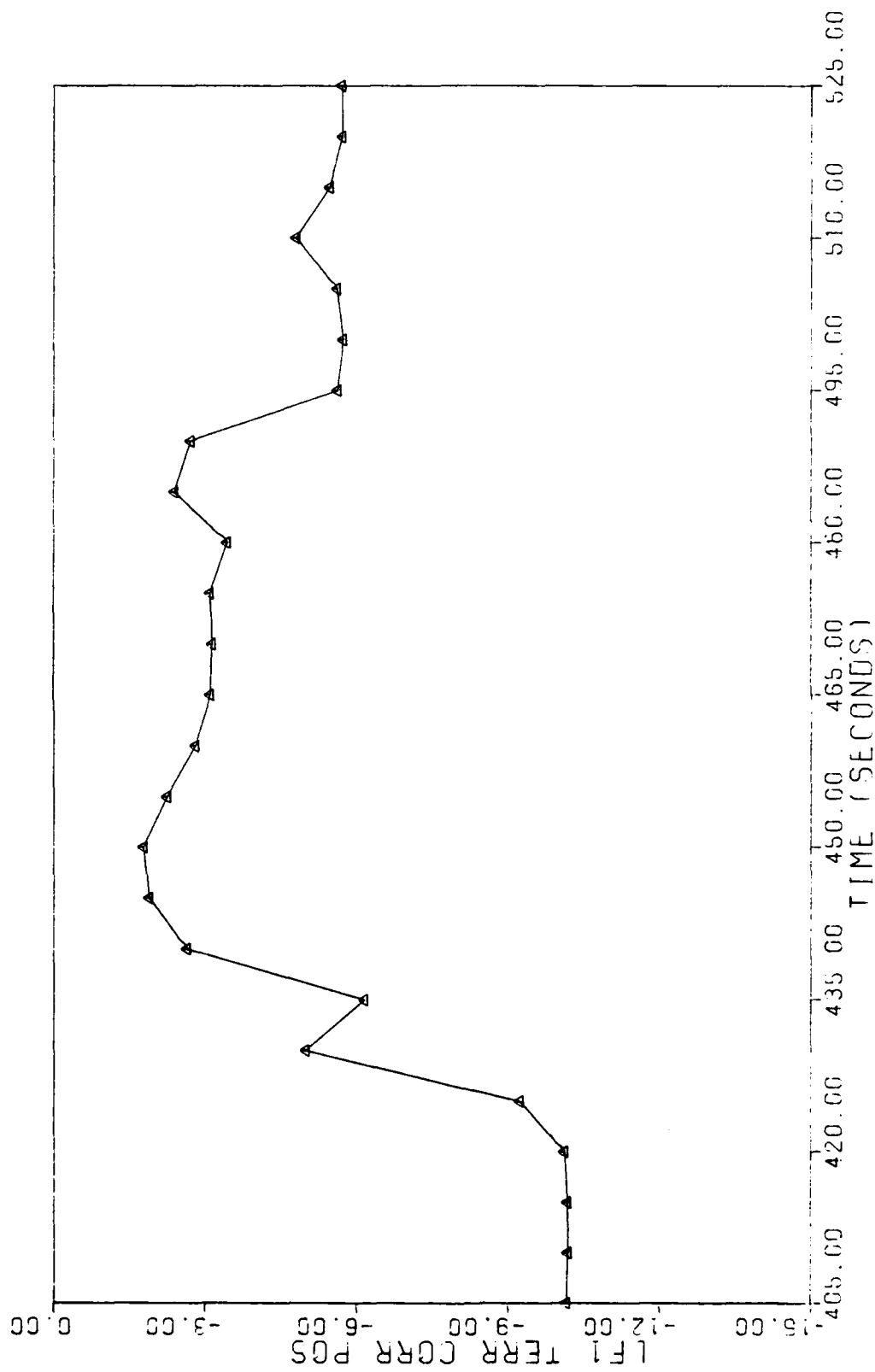


Fig. A.86. Soft Accelerometer 2 Failure--Terrain Correlator Measurement #1--Benign Flight

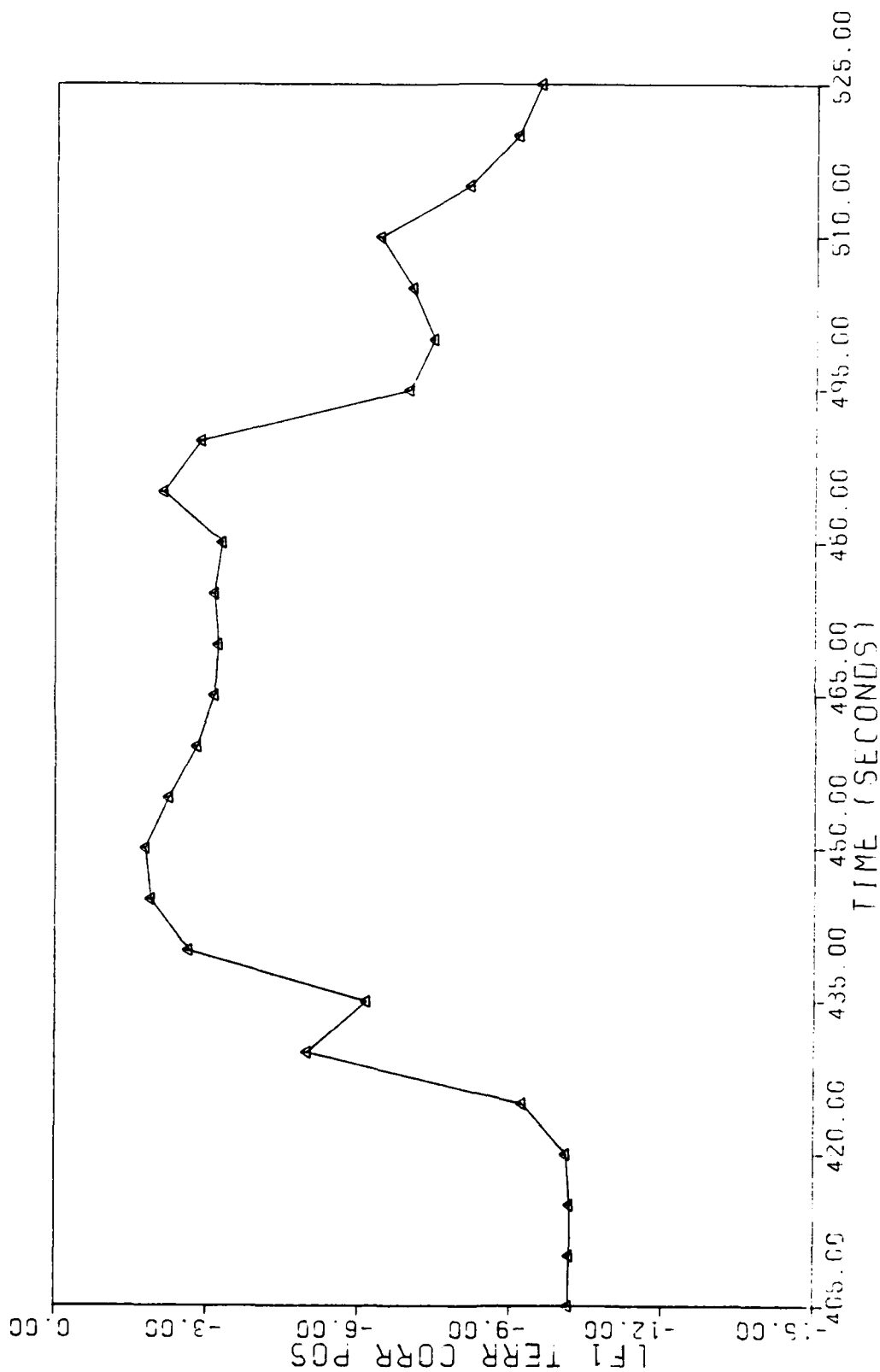


Fig. A.87. Hard Accelerometer 1 Failure--Terrain Correlator Measurement #1--Benign Flight

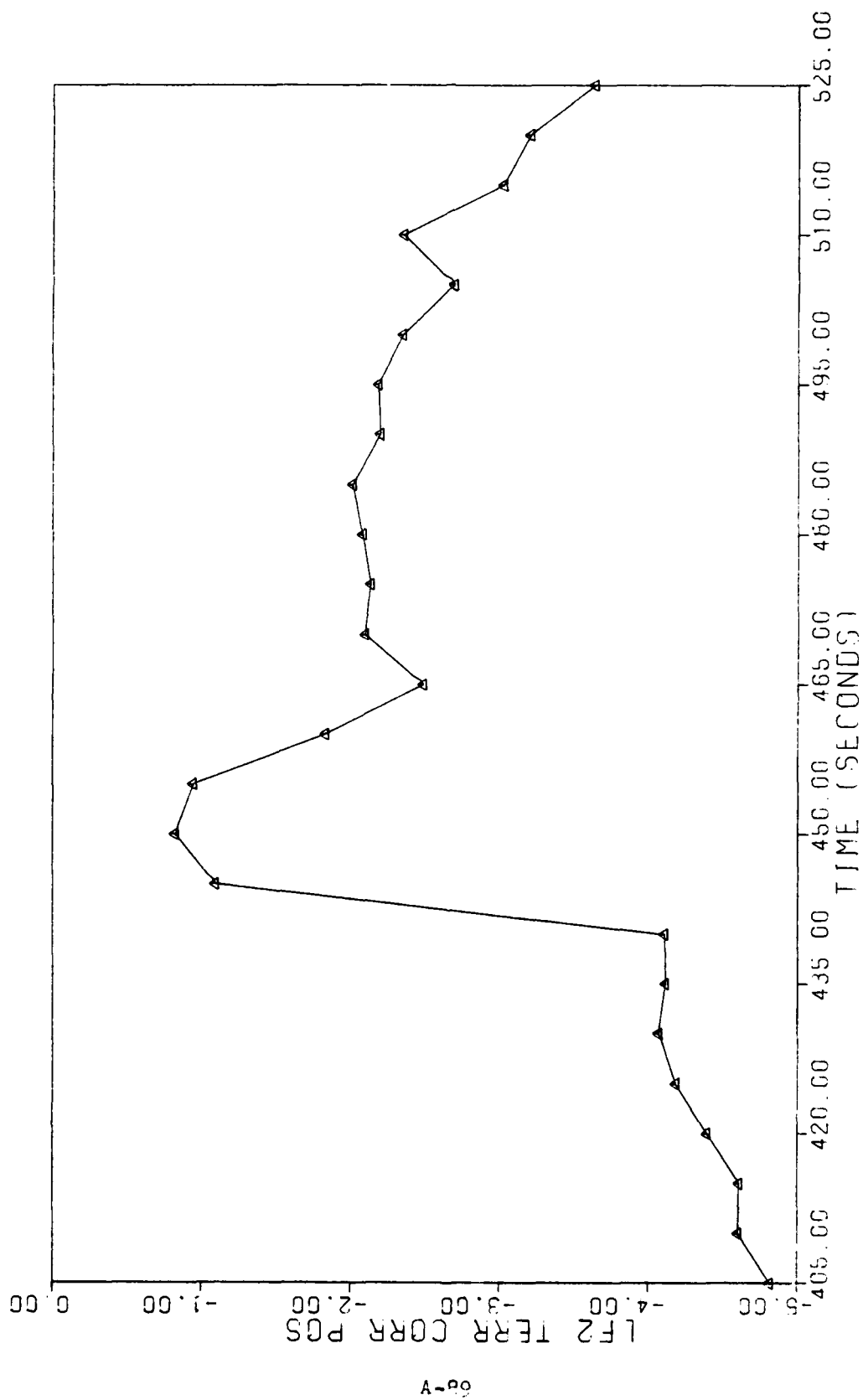


Fig. A.88. Hard Accelerometer 1 Failure--Terrain Correlator Measurement #1--Benign Flight

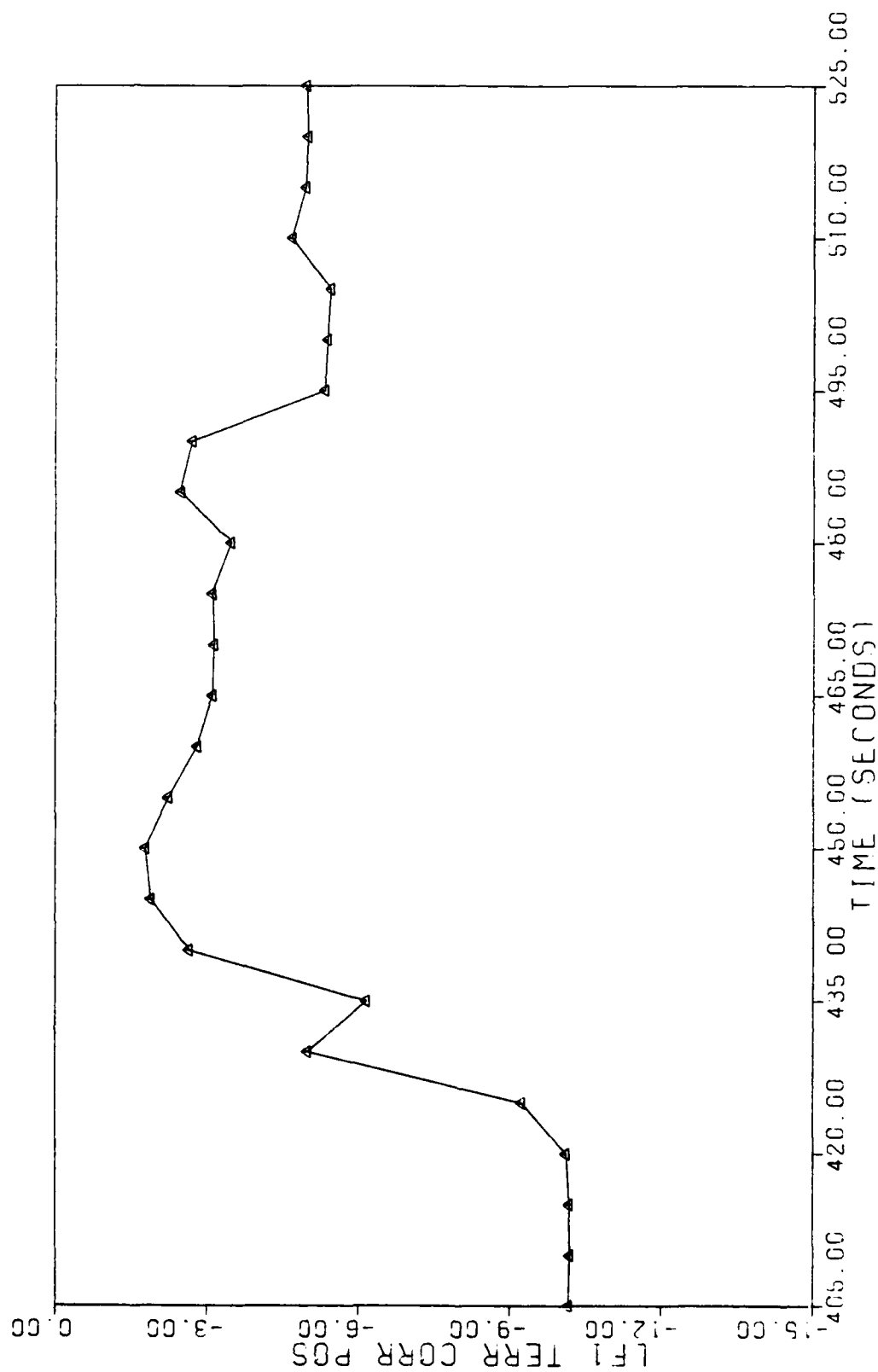


Fig. A.89. No Failure Condition--Terrain Correlator Measurement #1--Benign Flight

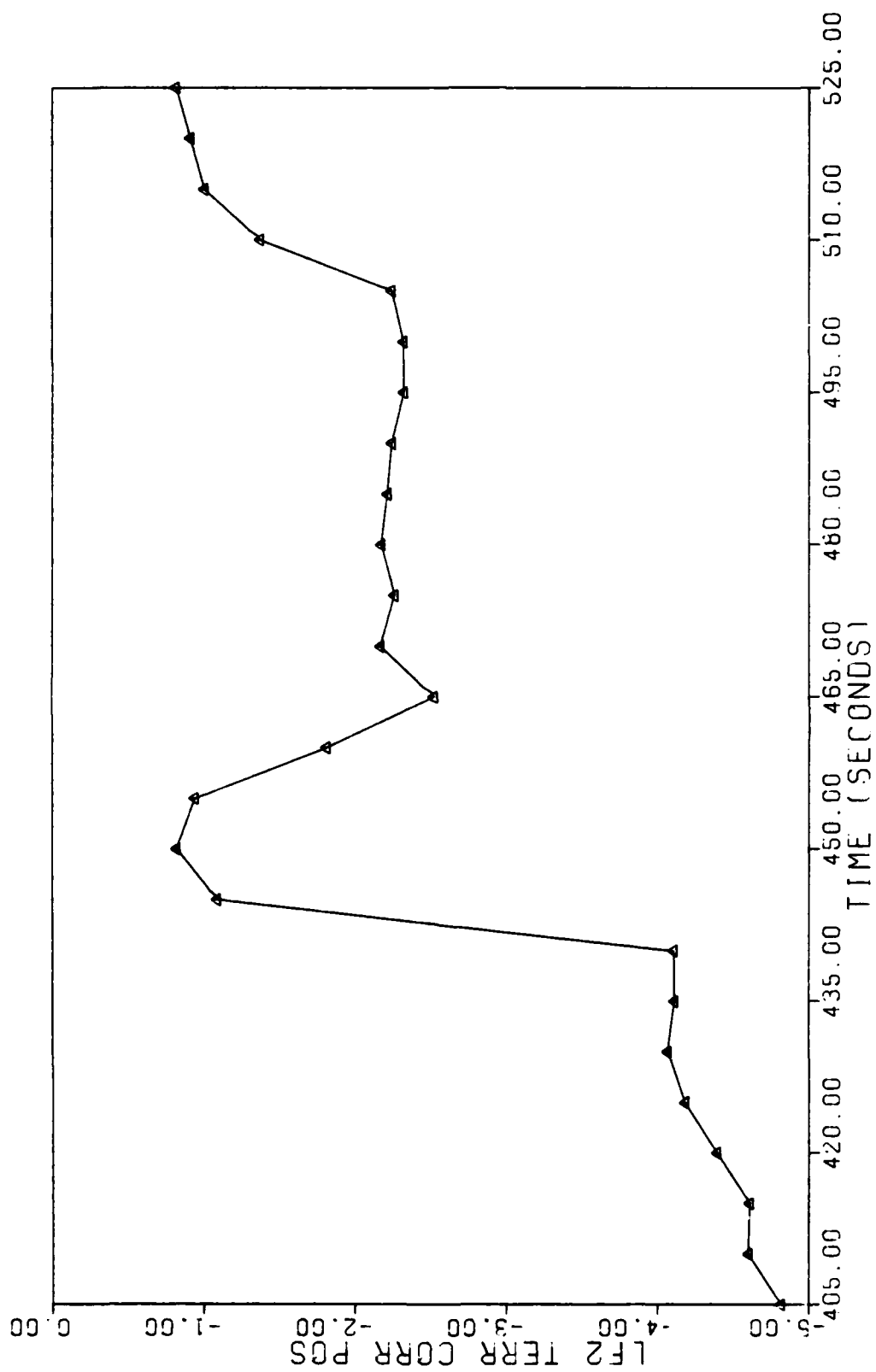


Fig. A.90. No Failure Condition--Terrain Correlator Measurement#2--Benign Flight

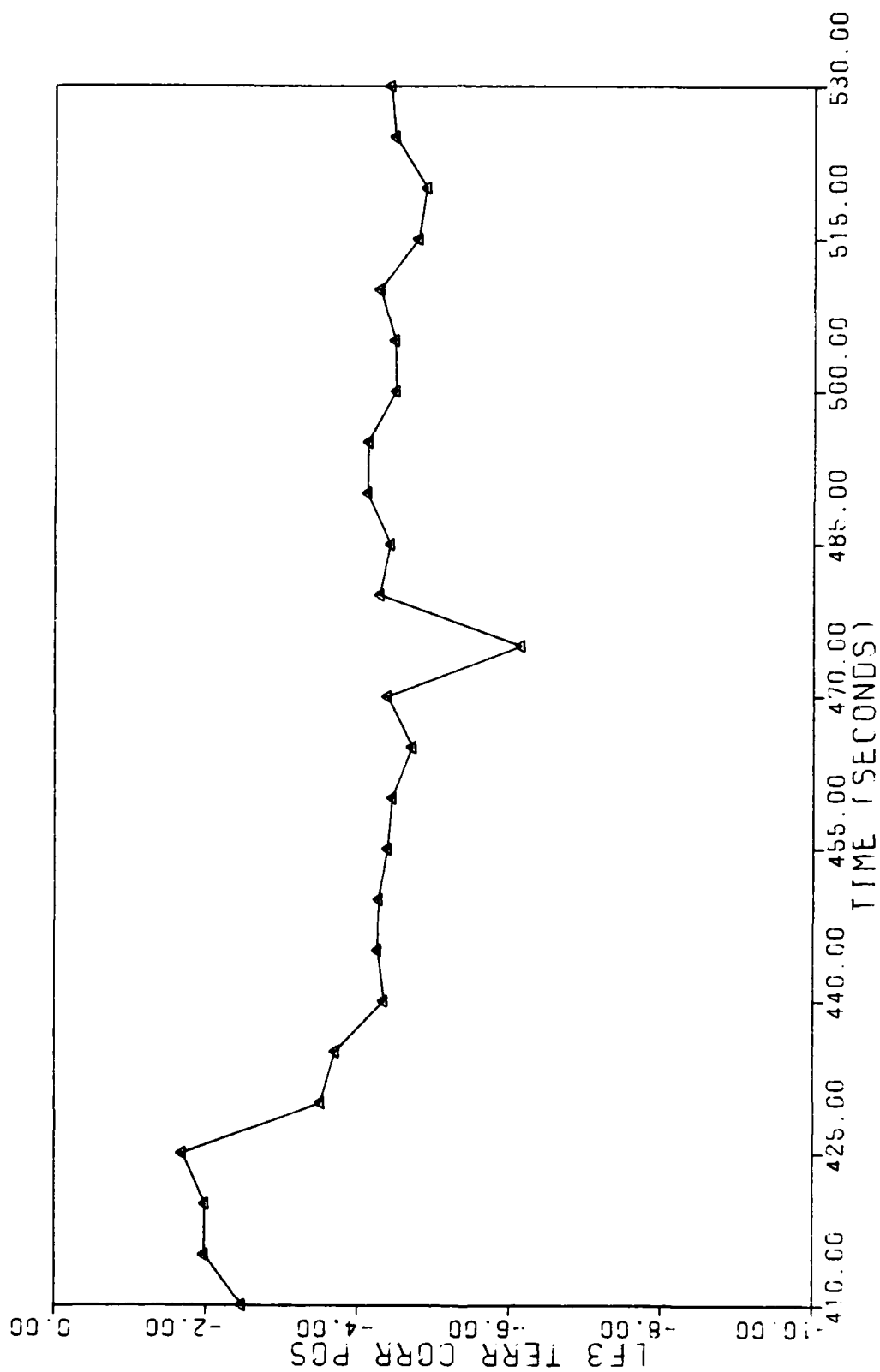


Fig. A.91. No Failure Condition--Terrain Correlator Measurement #3--Benign Flight

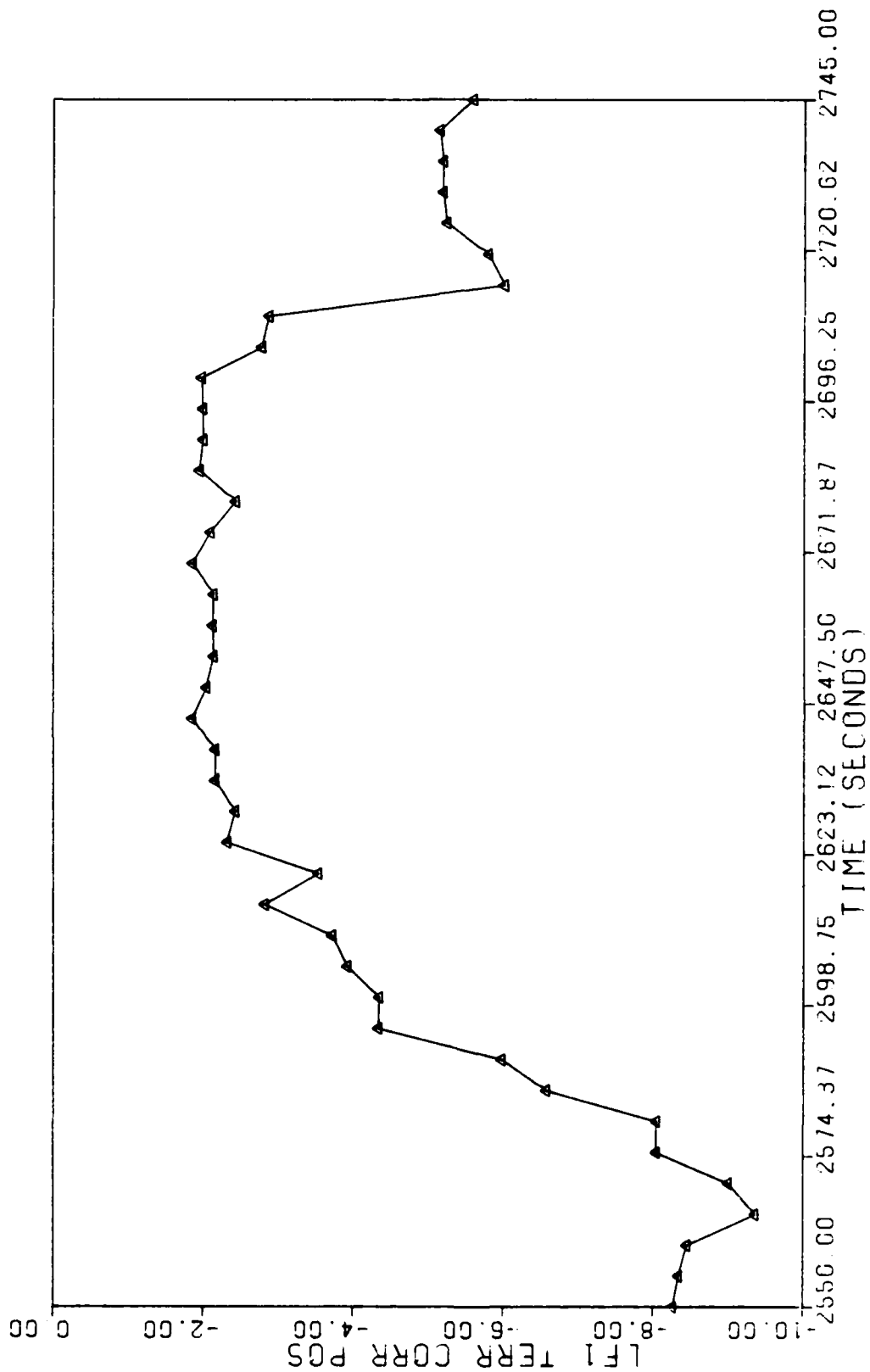


FIG. A.92. No Failure Condition--Terrain Correlator Measurement #1--Dynamic Flight

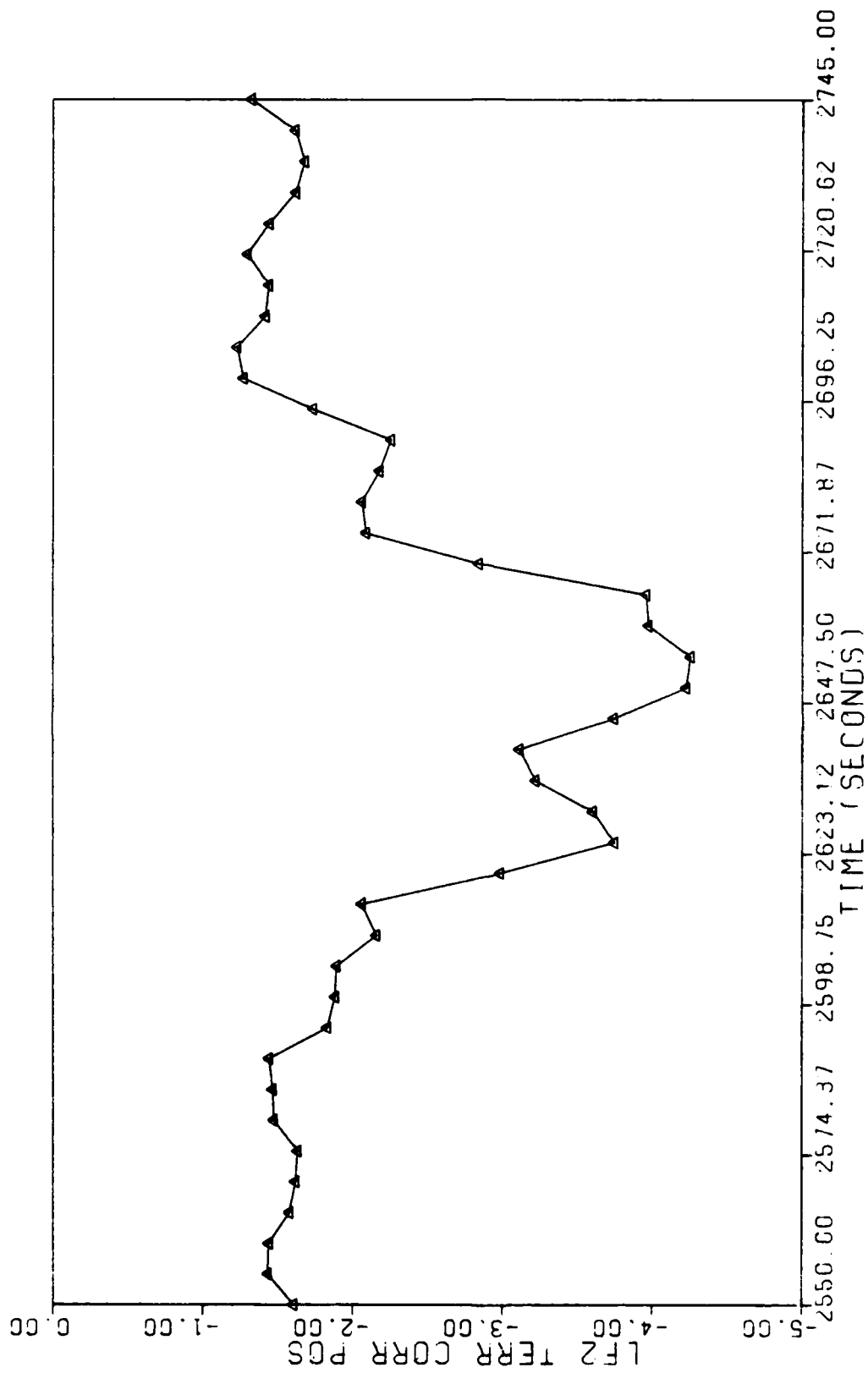


Fig. A.93. No Failure Condition--Terrain Correlator Measurement #2--Dynamic Flight



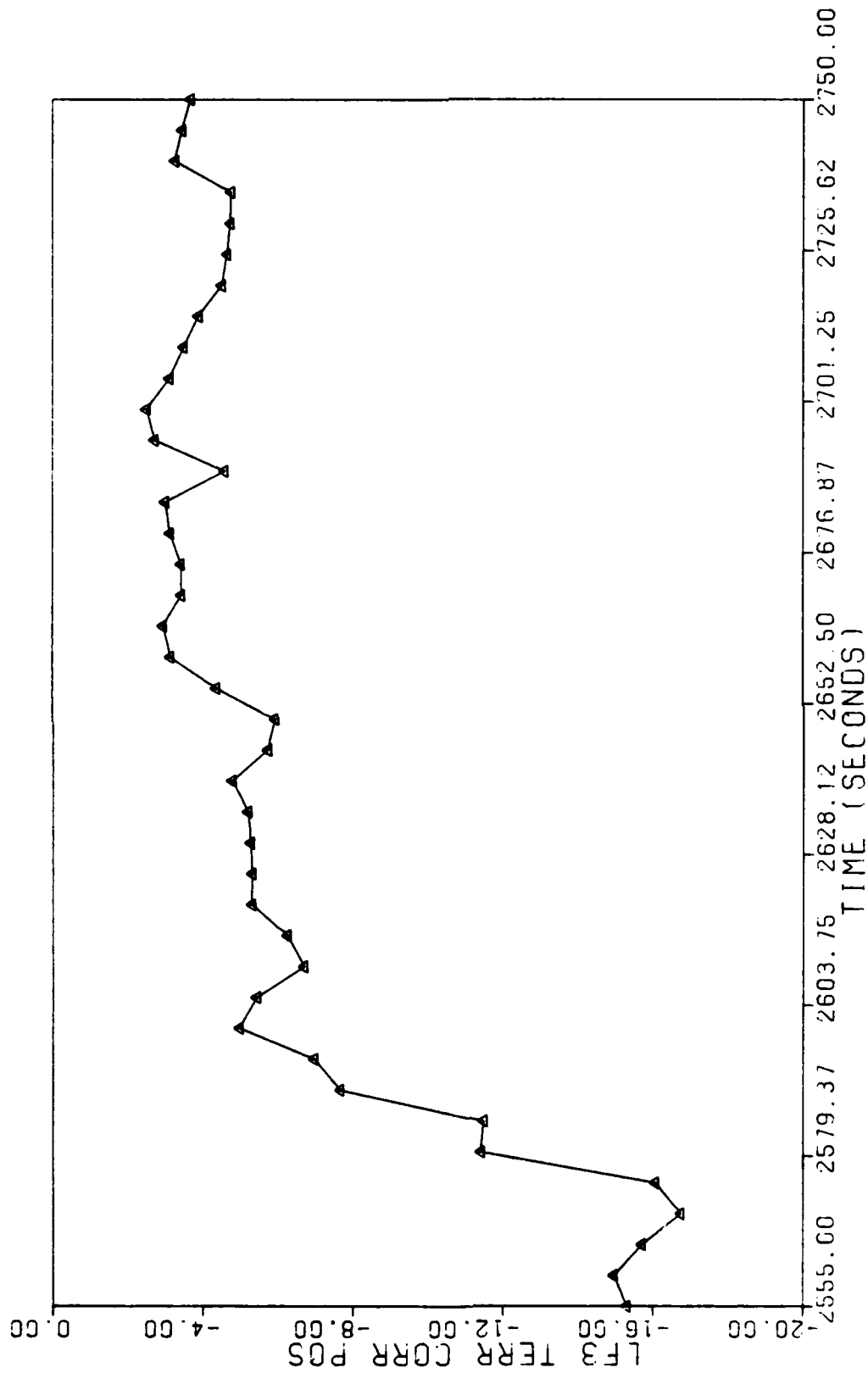


Fig. A.94. No Failure Condition--Terrain Correlator Measurement #3--Dynamic Flight

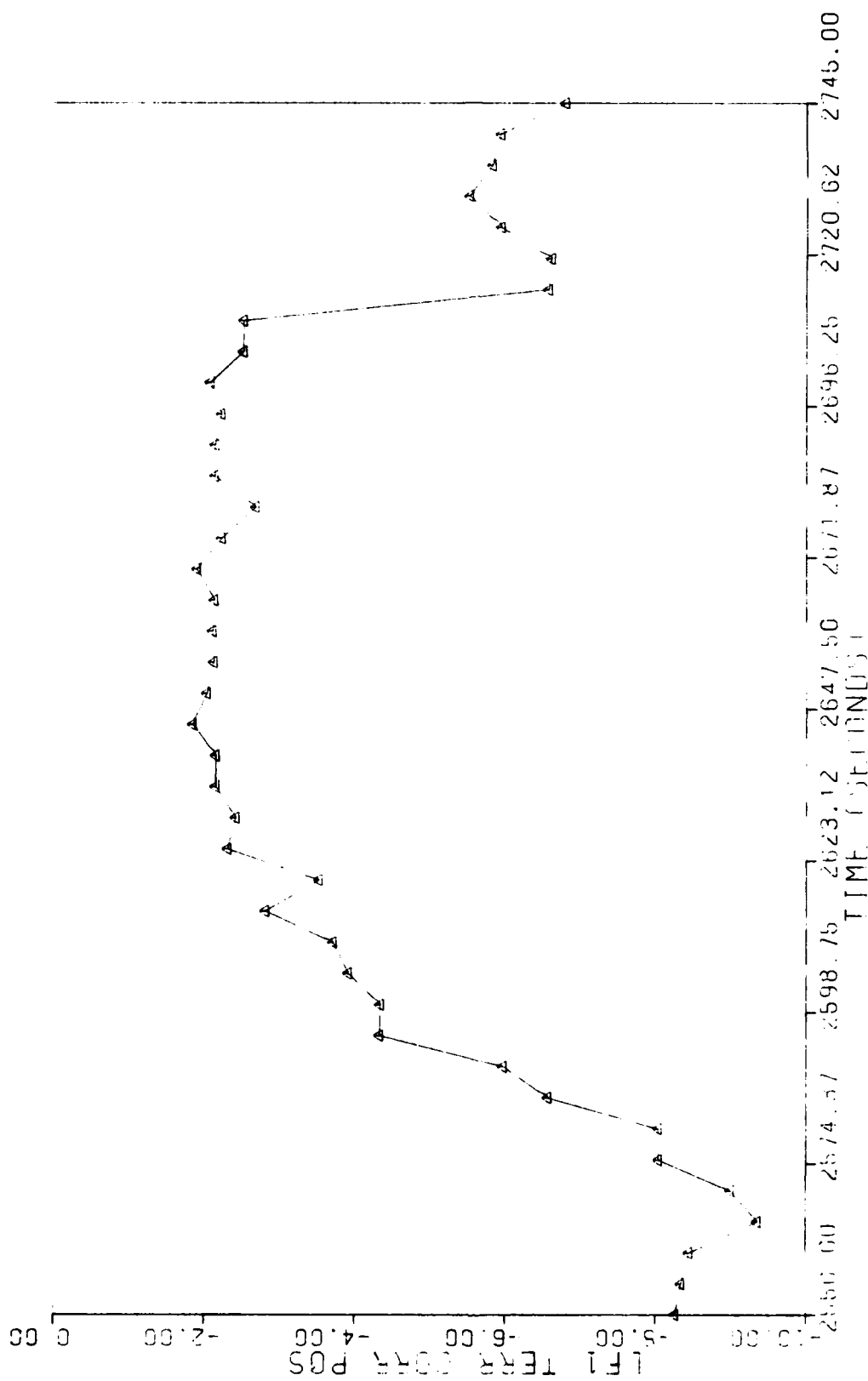


Fig. A.95. Soft Accelerometer 2 Failure--Terrain Correlator Measurement #1--Dynamic Flight

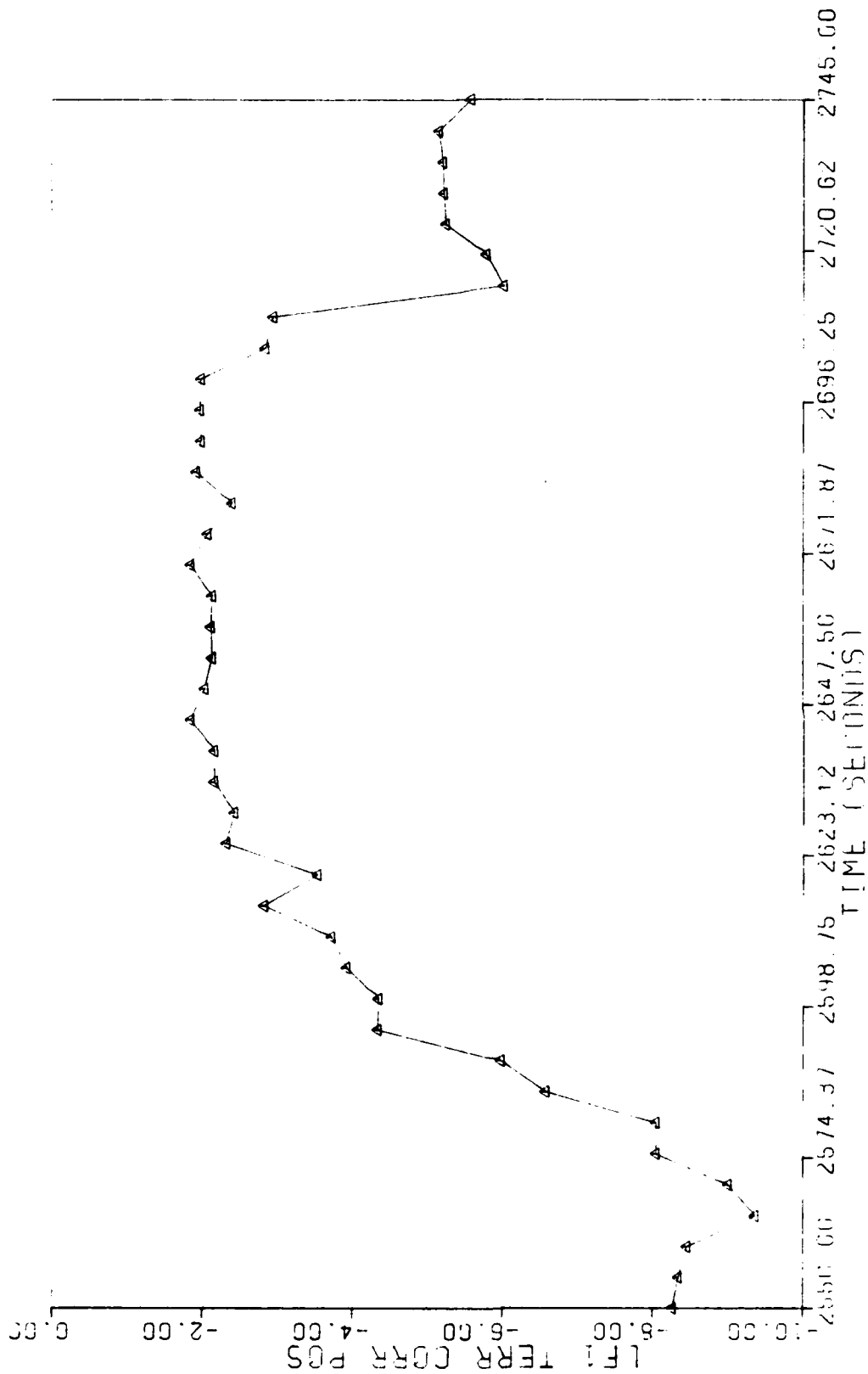


Fig. A.96. Soft Accelerometer 3 Failure--Terrain Correlator Measurement #1--Dynamic Flight

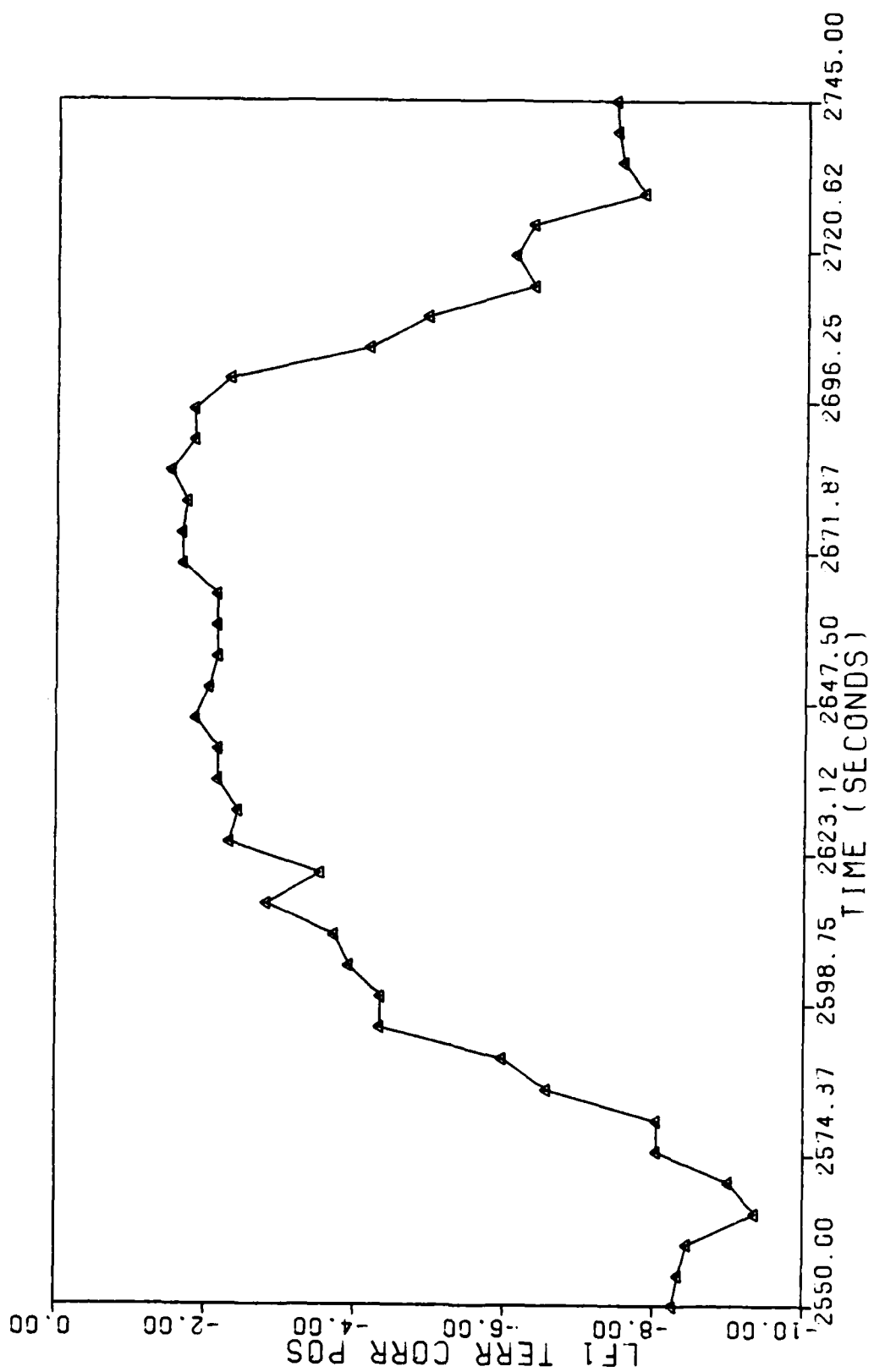


FIG. A.97. Hard Accelerometer 1 Failure--Terrain Correlator Measurement #1--Dynamic Flight

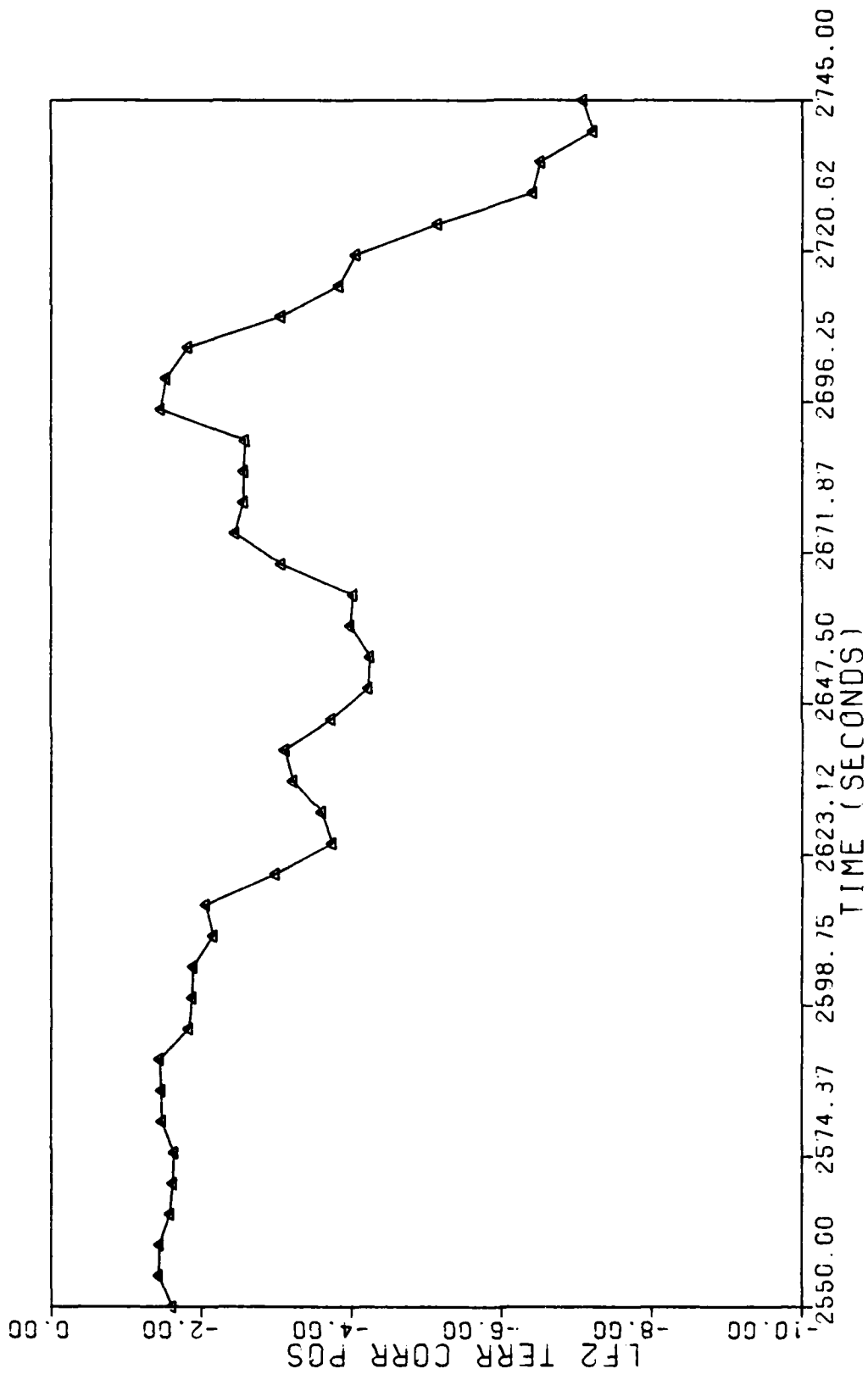


Fig. A.98. Hard Accelerometer 1 Failure--Terrain Correlator Measurement #2--Dynamic Flight

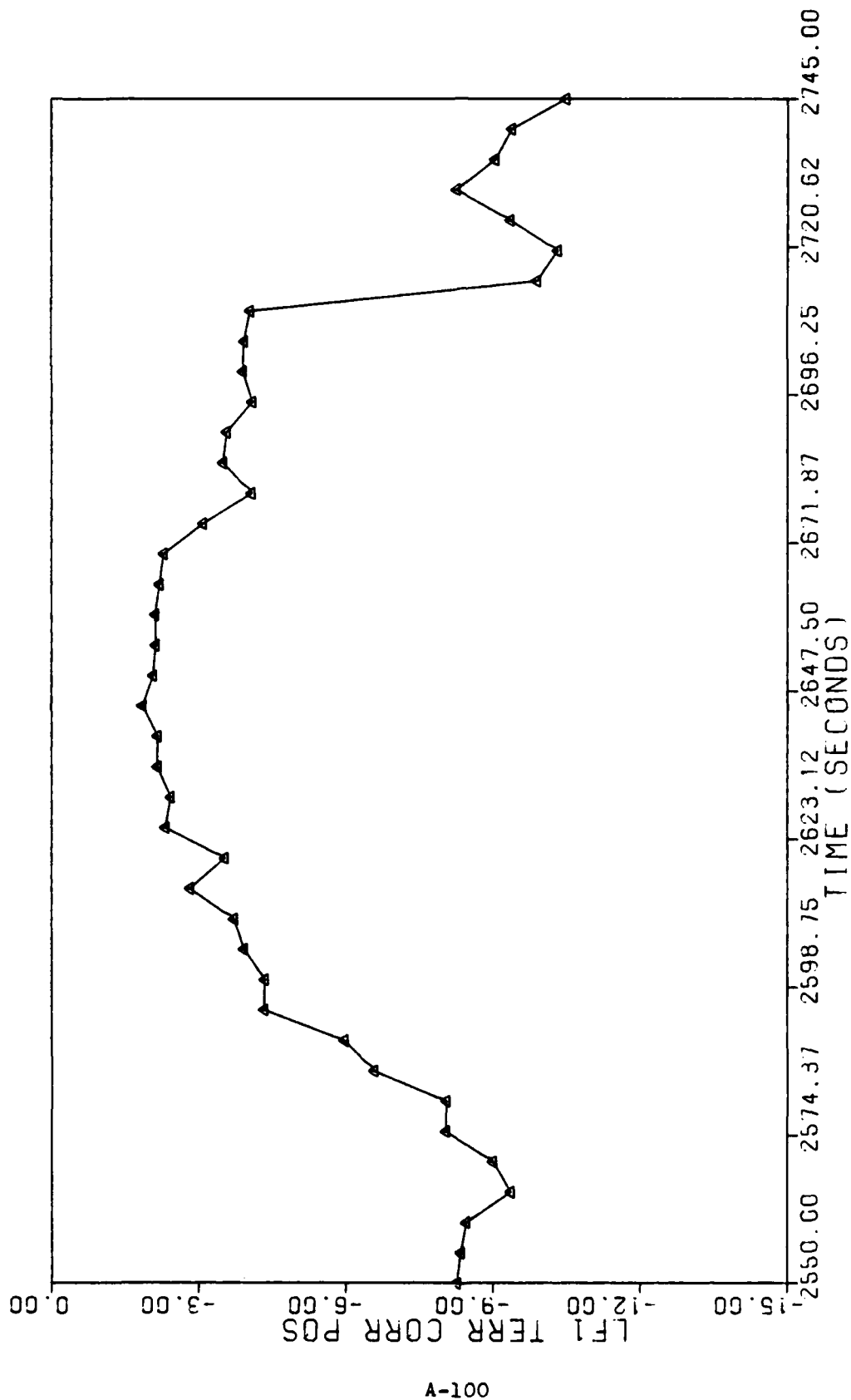


Fig. A.99. Hard Accelerometer ? Failure--Terrain Correlator Measurement #1--Dynamic Flight

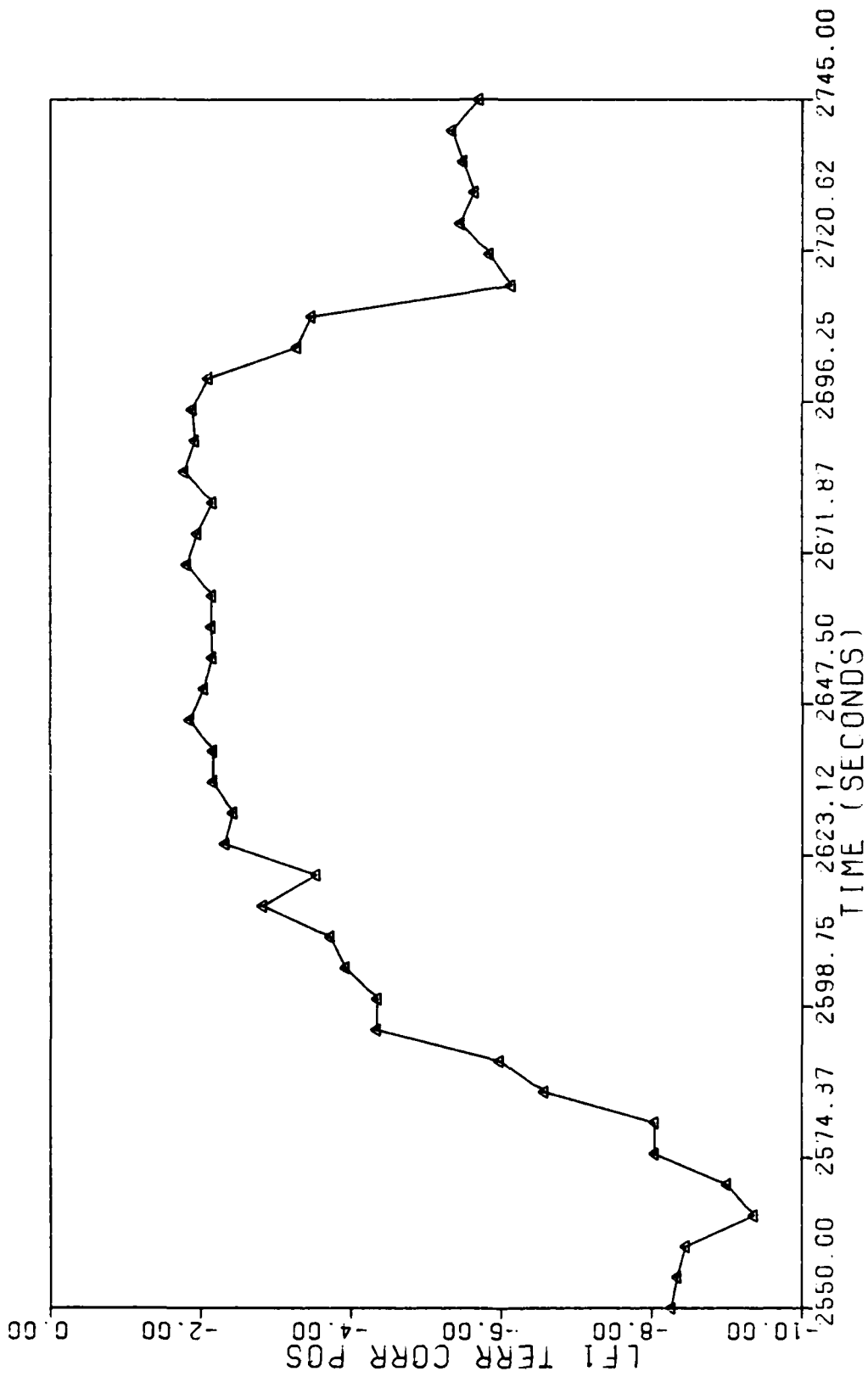


Fig. A.100. Hard Accelerometer 3 Failure--Terrain Correlator Measurement #1--Dynamic Flight

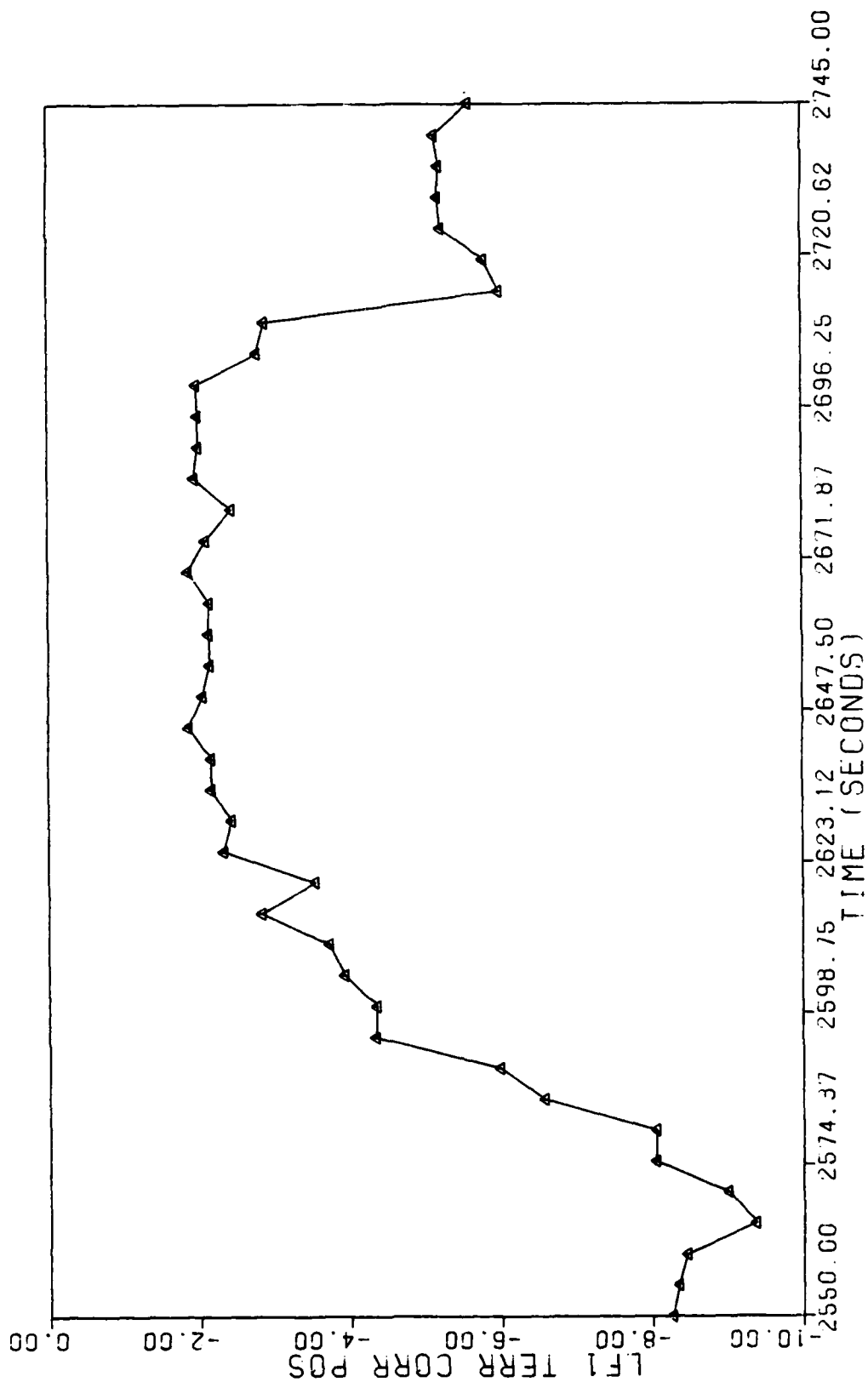


FIG. A.101. Soft Radar Altimeter Failure--Terrain Correlator Measurement #1--Dynamic Flight



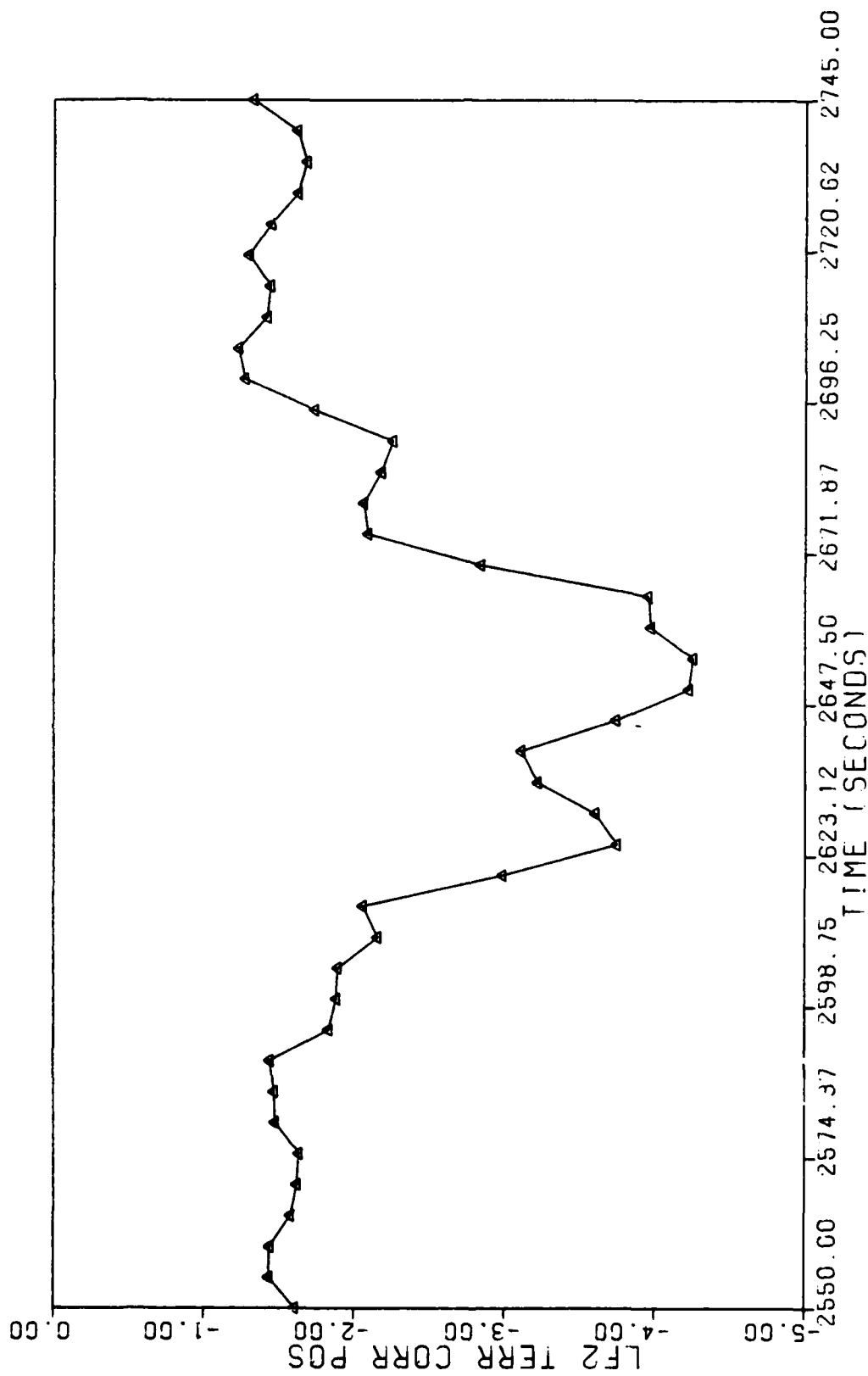


Fig. A.102. Soft Radar Altimeter Failure--Terrain Correlator Measurement #2--Dynamic Flight

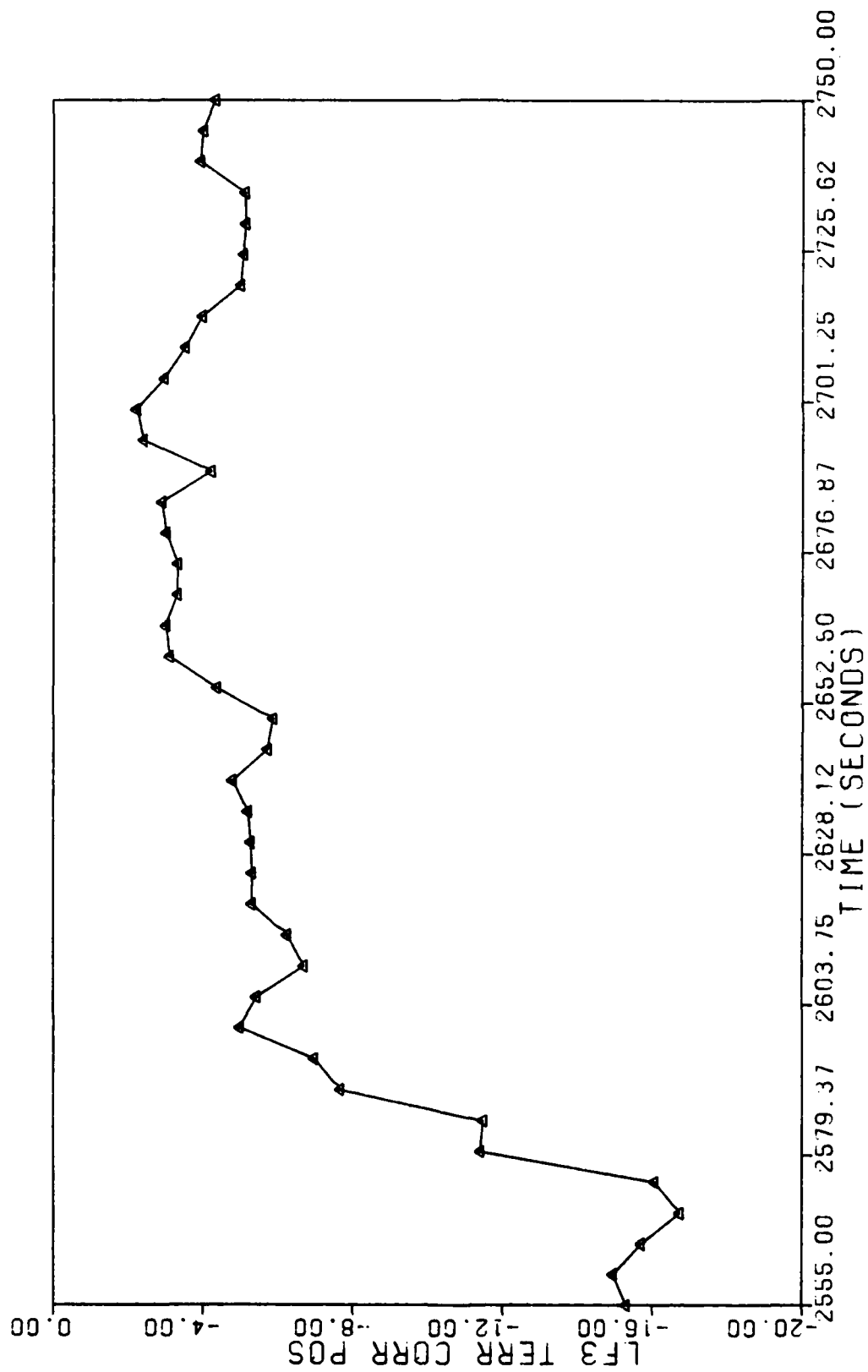


Fig. A.103. Soft Radar Altimeter Failure--Terrain Correlator Measurement #3--Dynamic Flight

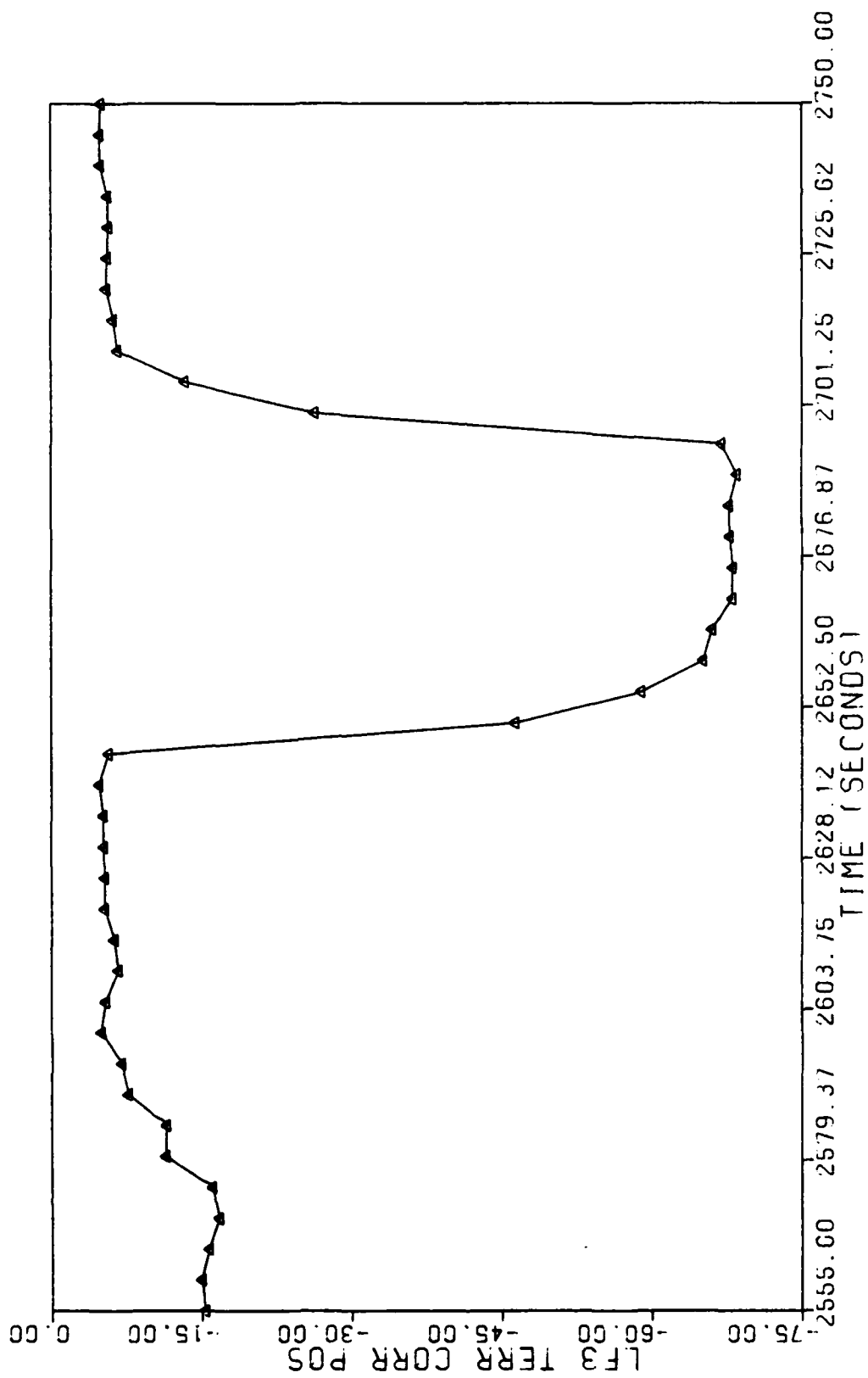


Fig. A.104. Hard Radar Altimeter Failure--Terrain Correlator Measurement #3--Dynamic Flight

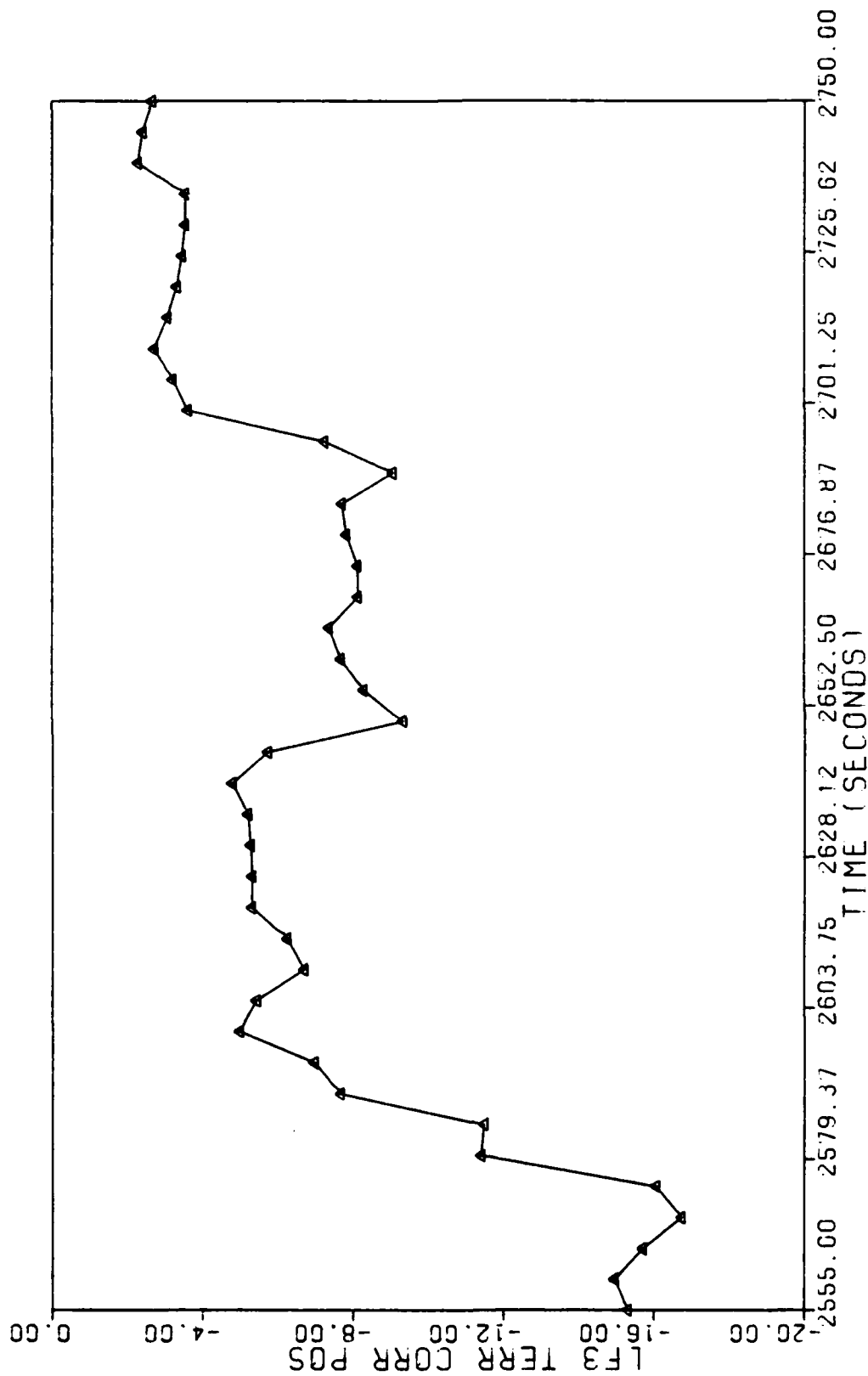


Fig. A.105. Hard Baro-altimeter Failure--Terrain Correlator Measurement #3--Dynamic Flight

### Bibliography

1. Britting, K.R. Inertial Navigation Systems Analysis. New York: John Wiley and Sons, Inc. 1971.
2. Broen, R.B. "A Non-linear Voter-Estimator for Redundant Systems," Proceedings of the 1974 IEEE Conference on Decision and Control, 743-748. IEEE Press, New York, 1974.
3. Butler, R. and G. Rhue. Kalman Filter Design for an Integrated Navigation System Aided by Non-synchronous Satellite Constellations. Wright-Patterson Air Force Base, Ohio: Air Force Institute of Technology Master's Thesis, March 1974. (AD-779724).
4. Buxbaum, P.J. and R.A. Haddad. "Recursive Optimal Estimation for A Class of Non-Gaussian Processes," Proceedings of the Symposium on Computer Processing in Communications, April 8-10, 1969.
5. Chang, C.B. and K.P. Dunn. "On GLR Detection and Estimation of Unexpected Changes in a Linear Discrete Systems," IEEE Transactions on Automatic Control, 24: 499-501 (June 1979).
6. Chang, Chaw-Bing and John A. Tabaczynski. "Application of State Estimation to Target Tracking," IEEE Transactions on Automatic Control, AC-29: 98-109 (February 1984).
7. Chow, Edward Y. and Alan S. Willsky. Analytical Redundancy and the Design of Robust Failure Detection Systems. Laboratory for Information and Decision Systems, MIT, Cambridge, MA, October 1982 (AD-A121771).
8. Chow, Edward Y. and others. Redundancy Relations and Robust Failure Detection. Department of Electrical Engineering and Computer Science, Massachusetts Institute of Technology, Cambridge, Massachusetts (AD-A138357).
9. Cross, S.E. Performance In a Jamming Environment of a Low-Cost GPS User Receiver Algorithm for Aiding a Tactical INS. Wright-Patterson Air Force Base, Ohio: Air Force Institute of Technology Master's Thesis, December 1977.
10. Davis, M.H.A. "The Application of Non-Linear Filtering to Fault Detection in Linear Systems," IEEE Transactions on Automatic Control, AC-20: 257-259 (April 1975).

11. Deckert, J.C. and others. "F-8 DFBW Sensor Failure Identification Using Analytic Redundancy," IEEE Transactions on Automatic Control, AC-22: 975-803 (October 1977).
12. Fagin, S.L. "Recursive Linear Regression Theory, Optical Filter Theory, and Error Analyses of Optimal Systems." IEEE Int. Conv. Record: 216-240 (March 1964).
13. Gilmore, J. and McKern. "A Redundant Strapdown Inertial System Mechanization - SIRU," Proceedings of the AIAA Guidance, Control and Flight Mechanics Conference. 1970.
14. Gupta, Narendra K. and W. Earl Hall. System Identification Methodology For Fault Detection and Isolation In Dynamic Systems. Interim Report, 1 Jan. 1976 - 1 May 1977. Contract N00014-76-C-0420. Systems Control, Inc., Palo-Alto, California, 1 Feb. 1978 (AD-A059126).
15. Heller, Warren G. Models For Aided Inertial Navigation System Sensor Errors. Contract DMA 700-74-C-005. The Analytical Sciences Corporation, Reading, Mass.
16. Ho, Y.C. and P.M. Newbold. "Detection of Changes In the Characteristics of a Gauss-Markov Process," IEEE Transactions on Aerospace Electrical Systems, AES-4: 707-718 (September 1968).
17. Jazwinski, A.H. "Limited Memory Optimal Filtering," IEEE Transactions on Automatic Control, AC-13: 558-563 (1968).
18. Jazwinski, A.H. Stochastic Processes and Filtering Theory. New York: Academic Press, 1970.
19. Lainiotis, D.G. "Joint Detection, Estimation, and System Identification," Information Control, 19: 75-92, (August 1971).
20. Lou, X: Cheng and others. "Failure Detection With Uncertain Models," Proceedings of the 1983 American Control Conference. Laboratory for Information and Decision Systems. MIT Cambridge, Massachusetts, March 1983 (AD-A127881).
21. Magill, D.T. "Optimal Adaptive Estimation of Sampled Processes" IEEE Transactions on Automatic Control, AC-10: 434-439 (Oct. 1965).
22. Maybeck, Peter S. Failure Detection Through Functional Redundancy, January 1972 - July 1973. AFFDL-TR-76-93. Wright-Patterson AFB, Ohio: Air Force Flight Dynamics Laboratory, September 1976 (AD-A076906).

23. Maybeck, Peter S. "Failure Detection Without Excessive Hardware Redundancy," Proc. IEEE Nat. Aerospace Electron Conf., Dayton, Ohio: 315-322 (May 1976).
24. Maybeck, Peter S. "Performance Analysis of a Particularly Simple Kalman Filter," Journal of Guidance and Control, 1: 391-396 (November-December 1978).
25. Maybeck, Peter S. Stochastic Models, Estimation and Control Volume 1. New York: Academic Press, 1979.
26. Maybeck, Peter S. Stochastic Models, Estimation and Control Volume 2. New York: Academic Press, 1982.
27. Maybeck, Peter S. Stochastic Models, Estimation and Control Volume 3. New York: Academic Press, 1982.
28. Maybeck, Peter S. and Steven K. Rogers. "Adaptive Tracking of Multiple Hot-spot Target IR Images," IEEE Transactions on Automatic Control, AC-28: 937 (October 1983).
29. Maybeck, Peter S. and William L. Zicker. Control Based on Multiple Model Adaptive Estimation For Space-Time Point Process Observations. Air Force Institute of Technology, AFIT/ENG, Wright-Patterson AFB, Ohio.
30. Maybeck, Peter S. and others. Investigation of Constant Turn-Rate Dynamics Models In Filters For Airborne Vehicle Tracking. Dept. of Electrical Engineering, Air Force Institute of Technology. Wright-Patterson AFB, Ohio.
31. McAulay, R.J. and E. Denlinger. "A Decision-Directed Adaptive Tracker," IEEE Transactions Aeronautical and Electrical Systems, AE5-9: 229-236 (March 1973).
32. Mehra, R.K. and J. Peschon. "An Innovations Approach to Fault Detection and Diagnosis In Dynamic Systems," Automatica, 7: 637-640.
33. Montgomery, R.C. and D.B. Price. "Management of Analytical Redundancy in Digital Flight Control Systems For Aircraft," AIAA Mechanics and Control of Flight Conference. August 1974.
34. Motyka, Paul. Reliability Analysis and Fault-Tolerant System Development for a Redundant Strapdown Inertial Measurement Unit. Contract NAS1-16887. The Charles Stark Draper Laboratory, Inc. Cambridge, Massachusetts, March 1983.

35. Motyka, Paul and others. Failure Detection and Isolation Analysis of a Redundant Strapdown Inertial Measurement Unit. Contract NAS1-15933. The Charles Stark Draper Laboratory, Inc., Cambridge, Mass., February 1981.
36. Musick, Stanton H. A Computer Program for Generation of Flight Profiles. AFAL-TR-76-247. Wright-Patterson AFB, Ohio: Air Force Avionics Laboratory, November 1976.
37. Musick, Stanton H. SOFE: A Generalized Digital Simulation For Optimal Filter Evaluation User's Manual, 1 January 1976 - 3 July 1980. Technical Report AFNAL-TR-80-1108. Avionics Laboratory (AFWAL/AARA) Air Force Aeronautical Laboratories, AFSC, Wright-Patterson AFB, Ohio, October 1980 (AD-A093887).
38. Musick, Stanton H. and others. SOFEPL: A Plotting Postprocessor for "SOFE", User's Manual, July 1979 - September 1981. AFWAL-TR-80-1109, Wright-Patterson AFB, Ohio: Air Force Avionics Laboratory, November 1981.
39. Nahi, N.E. "Optimal Recursive Estimation With Uncertain Observation," IEEE Transactions Information Theory, IT-15: 457-462 (July 1969).
40. Pierce, B.D. and D.D. Sworder. "Bayes and Minimax Controllers for a Linear System With Stochastic Jump Parameters," IEEE Transactions on Automatic Control, AC-16: 300-307 (August 1971).
41. Ratner, R.S. and D.C. Luenberger. "Performance Adaptive Renewal Policies for Linear Systems," IEEE Transactions on Automatic Control, AC-14: 344-351 (August 1969).
42. Robinson, V.G. and D.D. Sworder. "A Computational Algorithm For Design of Regulators For Linear Jump Parameter Systems," IEEE Transactions on Automatic Control, AC-19: 47-49 (February 1974).
43. Sanyal, P. and C.N. Shen. "Bayes' Decision Rule For Rapid Detection and Adaptive Estimation Scheme With Space Applications," IEEE Transactions on Automatic Control, AC-19: 228-231 (June 1974).
44. Stuckenberg, Norbert. A Diagnosis Scheme For Sensors of a Flight Control System Using Analytical Redundancy. Institut Fur Flugfuhrang, DFVLR, Flughafen D3300 Braunschweig, Germany (AD-P002282).
45. Tarn, T.J. and J. Zaborsky. "A Practical Non-Diverging Filter," AIAA Journal, 8: 1127-1133 (1970).



46. Widnall, W. and P. Grundy. Inertial Navigation System Error Models. AFSWC-TR-03-73. Holloman AFB, New Mexico: Air Force Special Weapons Center, March 1973 (AD-9124896).
47. Willsky, Alan S. "A Generalized Likelihood Ratio Approach To State Estimation In Linear Systems Subject to Abrupt Changes," Proceedings of the 1974 IEEE Conference on Decision and Control. 846-852. IEEE Press, New York, November 1974.
48. Willsky, Alan S. "A Survey of Design Methods For Failure Detection in Dynamic Systems," Automatica, 12: 601-611 (December 1976).
49. Willsky, Alan S. "Two Self-Test Methods Applied to an Inertial System Problem," J. Spacecraft, 12: 434-437 (July 1975).
50. Willsky, A.S. and H.L. Jones. "A Generalized Likelihood Ratio Approach to the Detection and Estimation of Jumps In Linear Systems," IEEE Transactions on Automatic Control, AC-21: 108-112 (February 1976).
51. Willsky, Alan. and others. Optimally Robust Redundancy Relations For Failure Detection In Uncertain Systems. Department of Electrical Engineering and Computer Science, MIT, Cambridge, Mass. (AD-A135949).
52. Willsky, A.S. and others. "Two Self-Test Methods applied to an Inertial System Problem," Proceedings of the 1974 JACC, June 19-21, 1974.

VITA

First Lieutenant Gary R. Johnston [REDACTED]  
[REDACTED] [REDACTED]  
[REDACTED]

After one year of college, he enlisted in the USAF in 1972. In 1978, he returned to Purdue University under the Airman Education and Commissioning Program (AECPP). He received the degree of Bachelor of Science in Electrical Engineering in December 1980. In April 1981, he received a USAF commission through Officer Training School (OTS). He worked as a TEMPEST engineer for the 6906th Electronic Security Squadron, Brooks AFB, Texas, until entering the School of Engineering, Air Force Institute of Technology, in June 1983.

[REDACTED] [REDACTED]  
[REDACTED]

UNCLASSIFIED

SECURITY CLASSIFICATION OF THIS PAGE

## REPORT DOCUMENTATION PAGE

|  |       |   |   |                |                                       |
|--|-------|---|---|----------------|---------------------------------------|
| 1. REPORT SECURITY CLASSIFICATION<br><b>UNCLASSIFIED</b>   |       |   | 1b. RESTRICTIVE MARKINGS  |                |                                       |
| 2a. SECURITY CLASSIFICATION AUTHORITY  |       |   | 3. DISTRIBUTION/AVAILABILITY OF REPORT<br><b>Approved for public release;<br/>distribution unlimited.</b> |                |                                       |
| 2b. DECLASSIFICATION/DOWNGRADING SCHEDULE  |       |   |   |                |                                       |
| 4. PERFORMING ORGANIZATION REPORT NUMBER(S)<br><b>AFIT/CE/ENG/84D-36</b>   |       |   | 5. MONITORING ORGANIZATION REPORT NUMBER(S)   |                |                                       |
| 6a. NAME OF PERFORMING ORGANIZATION<br><b>School of Engineering</b>  |       | 6b. OFFICE SYMBOL<br>(If applicable)<br><b>AFIT/ENG</b> | 7a. NAME OF MONITORING ORGANIZATION   |                |                                       |
| 6c. ADDRESS (City, State and ZIP Code)<br><b>Air Force Institute of Technology<br/>Wright-Patterson AFB, OH 45433</b>  |       |   | 7b. ADDRESS (City, State and ZIP Code)  |                |                                       |
| 8a. NAME OF FUNDING/SPONSORING ORGANIZATION<br><b>AFWAL</b>  |       | 8b. OFFICE SYMBOL<br>(If applicable)<br><b>AAAN-2</b>   | 9. PROCUREMENT INSTRUMENT IDENTIFICATION NUMBER   |                |                                       |
| 8c. ADDRESS (City, State and ZIP Code)<br><b>Wright-Patterson AFB, OH 45433</b>  |       |   | 10. SOURCE OF FUNDING NOS.  |                |                                       |
| 11. TITLE (Include Security Classification)<br><b>See Box 19</b>   |       |   | PROGRAM<br>ELEMENT NO.  | PROJECT<br>NO. | TASK<br>NO.                           |
| 12. PERSONAL AUTHOR(S)<br><b>Gary R. Johnston, B.S., 1Lt, USAF</b>   |       |   | WORK UNIT<br>NO.  |                |                                       |
| 13a. TYPE OF REPORT<br><b>MS Thesis</b>  |       | 13b. TIME COVERED<br>FROM _____ TO _____                | 14. DATE OF REPORT (Yr., Mo., Day)<br><b>1984 December</b>  |                | 15. PAGE COUNT<br><b>309</b>          |
| 16. SUPPLEMENTARY NOTATION<br><b>1472D</b>   |       |   |   |                |                                       |
| 17. COSATI CODES   |       |   | 18. SUBJECT TERMS (Continue on reverse if necessary and identify by block number)                         |                |                                       |
| FIELD  | GROUP | SUB. GR.  |   |                |                                       |
| 17   |       |   | Detection Detectors, Kalman Filtering   |                |                                       |
| 9  | 2     |   | Isolation Filters, Failure.   |                |                                       |
| 19. ABSTRACT (Continue on reverse if necessary and identify by block number)   |       |   |   |                |                                       |
| Title: <b>INVESTIGATION OF A FAILURE DETECTION/IDENTIFICATION<br/>SYSTEM FOR A TACTICAL AIRCRAFT NAVIGATION SYSTEM</b>   |       |   |   |                |                                       |
| Thesis Chairman: <b>Peter S. Maybeck, Ph.D.</b>  |       |   |   |                |                                       |
| Approved for public release: IAW AFR 190-17.<br>K. E. WOLVER<br>Organizational and Professional Development<br>Air Force Institute of Technology (AFIT)<br>Wright-Patterson AFB OH 45433 |       |   |   |                |                                       |
| 20. DISTRIBUTION/AVAILABILITY OF ABSTRACT<br><b>UNCLASSIFIED/UNLIMITED</b> <input checked="" type="checkbox"/> SAME AS RPT. <input type="checkbox"/> DTIC USERS <input type="checkbox"/> |       |   | 21. ABSTRACT SECURITY CLASSIFICATION<br><b>UNCLASSIFIED</b>   |                |                                       |
| 22a. NAME OF RESPONSIBLE INDIVIDUAL<br><b>Peter S. Maybeck, Ph.D.</b>  |       |   | 22b. TELEPHONE NUMBER<br>(Include Area Code)<br><b>513-255-2024</b>                                       |                | 22c. OFFICE SYMBOL<br><b>AFIT/ENG</b> |

This research effort aimed at the design of a suitable filter model and failure detection/identification (FDI) processor as a basis for the development of a fully simulated adaptive tactical navigation (ATN) system. A 52-state "truth" error model was developed from which a 26-state filter error model was derived. The measurement process <sup>uses</sup> utilized a six measurement satellite positioning system (three velocity measurements and three position measurements), a three measurement Doppler radar (three velocity measurements), and a terrain correlation system (three position measurements). The filter residuals for the different measurement processes are then utilized in N-step likelihood function computations to observe the residual behavior. Two different testing criteria have been developed for failure declaration. Simple threshold establishment and the tracking of the likelihood function N-step slope characteristics are utilized for this purpose. Based on the statistics of the observed failure characteristics, an isolation/identification processor isolates the fault and makes the correct identification.

The analysis was performed by simulating both "soft" and "hard" failures and monitoring the likelihood function behavior. The observed failure characteristics then triggered the appropriate isolation/identification logic and the failed sensor decision was made. The test results indicate that this FDI process warrants further consideration. Readdressing the basic issues of filter state reduction, tuning, threshold settings, and "window" size will undoubtedly improve the performance of this system.